Fragile X Related Protein 1 Associates with the Protein Synthesis Machinery and Controls Synaptic Plasticity in Mice

by

Denise Cook

Department of Neurology and Neurosurgery
Integrated Program in Neuroscience

The Faculty of Medicine
McGill University
Montreal, Quebec, Canada

April 2012

A thesis submitted in partial fulfillment of the requirements of the degree of
Doctorate of Philosophy

ABSTRACT

Long-lasting synaptic plasticity and memory storage rely on mRNA control mechanisms that allow for rapid changes in gene expression in response to synaptic activity. RNA-binding proteins, which affect the transport, stability and translational state of their target mRNAs, are an important component of these translational control mechanisms. Fragile X Related Protein 1 (FXR1P) is a member of the Fragile X family of RNA-binding proteins, which also includes Fragile X Mental Retardation Protein (FMRP) and Fragile X Related Protein 2 (FXR2P). FXR1P is known to both repress and enhance the translation of its target mRNAs in non-neuronal cells. However, its function in neurons is currently unknown. The central hypothesis of this thesis is that FXR1P controls the local translation of mRNAs important for spine development and synaptic plasticity in mice. To test this hypothesis, we used biochemical and confocal imaging techniques to study the expression pattern and subcellular localization of FXR1P in developing neurons and to look at the association of endogenous and exogenous FXR1P with the translational machinery. We then used a combination of confocal imaging, whole-cell electrophysiological recordings and two-photon glutamate uncaging approaches to measure the effect of increasing levels of FXR1P on spine number, spine morphology and spine function. Finally, we used a conditional mouse knockout approach to selectively delete FXR1P from postnatal forebrain neurons and studied the consequences of FXR1P loss on spine development and synaptic plasticity in adult mice. Interestingly, we found that FXR1P clustered with the translational machinery in dendrites and at a subset of large, functionally-strong dendritic spines. Genetic deletion of FXR1P decreased spine density and spine size and enhanced protein-synthesis dependent long-lasting long-term potentiation (L-LTP). Together, these results support the idea that FXR1P is positioned to control the local translation of a subset of mRNAs required for regulating the maintenance of spines and restraining the size of L-LTP. The results presented in this thesis expand on our understanding of the importance of translational control mechanisms in synaptic plasticity and cognition.

ABRÉGÉ

La plasticité synaptique de longue durée et l'entreposage des mémoires nécessitent des mécanismes de contrôle de l'ARNm qui permettent des changements rapides dans l'expression des gènes en réponse à l'activité synaptique. Les protéines d'attachement à l'ARN sont une composante importante des mécanismes de contrôle de la traduction de l'ARNm. Ces protéines affectent le transport et la stabilité de leurs ARNm cible. La protéine reliée à Fragile X (FXR1P) est un membre de la famille Fragile X, des protéines d'attachement à l'ARN qui incluent FMRP et FXR2P. FXR1P est capable de réprimer et d'augmenter la traduction des ARNm cibles dans des lignées cellulaires non neuronales. Cependant, sa fonction dans les neurones demeure inconnue. L'hypothèse centrale de cette thèse est que FXR1P contrôle la traduction locale des ARNm intégrales au développement des épines dendritiques et à la plasticité synaptique des souris. Dans l'objectif de tester cette hypothèse, nous avons utilisé des techniques en biochimie moléculaire et en imagerie confocale afin d'étudier le modèle d'expression et la localisation subcellulaire de FXR1P ainsi que son association endogène ou exogène avec la machine de traduction. Ces expériences ont été réalisées dans des neurones en cours de développement. En utilisant une combinaison d'imagerie confocale, d'enregistrements electrophysiologiques de cellule entière et de libération de glutamate à deux photons nous avons pu mesurer l'effet net de l'augmentation des niveaux de FXR1P sur le nombre d'épines, leur morphologie et leur fonction. Enfin, nous avons étudié l'effet de la perte de FXR1P sur le développement des épines et sur la plasticité synaptique des souris adultes. Ceci a été réalisé en utilisant un knockout conditionnel dans une lignée de souris où le gène FXR1P a été éliminé des neurones du cerveau antérieur. De façon intéressante, nous avons trouvé que FXR1P se rassemblait autour de la machine de traduction des cellules dendritiques, mais surtout dans un sous-groupe de grosses épines dendritiques fonctionnellement actives. La délétion génétique de FXR1P a eu pour résultat une diminution de la densité et de la taille des épines dendritiques, ainsi qu'une augmentation de la synthèse de protéines et de la potentialisation à long terme de longue durée (PLT-L). Ensemble, ces

résultats soutiennent l'idée que FXR1P est directement capable de contrôler la traduction locale dans un sous groupe d'ARNm requis dans la régulation du développement et de la gestion des épines dendritiques en restreignant l'amplitude de la PLT-L. Les résultats présentés dans cette thèse contribuent à notre savoir de l'importance que jouent les mécanismes de contrôle de la traduction protéinique dans la plasticité synaptique et la cognition.

DEDICATION

"If we knew what it was we were doing,
it would not be called research."

- Albert Einstein

To my husband Tadeu,
for his support, love and dedication

To my parents Rita and James
and my sister Paula,
for understanding that not even
I knew what it was I was doing.

ACKNOWLEDGMENTS

The years would not have gone by so fast without:

My supervisor, Dr. Keith Murai, who accepted me into his lab under exceptional circumstances five years ago and who has infected me with his unparalleled excitement, passion and dedication to science. He has provided me with the guidance, support and knowledge needed to complete the experiments in this thesis. Most importantly, he always made sure that no experiment was ever out of my reach.

My collaborator and future mentor, Dr. Jean-Claude Béique, for having the courage to accept me into his lab and teach me his trade. Without his help this project would not be complete.

My second collaborator, Dr. David Stellwagen, for allowing me, in the very final stages of this project, to use his equipment and knowledge to complete crucial experiments for this thesis.

My advisory committee, Drs. Wayne Sossin and Anne McKinney, and my mentor, Dr. Kathy Mullen, for keeping me on track and on my toes with their guidance, helpful suggestions and invaluable comments.

My co-authors and students who helped complete experiments that were just out of my reach. A special thanks to Dr. Maria Sanchez-Carbente for performing the fluorescent *in-situ* hybridization experiments, Edith Hanna for helping out with time-consuming sectioning, imaging and image stitching, Ling Tian for her technical support and Erin Nuro for happily taking over my mouse lines and experiments when the time came for me to write up this thesis.

My colleagues and friends, who helped shape the scientist I am today. Thanks for the scientific discussions, the many laughs and especially for helping through the inevitable doldrums of the PhD.

My parents and sister, who took an interest in this project even if it was far-removed from their daily lives and pursuits.

My husband, Tadeu, who waited patiently for seven long years for this day to finally come.

PREFACE

This thesis is manuscript-based in accordance with the guidelines from the Faculty of Graduate Studies and Research of McGill University and includes three original manuscripts, one of which has been published. The contributions of the authors included on these manuscripts are highlighted here.

CONTRIBUTIONS OF AUTHORS

Manuscript #1:

Fragile X Related Protein 1 Clusters with Ribosomes and Messenger RNAs at a Subset of Dendritic Spines in the Mouse Hippocampus. PLoS ONE 2011 6: e26120.

Denise Cook, Maria del Rayo Sanchez-Carbente, Claude Lachance, Danuta Radzioch, Sandra Tremblay, Edouard W. Khandjian, Luc DesGroseillers, Keith K. Murai

The candidate and Keith Murai conceived the project and designed the experiments. The candidate prepared all neuronal cultures, DNA constructs and other materials required for the experiments except for the material specifically mentioned below. The candidate performed experiments in Figures 1, 3-4, 6-8, 10, and S1-6, carried out the confocal microscopy and analyzed the data. Maria Sanchez-Carbente performed the FISH experiments for Figures 5 and 9. Edouard Khandjian and Sandra Tremblay performed the Coomassie staining and western blots for FXR1P (all isoforms), FMRP and L7 in Figure 1A and performed the polyribosome fractionation experiment in Figure 2. Claude Lachance and Danuta Radzioch provided FXR1P and eGFP-FXR1P constructs. Edouard Khandjian provided the FXR1P #ML13 antibody. The candidate prepared the figures and wrote the manuscript with help from Keith Murai. Edouard Khandjian and Luc DesGroseillers provided comments.

Manuscript # 2:

Fragile X Related Protein 1 preferentially clusters at large spines with strong synapses

Denise Cook, Jean-Claude Béique, Keith K. Murai

The candidate, Keith Murai and Jean-Claude Béique conceived the project and designed the experiments. The candidate performed the experiments and analyzed the data. Ling Tian prepared the rat organotypic hippocampal slices and performed the gene-gun transfections for all electrophysiology experiments performed in the lab of Jean-Claude Béique (Figures 3, 6). The candidate prepared the figures and wrote the manuscript with help from Keith Murai. Jean-Claude Béique provided comments.

Manuscript # 3:

Targeted deletion of the FMRP paralog FXR1P alters dendritic spines and enhances late-phase LTP

Denise Cook, David Stellwagen, Keith K. Murai

The candidate and Keith Murai conceived the project and designed the experiments. All mouse husbandry, including breedings, genotyping, perfusions, acute slice preparation and dissections were performed by the candidate. Edith Hanna helped with the cryostat sectioning, staining and imaging presented in Figures 1-3. The candidate performed the DiI experiments and confocal imaging presented in Figure 4. David Stellwagen provided the equipment and technical expertise for the candidate to perform the field recording experiments presented Figures 5-8. All data analysis was performed by the candidate. The candidate prepared the figures and wrote the manuscript with help from Keith Murai. David Stellwagen provided comments.

Overview:

The goal of this thesis was to determine whether the RNA-binding protein FXR1P plays an important role in controlling the local translation of mRNAs involved in synaptic plasticity. The structure of the thesis includes a brief introduction, which outlines the rationale, hypothesis and objectives we set to address this goal. This is followed by a thorough review of the past and current literature on the importance of new protein synthesis and translational control for long-lasting synaptic plasticity and memory creation and storage. Our results are presented in three original manuscripts, followed by a final summary of our major contributions to knowledge and conclusions with future perspectives on our work.

TABLE OF CONTENTS

LIST OF TABLES

Chapter 3

LIST OF FIGURES

Chapter 3

Chapter 3- Supplemental Figures

Chapter 4

Chapter 5

Appendix A

Appendix B

Appendix C

LIST OF ABBREVIATIONS

2P-EPSC	two-photon excitatory postsynaptic current
4E-BP	4E-binding protein
5'TOP	5′ terminal oligopyrimidine tract
AGO	argonaute
AMPA	2-amino-3-(5-methyl-3-oxo-1,2-oxazol-4-yl)propanoic acid
ANOVA	analysis of variance
Arc/Arg3.1	activity-regulated cytoskeleton-associated protein
ATF4	activating transcription factor 4
ATP	adenosine triphosphate
BAPTA	1,2-bis(o-aminophenoxy)ethane-N,N,N',N' tetraacetic acid
BDNF	brain-derived neurotrophic factor
BONCAT	bioorthogonal noncanonical amino acid tagging
BSA	bovine serum albumin
CA	cornu Ammonis
$CaCl_2$	calcium chloride
CaMKII	calcium calmodulin kinase 2
cHET	conditional heterozygote
cKO	conditional knockout
CMV	cytomegalovirus
CPEB	cytoplasmic polyadenylation element binding protein
CREB	cAMP response element-binding
CYFIP1	cytoplasmic FMR1 interacting protein 1
DG	dentate gyrus
DHPG	dihydroxyphenylglycine
DIC	differential interference contrast
DIG	digoxigenin
DiI	1,1' - Dioctadecyl - 3,3,3',3' - tetramethylindocarbocyanine iodide
DMEM	Dulbecco's modified essential medium
DMSO	dimethyl sulfoxide
DNA	deoxyribonucleic acid
ECL	enhanced chemiluminescence
EDTA	ethylenediaminetetraacetic acid
eEF	eukaryotic elongation factor
eIF	eukaryotic initiation factor
E-LTP	early-long-term potentiation
ER	endoplasmic reticulum
ERK	extracellular signal-regulated kinase
fEPSPs	field excitatory postsynaptic potentials
FISH	fluorescence *in situ* hybridization
FKBP12	FK506-binding protein
FMRP	Fragile X mental retardation protein
FXR1P	Fragile X related protein 1
FXR2P	Fragile X related protein 2

FXS	Fragile X Syndrome
GAPDH	glyceraldehyde 3-phosphate dehydrogenase
GCN2	general control nonrepressed 2
GFAP	glial fibrillary acidic protein
GFP	green fluorescent protein
GTP	guanosine triphosphate
HEPES	hydroxyethyl piperazineethanesulfonic acid
HRI	heme-regulated inhibitor kinase
HRP	horse radish peroxidase
ICA	intensity correlation analysis
ICQ	intensity correlation quotient
KCl	potassium chloride
L-LTP	late-long-term potentiation
LTD	long-term depression
LTP	long-term potentiation
MAP	microtubule associated protein
MAPK	mitogen activated protein kinase
MEF2	myocyte enhancer factor-2 (Mef2)
mEGFP	membrane-targeted enhanced green fluorescent protein
MEM	minimum essential media
mEPSC	miniature excitatory postsynaptic currents
Met-tRNA	methionine transfer ribonucleic acid
mGluR	metabotropic glutamate receptor
$MgSO_4$	magnesium sulfate
miRNA	micro-ribonucleic acid
MNI	4-methoxy-7-nitroindolinyl
mTOR	mammalian target of rapamycin
NaCl	sodium chloride
NaH_2PO_4	sodium phosphate dibasic
$NaHCO_3$	sodium bicarbonate
NeuN	neuronal nuclei
NMDA	N-Methyl-D-aspartate
PI3K	phosphoinositide 3-kinase
PAK1	serine/threonine p21-activated kinase 1
PDM	product difference of the mean
PERK	PKR-like ER kinase
PKMζ	protein kinase M zeta
PKR	protein kinase R
PMSF	phenylmethylsulfonyl fluoride
PSD95	postsynaptic density 95
PVDF	polyvinylidene fluoride
PVP	polyvinylpyrrolidone
RFP	red fluorescent protein
RIPA	radioimmunoprecipitation assay
RISC	RNA-induced silencing complex
RNA	ribonucleic acid

RNP	ribonucleoprotein particle
SDS-PAGE	sodium dodecyl sulfate polyacrylamide gel electrophoresis
SSC	saline-sodium citrate
TBS	tris-buffer saline
TEA	triethanolamine
TIA-1	T-cell intracellular antigen-1
TNF-α	tumor necrosis factor-α
TTX	tetrodotoxin
UTR	untranslated region
UV	ultraviolet
WT	wild-type
ZBP1	zipcode binding protein 1

CHAPTER 1: INTRODUCTION

Memories are thought to be stored as long-lasting changes to the size, strength or number of synapses in a neuronal network [1–3]. These changes rely on new protein synthesis which can occur locally from translational machinery found in dendrites and at synapses [4,5]. This local protein synthesis is regulated through a combination of general translational control mechanisms, which act on all mRNAs, and gene-specific mechanisms, which act on subsets of mRNAs. Together, these mechanisms ensure that the correct subsets of proteins are synthesized in response to specific patterns of synaptic activity [6]. Although several studies have shown that knocking-out components of the general translational control pathway alters synaptic plasticity and memory [7–11], more research is needed to elucidate the role of gene-specific mechanisms in these processes.

Gene-specific translational control mechanisms are composed of cis-acting sequences, located in the 3' and 5' untranslated regions of the mRNA, and the RNA-binding proteins which recognize these sequences [12]. In neurons, RNA-binding proteins control the activity-dependent transport, stability and translation of mRNAs, thereby allowing the metabolism of each mRNA to be independently controlled by its own specific complement of RNA-binding proteins [12]. Recent proteomic studies have identified large numbers of neuronal RNA-binding proteins; however, little is known about the function of the majority of these proteins and specifically, which of these proteins interact together to control the local translation of mRNAs required for long-lasting synaptic plasticity and memory storage [13,14].

One of the best characterized neuronal RNA-binding proteins is the Fragile X Mental Retardation Protein (FMRP). This protein is lost or reduced in Fragile X Syndrome, a disorder characterized by intellectual disability and autism [15–18]. Loss of FMRP in mice leads to changes in spine structure, synaptic plasticity

and learning and memory [19]. FMRP is therefore thought to control the translation of a subset of brain mRNAs involved in synaptic plasticity and behaviour [20].

FMRP is part of a family of RNA-binding proteins, the Fragile X Proteins, which also includes Fragile X Related Protein 1 (FXR1P) and Fragile X Related Protein 2 (FXR2P). All three proteins associate with ribosomes in the cytoplasm and dendrites of neurons [21–23]. Interestingly, they can homo and hetero-multimerize both *in vitro* and *in vivo*, suggesting that they share certain mRNA targets [24–27]. Loss of FXR2P also leads to deficits in synaptic plasticity and behaviour [28–31], however, very little is known about the function of FXR1P in the brain. In non-neuronal cells, FXR1P can both repress and enhance mRNA translation, providing evidence that it also functions as a translational regulator [32,33]. Research into whether FXR1P controls local protein synthesis in neurons is needed to help determine whether FXR1P has a similar or distinct role to its paralogs, and whether or not it can compensate for or be used as a drug target for treating memory impairments. **We hypothesized that FXR1P controls the local translation of mRNAs important for spine development, long-lasting synaptic plasticity and long-term memory creation and storage.**

To test this, we used a combination of biochemical, imaging, electrophysiology and behavioural techniques to characterize the expression pattern, gain-of-function and loss-of-function of FXR1P in the hippocampus, a structure important for learning and memory. To verify if FXR1P is expressed at the right time and place to control local protein synthesis in hippocampal neurons, we determined whether FXR1P localizes with ribosomes and mRNAs in dendrites and at spines (**Specific Aim 1 - Chapter 3**). To test if FXR1P is important for spine development and synaptic plasticity, we increased and decreased FXR1P expression and looked for changes in spine density, spine morphology and synaptic function. First, we determined if overexpression of FXR1P led to a change in spine density, structure or function (**Specific Aim 2 - Chapter 4**). Finally, we tested whether conditional loss of FXR1P altered spine development, synaptic function and long-lasting synaptic plasticity (**Specific Aim 3 - Chapter**

5). Our preliminary behavioural results, performed in collaboration with the Neurophenotyping Center at the Douglas Hospital, are suggestive of a role of FXR1P in learning and memory processes and are presented as future perspectives (**Chapter 6**).

The results presented in this thesis demonstrate that FXR1P associates with the translational machinery in dendrites and at a subset of large, mature dendritic spines and is required for proper spine development, long-lasting synaptic plasticity and behaviour. These results implicate FXR1P in the control of local translation of a subset of mRNAs important for synaptic plasticity and behaviour. Further research will be needed to identify and characterize the mRNA targets of FXR1P and to determine how the Fragile X Proteins coordinate their activities to ensure that the correct subsets of mRNAs are translated in response to synaptic activity.

CHAPTER 2: LITERATURE REVIEW

2.1 Memory formation and new protein synthesis

The ability to create, store and retrieve memories allows us to build upon previous knowledge and experiences and make connections between events, thoughts and ideas. It is with no surprise then that researchers have contemplated the neurological basis of memory formation and storage for over a hundred years. It was Santiago Ramón y Cajal who, in 1894, first postulated that memories were stored as a change in the strength of neuronal connections [34]. It took decades and several significant technological advances in the fields of physiology, pharmacology and imaging for researchers to demonstrate that synapses can show long-lasting changes in their strength and size [35]. To this day this form of synaptic plasticity remains the most likely explanation for how the brain stores long-term information.

How do neurons establish and maintain these long-lasting changes to their synapses, thereby allowing the brain to encode and store memories for long periods of time? Early evidence for the biochemical basis of long-term memory came from studies looking at the effects of protein synthesis inhibitors on the different stages of memory formation [36]. Memory can be divided into several stages: 1) acquisition 2) storage and consolidation 3) retrieval and 4) long-term maintenance. Flexner et al.[37] were the first to show that protein synthesis inhibitors could prevent the storage of long-term memories if injected into the cortices of mice shortly after training on a memory task. Studies over the next twenty years further clarified the role of *de novo* brain protein synthesis in memory [36]. Specifically, animals treated with protein synthesis inhibitors just before, during or shortly after training on a memory task were able to learn the task normally, however, were unable to remember the task when tested several hours or days later. If inhibitors were applied several hours after the training period, animals were able to remember the task. These results led to the following predictions about the biochemical basis of memory: 1) short-term memory formation is independent of new protein synthesis, 2) long-term memory

formation requires new protein synthesis during or shortly after training, 3) memory retrieval is not affected by protein synthesis inhibitors [36]. However, a brief increase in new protein synthesis at the time of training cannot by itself explain how some memories persist for months, years or even lifetimes despite regular protein turn-over. The biochemical mechanism for this long-term memory maintenance is still under intense investigation.

2.2 Cellular and molecular correlates of long-lasting memory in the hippocampus

Pioneering studies in the 1950s by Drs. Wilder Penfield, William Scoville and Brenda Milner on patients with bilateral damage to their hippocampi and surrounding structures in the medial temporal lobes, established the importance of these brain structures in forming and storing new episodic memories [38]. Subsequent studies from human patients and animal models confirmed the role of the hippocampal formation in long-term episodic memory formation [39]. The hippocampus, although only one of multiple memory systems in the brain, has continued to serve as the model system of choice to study the cellular and molecular correlates of long-lasting memories. This is mainly due to its simple neuronal circuit and planar structure which has facilitated electrophysiological research on the fundamental mechanisms of synaptic transmission and synaptic plasticity.

Indeed, it was the hippocampus that was first used to demonstrate the existence of synaptic plasticity. In 1973 Bliss and Lomo stimulated the perforant path of an anesthetized rabbit and demonstrated a long-lasting increase in excitatory synaptic strength in the dentate gyrus, a phenomenon referred to as long-term potentiation (LTP) [40]. This has since been repeated *in vivo* in many different animal models and *ex vivo* at different synapses in the hippocampus, most notably the CA3 Schaffer collateral-CA1 synaptic connection. Although the molecular mechanisms of LTP induction, expression and maintenance at different synapses are still hotly debated, at the CA3-CA1 synapse LTP is induced through a coincident depolarization of the postsynaptic cell (CA1) and glutamate release

from the presynaptic cell (CA3). These conditions have been achieved using many different experimental procedures, including high frequency tetanic stimulation, and serve to relieve the voltage-dependent magnesium block on the NMDA receptor, allowing calcium entry into the synapse and the activation of several signaling pathways leading to the expression of LTP. The need for coincident presynaptic glutamate release and postsynaptic depolarization to open NMDA receptors results in several interesting properties that make LTP an ideal cellular correlate for memory storage. First, LTP is only induced when the postsynaptic cell is depolarized above a certain threshold, a threshold that can be reached with strong tetanic stimulation of a single pathway, with weak stimulation of many pathways (cooperativity) or with a combination of strong tetanic stimulation and weak stimulation at two separate pathways (associativity) [41]. Second, LTP is induced at all active synapses, but not at adjacent inactive synapses, a property called input-specificity [41]. These properties could allow weaker memories to be strengthened and remembered alongside strong memories.

After induction, LTP is expressed and maintained through an increase in the number and conductance of AMPA receptors at the postsynaptic density (a measure of synaptic strength), an increase in the size or number of dendritic spines (small protrusions from the dendrite where excitatory synapses are formed) and in certain cases, a concomitant increase in the probability of release of neurotransmitter at the presynaptic terminal [42–44]. The increase in the size or number of dendritic spines is achieved through a combination of actin remodeling, addition of lipid membrane components and addition of new proteins [45–48]. Importantly, the size of the dendritic spine or postsynaptic density is correlated with the number of AMPA receptors in the postsynaptic density and therefore can be used as a read-out of synaptic strength [49,50]. LTP is therefore primarily thought to be expressed and maintained through an increase in the size and strength of dendritic spines.

Like memory, LTP can be divided into two phases. A short-lasting phase (1-3 hours) that depends on modifications to pre-existing proteins, referred to as early-LTP (E-LTP) and a long-lasting phase that depends on new protein

synthesis and new gene expression occurring at the time of induction, referred to as late-LTP (L-LTP) [51]. These two phases are thought to be the cellular equivalents of short-term memory and long-term memory, respectively. E-LTP is normally induced using a weak stimulus, for instance 1-2 trains of high-frequency tetanic stimulation, and L-LTP with a very strong stimulus, for instance 3-4 trains of high-frequency tetanic stimulation [7]. Interestingly, a weak E-LTP stimulus at one set of synapses can be converted into L-LTP if preceded or followed by (within 1-2 hours) a strong L-LTP stimulus at another set of synapses, a process also referred to as associativity [52]. Long-term memory and L-LTP are therefore linked by their dependence on new protein synthesis. Although a definite causal link between LTP and memory, or dendritic spines and memory has yet to be demonstrated, several correlational studies point to an important link between these synaptic properties and memory processes [35]. A striking link is the finding that dendritic spines are lost or abnormal-looking in several human diseases associated with intellectual disability or memory loss, including Alzheimer's [53], mental retardation and Fragile X Syndrome [54] and Down Syndrome [55]. More recently, researchers have found that learning induces several defining features of LTP in the rat hippocampus [56]. Learning has also been associated with long-lasting increases in the number of dendritic spines in the sensory and motor cortices [1,3]. These studies support the importance of studying the biochemical and molecular mechanisms underlying long-lasting LTP and structural spine plasticity, as potential underlying mechanisms of long-lasting memory storage.

2.3 Location of new protein synthesis in LTP: cell body, dendrite or synapse?

The demonstration that L-LTP is both input-specific and associative has helped shape theories on the cellular location of the new protein synthesis that is required for both long-lasting synaptic plasticity and memory formation. Since L-LTP is input-specific, occurring only at activated synapses, a cellular mechanism must exist to ensure that the newly synthesized mRNAs and proteins are inserted into the correct synapses. Since in the original descriptions of L-LTP nuclear transcription appeared to play a fundamental and regulatory role in the

maintenance of L-LTP, original hypotheses centered on the idea that new mRNAs were synthesized in the nucleus and translated in the cell body. The newly made proteins were then non-specifically shipped out into dendrites and captured by active synapses [57]. In this hypothesis, mRNA translation was thought to play only a permissive role.

However, this hypothesis was challenged by results that made it clear that L-LTP could be separated into two discrete phases: a translation-dependent, transcription-independent phase followed by a translation and transcription-dependent phase. The application of anisomycin, a protein synthesis inhibitor, before and during the induction of L-LTP led to a rapid decline in L-LTP, whereas application of actinomycin, a transcription inhibitor, over the same time-frame resulted in a decline only 60-90 minutes later [7]. In addition, metabotropic glutamate receptor-dependent long-term depression (mGluR-LTD) was also shown to require rapid new protein synthesis at the time of induction [58]. These results suggest that to maintain long-lasting forms of synaptic plasticity, new proteins must be synthesized and added rapidly to active synapses. The requirement for rapid new protein synthesis suggests that protein synthesis occurs through translation of pre-existing mRNAs.

Despite biochemical evidence for the existence of ribosomes in dendrites and incorporation of radioactive amino acids by synaptic fractions since the 1960s [59–61], researchers favored the hypothesis that new protein synthesis occurred on pre-existing mRNAs located in the cell body [57]. Again, this theory necessitated a way to tag the active synapses in order for them to capture the new proteins that were shipped non-specifically into dendrites. Although most housekeeping and synaptic proteins are probably constitutively produced from mRNAs in the cell body [62], the finding that new proteins are required within the first few minutes of induction of L-LTP make this an unlikely mechanism for activity-dependent protein synthesis, especially when synapses along the distal arbor of dendrites need to be potentiated [57].

Studies from Steward et al.[63–67] in the 1980s reinvigorated the lost idea that new protein synthesis could be occurring locally in dendrites and perhaps even at

the single-synapse level. They found that polysomes, the major workhorses of the translation machinery, are distributed throughout the dendrite and at the base, neck and head of a subset of dendritic spines in the developing and adult hippocampus. Subsequent papers from his laboratory used radioactive labeling in dissociated neuron cultures to demonstrate that newly synthesized RNAs are transported into dendrites [68], that new proteins are made in dendrites severed from the cell body [69] and that severed dendrites contain the machinery required to glycosylate newly synthesized proteins [70]. Studies since then have begun to dissect out the subset of mRNAs found in dendrites. Recent microarray studies have shown that approximately 400 distinct mRNAs are constitutively, although not exclusively, localized to dendrites [71–73]. This number is likely to be much higher due to the inability of these methods to detect mRNAs with low abundance in dendrites. Messenger RNAs with high abundance in dendrites include CaMKIIα, PKMζ, MAP2, GluA1/2, NR1 and β-actin [12,74]. In addition, certain mRNAs, such as the immediate-early gene Arc, are not constitutively localized to dendrites, but instead are transported to dendrites and synapses in an activity-dependent manner [75], demonstrating that neurons can use both localized translation and selective mRNA transport to ensure that the correct proteins are made at the appropriate time and place.

How "local" is this protein synthesis at synapses? Research has shown that synaptoneurosomes, biochemical entities containing both the pre- and postsynaptic compartments, are capable of synthesizing new proteins when depolarized [76], demonstrating that synapses can produce new proteins. In addition, researchers have noted increased translation of a fluorescent reporter in discrete locations along the dendrite, called "translational hotspots", in severed dendrites exposed to either BDNF or DHPG [77,78]. These hotspots colocalize with ribosomes and are partially colocalized with PSD95, a marker of excitatory synapses. These results argue for discrete zones of new protein synthesis in the dendrite and synapses, suggesting that new proteins could be made directly at active synapses.

However, Frey and Morris demonstrated that if a strong L-LTP stimulus was given to one set of synapses in the presence of anisomycin (which normally

would not induce L-LTP) one hour after L-LTP induction at an independent set of synapses, L-LTP was nevertheless induced at the second set of synapses [52]. This meant that somehow the new proteins induced by the first L-LTP induction were being shared with the second set of synapses, arguing that new protein synthesis is not confined to the activated synapses but instead may occur more generally across a dendritic segment. This is supported by the finding that a weak E-LTP inducing stimulus at one set of synapses is converted into L-LTP if an L-LTP stimulus is given at another set of synapses within 1-2 hours of the E-LTP stimulus. In order for this to occur, there must be sharing of L-LTP proteins across synapses [52]. Perhaps more intriguing is that finding that E-LTP at one set of synapses can be converted to L-LTP if preceded or followed by an L-LTD inducing stimulus at another set of synapses [79]. This suggests that stimuli inducing either L-LTP or L-LTD must lead to the synthesis of a set of proteins sufficient to express and maintain the structural and physiological changes characteristic of both L-LTP and L-LTD. These proteins, the identities of which are mostly unknown, are referred to as "plasticity-related proteins" and may include αCaMKII, PKMζ, Arc/Arg3.1 and MAP1B [6]. Strikingly, PKMζ is the only protein identified so far whose continued activity is both necessary and sufficient for L-LTP maintenance and memory storage [80,81]. The ability of synapses to share these plasticity-related proteins has lead to the synaptic tagging and capture model for L-LTP/L-LTD expression and maintenance. This model predicts that an E-LTP/E-LTD or L-LTP/L-LTD stimulus creates a short-lived (1-2 hours), synapse-specific and relatively immobile synaptic tag that does not require new protein translation and is unique for LTP versus LTD [57]. Although the identity of this tag is unknown and may involve multiple synaptic changes, it has been postulated to involve a phosphorylation change to a pre-existing protein, a cytoskeletal change or conversion of an RNA-binding protein into a persistent prion-like conformation [57,82]. The creation of this tag would then allow for the selective capture of dendritically synthesized proteins involved in LTP or LTD ("LTP proteins", "LTD proteins"). More recently, Govindarajan et al.[47] were able to tackle outstanding questions about the spatial and temporal limits of the synaptic tagging

and capture process. Using sophisticated two-photon glutamate uncaging and electrophysiology techniques, they were able to show that plasticity-related proteins could be shared between two synapses on the same dendritic branch up to a distance of 70 μm, and between two synapses on sister branches up to a distance of 50 μm. They also demonstrated that under their conditions the synaptic tag had a lifetime of two hours and the rate-limiting plasticity-related proteins had lifetimes up to ninety minutes. It was also shown that synapses stimulated close together in space and time competed for these limiting plasticity-related proteins [47]. Altogether, these results provide convincing evidence that high levels of synaptic activity cause new protein synthesis in the dendrite. This creates a pool of plasticity-related proteins with short lifetimes that have the ability to diffuse across the dendritic branch and be shared with other weakly stimulated synapses, potentially leading to long-lasting synaptic strengthening of spines in a clustered fashion along a dendritic branch [2].

These results demonstrate that dendrites have the capacity to synthesize new proteins. However, an important issue is whether dendritic protein synthesis is necessary and sufficient for synaptic plasticity and memory formation. The ability of dendritic protein synthesis to support synaptic plasticity in the absence of synthesis from the cell body was accomplished by severing CA1 dendrites and demonstrating that L-LTP and mGluR-LTD could still be induced [58,83]. Frey et al.[84] also demonstrated that severed CA1 dendrites could support tetanus-induced L-LTP, although L-LTP could not be maintained beyond three hours, suggesting that nuclear transcription is required to replenish the stores of dendritic mRNAs and maintain L-LTP over longer periods of time. The best evidence for the necessity of dendritic protein synthesis in synaptic plasticity and learning and memory comes from a mouse model in which *αCaMKII* mRNA is no longer targeted to dendrites. This mouse has a deficit in L-LTP and an inability to store long-lasting memories [85]. Whether dendritic translation of other plasticity-related mRNAs is also required is currently unknown. Together, these results demonstrate that dendritic protein synthesis is sufficient to support the initial

phase of long-lasting synaptic plasticity, and dendritic targeting of at least one plasticity-related mRNA is required for synaptic plasticity and memory storage.

2.4 General translational control mechanisms in long-lasting synaptic plasticity

If new protein synthesis occurs at the level of the dendritic branch, an important question that emerges is what molecular mechanisms exist in the dendrite to control the burst of new protein synthesis during the induction phase of L-LTP and L-LTD? New protein synthesis from an mRNA begins with the binding of the initiation factor eIF2 to GTP and Met-$tRNA_i^{Met}$ to form a ternary complex which then associates with the small 40S ribosomal subunit to form the 43S pre-initiation complex. The 43S complex is then guided to 5' capped mRNAs, which make up the majority of nuclear-transcribed mRNAs, by interaction with the cap-binding complex eIF4F (made up of the cap-binding protein eIF4E, the RNA helicase eIF4A and eIF4G) [6]. The complex then scans the mRNA until it reaches the initiation codon, at which point it is joined by the 60S complex, a complex composed of the large ribosomal subunit and its associated translation factors. Translation elongation proceeds with the help of elongation factors, such as eEF2. Translation termination occurs when the ribosome reaches the stop codon and is released from the mRNA with the help of termination factors [6].

The rate-limiting and major regulatory step in mRNA translation is at the point of initiation. This step is regulated by 4E-BPs which bind to eIF4E and prevent joining of eIF4G and the small ribosome to the mRNA, thereby blocking initiation. Hyperphosphorylation of the 4E-BPs causes them to dissociate from eIF4E, allowing initiation from capped mRNAs to occur. Other points of regulation which are less well understood include phosphorylation of eIF4E and the small ribosomal subunit S6. Phosphorylation of S6 increases the translation of mRNAs containing highly structured repressor sequences known as 5' oligopyrimidine tracts (5'TOP) which are found on the mRNAs of ribosomal proteins and translation factors, thereby increasing the availability of the

translation machinery [57]. Another key point of control is the phosphorylation status of eIF2α. Phosphorylation of eIF2α prevents the ternary complex from forming and therefore halts translation initiation. Since translation of the majority of capped mRNAs is thought to be influenced by phosphorylation of eIF4E, 4E-BPs, S6 and eIF2α, any signaling pathways acting on these molecules are considered part of the general translational control machinery and may be involved in regulating activity-dependent new protein synthesis.

The importance of the ERK-MAPK and PI3K-mTOR pathways in general translational control has been thoroughly investigated in non-neuronal cells. However, it was not until recently that these pathways have been looked at in the context of synaptic plasticity. In 2004, Kelleher et al.[7] first demonstrated that the ERK-MAPK pathway plays a key regulatory role in activity-dependent new protein synthesis. They demonstrated that L-LTP induction leads to the ERK-dependent phosphorylation of 4E-BPs, eIF4E and S6. In addition they found that expression of a dominant-negative form of ERK kinase impaired L-LTP, but not E-LTP, and caused mice to exhibit deficits in forming and storing long-lasting spatial memories [7]. To further delineate the signaling pathways involved, they added rapamycin, a drug which inhibits mTOR, to cultured hippocampal neurons and found that it also inhibited the activity-dependent phosphorylation of 4E-BPs, eIF4E and S6 [7]. Rapamycin had also been shown previously to inhibit tetanus and BDNF-induced L-LTP [86]. The mTOR and ERK pathways are also required for mGluR-dependent LTD [87,88]. Importantly, several components of the ERK-MAPK and mTOR signaling pathways, as well as several initiation and elongation factors, have been localized to dendrites and synapses [86]. Together, these results demonstrate that dendritic protein synthesis is stimulated by the synergistic action of the mTOR and ERK-MAPK signaling pathways acting to activate translation initiation.

Further support for the importance of general translational control mechanisms in long-lasting synaptic plasticity has come from the creation of mouse models where activity-dependent general translation initiation has been enhanced through the deletion of a translational repressor. Hoeffer et al.[8] created a

forebrain-specific conditional knockout of FKBP12, an endogenous inhibitor of the mTOR pathway, and found that although E-LTP was unchanged, protein-synthesis dependent L-LTP was significantly enhanced. Additionally, they found that the FKBP12 conditional knockout (cKO) mice displayed enhanced contextual fear memory and perseveration for previous escape locations in the Y-Maze test, although performance on the Morris Water Maze was similar to wild-type mice [8]. This suggests that by removing a repressor of the mTOR pathway, more plasticity-related proteins are synthesized in response to high levels of synaptic activity, leading to increased levels of L-LTP and memory storage. As mentioned in the previous section, the phosphorylation status of eIF2α also controls general translation initiation. Increased eIF2α phosphorylation inhibits general translation but paradoxically increases the translation of ATF4, an inhibitor of CREB, a transcription factor which increases the transcription of genes required for long-lasting synaptic plasticity [89–91]. Importantly, induction of L-LTP in the hippocampus leads to dephosphorylation of eIF2α [10]. The phosphorylation status of eIF2α is controlled by four kinases, GCN2, PERK, PKR and HRI, with each kinase activated in response to different types of cellular stresses [92]. GCN2, which is activated by amino acid deprivation, is the main eIF2α kinase in the brain and was therefore the first kinase to be studied with respect to synaptic plasticity and memory [10]. Intriguingly, they found that GCN2 knockout mice were able to convert weak memories into long-lasting ones and E-LTP into protein-synthesis dependent L-LTP, arguing for a decrease in the threshold for induction of L-LTP. This finding has been recapitulated, with some minor differences, in the knockout mouse of PKR and a knock-in mouse with reduced eIF2α phosphorylation [11,93]. Although these phenotypes could be due to a direct influence of eIF2α dephosphorylation on enhanced activity-dependent new protein synthesis, the authors' results instead support a view whereby decreased ATF levels lead to constitutive transcription of CREB-dependent plasticity-related mRNAs, even in the absence of synaptic activity [10,11]. This may mean that the levels of plasticity-related mRNAs in dendrites are increased, thereby making it quicker and easier to induce long-lasting synaptic plasticity even with a weak stimulus. Altogether,

these studies demonstrate that several signaling pathways acting at the initiation step of mRNA translation play important roles in the creation of long-lasting synaptic plasticity and memories.

Another level of general translational control occurs at the elongation step. Although not generally considered a rate-limiting and major point of control, there are nevertheless specific examples in the literature where translation is regulated at elongation [94–96]. Several studies have found that synaptic activity changes the phosphorylation state of eEF2, an elongation factor that, when not phosphorylated, promotes movement of the ribosome along the mRNA after peptide-bond formation [6]. In one study, NMDA-induced phosphorylation of eEF2 decreased global translational rates, but at the same time increased the translation of αCaMKII [97]. Another study demonstrated a strikingly similar result where induction of mGluR-LTD led to eEF2 phosphorylation, decreased general protein synthesis but a rapid increase in Arc/Arg3.1 synthesis [98]. This paradox, similar to the situation that occurs with the phosphorylation of eIF2α, is thought to occur when partial inhibition of elongation frees up translation factors for a small subset of mRNAs with low basal translational efficiency [99]. The role of eEF2 phosphorylation as a bidirectional control of local dendritic protein synthesis has recently been studied by Sutton et al.[100]. Using cultured hippocampal neurons they showed that eEF2 is kept in a dephosphorylated state under normal action-potential dependent network activity. However, high levels of excitatory miniature neurotransmission, the spontaneous release of neurotransmitter at excitatory synapses in the absence of action potentials, increased eEF2 phosphorylation and decreased dendritic protein synthesis [100]. Blocking excitatory miniature neurotransmission, even locally on a dendritic branch, decreased eEF2 phosphorylation and increased local dendritic protein synthesis. These results suggest that miniature neurotransmission could control local dendritic protein synthesis via eEF2 phosphorylation. Whether specific subsets of mRNAs are regulated in the opposite direction to the general changes in dendritic protein synthesis seen here was not investigated. These results demonstrate that synaptic activity can regulate translation at the elongation step, which, while globally

affecting rates of translation, offers an opportunity to regulate the translation of a small subset of special mRNAs in the opposite direction. Whether this is a more general mechanism used by neurons to focus their efforts on the rapid synthesis of plasticity-related proteins during induction of long-lasting synaptic plasticity is an important outstanding question.

2.5 Gene-specific translational control mechanisms in long-lasting synaptic plasticity

In addition to being under general translational control, each mRNA is bound by its own unique set of RNA-binding proteins. *Cis*-acting sequences, usually in the 3' and 5' untranslated regions (UTRs), serve as zipcodes or localization elements to attract trans-acting RNA-binding proteins which guide the localization of mRNAs within the cell [12]. Due to the complicated sequence-dependent and/or secondary-structure dependent way in which RNA-binding proteins recognize mRNAs, it has been impossible so far to develop algorithms to predict which mRNAs are bound by which RNA-binding proteins. Regardless, each pre-mRNA is bound by a specific complement of RNA-binding proteins as it is processed in the nucleus, creating a ribonucleoprotein particle (RNP). This RNP then exits the nucleus and is remodeled in the cytoplasm by the joining of more specific RNA-binding proteins. This RNP therefore contains the complete set of gene-specific translational control mechanisms for that mRNA. The translation of each mRNA is therefore controlled through the interplay of both general and gene-specific translational control mechanisms [57].

In neurons, these RNA-binding proteins help stabilize and transport mRNAs in a translationally repressed state. This control allows mRNAs to be translated only when and where they are needed. RNA-binding proteins will then store and anchor mRNAs at their final destinations, and will help with their activity-dependent translational derepression/activation [12]. It is becoming increasingly clear that RNA-binding proteins exist with their cognate mRNAs in a variety of different RNPs. Researchers have found that RNPs are actually a heterogeneous population with different compositions and functions. Broadly

speaking, RNPs can be categorized into RNA transport particles, stress granules, P-bodies and RNA granules [101]. RNA transport particles are small particles containing mRNAs and RNA-binding proteins, but not ribosomal subunits, which travel along microtubules from the nucleus out into the dendrites. Since they do not contain ribosomes, transport particles likely contain RNA-binding proteins capable of repressing translation at the initiation stage. Stress granules form when cells are exposed to an environmental stress, such as UV irradiation, heat shock or oxidative stress. This activates kinases which phosphorylate eIF2α, leading to global translational arrest and the formation of particles containing mRNAs, RNA-binding proteins and small ribosomal subunits arrested on the mRNAs. These particles store and protect the majority of mRNAs—possibly allowing for the translational upregulation of a subset of mRNAs for proteins involved in counteracting the stress—and disappear when the threat is eliminated. P-bodies contain mRNAs, RNA-binding proteins, micro-RNAs (miRNAs) and proteins found in the RNA-induced silencing complex (RISC) as well as decapping and deadenylation enzymes involved in RNA silencing and degradation [101,102]. These three categories of RNPs have been identified in neuronal dendrites [103–105]. RNA granules, thought to be specific to neurons, contain all the components necessary to translate mRNAs, including mRNAs, RNA-binding proteins, small and large ribosomal subunits, initiating and elongation factors [101,106]. Ribosomes in RNA granules are thought to be arranged in a disorganized fashion or stalled along the mRNA, precluding translation elongation. However, synaptic activity partially dissolves the RNA granule, potentially leading to the release of mRNAs and ribosomes for translational activation [106,107]. These granules may serve to transport and store fully functional translational units which rapidly release and translate mRNAs required for long-lasting synaptic plasticity.

Paradoxically, when looking at the movement of fluorescently-tagged RNA-binding proteins or mRNAs in cultured neurons, the majority of the RNPs, usually of unknown composition, are immobile [13,103,108–112]. However, fluorescent recovery after photobleaching experiments have demonstrated that there is rapid exchange between the cytoplasm and these particles, suggesting that the transport

particles which replenish these more stable stores of RNPs may fall below the level of detection of the method [103,108]. However, a small fraction (5-10%) of RNPs does display bidirectional movements. This fraction can be increased by enhancing network activity using either KCl depolarization or BDNF treatment [13,108]. However, since all of the studies performed so far used bath application of these agents, it is impossible to tell whether RNPs display directed movements towards activated synapses.

Using proteomic analysis, researchers have recently begun to dissect out the complement of RNA-binding proteins found in the biochemically-isolated neuronal RNA granule [13,14]. These studies, performed at two different developmental time-points, have identified a large number of known and unknown components of the RNA granule. Although these RNA granules had many RNA-binding proteins in common, there were some notable differences. This heterogeneity in protein composition between the two granules perhaps reflects methodological differences or developmental changes in the composition of RNA granules. This complexity in RNA granule composition emphasizes the need for continued research into the function of each of these RNA-binding proteins and how they interact with each other to influence the transport, stability and translational control of their target mRNAs.

The best characterized neuronal RNA-binding proteins are zipcode-binding protein 1 (ZBP1), Staufen, cytoplasmic polyadenylation element binding protein (CPEB) and Fragile X Mental Retardation Protein (FMRP). ZBP1 is best known for its role in transporting β-actin mRNA to neuronal growth cones and controlling its translation [113]. BDNF application to growth cones increases the phosphorylation of ZBP1 by Src kinase causing its dissociation from β-actin mRNA, translational derepression and growth cone turning [114,115]. In dendrites, ZBP1 is present in granules at the base of dendritic spines, traffics into spines in response to activity and is required for β-actin mRNA localization and proper spine growth [116,117].

Staufen is best characterized for its role in controlling the transport, localization and translational control of *bicoid* and *oskar* mRNAs, two mRNAs

critical for anterior-posterior patterning of the Drosophila oocyte [118]. The two neuronal Staufen family members, Stau1 and Stau2, form distinct RNPs and associate with two different but overlapping subsets of mRNAs [119–121]. Knockdown of both Stau1 and Stau2 causes alterations in spine morphology and synaptic function [122–124]. Interestingly, Stau1 and Stau2 appear to participate in distinct forms of protein-synthesis dependent synaptic plasticity, with knockdown of Stau1 causing a selective deficit in L-LTP whereas knock-down of Stau2 causes a selective deficit in mGluR-LTD [122,123]. These results suggest that Stau1 and Stau2 could be controlling two distinct populations of mRNAs involved in L-LTP and mGluR-LTD, respectively.

CPEB is another important neuronal RNA-binding protein first characterized in a non-neuronal cell, the Xenopus oocyte. In Xenopus oocytes, CPEB functions as a translational switch, controlling both translational repression and activation. It functions as a repressor in two ways: 1) by keeping the poly (A) tail short, preventing circularization of the mRNA and 2) by recruiting Maskin, a protein that displaces eIF4G from eIF4E, which blocks binding of the 43S complex to the mRNA [125]. Phosphorylation by Aurora A kinase in response to external signals converts CPEB from a repressor into an activator. Phosphorylated CPEB displaces Maskin and leads to the lengthening of the poly(A) tail, allowing for translation initiation and circularization of the mRNA [125]. In neurons, CPEB binds to the 3'UTR of αCaMKII and controls its activity-dependent polyadenylation and translational activation [126,127]. Curiously, CPEB knock-out mice display deficits in E-LTP and E-LTD, but not L-LTP nor L-LTD [128] and display normal learning, but an impaired ability to extinguish memories [129], which suggests that loss of CPEB-mediated translational control has complex effects on synaptic plasticity and memory formation.

It is becoming increasingly evident that miRNAs, small non-coding RNAs which bind to mRNAs in a sequence-dependent manner, also play an important role in controlling the translation of specific subsets of mRNAs important for synaptic plasticity. The RISC complex, which includes miRNAs bound by Dicer and argonaute proteins, normally functions to repress or degrade its target

mRNAs [32,130,131]. All components of the RISC, including Dicer, argonaute 2 (AGO2), pre-miRNAs and miRNAs, are found in dendrites and at synapses [132]. In addition, the brain-specific miR-134 and miR-138 regulate the size and morphology of dendritic spines through translational regulation of their target mRNAs [133,134]. More recently, Edbauer et al.[135] demonstrated that miR-125b and miR-132 regulate synaptic function and dendritic spine morphology and that this effect requires the RNA-binding protein FMRP, lending support to the idea that Fragile X proteins may function through the miRNA pathway. Together, these results have begun to elucidate the important role of the miRNA-RISC complex in local gene-specific translational control.

2.6 Importance of Fragile X Proteins in translational control and synaptic plasticity

Despite all of the research presented above, very little is known about the RNA-binding proteins involved in local translational control during long-lasting synaptic plasticity. The best characterized example to-date is the involvement of FMRP in metabotropic glutamate receptor dependent LTD (mGluR-LTD). FMRP is lost in Fragile X Syndrome, a disorder characterized by intellectual disability and an overabundance of abnormally long, thin spines [18,54]. Huber et al.[136] provided the first evidence of the link between FMRP and mGluR-LTD when they demonstrated that this form of plasticity was actually enhanced in the knockout mouse of *Fmr1*. Later, Nosreyva et al.[58,137] showed that this enhanced mGluR-LTD persisted in the presence of protein synthesis inhibitors. These results, in addition to results showing that FMRP repressed translation of specific mRNAs *in vitro* and at synapses [138–140], has led to the hypothesis that FMRP represses translation of mRNAs important for mGluR-LTD [141]. Several recent papers have shed light on the potential mechanisms through which FMRP represses its target mRNAs. Napoli et al.[142] provided evidence that FMRP blocks translation initiation by binding to the novel 4E-BP, CYFIP1. Synaptic activity caused the dissociation of CYFIP1 from the complex, allowing for ribosome recruitment and translation initiation [142]. Darnell et al provided evidence for a different mechanism, when they found, using high-throughput sequencing of

RNAs isolated by crosslinking immunoprecipitation (HITS-CLIP), that FMRP bound to the 3'UTR, 5'UTR and all along the open reading frames of approximately 800 brain mRNAs [20]. Using polyribosome profile analyses, they argue that FMRP represses translation by stalling ribosomes along the mRNA, a mechanism which supports results from previous publications [20,143,144]. This translational repression may be alleviated by activity-dependent dephosphorylation of FMRP, which is thought to convert FMRP-bound stalled ribosomes into actively translating polyribosomes [144]. Therefore, FMRP, like CPEB, may function as a translational switch converting from a repressor to an activator of mRNA translation in response to synaptic activity [145]. In support of this view, studies have shown that FMRP can enhance translation of certain mRNA targets [146–149]. In addition to, or in combination with, the mechanisms described above, FMRP may also function with the miRNA-RISC pathway. Several studies have demonstrated that FMRP interacts with Dicer, argonaute 1 (AGO1) or AGO2, pre-miRNAs and miRNAs [150]. Researchers have also demonstrated that FMRP functions with miRNAs and AGO2 to control the translation of certain target mRNAs [135,145]. FMRP is therefore a prime candidate to be involved in the local translational control of the subset of mRNAs involved in mGluR-LTD, so called "LTD proteins". The identity of the RNA-binding proteins that may be more selectively involved in the local translational control of "LTP proteins" is currently unknown.

FMRP is one of a triad of RNA-binding proteins, which also includes Fragile X Related Protein 1 (FXR1P) and Fragile X Related Protein 2 (FXR2P). These proteins are highly conserved in vertebrates and contain three functional RNA binding domains, a nuclear localization signal (NLS) and a nuclear export signal (NES) [27,151]. Reports suggest that there could be up to twenty FMRP isoforms, seven FXR1P isoforms (a-g) and two FXR2P isoforms, which further increases the complexity of their potential functions and mRNA targets [152,153]. All three proteins are highly expressed in the cytoplasm and dendrites of many types of neurons [21,22]. They have been found to fractionate with polyribosomes and coimmunoprecipitate with the large ribosomal subunit [24,154]. Researchers have

shown that FMRP, FXR1P and FXR2P bind to themselves and to each other in overexpression studies [25]. However, later experiments in cell culture concluded that the proteins formed homomers and not heteromers *in vivo* [27]. This suggests that the Fragile X Proteins function independently in separate mRNA containing particles.

In support of this view, results from *Fxr2* knockout mice suggest that FMRP and FXR2P may share similar functions, but work in two different pathways. In contrast to the enhanced mGluR-LTD seen in *Fmr1* knockout mice, *Fxr2* knockout mice display reduced protein-synthesis dependent mGluR-LTD [28]. L-LTP is unaltered in both *Fmr1* and *Fxr2p* knockout mice [28]. A more complicated phenotype arises in the *Fmr1*/*Fxr2p* double knockout where mGluR-LTD is enhanced beyond what is seen in the *Fmr1* knockout alone, but is still partially dependent on new protein synthesis, and L-LTP remains unaltered [28]. Therefore, FMRP and FXR2P both function in mGluR-LTD, but neither seems to play an important role in L-LTP.

Despite its high expression in neurons, most of the functional studies on FXR1P have focused on non-neuronal cells. A knockout mouse of the *Fxr1* gene dies at birth because of severe defects in the development of heart and skeletal muscle [155]. More recently, FXR1P has been shown to directly repress the translation of *talin2*, *desmoplakin* and its own mRNA in heart muscle, potentially contributing to the lethality [156]. Garnon et al.[32] and Vasudevan et al.[33] independently demonstrated that, in macrophages and monocytes, FXR1P binds to the AU-rich element of the mRNA for tumor necrosis factor alpha (TNF-α). Garnon et al.[33] and Lachance et al.[157] found that macrophages lacking FXR1P secreted higher levels of TNF-α in response to lipopolysaccharide and Toll receptor activation. This was due to an increase in translation and stability of the TNF-α mRNA in the absence of FXR1P. These results suggest that FXR1P directly or indirectly represses the translation and increases the degradation of TNF-α mRNA. In contrast, Vasudevan et al.[32] concluded that FXR1P, in combination with a miRNA-AGO2 complex, actually enhances the translation of TNF-α mRNA. They demonstrated that serum-starved monocytes and human

embryonic kidney cells increased their translation of a TNF-α reporter mRNA. This increase was dependent on the presence of FXR1P and suggests that FXR1P responds to serum starvation by binding to the miRNA-AGO2 complex and converting it from a repressor to an activator of TNF-α mRNA translation [32]. Furthermore, direct tethering of overexpressed FXR1P to a reporter mRNA resulted in an increase in the translation of the reporter, even in the absence of serum starvation [32]. This suggests that overexpressed FXR1P does not require an external signal to enhance protein synthesis and that FXR1P can directly promote mRNA translation. Overall, these results in non-neuronal cells suggest that FXR1P, like FMRP, can act as both a repressor and an enhancer of mRNA translation depending on the external signal.

Despite an abundance of studies on FMRP function in the brain, relatively little is known about the neuronal function of its paralog FXR1P. Although no neurological disorders have been associated with loss of FXR1P thus far, probably due to its crucial role in muscle development, studies have shown an association between polymorphisms in the *Fxr1* gene and cases of autism spectrum disorders and schizophrenia [158,159]. This elevates the need to study the function of this molecule in the brain. We therefore decided to employ both loss-of-function and gain-of-function techniques to characterize the potential role of FXR1P in controlling the activity-dependent local translation of mRNAs involved in spine development and synaptic plasticity. Chapter 3 is a descriptive study demonstrating that FXR1P associates with ribosomes and mRNAs in dendrites and at a subset of dendritic spines. Chapter 4 presents our findings from the gain-of-function of FXR1P and shows that over-expressed FXR1P localizes to a subset of large, mature dendritic spines. Finally, Chapter 5 describes the creation of a forebrain-specific conditional knockout for FXR1P and demonstrates that loss of FXR1P alters spine development and enhances L-LTP. Chapter 6 includes a final summary and discussion of our results.

CHAPTER 3:

FRAGILE X RELATED PROTEIN 1 CLUSTERS WITH RIBOSOMES AND MESSENGER RNAS AT A SUBSET OF DENDRITIC SPINES IN THE MOUSE HIPPOCAMPUS

Authors: Denise Cook, Maria del Rayo Sanchez-Carbente, Claude Lachance, Danuta Radzioch, Sandra Tremblay, Edouard W. Khandjian, Luc DesGroseillers, Keith K. Murai

Published in October 2011 PLoS ONE 6: e26120

3.1 Relationship to overall project

The overarching hypothesis for this body of work is that FXR1P controls the local translation of mRNAs important in spine development, synaptic plasticity and memory. The experiments described in this manuscript were designed to address our first objective, which was to determine whether FXR1P is expressed at the right time and place to be involved in local translational control in the hippocampus. We therefore performed a series of experiments to look at the developmental expression pattern of FXR1P, its subcellular localization and whether it colocalized with components of the translational machinery in hippocampal neurons. The results of these experiments are presented here.

3.2 Abstract

The formation and storage of memories in neuronal networks relies on new protein synthesis, which can occur locally at synapses using translational machinery present in dendrites and at spines. These new proteins support long-lasting changes in synapse strength and size in response to high levels of synaptic activity. To ensure that proteins are made at the appropriate time and location to enable these synaptic changes, messenger RNA (mRNA) translation is tightly controlled by dendritic RNA-binding proteins. Fragile X Related Protein 1 (FXR1P) is an RNA-binding protein with high homology to Fragile X Mental Retardation Protein (FMRP) and is known to repress and activate mRNA translation in non-neuronal cells. However, unlike FMRP, very little is known

about the role of FXR1P in the central nervous system. To understand if FXR1P is positioned to regulate local mRNA translation in dendrites and at synapses, we investigated the expression and targeting of FXR1P in developing hippocampal neurons *in vivo* and *in vitro*. We found that FXR1P was highly expressed during hippocampal development and co-localized with ribosomes and mRNAs in the dendrite and at a subset of spines in mouse hippocampal neurons. Our data indicate that FXR1P is properly positioned to control local protein synthesis in the dendrite and at synapses in the central nervous system.

3.3 Introduction

New protein synthesis is required for long-lasting changes to synapses, changes thought to underlie long-term memory formation [160]. With the discovery of ribosomes and mRNAs in dendrites and at dendritic spines as well as evidence that dendrites can synthesize proteins in the absence of the cell body, we now know that new protein synthesis can occur locally in the dendrite and at spines [4,67–69]. Local protein synthesis is thought to support rapid, signal-dependent increases in protein expression required for synaptic plasticity as well as long-term memory formation [58]. Indeed, analysis of single spines using focal uncaging of glutamate has revealed the importance of dendritic protein synthesis in controlling long-lasting structural and physiological changes at individual synapses [47]. Despite the known importance of local protein synthesis in supporting synaptic plasticity, the actual proteins involved in repressing or enhancing mRNA translation at synapses remain poorly defined. A collection of RNA binding proteins has been identified biochemically as components of ribosomes and/or mRNA-containing granules in neurons [13,14]. However, it remains unclear which RNA proteins are important for regulating local protein synthesis in the dendrite and at dendritic spines [161].

Kanai et al.[14] identified Fragile X Related Protein 1 (FXR1P) as a component of their biochemically isolated neuronal mRNA granule. FXR1P is a member of a small family of RNA binding proteins that also includes Fragile X Related Protein 2 (FXR2P) and Fragile X Mental Retardation Protein (FMRP)

[25,151]. It is well established that loss of FMRP is the cause of Fragile X Syndrome, a syndrome characterized by mental retardation and autism [18,162,163]. FMRP controls the trafficking and translation of a subset of mRNAs important for certain forms of protein synthesis-dependent plasticity including mGluR-mediated long-term depression [136,164,165]. Interestingly, FXR2P is believed to participate with FMRP in regulating synaptic plasticity and behaviour [28–30]. However, the role of FXR1P in the central nervous system remains unknown. Like FMRP, FXR1P associates with mRNAs and ribosomes in messenger ribonucleoprotein particles (mRNPs) [22,24,166], is expressed by neurons [21,22] and can form homo- and hetero-multimers with FMRP and FXR2P both *in vitro* and *in vivo* [24–27]. Interestingly, FXR1P can either repress or activate the translation of target mRNAs in non-neuronal cells depending on the cellular context [32,33]. However, whether FXR1P is positioned to control local protein synthesis at or near synapses remains to be demonstrated. If FXR1P is involved in this process, it should be localized with ribosomes and mRNAs in the dendrite and at spines. We investigated this possibility by determining the expression and localization pattern of FXR1P in the developing mouse hippocampus, a system that is critical for learning and memory processes. We performed co-labeling studies using dissociated mouse hippocampal neurons to more precisely determine if FXR1P colocalizes with protein translational machinery and mRNAs in the dendrite and at spines. Remarkably, we found that FXR1P was highly co-localized with the translational machinery at a subset of spines. These findings suggest that FXR1P is well-positioned to regulate local protein synthesis at synapses and cooperate with other Fragile-X gene family members to control synaptic plasticity.

3.4 Materials and Methods

Ethics Statement with regards to animal use. All mice used in this study (both male and female) were from a wild-type C57BL/6 strain bred in our animal facility. All experiments involving mice were approved by the Montreal General Hospital Facility Animal Care Committee (Protocol ID#5758) and followed the guidelines of the Canadian Council on Animal Care.

cDNA plasmids. Farnesylated monomeric RFP in pcDNA3 was described previously . pcDNA 3.1Hyg(+) eGFP-FXR1P (isoform d) and pcDNA3.1Zeo(+) FXR1P (isoform d) plasmids were characterized in a previous publication [33]. EST clones containing full-length mouse cDNAs for FXR1P (isoform a), FXR2 and FMRP (isoform 1) were obtained from Open Biosystems (Clone IDs: 5041635, 9498022, 30532682 respectively). cDNA inserts were PCR amplified and subcloned into pcDNA3 (Clontech) and pcDNA3.1myc-His(-) (B) (Invitrogen). mCherry (courtesy of Dr. R. Tsien) and eGFP were added in-frame to the N-terminus of the Fragile X proteins. All plasmids were verified by sequencing and matched their respective sequences on GenBank, except for the plasmids pcDNA3.1Hyg(+) eGFP-FXR1P and pcDNA3.1Zeo(+) FXR1P, which started with ATG GCG GAC GTG instead of ATG GCG GAG CTG (discrepancy is underlined; see [33]). This discrepancy leads to an amino acid change of MAEL to MADV, which corresponds to the original reported sequence for human FXR1P (Accession number: AAC50155.1, see [151]). This discrepancy was corrected in the pcDNA3.1-FXR1P-myc-his construct. Expression from all constructs was driven by the CMV promoter.

Antibodies. For detecting FXR1P, we used a rabbit polyclonal antibody against FXR1P (#ML13) which has been described previously [167]. Other antibodies used included mouse monoclonal antibodies against FMRP (mAb1C3; [168]), FXR1P (mAb3FX; [166]), FXR2P (mAbA42, Abcam), myc (Santa Cruz; 9E10), MAP-2 (Sigma-Aldrich; HM-2) and GAPDH (Abcam; ab9484), human anti-ribosomal P antibodies (Immunovision), a rabbit anti-ribosomal large protein L7 (Cell Signaling), a rabbit monoclonal antibody against S6 (Cell Signaling; 5G10) and a goat polyclonal antibody against TIA-1 (Santa Cruz; sc-1751). The specificity of the anti-ribosomal P antibodies for the large ribosomal subunits P0, P1 and P2 was verified previously by others [24].

HEK cell culture, transfection and western blotting. Human embryonic kidney cells with the SV-40 T antigen (293-T) were cultured in high glucose Dulbecco's Modified Essential Medium (DMEM, Invitrogen) containing L-glutamine, 110 mg/L sodium pyruvate, 10% fetal bovine serum and 1% penicillin-streptomycin.

One day before transfection, cells were split and plated at a density of 1.2 x 10^6 cells per 6 cm dish. Cells were transfected with various Fragile X plasmids using Polyfect (Qiagen) according to the manufacturer's instructions. Cells were lysed after 48 hours in 400 µl RIPA buffer (1% Triton X-100, 1% sodium deoxycholate, 0.1% SDS, 20 mM Tris pH 8.0, 150 mM NaCl and 1 mM EDTA) containing 1 µg/ml each of leupeptin, aprotinin, pepstatin, 10 mM NaF, 1 mM sodium ortho-vanadate and 1 mM PMSF. Lysates were diluted with 3X sample buffer and equal quantities of each lysate were run on a 10% polyacrylamide gel and transferred to PVDF membranes following standard protocols. Membranes were blocked for 40 minutes with 5% BSA/TBS-0.1% Tween, and incubated overnight at 4°C with either #ML13 (1:100,000) or anti-myc (1:2000) in TBS-0.1% Tween. The next day membranes were incubated for 1 hour at room temperature with secondary antibodies conjugated to HRP. Chemiluminescent signal was obtained using Amersham ECL Plus Western Blotting Detection Reagents (GE Healthcare) and captured on X-ray film.

Hippocampal Lysates and Western Blotting. We dissected out the hippocampus from mice at different points in development (postnatal day 2, 5, 10, 15, 21, 60). Whole cell lysates were obtained by homogenizing the hippocampi in an appropriate volume of RIPA buffer (1% Triton X-100, 1% sodium deoxycholate, 0.1% SDS, 20 mM Tris pH 8.0, 150 mM NaCl and 1mM EDTA) using a dounce homogenizer. Lysates were left on ice for 30 minutes, sonicated for 10 seconds and spun at 13,200 rpm for 10 minutes. Supernatants were collected and protein concentration was determined using a BCA assay (Pierce). 20 µg of total protein at each time point was run on 10% SDS-PAGE gels and subjected to Coomassie blue staining and immunoblotting as described above. Membranes were incubated with either mAb3FX (1:2000), mAb1C3 (1:1), #ML13 (1:100,000), #anti-L7 (1:2000) or anti-GAPDH (1:10,000) as a loading control. We quantified the developmental expression profile of FXR1P relative to GAPDH using densitometry and the ImageJ Gel Analysis Plugin. We first normalized the intensity of FXR1P bands to GAPDH by dividing the area measurements returned by ImageJ and then expressed the level of FXR1P as a percentage of the level at

the earliest time-point studied (P0-P2). This was repeated across 3 independent experiments. The averages and standard errors of the mean at each developmental time-point are displayed in Figure 1B.

Cryostat sections and immunohistochemistry. A P14 mouse was transcardially perfused with ice cold Dulbecco's phosphate buffered saline followed by 20 ml of fixative (4% paraformaldehyde/0.1 M phosphate buffer; pH 7.4) using a syringe-pump (Harvard Apparatus). The brain was post-fixed overnight in 10 mL of fixative and transferred to a solution of 30% sucrose/0.1 M phosphate buffer pH 7.4 for 24-48 hours. The brain was then embedded in O.C.T. Compound (EM Sciences) and cut into 30 μm free-floating sagittal sections using a cryostat. Sections were collected in Tris buffered saline (TBS), blocked and permeabilized using 10% normal goat serum/TBS/0.2% Triton-X 100 for 1 hour at room temperature and incubated overnight at 4°C with primary antibody (#ML13; 1:500) diluted in 1% normal goat serum/TBS/0.2% Triton-X 100. Sections were washed three times for 20 minutes in TBS and incubated with Alexa Fluor goat anti-rabbit 647 (Invitrogen; 1:500) for 2 hours. Sections were washed three times for 20 minutes and then mounted using SlowFade Gold antifade reagent (Invitrogen). Sections were imaged at 10X (0.4 numerical aperture) using an Ultraview spinning disk confocal system (PerkinElmer, Wellesley, MA) connected to an Eclipse TE2000 (Nikon, Tokyo, Japan) and a cooled CCD 12-bit Hamamatsu ORCA-ER camera. Exposure time was 3000 milliseconds. We created an image of the entire hippocampus by stitching together neighboring single plane images with at least 20% overlap using the Photomerge application of Photoshop CS3 Extended.

Polyribosome preparation and analyses. Total brain polyribosomes were prepared from 10 day old C57BL/6 mice as described [169] and treated with 25 mM EDTA or 100 μg/ml of RNAse. Ten to fifteen OD at 260 nm were loaded onto 10 ml of 15-45% (w/w) linear sucrose gradients and centrifuged in a Beckman SW40 rotor for 2 hours at 34,000 rpm and 4°C. Gradients were fractionated by upward displacement using an ISCO UA-5 flow-through spectrophotometer set at 254 nm and connected to a gradient collector. Each collected fraction was precipitated

overnight at –20°C after addition of 2 volumes of ethanol. The precipitated material was collected by centrifugation at 12,000 rpm for 20 min and solubilized in SDS-sample buffer before immunoblot analyses. FXR1P was detected with mAb3FX, and the ribosomal L7 protein with rabbit anti-L7 serum.

Dissociated mouse hippocampal neurons. Primary mouse hippocampal neurons were cultured using a modified version of the Banker method [170]. Briefly, astrocytes were isolated from the hippocampi of P1-P2 mice and maintained in Glial Growth Medium (Minimal Essential Medium containing Earle's salts and L-glutamine supplemented with 10% Horse serum, 0.6% glucose and 1% penicillin/streptomycin (Invitrogen)) until they reached confluency (approximately 7-10 days). At this point, astrocytes were seeded at a density of 80,000 cells/well in 12 well dishes (with 3 paraffin dots/well) coated overnight with poly-D-lysine (0.1 mg/ml). After 4 days medium was changed to Neuronal Growth Medium (Neurobasal A containing 2% B27, 1 mM Glutamax and 1% penicillin/streptomycin (Invitrogen)) to condition the medium overnight. The next day, hippocampi from P0 mice were dissociated in Neuronal Growth Medium containing 1 mg/ml papain and 0.02% BSA for 15 minutes at 37°C. Hippocampi were then transferred to Neuronal Growth Medium containing 1% trypsin inhibitor (Sigma) and 1% BSA and triturated using a fire-polished pipette. Cells were then resuspended in Neuronal Growth Medium and counted. We plated neurons at a density of 80,000 cells/well onto poly-L-lysine (0.1 mg/ml) coated coverslips (15 mm, Fisher). After 3 hours, coverslips with neurons were transferred onto the paraffin dots and placed face-up on the astrocyte feeder layer. After 3 days, 3 μM Ara-C was added to inhibit glial growth. One-third of the medium was changed every 3-4 days.

Lipofectamine 2000 transfection of primary hippocampal neurons. Primary neurons were transfected at 7 or 14 days *in vitro* using Lipofectamine 2000. Briefly, 1.5 μg of cDNA and 3 μl Lipofectamine 2000 (Invitrogen) were separately diluted in 100 μl of Minimum Essential Medium and incubated for 5 minutes at room temperature. DNA/Lipofectamine complexes were combined, vortexed for 2 seconds and incubated for 30 minutes. During this time, coverslips

with neurons were transferred to wells in a separate 12 well dish containing 1 ml of pre-warmed plain Neurobasal A Medium. The DNA/Lipofectamine complexes (200 µl) were then added dropwise to each well. After 3-4 hours the coverslips were returned to the astrocyte feeder layer. We routinely checked the health of our transfected neurons using MAP2 labelling [171]. We found that unhealthy transfected neurons had little or no MAP2 staining. We obtained approximately 5-15 healthy transfected cells per coverslip using this method.

Immunostaining of dissociated neurons. Neurons were fixed at 7 or 14 days *in vitro* using ice cold 4% paraformaldehyde/4% sucrose/0.1 M phosphate buffer for 15 minutes. Neurons were then washed once with a solution of Dulbecco's phosphate buffered saline (DPBS)/10 mM glycine and permeabilized using a solution of DPBS/10 mM glycine/0.2% Triton-X 100 for 15 minutes at room temperature. We then washed the neurons using DPBS/10 mM glycine/0.1% Triton-X 100 and blocked them in 5% BSA/DPBS for 1 hour at room temperature. Neurons were then incubated overnight at 4°C with primary antibodies diluted in 5% BSA/DPBS (mouse anti-MAP2 HM-2, 1:200; #ML13, 1:200; P0, 1:500; rabbit anti-S6, 1:200, goat anti-TIA-1 (Santa Cruz, 1:200), FMRP mAb1C3 (tissue culture supernatant, neat), FXR2P mAbA42 (Millipore, 1:50), mouse anti-AGO2 (Abnova, 1:300), mouse anti-PAK1 (Abnova, 1:300)). Neurons were washed 3 times for 5 minutes using DPBS/0.1% Triton-X 100 and incubated with suitable Alexa Fluor conjugated secondary antibodies (-488, -568, -647) diluted to 1:300 in 5% BSA/DPBS. Neurons were then washed three times and mounted using SlowFade Gold Reagent (Invitrogen).

Fluorescence in situ hybridization of dissociated neurons. Oligonucleotide probes (27-mer poly(dT) or poly(dA)) were 3' end labelled with digoxigenin (DIG) as indicated by the manufacturer (Roche). DIG incorporation was checked by dot blot. Fixed cells were subjected to fluorescence *in situ* hybridization (FISH) with the DIG-labelled poly(dT) or control poly(dA) probes as described previously with some modifications [172]. Cells were washed in PBS containing 5 mM $MgCl_2$ (PBSM) and 0.1 M glycine, dehydrated in 50% ethanol and finally in 70% ethanol for at least 3 hours. Cells were then rehydrated with PBSM, permeabilized with

0.25% Triton-X 100 in PBSM and washed with PBSM. The cells were treated for 10 minutes with acetic anhydride in 0.1 M TEA, washed with 1X SSC and equilibrated with 1X SSC and 20% formamide for 5 minutes at room temperature. Probe mixture (10 ng) was dried down with *Escherichia coli* tRNA (10 mg) and sonicated salmon sperm DNA (10 mg), then suspended in 15 µl of 40% formamide and 4X SSC pH 7.0. Probes were mixed with 15 µl of hybridization buffer (20% dextran sulfate, 0.4% BSA and 4 mM Vanadyl Ribonucleotide Complex). The coverslips were covered with parafilm containing 30 µl of probe mixture and hybridized overnight at 37°C in a humid chamber. After hybridization, coverslips were washed for 20 minutes in 20% formamide/1X SSC at 37°C and followed by three 10 minute washes in 1X SSC and two 20 minute washes in 0.1X SSC at room temperature. Hybridized probes, eGFP-FXR1P fusion protein and endogenous FXR1P and P0 were detected by immunofluorescence using an anti-DIG antibody conjugate with rhodamine (1:25; Roche), a mouse anti-GFP antibody (1:250; Roche Molecular Biochemicals), a rabbit anti-FXR1P antibody (1:100; #ML13) and a human anti-P0 antibody (1:200, Immunovision) respectively. The primary antibodies were incubated overnight at 4°C. Secondary antibodies used were Alexa 488-conjugated goat anti-mouse IgG (1:500; Molecular Probes) and Alexa 647-conjugated goat anti-human IgG (1:500; Molecular Probes).

Imaging of dissociated neurons. Neurons were imaged at 60X using an oil immersion objective (60X Plan Fluor 1.25 numerical aperture) using an Ultraview spinning disk confocal system (PerkinElmer, Wellesley, MA) connected to an Eclipse TE2000 (Nikon, Tokyo, Japan). Excitation band pass filters are as follows: 488, 568 and 647 nm (+/- 10nm). Emission band pass filters are as follows: 525 +/-50 nm, 607 +/- 45 nm and 700 +/-75 nm. Exposure time was adjusted to obtain maximal signal to noise without saturating pixels in the dendrites (as a consequence, pixels within the cell body were sometimes saturated; however, the cell body was never used for analysis). Single plane images or image stacks were acquired using a Z-step of 0.6 µm.

Colocalization Analysis. We used 0.1 µm, 0.5 µm and 4 µm Tetraspeck Fluorescent Microspheres (Invitrogen) to check for chromatic aberration. These microspheres emit fluorescence in the blue/green/red/far red channels and we used them to test whether the green/red/far red signals properly overlap. We found close apposition of signals in the green and red channels with a slight off-set in the far red channel. Therefore, most of our colocalization experiments were performed using red and green signals. Control experiments using single primary and secondary antibodies, secondary antibodies only and single primary antibodies with both secondary antibodies were performed to rule out bleed-through of signals and cross-reactivity of antibodies. We quantified colocalization between FXR1P and ribosomal proteins using the Intensity Correlation Analysis Plugin in ImageJ [173]. We first converted 16-bit monochromatic single plane images or maximum projection images to 8-bit, selected a background region of interest (ROI) and subtracted background using the ImageJ plugin "Background subtract from ROI" with default setting of 2 standard deviations (except for *in situ* hybridization experiments where 0.5 standard deviations was used). No thresholds were set. We then drew a line ROI along a dendrite and ran the Intensity Correlation Analysis (ICA) Plugin. At least 2 dendrites per cell were analyzed. This plugin generates multiple coefficients of colocalization, including Pearson's (Rr), Mander's M1 and M2 and the Intensity Correlation Quotient (ICQ). Since each of these values is influenced in different ways by image quality, background and differences in signal intensity, relying on any one measure can misrepresent the degree of colocalization in images [174]. Thus, for a more complete understanding of the degree of colocalization, we have decided to present the results obtained from each of these measures. Pearson's coefficient measures how correlated the intensities of both channels are and varies between -1 and 1. A value from 0.5 to 1.0 indicates colocalization [174]. M1 and M2 describe how much of the green signal overlaps with red signal and vice-versa. They vary between 0 and 1 with anything more than 0.5 indicating colocalization. The ICQ measures whether the signals in both channels vary in synchrony. It is calculated on a pixel by pixel basis by first subtracting the mean intensity from the pixel intensity of

each channel and then multiplying the values obtained for both channels. If the signals vary in synchrony, then the differences from the mean will be both positive or both negative, resulting in a positive multiplication product. The ICQ is then calculated by summing up the number of pixels with positive multiplication products (product of the differences from the mean (PDM)), dividing by the total number of pixels and subtracting 0.5. This results in a value that varies between -0.5 (segregated staining) and 0.5 (perfect colocalization). A value close to 0 signifies random staining. To calculate the number of overexpressed FXR1P clusters containing ribosomal markers we ran the ICA Plugin and generated an image displaying the location of the positive PDMs. This image contains PDMs from pixels that are both above the mean (+ x +) and below the mean (- x -). Since pixels below the mean are mostly 0, 0 pixels, we used the PDM image for pixels above the mean (see Figure 3E for example). This image was thresholded, converted to a binary image and the number of particles was calculated using the Analyze Particles plugin in ImageJ. This process was repeated for the FXR1P image. The number of FXR1P clusters containing colocalized signal was determined by dividing the number of colocalized particles by the total number of FXR1P clusters.

Mouse organotypic hippocampal slices. Hippocampal slices were prepared according to previously published methods [175,176]. Briefly, the hippocampus was removed from P7 mouse pups and cut into 300 µm transverse slices using a tissue chopper (McIllwain). Approximately 4-6 slices were placed in a circle in the center of a semi-porous tissue culture insert (0.4 µm pore size; Millipore) and maintained in culture media consisting of 50% Minimum Essential Medium (+ Glutamax), 25% heat-inactivated horse serum, 25% Hank's Balanced Salt Solution and 6.5 mg/ml D-glucose (Sigma). Medium was replaced every two days.

Gene Gun transfection and imaging of CA1 pyramidal cells. We prepared the cartridges for transfection according to previously published methods [177]. Briefly, we precipitated 25 µg of eGFP-FXR1P and 25 µg of RFPf plasmid DNA onto 25 mg of 1.6 µm gold particles (Bio-Rad) using 100 µl 0.05 M spermidine and 100

µl 1M $CaCl_2$. Gold particles with precipitated DNA were then washed three times with 1 ml absolute ethanol, resuspended in 3 ml of 0.05 mg/ml polyvinylpyrrolidone in absolute ethanol (PVP, Bio-Rad) and drawn into pre-dried Tefzel tubing. The tubing was placed into the Bio-Rad preparation station and the gold particles were allowed to settle for 3 minutes. We then slowly withdrew the ethanol and allowed the tubing to dry for 5 minutes. Hippocampal slices were transfected at 7 days in vitro using helium at 110-130 psi. A 3.0 µm membrane filter (Millipore) was placed between the gene gun nozzle and the hippocampal slices to decrease the shock-wave and improve transfection efficiency. Slices were fixed 48 hours after transfection and imaged using the 60X oil immersion objective and confocal microscopy as described previously. The primary apical dendrites of CA1 pyramidal cells (~100 µm from the cell body) in both green (eGFP-FXR1P) and red (RFPf) channels were acquired using Metamorph (Molecular Devices). Z-stacks were produced using a z-step of 0.3 µm. We imaged 17 CA1 apical dendrites across multiple slices cultured from four mouse litters.

Analysis of FXR1P cluster location in CA1 dendrites. To analyze FXR1P cluster location, we first created separate maximum projection images for eGFP-FXR1P and RFPf. The RFPf images were thresholded linearly in Photoshop (Adobe Systems, Seattle, WA) and imported into Reconstruct. For each image, using only the RFPf channel, (and therefore blind to the location of FXR1P clusters) we measured the length of a small dendritic segment (30-70 µm) and counted the number of spines along that length (30-80 spines). We then manually traced the total perimeter and spine head perimeter of each of the spines along the segment. The perimeter drawings were saved and overlaid with the eGFP-FXR1P images. We counted the number of FXR1P clusters along the dendritic segment. A cluster was defined as being at a spine if it was found within the spine's traced perimeter. A cluster was scored as being in the spine head if it was found within the spine head perimeter and as being in the base/neck if it was found outside the spine head perimeter. For spines lacking clear spine heads (ie. stubby spines), the cluster was scored as being in both the spine head/base/neck ("all").

Statistical Analysis. All statistical analyses were performed using R (http://www.R-project.org) [178]. The package Hmisc was used to calculate means and standard deviations plotted in Figure 9 [179]. All graphs were produced in R using ggplot2 [180]. Confidence intervals were calculated using resampling techniques (bootstrapping) implemented in the base R package boot using values from individual observations (cells). Standard errors for colocalized granules were calculated using the average percent colocalization from each independent culture.

3.5 Results

FXR1P is expressed in neurons of the developing hippocampus.

In contrast to FMRP, very little is known about the expression and localization pattern of FXR1P in the developing and adult mouse brain. In order to determine whether FXR1P is in a position to regulate local protein synthesis in neurons we first examined the expression of FXR1P in the developing mouse hippocampus. We were particularly interested in the expression of FXR1P in the first three postnatal weeks since this corresponds to a time period when there is the highest presence of translational machinery in dendrites and at spines and maximal synapse growth [66]. Whole lysates were prepared from mouse hippocampi at different developmental stages, loaded onto an SDS-PAGE gel and analyzed by Coomassie blue staining. Staining revealed even loading of total protein with only subtle changes in the intensity of labeled bands during development (Figure 1A). To determine whether FXR1P expression changes during development, we used mAb3FX which detects all FXR1P isoforms (a to f). The results showed that FXR1P isoforms a, b, c, and d were highly expressed in early postnatal development (P2-P10) with a substantial drop in expression after P15 (Figure 1A). Since mAb3FX also reacts with FXR2P, we further resolved the expression of the 78 kDa (iso d) and 80 kDa (iso c) isoforms of FXR1P using the FXR1P specific antibody #ML13 (Figure 1A, Figure S1A), which gave a similar pattern as mAb3FX. As expected, the muscle-specific long isoforms (e, f), which run at 84-88 kDa [166], were not present in hippocampal lysate. We also blotted for

FMRP and FXR2P and observed a similar decrease in expression across development. Importantly, we observed that the decay of the ribosomal protein L7 was similar to the Fragile X proteins. This suggests a global decrease in the abundance of translational machinery as compared to other proteins such as GAPDH (Figure 1A). Normalizing FXR1P levels with GAPDH expression showed a significant decrease in FXR1P expression across postnatal development compared to GAPDH (Figure 1B). These results indicate that FXR1P was highly expressed during early postnatal stages, a time when synapses are actively forming and reorganizing during hippocampal development.

To define the cellular localization pattern of FXR1P, we performed immunofluorescence labeling on sections from mouse hippocampus at multiple developmental time points using the FXR1P specific serum #ML13. FXR1P (isoforms c and d) were enriched in the cytoplasm of pyramidal and non-pyramidal neurons at all time points studied (P10, P12, P14, P16, P18, P30 and P63). A representative image from postnatal day 14 is shown in Figure 1C. At high magnification the majority of the FXR1P staining was found in the perinuclear cytoplasm and proximal dendrites of pyramidal neurons and observed as small punctae in the stratum radiatum. FXR1P was also detected in large interneurons in the stratum oriens, radiatum, and lacunosum moleculare. In contrast, we observed very limited expression of FXR1P in glia. Control experiments with application of secondary antibody alone did not reveal significant labeling (Figure S1B). Therefore, FXR1P is strongly expressed by developing neurons in the mouse hippocampus and localized in dendrites.

While it is established that FXR1P, similarly to FMRP, is physically associated with translation machinery in non-neural cells [33,166,181], it has been assumed that this is also the case in the central nervous system. To determine whether FXR1P is associated with the translational apparatus in brain, total polyribosomes were prepared from P10 brain as previously described [169] and analyzed by velocity sedimentation through sucrose density gradients. In the presence of Mg^{2+}, all FXR1P isoforms were detected in fractions corresponding to heavy sedimenting polyribosomes (Figure 2). The presence of the ribosomal

protein L7 in the fractions was used as a control. Upon addition of EDTA, which dissociates ribosomes into their subunits concomitant with the release of free mRNP complexes, FXR1P was displaced to the upper part of the gradient with sedimentation values corresponding to mRNPs. Finally, treatment with RNase A resulted in the complete destruction of polyribosomes and all FXR1P isoforms were displaced to the top fractions of the gradient (data not shown). Since mAb3FX was used in this analysis, these results established that both FXR1P and FXR2P co-sediment in the same fractions (Figure 2).

FXR1P forms clusters in the dendrite and at spines.

Having established that FXR1P was expressed by developing neurons in the mouse hippocampus and present in dendrites, we performed a more detailed subcellular characterization of endogenous FXR1P along dendrites. To do this, we used low-density dissociated mouse hippocampal neurons which allowed us to resolve the discrete localization of FXR1P in isolated dendrites and to colocalize FXR1P with other proteins. Similar to what we found *in vivo*, FXR1P was highly expressed in the perinuclear region and found as individual punctae in MAP2-positive dendrites (Figure 3A). Large punctae were especially prevalent in proximal dendritic regions while smaller punctae were found in more distal dendritic segments. FXR1P was found in punctae of different sizes that, in general, became progressively larger with the age of neuronal cultures (Figure 3A). Due to the heterogeneous size of these punctae and the fact that FXR1P is known to multimerize, we will refer to these punctae as "clusters". We next followed up on the distribution of FXR1P clusters with respect to dendritic spines and filopodia, a subset of which are known to contain protein translation machinery at their bases [67]. To fully delineate dendrites, filopodia and spines we used a construct encoding farnesylated red fluorescent protein (farnesylated RFPf) which is targeted to the cell membrane. We transfected hippocampal neurons with an RFPf construct at 14 days *in vitro* and then immunostained for endogenous FXR1P (Figure 3B). Upon close examination of FXR1P clusters we found that some of these clusters were in close proximity with the base of a subset of dendritic filopodia or spine-like extensions (Figure 3C, I and II). FXR1P was also

detected in axons, however the clusters were smaller and more infrequent than in the dendrites (data not shown). These experiments demonstrate that FXR1P accumulates in discrete clusters in the dendrite and at dendritic spine-like protrusions.

FXR1P colocalizes with ribosomal subunits and mRNAs in clusters along the dendrite.

We have shown that FXR1P physically associates with polyribosomes in the developing mouse brain (Figure 2). However, this analysis does not allow us to determine whether this association takes place in dendrites and at spines. If FXR1P plays a role in local protein synthesis, then it should colocalize in dendrites with components of the translational machinery, for example ribosomes and/or mRNAs. We investigated this by quantifying the degree of colocalization between FXR1P and ribosomes or mRNAs in dissociated hippocampal neurons at 14 days *in vitro* (Figures 4, 5). Immunostaining for the large ribosomal subunit P0 was used to detect ribosomes while fluorescence *in situ* hybridization (FISH) with a poly (dT) probe was used to detect polyadenylated mRNAs. FISH labeling with a poly (dA) probe was used in control experiments (Figure S2). First, using a qualitative method to look at colocalization, we saw a large amount of overlapping signal on the merged image of FXR1P and P0 as well as FXR1P and mRNAs in both the perinuclear region and proximal dendrites (Figures 4A and 5A). We used ImageJ to measure the intensity changes of the two signals along the dendritic segment shown in Figures 4B and 5B. This displayed a strong co-variance in the FXR1P/P0 and FXR1P/mRNA signals (Figures 4C and 5C). However, since determining the degree of overlap with these methods is subjective and influenced by differences in intensities between the two channels, we used the Intensity Correlation Analysis (ICA) Plugin in ImageJ to quantify the degree of colocalization in dendritic segments using multiple methods [173] (see methods). All coefficients indicated significant levels of colocalization between FXR1P/P0 and FXR1P/mRNA (Table 1). Importantly, Intensity Correlation Analysis (ICA) reveals not only the degree of correlated signal but also non-correlated signal. Typical results obtained from this type of analysis are shown in

Figures 4D, E and 5D, E. Figures 4D and 5D present the grayscale and merged images of the dendritic segments used in ICA. Plots of fluorescence intensity versus product difference of the mean (PDM) are shown in Figures 4E and 5E. A positive PDM indicates a pixel with correlated FXR1P and P0 or mRNA intensities (right of the red line), whereas a negative PDM indicates a pixel with non-correlated FXR1P and P0/mRNA intensities (left of the red line). The majority of FXR1P and P0/mRNA pixels fall to the right of the red line, indicating a high level of co-dependence of the signals. The location of these correlated pixels is shown in the inset. Interestingly, a number of high intensity FXR1P pixels contained uncorrelated P0 intensities (left of the red line), whereas most of the pixels for FXR1P and mRNA were correlated (Figures 4E and 5E). This demonstrates that most FXR1P clusters contain mRNAs and ribosomes and a fraction of FXR1P clusters lack ribosomes. These collective results demonstrate that FXR1P clusters are colocalized with protein synthesis machinery in dendrites.

To validate our method of quantifying colocalization, we repeated the analysis using co-immunostaining of FXR1P and PSD95. PSD95 is discretely localized to postsynaptic sites including the heads of dendritic spines [182]. As shown in Figure 6A, the staining patterns of FXR1P and PSD95 are different. Measuring the intensities of the two signals along the dendritic segment shown in the bottom panel of Figure 6A confirms the lack of co-variance in the two signals (Figure 6B). In addition, most of the measures of colocalization demonstrated a lack of colocalization between the two channels (Table 1), and the intensity correlation analysis showed that most of the FXR1P and PSD95 pixels had PDM values less than 0, demonstrating a lack of co-dependence of the two signals (Figure 6C). These results demonstrate a lack of colocalization between FXR1P and PSD95 and is consistent with findings showing that protein synthesis machinery is concentrated mostly near the base of dendritic spines and not at the postsynaptic density [66].

Previous studies have found that FXR1P can interact with its homologues FMRP and FXR2P [25], with the miRNA-induced silencing complex (RISC)

protein, argonaute 2 [32] and with the actin modulator, PAK1 [183]. To determine whether FXR1P colocalizes with these proteins in neuronal dendrites we performed immunostaining for FXR1P, P0 and each of these interacting proteins. Qualitatively, we saw partial colocalization of FXR1P with FMRP, FXR2P, and argonaute 2 in P0 positive dendritic clusters (Figure S3). However, in most cases argonaute 2 clusters were located on the edge of the P0 clusters, whereas FXR1P occupied the majority of the P0 cluster. In contrast, PAK1 was ubiquitously expressed throughout the neuronal dendrites and axon of neurons, a pattern shown previously [184], and showed no specific colocalization with FXR1P (data not shown). These results demonstrate that a subset of FXR1P/P0 clusters also contain the RNA-binding proteins FXR2P, FMRP and argonaute 2.

eGFP-FXR1P colocalizes with ribosomal subunits and mRNAs in clusters along the dendrite.

We next tested whether a fluorescently tagged version of FXR1P would behave similarly to the endogenous protein when overexpressed in neurons at both 7 and 14 days *in vitro* (Figure 7). Similar to endogenous FXR1P, eGFP-FXR1P formed clusters of various sizes in the perinuclear region and dendrites. However, these clusters were often larger and more defined than the clusters seen with endogenous FXR1P staining. This was not due to aggregation of eGFP, since both untagged FXR1P and myc-tagged FXR1P showed similar cluster sizes when overexpressed in neurons (data not shown). Similar to endogenous FXR1P, eGFP-FXR1P clusters were found at the base of a subset of dendritic spine-like protrusions.

We next asked whether these clusters contained ribosomal proteins. We immunostained neurons expressing eGFP-FXR1P with antibodies against the large and small ribosomal subunits (P0 and S6 respectively) and quantified the number of FXR1P clusters containing either P0 or S6 signal (Figure 8A, B and Table 2). The majority (~ 70%) of FXR1P clusters contained correlated P0 or S6 signal. All other measures of colocalization also demonstrated high levels of colocalization (Table 2). Most surprisingly, we noted that the staining pattern of P0 and S6 changed to follow the cluster pattern of overexpressed FXR1P.

Specifically, the clusters became larger, brighter and more defined upon FXR1P overexpression (compare P0 staining in Figure 8A with staining in Figure 4A). To rule out the fact that eGFP-FXR1P was forming a non-specific cluster of RNA binding proteins or a stress granule [102,185], we repeated the analysis using staining against T cell immunoantigen-1 (TIA-1). TIA-1 is an RNA binding protein that normally resides in the nucleus and perinuclear region of non-neuronal cells and redistributes to stress granules when cells are stressed [102,186]. We first verified that our antibody was capable of detecting TIA-1 positive stress granules in both heterologous cells and neurons challenged with puromycin or arsenite (Figure S4) [102]. We found that TIA-1 redistributed into cytoplasmic granules in stressed heterologous cells and neurons (Figure S4), demonstrating that our antibody does detect TIA-1 positive stress granules. In contrast, we found that overexpression of eGFP-FXR1P in neurons did not cause a redistribution of TIA-1 into cytoplasmic granules and TIA-1 was not colocalized with eGFP-FXR1P clusters (Figure 8C and Table 2). This indicates that overexpressed eGFP-FXR1P is not causing a general redistribution of RNA binding proteins or causing cellular stress.

To determine whether the colocalization of FXR1P with ribosomes was unique to eGFP-FXR1P (isoform d), we repeated the P0 staining using untagged FXR1P, myc-tagged FXR1P, mCherry-FXR1P (isoform a), eGFP-FXR2P and eGFP-FMRP (isoform 1). We found that regardless of the tag, family member or isoform tested, these proteins formed clusters that contained high levels of P0 (data not shown) and hence likely reflect the true distribution of overexpressed Fragile X proteins.

In addition, we tested whether overexpressed Fragile X proteins colocalize in clusters with their endogenous counterparts (Figure S5). We found that eGFP-FXR1P partially colocalized with FXR2P in large clusters (Figure S5A). eGFP-FXR2P and eGFP-FMRP clusters both contained FXR1P (Figures S5B,C). We were unable to verify whether FXR1P clusters contain endogenous FMRP due to the slight cross-reactivity of antibody 1C3 with FXR1P [166]. These results demonstrate that over-expressed Fragile X proteins, similar to the endogenous

proteins (Figure S3), retain their ability to colocalize with their endogenous counterparts in clusters.

Finally, we tested whether FXR1P clusters also contained mRNAs. We performed FISH with a poly(dT) probe on neurons transfected with eGFP-FXR1P. Similar to the ribosome staining, we found that the majority of FXR1P clusters (approximately 80%) contained mRNAs (Figure 9 and Table 2). Together, these results demonstrate that eGFP-FXR1P forms clusters containing ribosomes and mRNAs along the dendrite and at spine-like protrusions.

eGFP-FXR1P clusters are found at the base of a subset of dendritic spines.

Our previous experiments showed that both endogenous and overexpressed FXR1P are localized to the base of only a small number of spine-like extensions and are co-localized with protein synthesis machinery (see Figures 3C and Figure 7). To quantify the distribution of FXR1P clusters with respect to the dendrite and spines as well as to determine the proportion of spines containing FXR1P clusters, we transfected plasmids expressing eGFP-FXR1P and RFPf into organotypic hippocampal slices from mice. We chose to quantify the distribution of eGFP-FXR1P clusters instead of endogenous FXR1P clusters because we could focus our analysis on dendritic FXR1P clusters without influence from clusters found in neighboring cells. Furthermore, using exogenous eGFP-FXR1P, we could perform the analysis in organotypic slices, which provide a useful model system for studying dendritic spines on CA1 pyramidal neurons [175,187]. Indeed, our previous work has shown that the majority of dendritic spine protrusions have associated presynaptic terminals and likely represent actual synapses [176]. Qualitatively, the distribution of eGFP-FXR1P clusters in slices was similar to that in dissociated hippocampal neurons (Figure 10A). Further analysis showed that eGFP-FXR1P cluster density was highly variable across the 17 dendritic segments analyzed (Figure 10B). The majority of clusters were found on the dendritic shaft and an average of 23.6% of spines contained at least one eGFP-FXR1P cluster (Figure 10C, D). Within this 23.6%, we found that FXR1P was more than twice as likely to be present at the base or neck of the spine than in the head of the spine (Figure 10E). Interestingly, the majority of eGFP-FXR1P

clusters are immobile over time periods of 10 minutes to 1 hour in both young dissociated hippocampal neurons (Figure S6) and organotypic slice cultures (data not shown). These results indicate that FXR1P clusters are found at stable structures containing protein synthesis machinery and are located at the base of a subset of spines in hippocampal neurons.

3.6 Discussion

The goal of the study was to determine whether FXR1P localizes with the translational machinery in the dendrite and at spines of mouse hippocampal neurons. Using biochemistry and confocal imaging with colocalization analysis, we demonstrate that FXR1P has enriched expression during hippocampal development and that the majority of FXR1P associates with polyribosomes and colocalizes with components of translational machinery including ribosomes and mRNAs in dendrites and at the base of a subset of dendritic spines. Our results support a role for FXR1P in local mRNA translation in neurons.

Local mRNA translation is regulated by RNA binding proteins which play a role at many different steps in the mRNA life cycle. In neurons, some mRNAs must be processed and trafficked out of the nucleus, repressed en-route to their destinations, and then stored safely until a signal is received at which point they need to be rapidly translated and then stored again for future use or degraded [188]. Our study suggests that FXR1P may function in controlling mRNAs at multiple steps in neurons.

Firstly, we found that FXR1P is associated with polyribosomes in developing brain and localized with mRNAs in discrete clusters in the dendrites. In addition, we noted that the majority of these FXR1P clusters are immobile (Figure S6). The properties of these clusters are reminiscent of RNA granules – large aggregates of mRNAs, ribosomes and RNA binding proteins that are thought to store and traffic repressed mRNAs [101,106,110,189]. In fact, the observation that overexpressing FXR1P increases the degree of co-localization with ribosomes and mRNAs, suggests that high levels of FXR1P can actively recruit

ribosomes and mRNAs into RNA granules. This suggests that FXR1P could play a role in storing and protecting repressed mRNAs in neuronal RNA granules.

Secondly, FXR1P may function as a regulator of local mRNA translation. FXR1P is known to both repress and enhance the translation of target mRNAs in monocytes and macrophages depending on external cues [32,33]. These findings raise the intriguing possibility that FXR1P may act as a switch for mRNA translation in response to external signals. This would be relevant for neurons, where synaptic activity leads to rapid local protein synthesis in dendrites [77,78]. The stable localization of FXR1P with ribosomes at the base of dendritic spines is consistent with a role in controlling activity-dependent local protein synthesis [77,78]. To address this possibility, future studies will be needed to determine if synaptic activity changes the localization or mobility of FXR1P clusters near spines and whether FXR1P can directly affect activity-dependent local mRNA translation. Indeed, this hypothesis fits well with results showing that synaptic activity can change the distribution of ribosomes, mRNAs and other RNA-binding proteins in order to modulate local protein synthesis, remodel spines, and adjust synaptic strength [116,190,191].

Lastly, FXR1P could also play a role at the level of mRNA trafficking. In support of this, we found that the degree of co-localization was greatest with mRNAs versus the large ribosomal subunit. This was reflected by a minor fraction of small FXR1P clusters that did not contain discernible P0 staining (Figures 4D, E). These small, non-ribosome containing mRNA protein particles (mRNPs) may represent mRNAs trafficking from the nucleus to the dendrites and spines. Further experimentation is needed to test whether FXR1P is involved in trafficking mRNAs into the dendrites and spines, for example by reducing the level of FXR1P in neurons and tracking the fate of candidate target mRNAs.

A major unanswered question is the actual identity of mRNA targets of FXR1P in neurons. Previous studies have shown that FMRP and FXR1P both bind to kissing complex containing RNAs *in vitro*, suggesting that FMRP and FXR1P share some mRNA targets [192]. However, a more recent study using *in vivo* crosslinking-immunoprecipation to identify FMRP targets from mouse brain has

questioned the view that FMRP binds to specific RNA structures since FMRP seems to be present along the entire length of target mRNAs [20]. Nevertheless, our results showing colocalization between FXR1P, FMRP and FXR2P in large dendritic clusters (Figures S3, S4) supports a model whereby FXR1P, FMRP and FXR2P cooperate to control the translation of certain neuronal mRNAs. If this is true, FXR1P, like FMRP, may regulate the translation of proteins important for building and maintaining the structure and function of the synapse.

To perform these diverse functions, FXR1P may coordinate with different protein partners including argonaute 2 and PAK1 in addition to FMRP and FXR2P [27,32,183]. Although FXR1P showed some partial colocalization with argonaute 2, we found that FXR1P and argonaute 2 showed mainly complementary expression patterns, with argonaute 2 being found at the edges of the P0 positive clusters (Figure S3). This localization pattern is consistent with reports of P-bodies (which contain argonaute 2) being closely located to, but non-overlapping with RNA transport particles or RNA granules [104]. We also did not observe selective colocalization between FXR1P and PAK1 in dendrites. It is possible that FXR1P may increase its interactions with argonaute 2 and PAK1 only under certain circumstances [32].

Currently, many aspects of FXR1P function in neurons remain unsolved, including its mechanism of action, its mRNA targets and its physiological importance. What might be the functional role of FXR1P at the synapse? Our results showing increased expression of FXR1P during early postnatal development of the mouse hippocampus suggests that FXR1P functions predominantly during synapse formation and synapse maturation. This is consistent with studies showing an important role for FXR1P in the early development of the eye, neural crest and muscle [155,193]. Based upon our results, we propose that FXR1P is involved in local translational control of mRNAs in dendrites and may be involved in expressing proteins important for structural or physiological plasticity of dendritic spines. Further investigation is needed to determine how selective loss or overexpression of FXR1P in the brain affects

neuronal and synaptic properties and whether FXR1P, like its homolog FMRP, is important for cognitive processes such as learning and memory formation.

3.7 Acknowledgements

This work was supported by the Canadian Institutes of Health Research, Canada Research Chairs Program, Canadian Foundation for Innovation and the National Institutes of Health grant 1R21DA026053-01 (U.S.A) (K.K.M.). The authors thank Dr. Roger Tsien (Howard Hughes Medical Institute; UCSD) for the mRFP construct, Jean-Louis Mandel (IGBMC, Strabourg) and Barbara Bardoni (IPMC, Nice Sophia-Antipolis) for FMRP and FXR1P antibodies, and members of the Murai Lab for helpful discussions. D.C. was supported through a Frederick Banting and Charles Best CIHR Doctoral Research Award and an FRSQ Doctoral Award. L.D.G. was funded by the Canadian Institutes of Health Research. E.W.K. by the NSERC, and M.S.-C. received a postdoctoral fellowship from Consejo Nacional de Ciencia y Tecnologia (CONACYT).

3.8 Tables

Table 1: FXR1P colocalizes with ribosomes and mRNA (Means, 95% Confidence Intervals)

	Pearson's Coefficient	Mander's 1[a]	Mander's 2[b]	Intensity Correlation Quotient
FXR1P/ P0[c]	0.63 (0.59-0.67)	0.86 (0.80-0.93)	0.89 (0.87-0.92)	0.26 (0.25-0.28)
FXR1P/ mRNA[d]	0.74 (0.70-0.77)	0.97 (0.96-0.99)	0.90 (0.87-0.93)	0.31 (0.28-0.32)
FXR1P/ PSD95[e]	-0.05 (N/A)	0.22 (N/A)	0.76 (N/A)	0.11 (N/A)

[a] Overlap of FXR1P with label of interest

[b] Overlap of label of interest with FXR1P

[c] Number of independent cultures = 4; Number of cells = 38

[d] Number of independent cultures = 2; Number of cells = 21

[e] Number of independent cultures = 1; Number of cells = 6

Table 2: eGFP-FXR1P colocalizes with ribosomes and mRNA (Means, 95% confidence intervals).

	Pearson's Coefficient	Mander's 1[a]	Mander's 2[b]	Intensity Correlation Quotient	% colocalization (SE) [c]
FXR1P/ P0[d]	0.76 (0.71-0.82)	0.96 (0.92-0.99)	0.80 (0.77-0.89)	0.32 (0.30-0.34)	72.8 (3.5)
FXR1P/ S6[e]	0.74 (0.65-0.83)	0.96 (0.92-0.99)	0.73 (0.65-0.80)	0.32 (0.28-0.34)	68.1 (3.9)
FXR1P/ mRNA[f]	0.69 (0.61-0.80)	0.88 (0.84-0.92)	0.83 (0.75-0.92)	0.33 (0.30-0.35)	79.3 (N/A)
FXR1P / TIA-1[g]	-0.04 (-0.09-0.02)	0.27 (0.21-0.37)	0.27 (0.21-0.33)	0.17 (0.16-0.19)	23.5 (6.3)

[a] Overlap of FXR1P with label of interest

[b] Overlap of label of interest with FXR1P

[c] % colocalization (standard error) = # of FXR1P clusters with correlated signal from label of interest/total number of FXR1P clusters on dendritic segment.

[d] Number of independent cultures = 3; Number of cells = 22; Number of granules = 558

[e] Number of independent cultures = 4; Number of cells = 28; Number of granules = 576

[f] Number of independent cultures = 1; Number of cells = 12; Number of granules = 589

[g] Number of independent cultures = 5; Number of cells = 51; Number of granules = 1367

3.9 Figures

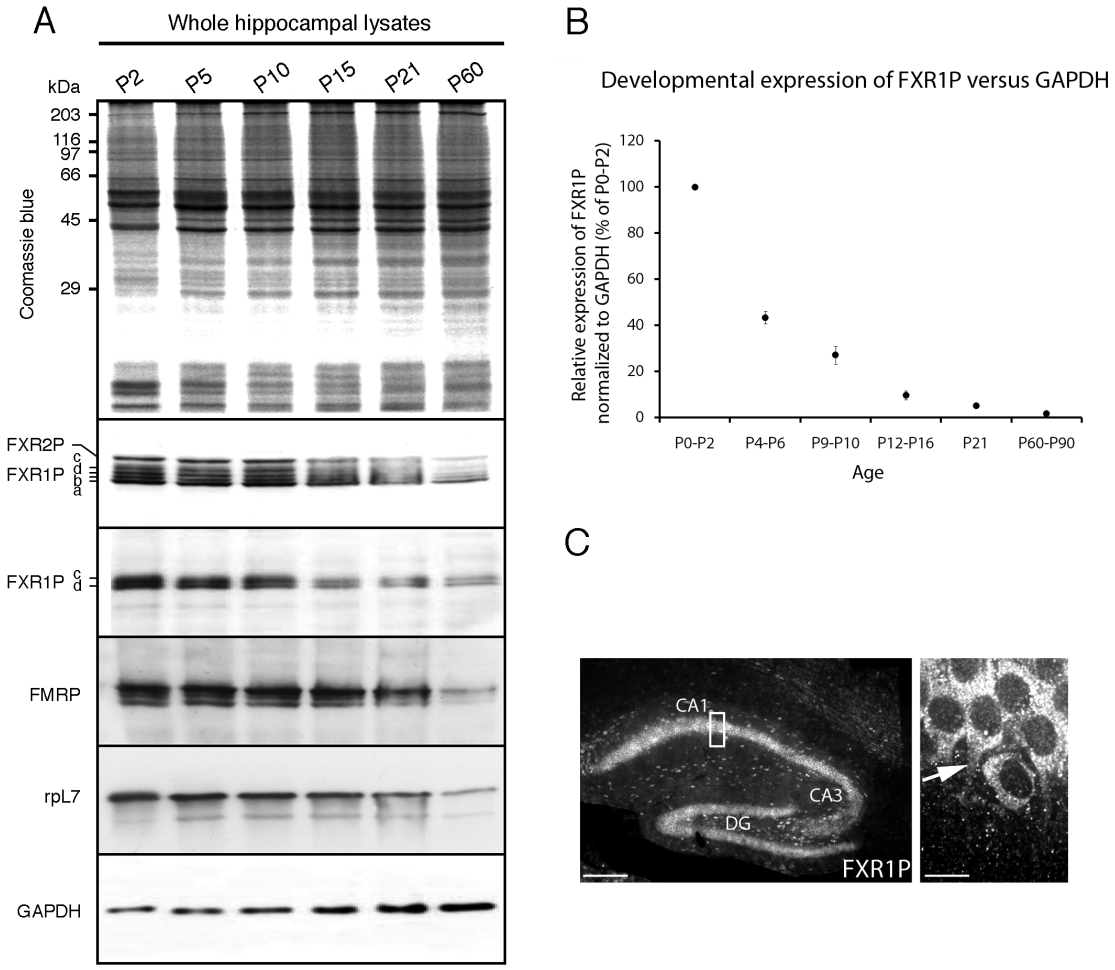

Figure 1: FXR1P is expressed in neurons of the developing hippocampus. A. Hippocampal lysates were prepared from mice at different developmental stages (P2= postnatal day 2) and analyzed for FXR1P, FXR2P, FMRP, L7 ribosomal protein and GAPDH. Isoforms of FXR1P (a.b,c,d), FXR2P, FMRP and ribosomal protein L7 were all highly expressed during early postnatal development in the hippocampus. **B.** FXR1P (isoforms c, d) expression across postnatal development was quantified and normalized against GAPDH expression. FXR1P levels decrease relative to GAPDH. **C.** We immunostained cryostat sections prepared from a P14 mouse with #ML13 and imaged the hippocampus at 10X (left panel). We found that FXR1P was highly expressed in neurons at P14. A 60X image of pyramidal neurons in area CA1 of the hippocampus (red box in 10X image) showing FXR1P expression in the cell body and proximal dendrites of CA1 neurons (right panel). Arrow points to a proximal dendrite found in the plane of the image. Scale bar = 60 µm (low magnification) and 10 µm (high magnification).

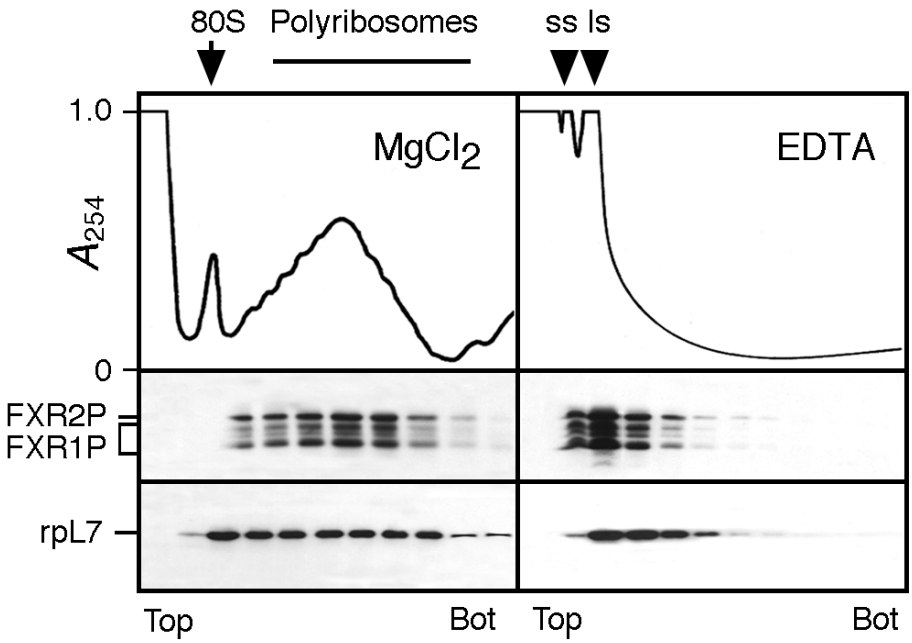

Figure 2: FXR1P is associated with polyribosomes in mouse brain extracts. Aliquots of native polyribosomes and EDTA treated polyribosomes were loaded onto linear 15-45% (w/w) sucrose gradients and centrifuged for 2 hr at 34 000 rpm at 4°C in a Beckman SW40 rotor. Each collected fraction was assayed for the presence of FXR1P and L7 ribosomal protein. Fractions from the top to the bottom of the gradient are shown from left to right and the position of the 80S ribosome monomer is indicated. SS, LS: ribosomal small and large subunits, respectively.

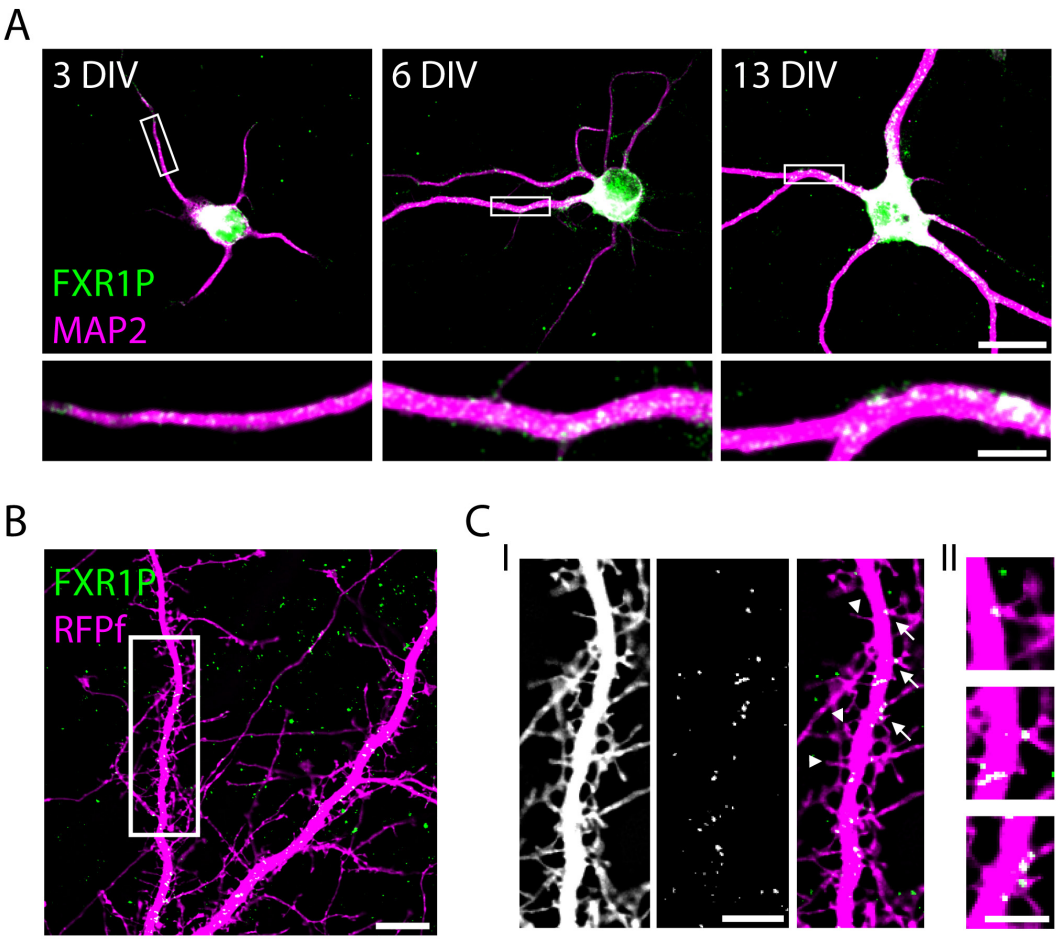

Figure 3: FXR1P forms clusters along the dendrite and at a subset of spine-like protrusions. A. We fixed dissociated hippocampal neurons at different developmental time-points and immunostained them with antibodies against FXR1P (#ML13; green) and MAP2 (dendritic marker; magenta). FXR1P formed clusters along dendrites at all developmental time-points. High magnification views of the segments outlined in white are shown below each image. We noted an increase in cluster size and intensity over time. Scale bar = 20 µm (low magnification) and 5 µm (high magnification). **B.** We transfected hippocampal neurons at 14 days *in vitro* with a plasmid encoding membrane targeted red fluorescent protein (RFPf) and immunostained for FXR1P. The single plane FXR1P image was thresholded to highlight the brightest clusters. FXR1P was found in clusters along the dendrite and at a subset of spine-like protrusions. Scale bar = 10 µm**. C. (I)** High magnification view of the segment of dendrite boxed in white in B. FXR1P clusters were found in the base, neck or head of a subset of dendritic spine-like protrusions. Arrows denote spine-like protrusions with an FXR1P cluster; arrowheads denote spine-like protrusions without an FXR1P cluster. DIV= days *in vitro*. Scale bar = 5 µm **C. (II)** High magnification view of the FXR1P-positive spine-like protrusions labeled in C. (I). Scale bar = 2.5 µm (high magnification).

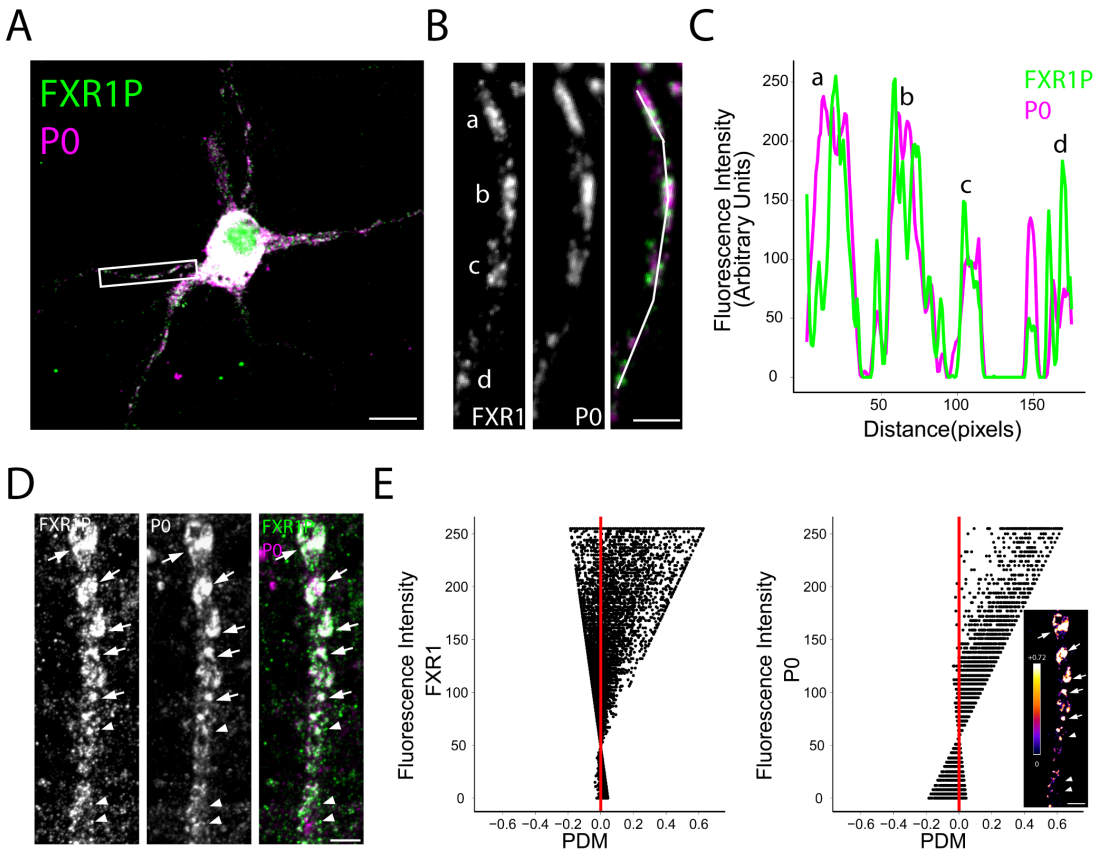

Figure 4: FXR1P colocalizes with ribosomes in clusters along the dendrite. A. Immunostaining of dissociated hippocampal neurons at 14 days *in vitro* with anti-FXR1P (#ML13) and anti-P0 shows a high degree of colocalization between FXR1P and P0 (white signal). Scale bar = 10 µm. **B.** High magnification view of the dendritic segment outlined in A. showing colocalization between FXR1P and P0 in clusters along the dendrite. Scale bar = 2.5 µm. **C.** Graph demonstrating the covariance in the fluorescence intensities of FXR1P and P0 along the dendritic segment traced in B. **D, E.** Example of the results obtained from the Intensity Correlation Analysis (ICA). Images showing FXR1P, P0 and merged staining (D). Arrows point to colocalized clusters of FXR1P/P0, whereas arrowheads point to bright FXR1P clusters lacking P0. Scale bar = 5 µm. In E, the fluorescence intensity of FXR1P and P0 was plotted against the Products of the Differences from the Mean (PDM) of that pixel. Pixels where fluorescence intensities are correlated are shown to the right of the red line; uncorrelated pixels are shown on the left. These graphs show that a large number of high intensity P0 and FXR1P pixels are correlated. However, a fraction of high intensity FXR1P pixels are not correlated with P0 intensity, whereas a fraction of low intensity P0 pixels are not correlated with FXR1P intensity. (Inset) Image showing the positive PDM produced using the ICA plugin in ImageJ. For clarity, only the PDMs for pixels with intensities above the mean are shown. An intensity lookup table has been applied to the image and is shown on the right. Scale bar = 5 µm.

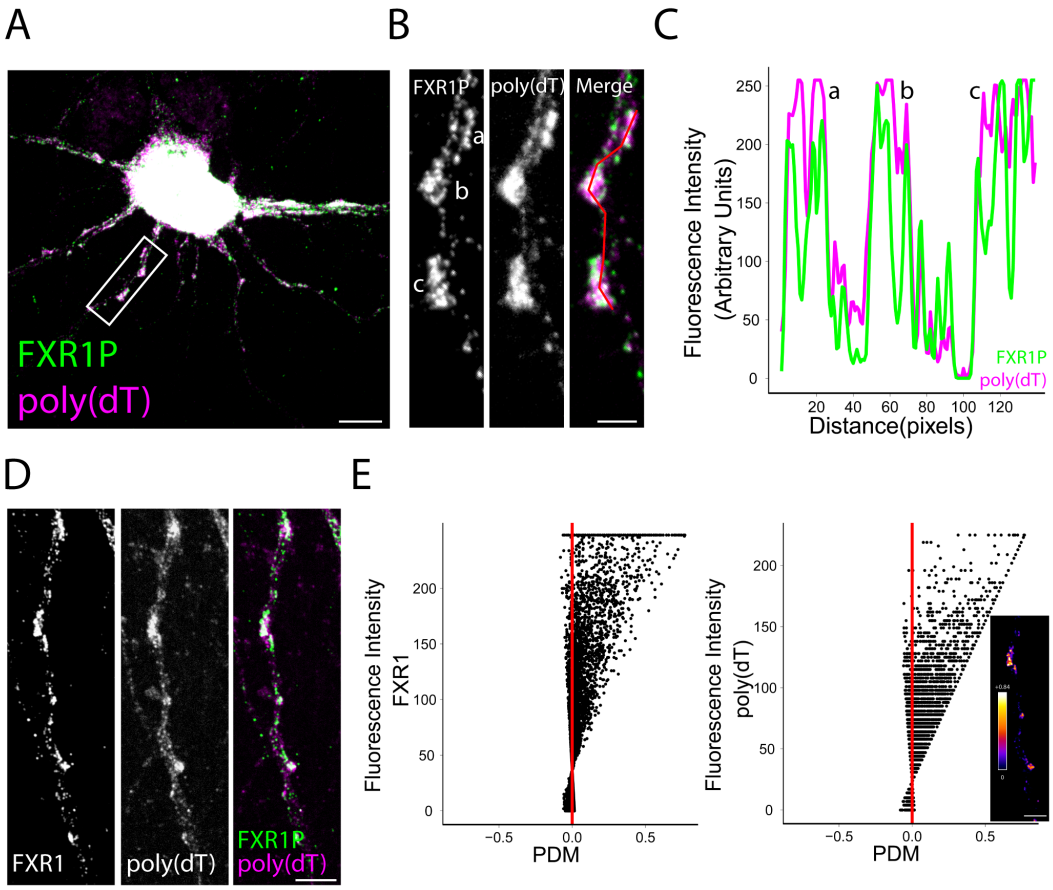

Figure 5: FXR1P colocalizes with mRNAs in clusters along the dendrite. A. We performed fluorescence *in situ* hybridization on dissociated hippocampal neurons at 14 days *in vitro* using a digoxigenin-labeled poly(dT) probe to detect poly(A)+ mRNAs. *In situ* hybridization was followed by immunostaining using anti-FXR1P (#ML13) and anti-P0 antibodies (data not shown). This merged image shows a high degree of colocalization between FXR1P and poly(dT) (white signal). Scale bar = 10 µm. **B.** High magnification view of the dendritic segment outlined in A. showing colocalization between FXR1P and poly(dT) in clusters along the dendrite. Scale bar = 2.5 µm**. C.** Graph showing covariance in the fluorescence intensities of FXR1P and poly(dT). **D, E.** Example of results obtained from the Intensity Correlation Analysis (ICA). D. Images showing FXR1P, poly(dT) and merged staining. Scale bar = 5 µm E. The fluorescence intensity of poly(dT) and FXR1P was plotted against the Product of the Differences from the Mean (PDM) of that pixel. Pixels where fluorescence intensities are correlated are shown to the right of the red line; uncorrelated pixels are shown on the left. These graphs show that the majority of FXR1P and poly(dT) pixels are correlated. Inset. Image showing the positive PDMs produced using the ICA plugin in ImageJ. For clarity, only the PDMs for pixels with intensities above the mean are shown. An intensity lookup table has been applied to the image and is shown to the right. Scale bar = 5 µm.

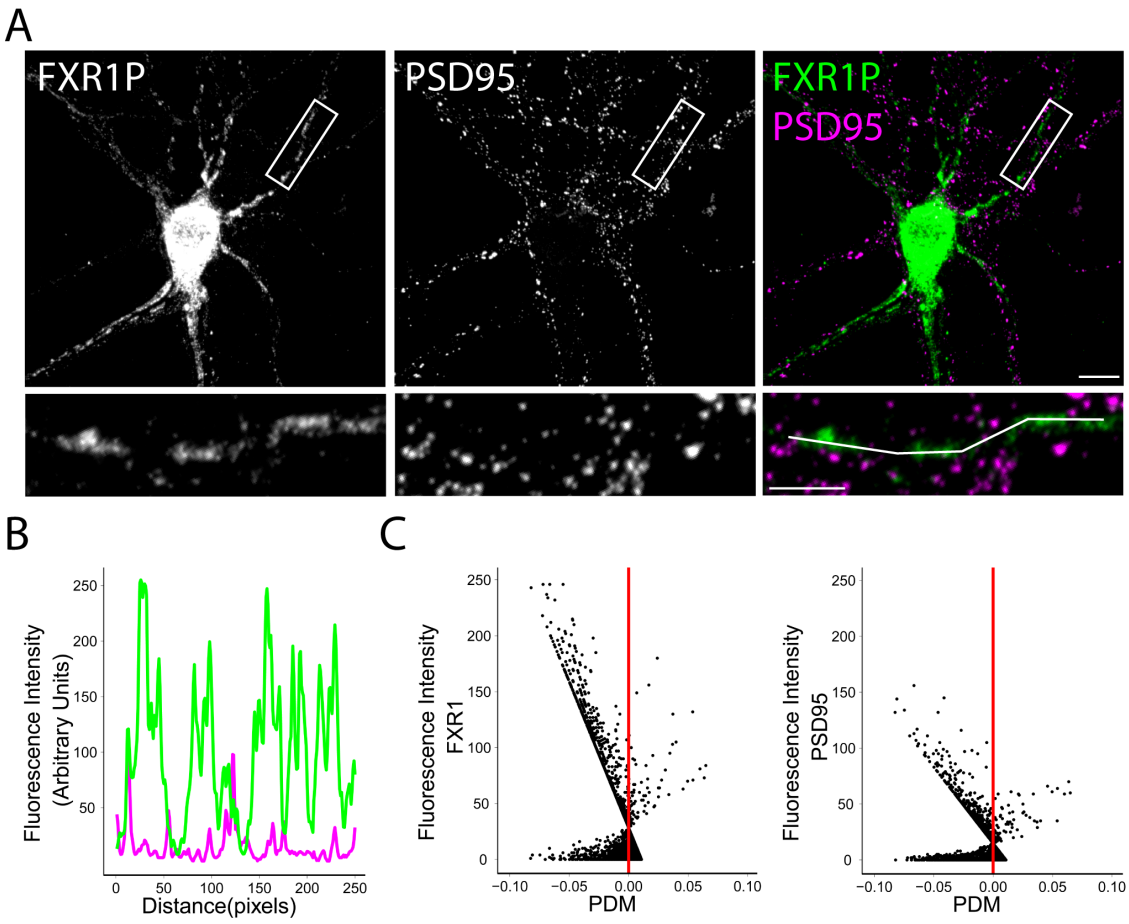

Figure 6: FXR1P does not colocalize with PSD95. A. We immunostained dissociated hippocampal neurons at 14 days *in vitro* using anti-FXR1P (#ML13) and anti-PSD95 antibodies. Single channel and merged images showing the lack of colocalization between FXR1P and PSD95. Scale bar = 10 µm. High magnification view of the dendritic segment outlined above are shown below. **B.** Graph showing the lack of covariance in the fluorescence intensities of FXR1P and PSD95 along the drawn line shown in A. **C.** Intensity correlation analysis of the segment shown in A. The fluorescence intensity of each PSD95 and FXR1P pixel was plotted against the Product Difference of the Mean (PDM) of that pixel. Pixels where fluorescent intensities are correlated are plotted to the right of the red line; uncorrelated pixels are plotted on the left. These graphs show that most of the pixels lie to the left of the red line, demonstrating a lack of colocalization between FXR1P and PSD95.

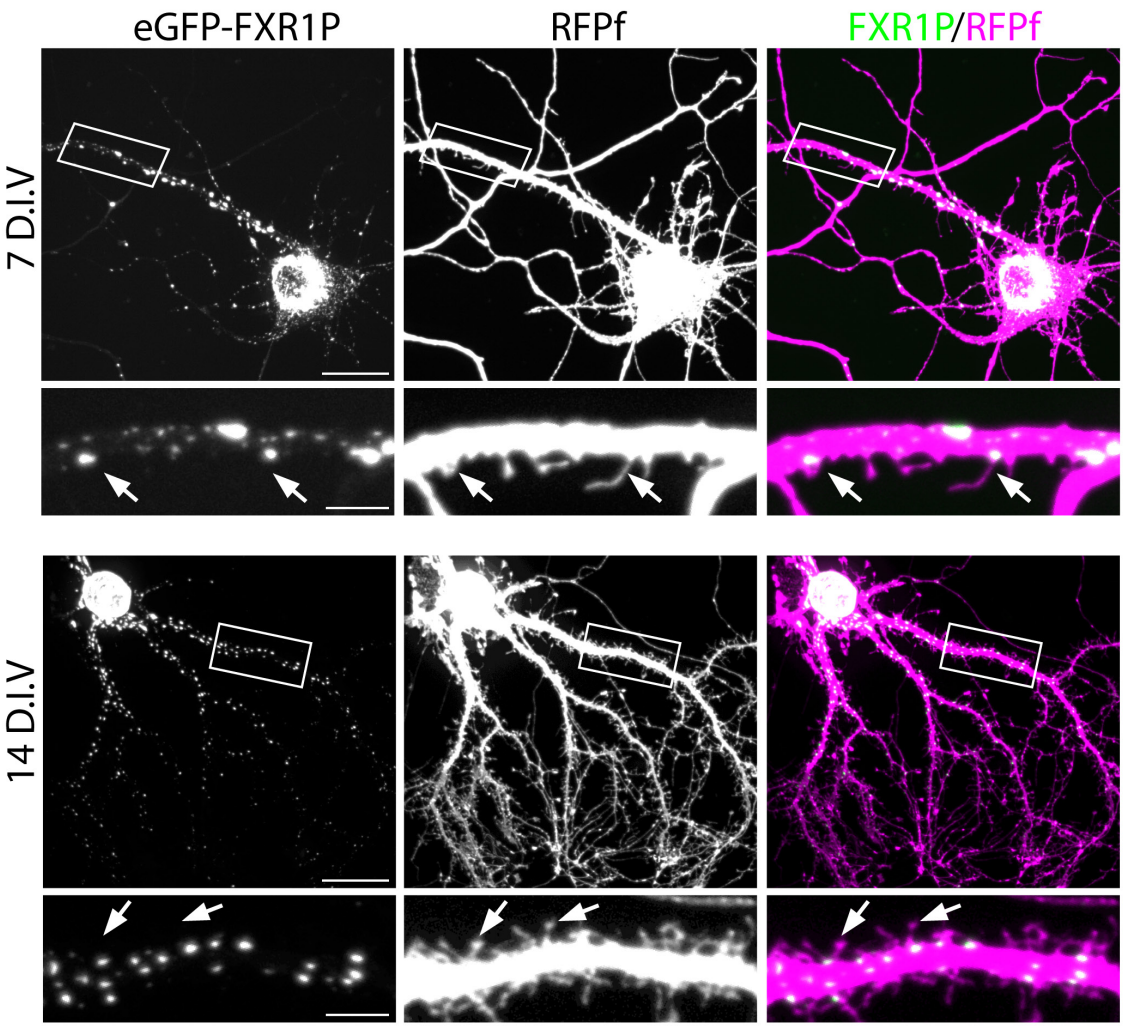

Figure 7: eGFP-FXR1P forms clusters along the dendrite and at spine-like protrusions in cultured neurons. We co-transfected hippocampal neurons grown for either 7 or 14 days *in vitro* with plasmids encoding membrane-targeted red fluorescent protein (RFPf) and eGFP-FXR1P. RFPf was used to visualize filopodia and spine-like protrusions. Here we show both low magnification and high magnification images of RFPf and eGFP-FXR1P at 7 and 14 days *in vitro.* We find that similar to endogenous FXR1P, overexpressed eGFP-FXR1P forms clusters of different sizes all along the dendritic shaft, with some of these clusters found close to filopodia and spine-like protrusions. Arrowheads point to filopodia and spines that are closely apposed by a bright eGFP-FXR1P cluster. Scale bar = 20 µm (low magnification) and 5 µm (high magnification). D.I.V= days *in vitro*.

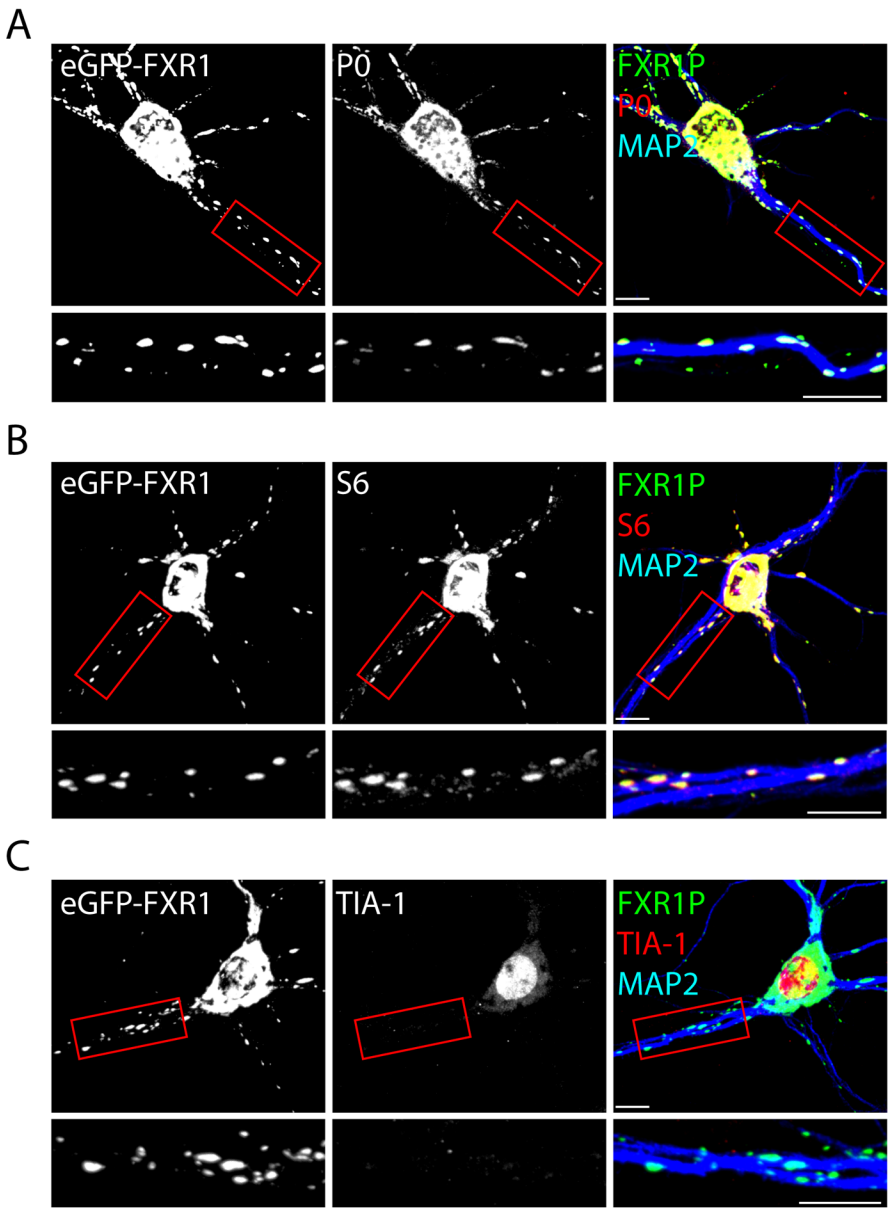

Figure 8: eGFP-FXR1P colocalizes with ribosomes. Dissociated hippocampal neurons were transfected with eGFP-FXR1P at 7 days *in vitro*. Cells were fixed after 24 hours and immunostained using an antibody against P0, a marker of the large ribosomal subunit (A), S6, a marker of the small ribosomal subunit (B), and TIA-1, an RNA-binding protein and marker of stress granules (C). In all cases, neurons were also immunostained with an antibody against MAP2 to delineate the proximal dendrites. We find that the majority of eGFP-FXR1P clusters contain strong signals for P0 and S6, but not TIA-1. The same results are seen at 14 days *in vitro* (data not shown). Results of the colocalization analyses are shown in Table 2. Scale bar = 10 µm.

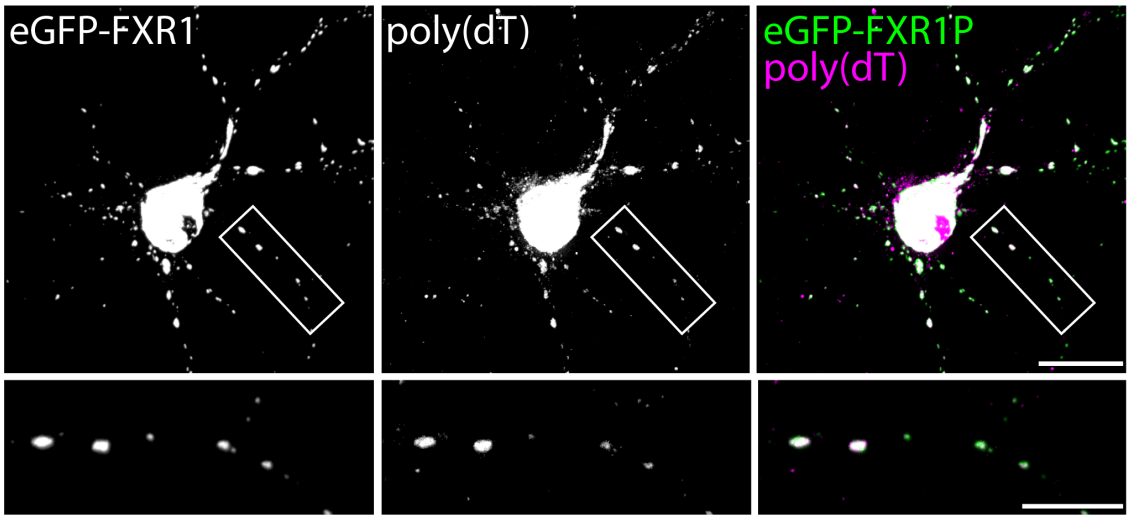

Figure 9: eGFP-FXR1P colocalizes with mRNAs. Dissociated hippocampal neurons were transfected with eGFP-FXR1P at 14 days *in vitro*. Cells were fixed after 24 hours and hybridized with a digoxigenin-labeled poly(dT) probe to detect poly(A)+ mRNAs. *In situ* hybridization was followed by immunostaining for GFP and P0 (data not shown). We found that the majority of eGFP-FXR1P clusters contain mRNAs. Results of the colocalization analyses are shown in Table 2. Scale bar = 20 μm (low magnification) and 10 μm (high magnification).

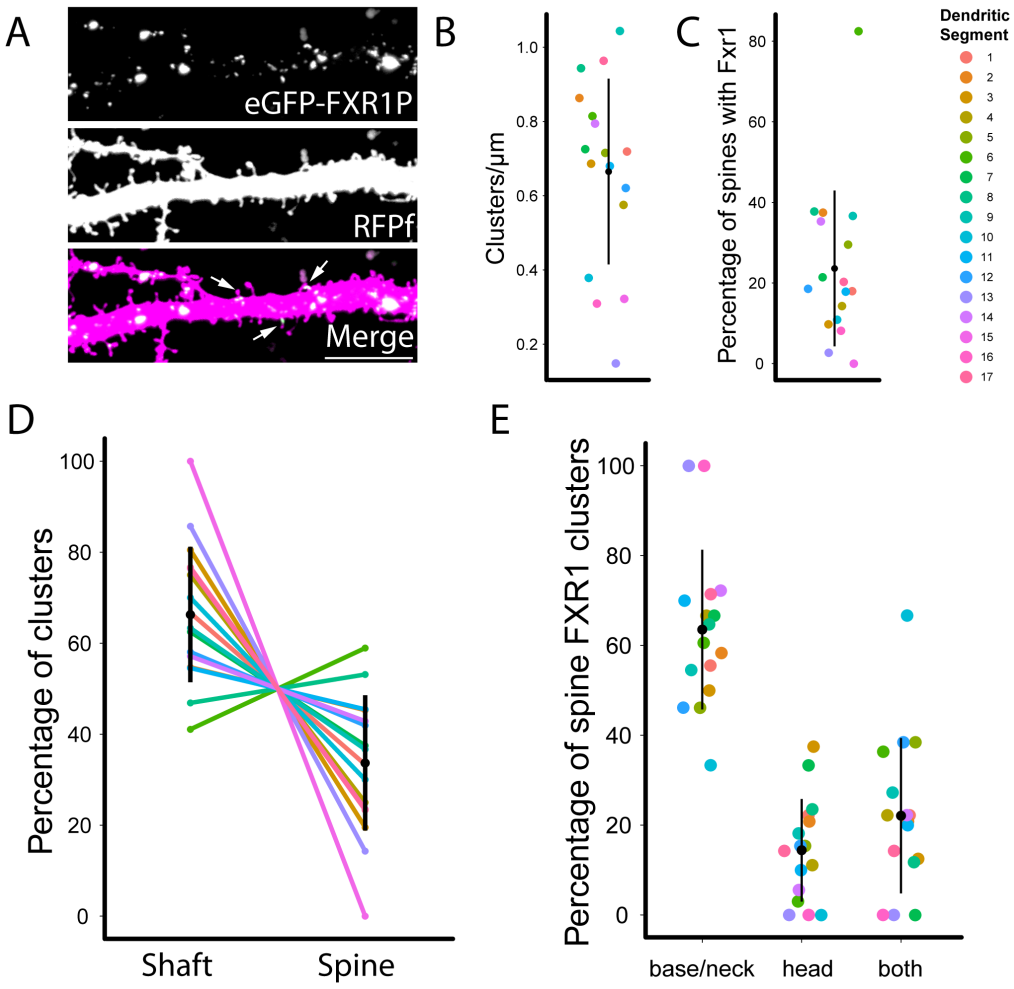
A
eGFP-FXR1P
RFPf
Merge
B
Clusters/µm
1.0
0.8
0.6
0.4
0.2
C
Percentage of spines with Fxr1
80
60
40
20
0
Dendritic Segment
1
2
3
4
5
6
7
8
9
10
11
12
13
14
15
16
17
D
Percentage of clusters
100
80
60
40
20
0
Shaft
Spine
E
Percentage of spine FXR1 clusters
100
80
60
40
20
0
base/neck
head
both

Figure 10: eGFP-FXR1P clusters are found at the base of a subset of dendritic spines. We transfected organotypic hippocampal slices at 7 days *in vitro* with plasmids encoding eGFP-FXR1P and membrane targeted red fluorescent protein (RFPf). The slices were fixed after 48 hours and CA1 apical dendrites were imaged using confocal microscopy. We quantified the subcellular localization of eGFP-FXR1P with respect to the dendrite and dendritic spines. **A.** A representative image of an apical dendrite of a CA1 cell. eGFP-FXR1P clusters are found along the dendrite and at a subset of spines. Arrows point to spines with a closely apposed eGFP-FXR1P cluster. **B.** We found that the density of eGFP-FXR1P clusters was variable and averaged 0.67 ± 0.25 clusters/μm (mean ± SD). **C.** eGFP-FXR1P clusters were found at a subset of dendritic spines. On average, eGFP-FXR1P clusters were found at 23.6 ± 19.34% of spines (mean ± SD). **D.** The majority of clusters were found in the dendritic shaft (shaft = 66.3%, spine = 33.7%). **E.** eGFP-FXR1P spine clusters are more likely found at the base and neck of the dendritic spine versus the spine head (base/neck = 63.5%, head = 14.4%). Each dendritic segment is color coded to allow comparison between the different measurements. The black dot and vertical bar represent mean ± standard deviation (SD). Data represent 17 dendrites imaged from 4 independent slice cultures.

3.10 Supplementary Figures

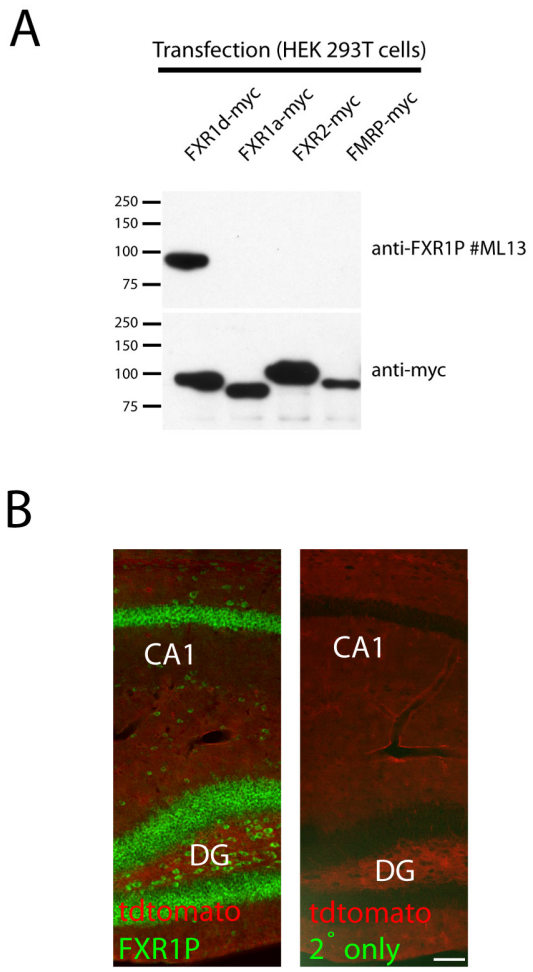

Figure S1: #ML13 is specific for FXR1P. A. We transfected HEK 293T cells with plasmids encoding myc-tagged Fragile X proteins. We found that antibody #ML13 recognized FXR1P isoform d and did not cross-react with closely related family members FXR2 and FMRP. An antibody against myc confirmed that all proteins were successfully overexpressed. **B.** We immunostained cryostat sections prepared from a P18 td-tomato expressing mouse with #ML13 and secondary antibody only (Alexa Fluor goat anti-rabbit 647; Invitrogen) and imaged the hippocampus at 10X (left panel). Scale bar = 80 µm.

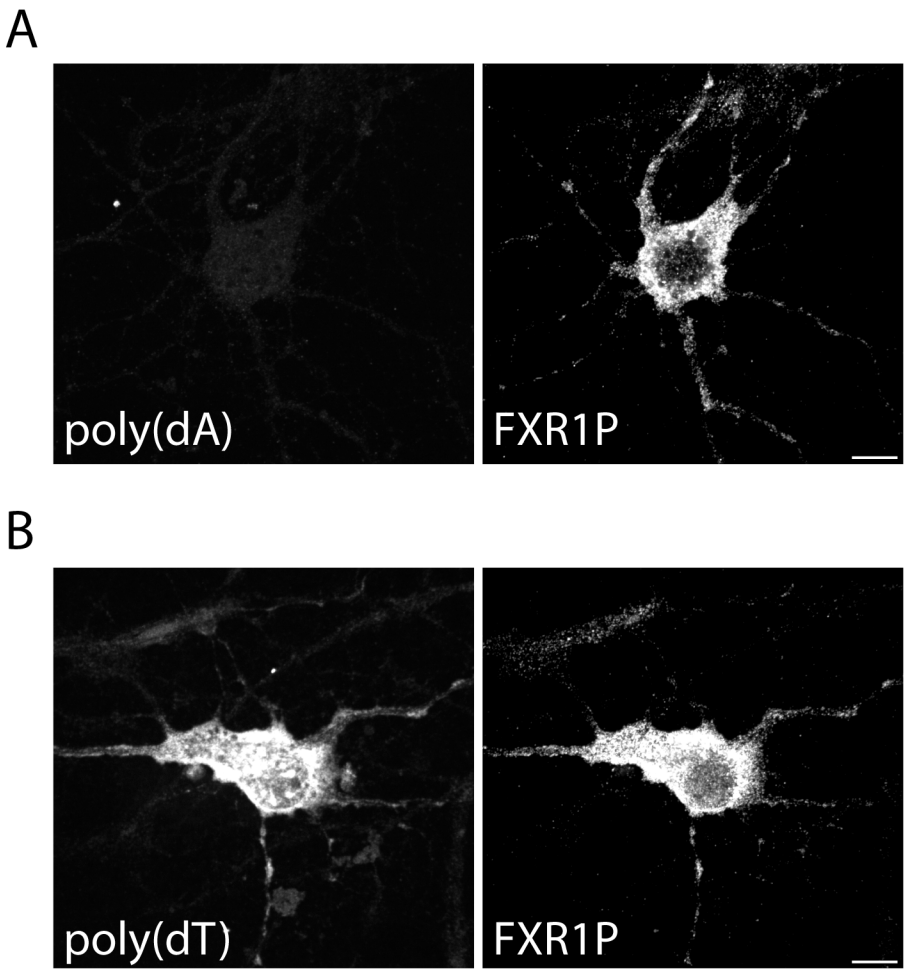

Figure S2: poly (dA) control shows no staining. Fluorescence *in situ* hybridization using a digoxigenin-labeled poly(dA) probe as an antisense control and immunostaining for FXR1P (#ML13). Brightness and contrast have been adjusted equally on the images to demonstrate the level of background staining from the poly (dA) probe. Scale bars = 10 μm.

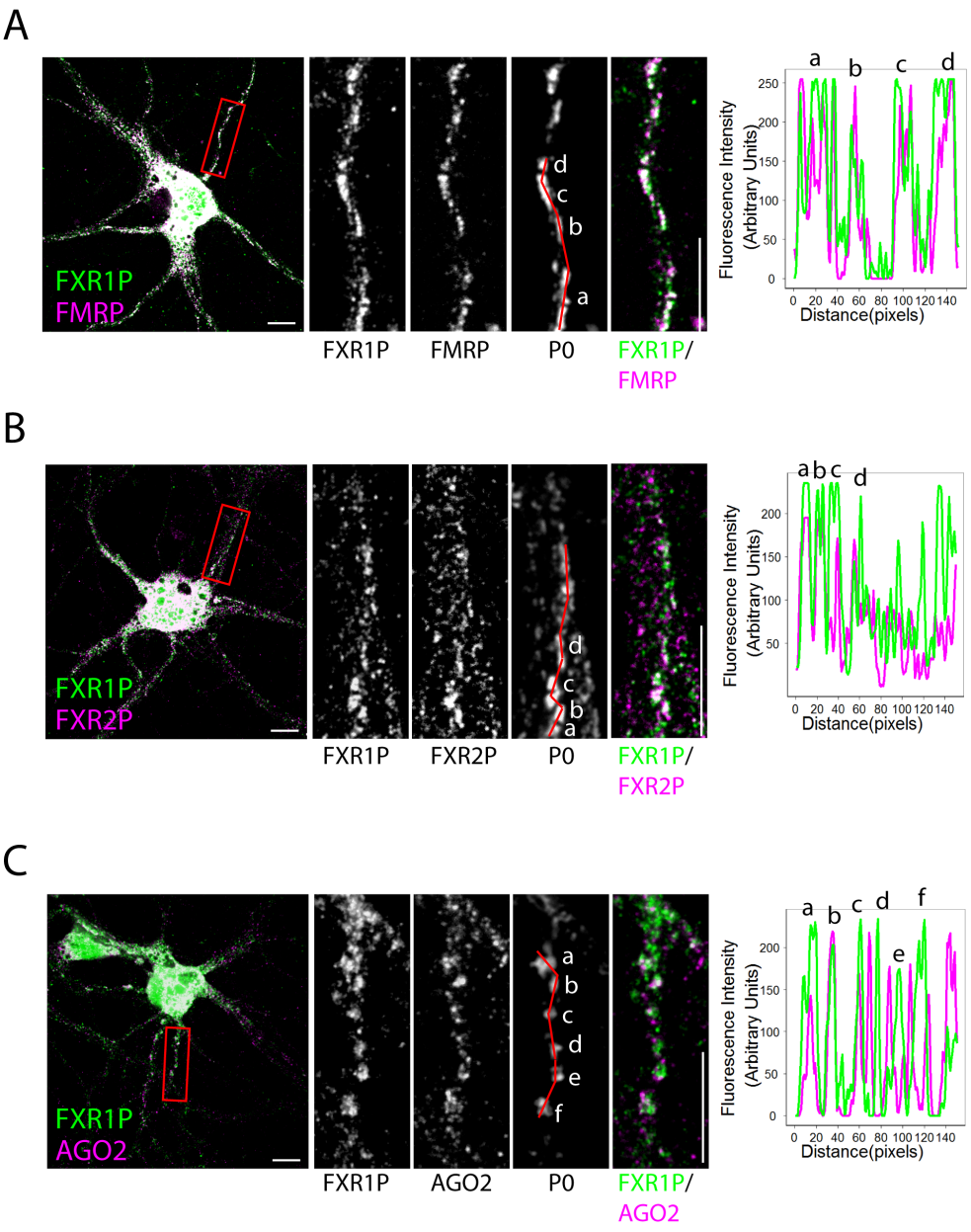

Figure S3: FXR1P partially colocalizes with FMRP, FXR2P and Argonaute 2 in clusters along the dendrite. Immunostaining of dissociated hippocampal neurons at 14 days *in vitro* with anti-FXR1P (#ML13) and A. anti-FMRP (1C3), B. anti-FXR2P (A42) and C. anti-Ago2 antibodies demonstrate partial colocalization of FXR1P with these three known interacting proteins (P0 staining is also shown for comparison). Note that Ago2 also shows complementary staining with FXR1P, with Ago2 more likely to be found at the edges of the P0 clusters and FXR1P in the center. Graphs with labeled peaks demonstrating the covariance (or complementary staining in the case of Ago 2) in the fluorescence intensities along the dendritic segment are shown at the right. Scale bars = 10 µm.

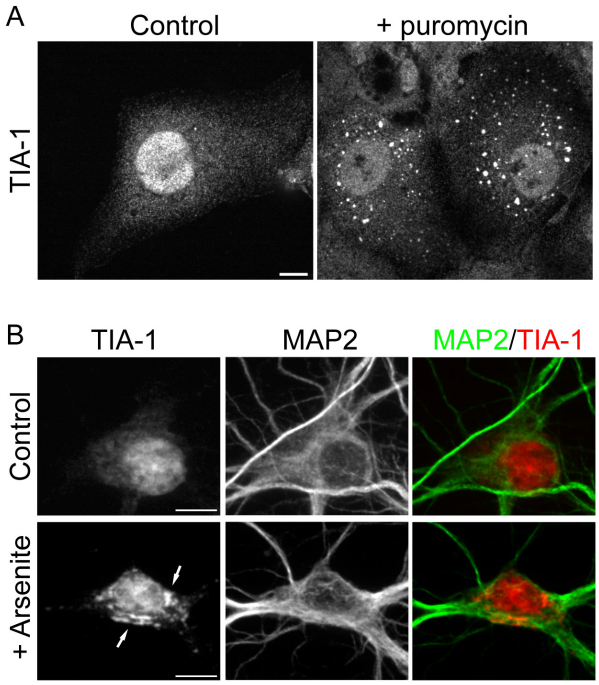

Figure S4: TIA-1 redistributes to stress granules. A. COS-7 cells were treated with 20 µg/ml puromycin for 2 hours, followed by immunostaining for TIA-1. A small percentage of COS-7 cells display clearly visible TIA-1 positive cytoplasmic granules. Scale bar = 10 µm. **B.** Dissociated hippocampal neurons were treated with 0.5 mM arsenite for 30 minutes and immunostaining for TIA-1. Neurons showed the characteristic redistribution of TIA-1 into cytoplasmic granules. Scale bar = 10 µm.

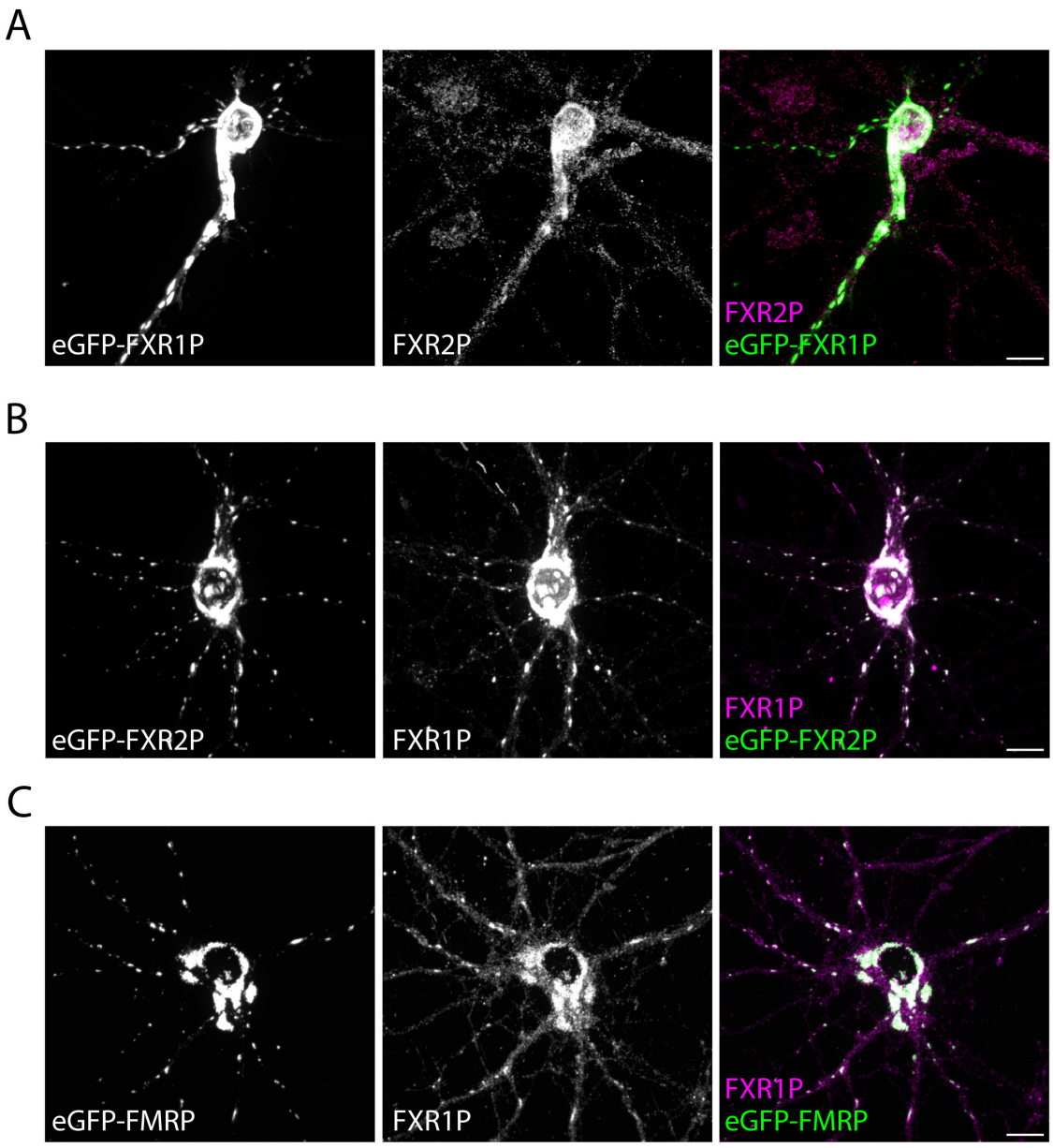

Figure S5: Fragile X Proteins colocalize with each other. Dissociated hippocampal neurons were transfected with **A.** eGFP-FXR1P, **B.** eGFP-FXR2P and **C.** eGFP-FMRP at 7 days *in vitro*. Cells were fixed after 24 hours and immunostained using an antibody against **A.** FXR2P (A42), **B, C.** FXR1P (#ML13). **A.** Endogenous FXR2P partially colocalizes with eGFP-FXR1P in large clusters. **B, C.** Endogenous FXR1P colocalizes with eGFP-FMRP (B) and eGFP-FXR2P (C). Scale bars = 10 µm.

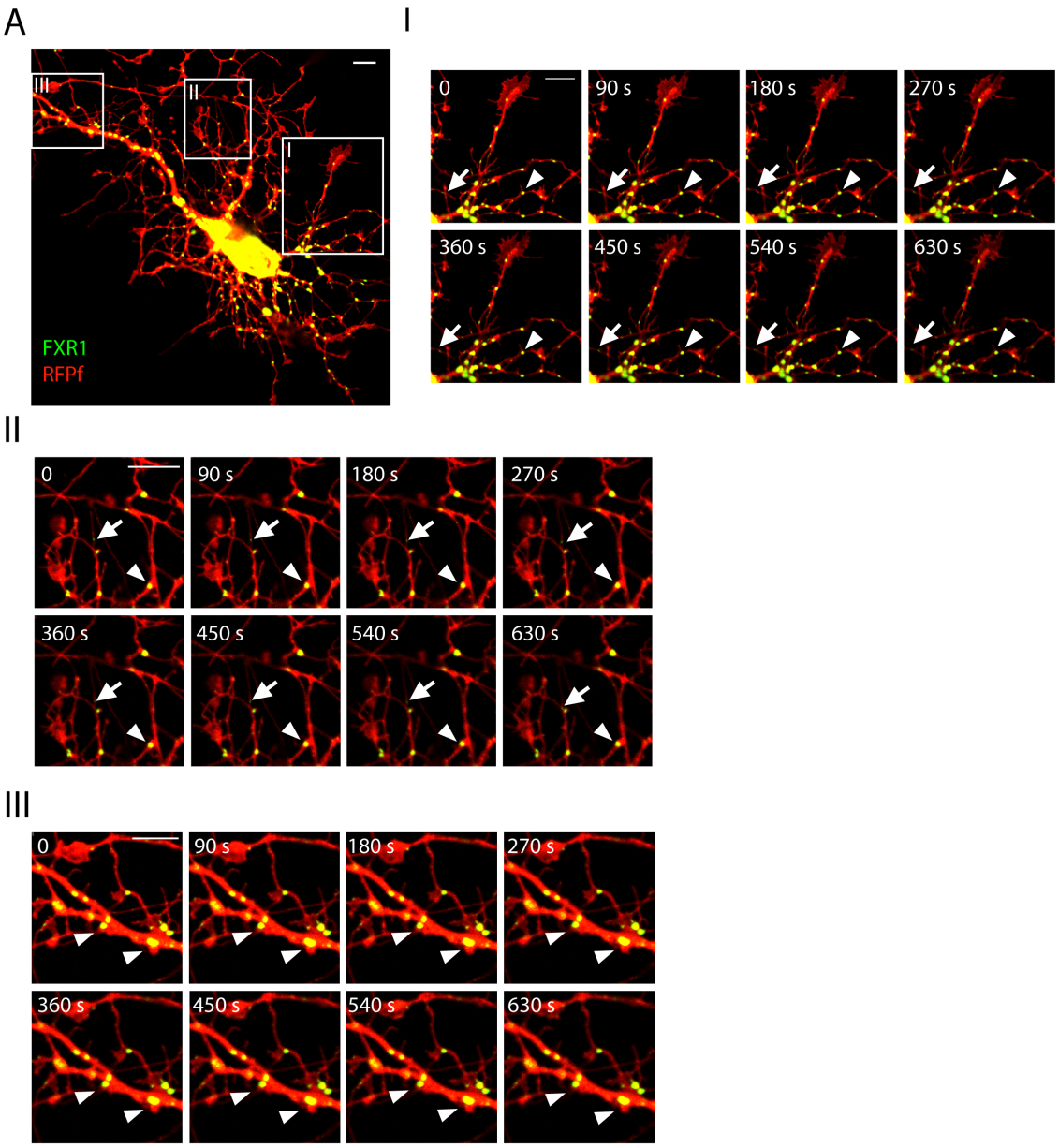

Figure S6: FXR1P clusters are immobile. A. Live hippocampal neuron transfected with RFPf and eGFP-FXR1P. **I, II, III.** Three examples of the FXR1P clusters imaged over time (images were taken every 8 seconds over 15 minutes). The majority of the FXR1P clusters were found to be immobile over this time-frame. Arrowheads denote immobile clusters while Arrows in I and II denote small clusters that were found to move over time. Scale bar = 10 μm.

CHAPTER 4:

FRAGILE X RELATED PROTEIN 1 PREFERENTIALLY CLUSTERS AT LARGE SPINES WITH STRONG SYNAPSES

Denise Cook, Jean-Claude Béique, Keith K. Murai

4.1 Relationship to overall project

In chapter 3 we presented results demonstrating that endogenous and exogenous FXR1P associates with ribosomes and mRNAs at a subset of dendritic spines in hippocampal CA1 neurons. These results suggested to us that FXR1P could be controlling the local translation of mRNAs important for spine plasticity. To test this, we decided to study the effect of overexpressing FXR1P on the structural and functional properties of spines. This chapter presents our results from these experiments.

4.2 Abstract

Memory formation and storage in the brain rely on rapid and sustained changes in the number, size and strength of dendritic spines. These rapid changes require the synthesis of new proteins from messenger RNAs, a process which can occur locally in the dendrite and at activated spines. The translation of specific messenger RNAs is controlled by several neuronal RNA binding proteins, including Fragile X mental retardation protein (FMRP) and Fragile X related protein 1 (FXR1P). FMRP associates with the translational machinery at dendritic spines and is thought to control the local translation of mRNAs important for synapse elimination. We recently showed that like FMRP, FXR1P associates with ribosomes and mRNAs in the dendrite and at a subset of dendritic spines. However, it is not known whether FXR1P also controls the translation of mRNAs important for maintaining spine number, structure and function. Here, we wanted to investigate whether overexpressing FXR1P would lead to a change in the number, structure or function of dendritic spines. To test this we used confocal imaging and whole-cell electrophysiological recordings to compare spine number,

spine size and synaptic function between control and FXR1P-expressing CA1 cells in organotypic hippocampal slice cultures. We found no overall differences in spine number, spine morphology or spine shape. As FXR1P clusters are found at only a subset of dendritic spines, we then went on to compare the structure and function of FXR1P-positive and FXR1P-negative spines using confocal imaging and two-photon glutamate uncaging. We found that FXR1P-positive spines were larger and stronger than their negative counterparts. Since large, strong spines are generally considered to be more mature, our results suggest that FXR1P may be locally regulating the translation of mRNAs important for spine maturation or maintenance.

4.3 Introduction

Memories are thought to be stored through the strengthening or weakening of excitatory synaptic connections in the brain. The vast majority of these synaptic connections form onto dendritic spines, small protrusions from the dendrite which come in a variety of shapes and sizes [194]. The different spine shapes and sizes offer a structural correlate of synaptic function, since spine volume is correlated with synaptic strength [49,50]. Despite the majority of spines being relatively stable over long periods of time [195,196], their sizes and shapes are constantly in flux, reflecting both intrinsic fluctuations and activity-dependent changes to spines [197–200]. Indeed, researchers have found that small spines are more likely to undergo activity-dependent increases in size than large spines, which are relatively stable with life expectancies of months to years [197]. This has led to the proposal that small spines are likely to function in learning whereas large spines are more likely to be involved in the storage of old memories [198]. Although spine size is regulated by the increase in expression of many proteins, including scaffolding proteins such as PSD95 and Shank [201], exactly how synaptic activity leads to a spine-specific increase in the levels of these proteins is currently unknown.

There is growing evidence that local protein synthesis plays an important role in the rapid and sustained increases in dendritic spine structure and function that occur after synaptic stimulation. Local protein synthesis occurs through the

activity-dependent recruitment of polyribosomes and mRNAs to dendritic spines [75,190] and is required for long-lasting increases in spine size and synaptic strength [47,48,58,83]. This process is tightly controlled by several neuronal RNA-binding proteins, including Fragile X mental retardation protein (FMRP), which bind to subsets of mRNAs and control either their transport, local translation or stability [12]. The importance of these regulatory processes to spine structure, as well as learning, is supported by the fact that patients who do not express FMRP have Fragile X syndrome, a disorder characterized by immature-looking spines and intellectual disability [18,54]. FMRP binds to approximately 800 brain mRNAs and controls their activity-dependent translation [20,136]. Accumulating evidence suggests that FMRP functions downstream of the transcription factor MEF2 to control mRNAs involved in spine elimination [143,202], further implicating the control of local protein synthesis as an important mechanism for regulating spine number and size.

We recently began to characterize the expression and localization of another Fragile X protein, Fragile X Related Protein 1 (FXR1P), in the developing mouse hippocampus. FXR1P is an RNA-binding protein which controls the translation of several mRNAs in non-neuronal cells [32,33,156]. Although present in several brain regions, including the hippocampus and Purkinje cells in the cerebellum, very little is known about the function of FXR1P in neurons [21,22]. We have previously shown that FXR1P, similar to FMRP, associates with polyribosomes and mRNAs in the dendrite and at a subset of dendritic spines [23]. However it is not known whether FXR1P, like FMRP, controls the local translation of mRNAs required for spine plasticity. Studying this will help elucidate FXR1P's functional role in neurons and may point to a fundamental role for FXR1P in synaptic plasticity and memory formation. We hypothesized that increasing FXR1P levels in hippocampal neurons would change spine density, spine morphology or synaptic function. To test this, we compared FXR1P expressing neurons with control neurons using a combination of confocal imaging, electrophysiological recordings and two-photon glutamate uncaging. We found that FXR1P expressing neurons had similar spine properties and synaptic

function to control cells. However, further analysis comparing FXR1P-containing spines with their negative neighbors determined that FXR1P was more likely to associate with large, mushroom-shaped spines with strong synapses. These results support the idea that FXR1P controls or maintains spine size and synaptic function through an influence on local mRNA translation.

4.4 Materials and Methods

Ethics Statement with regards to animal use. Mice: All mice used in this study (both male and female) were from a wild-type C57BL/6 strain bred in our animal facility. All experiments involving mice were approved by the Montreal General Hospital Facility Animal Care Committee (Protocol ID#5758) and followed the guidelines of the Canadian Council on Animal Care.

Rats: All rats used in this study were Sprague-Dawley pups obtained from timed-pregnancies ordered from Charles River (Charles River Laboratories International, Wilmington, MA).

cDNA plasmids. Farnesylated monomeric red fluorescent protein (RFPf) in pcDNA3 and eGFP-FXR1P were described previously [23,176]. We have previously shown that eGFP-FXR1P clusters with translational machinery at spines, similar to endogenous FXR1P [23]. The mCherry plasmid was a kind gift from Dr. Mollie Meffert. Expression from all constructs was driven by the CMV promoter.

Mouse organotypic hippocampal slices and RFPf/eGFP-FXR1P transfection (for imaging experiments). Hippocampal slices were prepared from postnatal day 7 (P7) mouse pups according to previously published methods [23,175]. Slices were transfected using the Helios Gene Gun system [203] (Bio-Rad, Hercules, CA). Gold bullet preparation and biolistic transfection have been previously described [23]. Briefly, 25 µg of RFPf and 25 µg of empty pcDNA3 plasmid (control) or 25 µg of eGFP-FXR1P and 25 µg of RFPf plasmid DNA (FXR1P) were precipitated onto 25 mg of gold and propelled into hippocampal slices at 7 days in vitro using helium at 110-130 psi. Slices were fixed for imaging 48 hours after transfection.

*Rat organotypic hippocampal slices and mCherry/eGFP-FXR1P transfection (for electrophysiological experiments and two-photon glutamate uncaging).*Rat hippocampal slices were prepared from P8 rat pups sacrificed by rapid decapitation after halothane or isoflurane anesthesia. The brains were removed and placed in ice-cold dissection medium (in mM): 119 choline chloride, 2.5 KCl, 4.3 $MgSO_4$, 1 $CaCl_2$, 1 NaH_2PO_4, 26.2 $NaHCO_3$, 1 kynurenic acid, 11 glucose, 1.3 ascorbic acid. The hippocampi were removed and then placed on a piece of agar and sliced using a guillotine-like tissue slicer (San Diego Instruments, San Diego, CA). Slices were then transferred back into cold dissection medium, separated using fine forceps and placed onto individual filter membranes on top of membrane inserts (Millipore, Billerica, MA) in 1 ml of MEM Media (50% Minimal Essential Media, 25% Hank's Balanced Salt Solution, 25% heat-inactivated horse serum, 1% penicillin/streptomycin and 0.5% L-glutamine) or Neurobasal Media (85% Neurobasal A, 10% heat-inactivated horse serum, 2% B27, 2% Glutamax, 1% penicillin/streptomycin, 0.5% HEPES, 0.68% D-glucose). Media was changed every two-three days. Unless otherwise noted, chemicals were obtained from Sigma-Aldrich (St.Louis, MO) and media solutions were obtained from Gibco (Invitrogen, Burlington, ON).

Slices were transfected at 8 days in vitro using the Helios Gene Gun system. In this case, gold bullets were prepared using 40 µg of eGFP-FXR1P and 10 µg mCherry. Bullets were coated onto Tefzel tubing according to standard protocols, except polyvinylpyrrolidone (PVP) was omitted to facilitate gold removal from the tubing during shooting. Gold was propelled into the slices at 180 psi through a 100 um nylon filter. All electrophysiological experiments were performed two days after transfection.

Confocal imaging CA1 dendrites were imaged using an oil immersion objective (60X Plan Fluor, 1.25 numerical aperture) mounted on an Ultraview spinning disk confocal system (PerkinElmer, Wellesley, MA) connected to an Eclipse TE2000 (Nikon, Tokyo, Japan). Excitation band pass filters are as follows: 488, 568 and 647 nm (+/- 10nm). Emission band pass filters are as follows: 525 +/- 50 nm, 607 +/- 45 nm and 700 +/- 75 nm. The primary apical dendrites of CA1 pyramidal

cells (~100 μm from the cell body and close to the point of bifurcation of the apical dendrite) were acquired in the red (RFPf, control dendrites) or both red and green channels (RFPf/eGFP-FXR1P, FXR1P expressing dendrites) using Metamorph (Molecular Devices). Z-stacks were produced using a z-step of 0.3 μm. We imaged 26 control dendrites and 17 FXR1P expressing dendrites across multiple slices cultured from four mouse litters. Note that the 17 FXR1P expressing dendrites are the same as those used to quantify FXR1P cluster location in our previous publication [23].

Analysis of spine parameters using Reconstruct. To analyze spine density and spine morphology in Reconstruct, we created separate maximum projection images for eGFP-FXR1P and RFPf. The RFPf images for both control and FXR1P expressing dendrites were thresholded linearly in Photoshop (Adobe Systems, Seattle, WA) and imported into Reconstruct with the proper X, Y calibration settings. Since only RFPf images were used, analysis of spines was performed blind to the treatment of the dendrite and also blind to the location of FXR1P clusters. For each image, we measured the length of a small dendritic segment (range: 20-70 μm) and counted the number of spines along that length (range: 20-90 spines). A threshold was set in Reconstruct for semi-automated tracing of dendritic spines using the wildfire tool. We then manually traced the spine head perimeter, spine head length and width, neck width and total spine length. Average spine density and spine morphology was then compared between control and FXR1P expressing dendrites.

In order to determine whether FXR1P-positive spines differed in morphology from FXR1P-negative spines, we overlaid the perimeter drawings from the RFPf images with the eGFP-FXR1P images. Spines were labeled as "FXR1P-positive" if an FXR1P cluster was found within its traced perimeter [23]. Average spine parameters were compared between "FXR1P-positive" and "FXR1P-negative" spines on the same dendrite. Dendrites with less than four FXR1P-positive spines were excluded from the analysis.

Analysis of spine parameters and spine shapes using three-dimensional automated quantification in NeuronStudio. In order to determine whether FXR1P expression changed spine shapes or whether FXR1P preferentially localized to a particular type of spine, we repeated the above analysis using NeuronStudio, a program which allows for three-dimensional automated quantification of spine shapes and parameters [204]. This program uses local adaptive thresholding and rayburst sampling techniques in order to detect and classify spines. Spine parameters are measured using a two-dimensional rayburst algorithm in order to find the maximum three-dimensional spine length and spine head diameter from an image stack while minimizing the effect of optical smear in the axial direction. Three-dimensional analysis eliminates potential artifacts produced by analyzing spines in two-dimensions. A dendritic segment was first cropped from each image stack and deconvolved using AutoDeblur's 3D blind deconvolution algorithm with standard settings for confocal microscopy (Autoquant, Media Cybernetics, Maryland). 16-bit deconvolved image stacks were then loaded into NeuronStudio. All analysis was performed blind to condition. Voxel size was set to X: 0.109 μm Y: 0.109 μm, Z: 0.300 μm. Neurites and spines were detected and classified as mushroom, stubby or thin using default settings. Neurite lengths ranged from 30-80 μm with 30-130 spines analyzed per segment. Spine detection was verified using the 3D viewer and any erroneous spines were removed. Average spine parameters and proportion of spine shapes were then compared between control and FXR1P expressing dendrites.

Since NeuronStudio only supports single-channel images, deconvolved images were then opened in Imaris (Bitplane, Zurich, Switzerland) and each spine quantified by NeuronStudio was scored manually for the presence or absence of an FXR1P cluster using Imaris's 3D volume rendering tools. Measurements and spine shape classification were then used to determine whether FXR1P spines differed in size and shape from FXR1P-negative spines.

Whole-cell electrophysiological recordings. Transfected and untransfected hippocampal CA1 cells in cultured slices were detected using a 40X water-objective with a 0.80 numerical aperture (Olympus LUMPlanFL N) or a 60X

water-objective with a 1.00 numerical aperture (Olympus LUMPlanFL N; for two-photon uncaging experiments) with infrared differential interference contrast imaging (DIC) and epifluorescence imaging mounted on an Olympus Fluoview FV1000 MPE Twin multiphoton system or using Dodt contrast and epifluorescence imaging on a Zeiss AX10 upright microscope. Once identified using epifluorescence imaging, targeting of transfected cells for whole-cell patch-clamp recording using DIC or Dodt imaging was facilitated by the presence of a gold particle inside the cell nucleus. Slices were maintained in a submersion chamber perfused at approximately 1 ml/min with normal Ringer solution (in mM): 119 NaCl, 2.5 KCl, 1.3 $MgSO_4$-$7H_2O$, 2.5 $CaCl_2$-$2H_2O$, 1 NaH_2PO_4-H_2O, 26.20 $NaHCO_3$, 11 Glucose (295-300 mOsm) saturated with 95% O_2/5% CO_2. For intracellular recordings, cells were voltage clamped at -70 mV using whole-cell recording pipettes (World Precision Instruments PG10165-4; 3-4 MΩ) pulled with a vertical puller (Narishige model PC-10) and filled with one of two internal solutions (in mM): 115 cesium methanesulfonate, 0.4 EGTA, 5 TEA-Cl, 2.8 NaCl, 20 HEPES, 4 Mg ATP, 0.5 GTP, 5 QX-314 and 10 Na_2 phosphocreatine (mEPSC recordings) or 77 cesium methanesulfonate, 10 tetracesium BAPTA, 5 TEA-Cl, 3 CaCl2, 20 HEPES, 4 ATP (Mg salt), 0.50 GTP, 5 QX-314, 10 sodium phosphocreatine (two-photon experiments) with or without 30 μM Alexa 594. The pH was adjusted to 7.3 and osmolality to 280-290 mOsm. Electrical signals were recorded using a Multiclamp 700B amplifier (Axon Instruments, Foster City, CA). All recordings were carried out at room temperature. Recordings were filtered at 2 KHz, digitized at 10 KHz and acquired with Clampex (Axon Instruments). Liquid junction potentials and voltages were left uncompensated. Starting access resistance was typically below 20 MΩ and was monitored continuously by delivering a 3-5 mV hyperpolarizing voltage step at the beginning of each sweep. Experiments were discarded if the access resistance was unstable.

For mEPSCs recordings, normal Ringer solution was supplemented with 0.1 mM picrotoxin (dissolved in DMSO, 0.05% final concentration) and 0.5 μM TTX. Analysis was carried out using a template search in Clampfit 10.3. The

template was created using a minimum of 10 events taken from an experimental trace. Events were detected using a combination of automatic detection by the software and visual inspection. Analysis was performed blind to transfection state of the neuron. The average amplitude and frequency of mEPSCs was first determined for each cell and then averaged together according to the experimental group. Cumulative probability plots were constructed using a random sampling of 200 events from each experimental group.

Two-photon uncaging of MNI-Glutamate. Whole-cell recordings were obtained following the standard procedures mentioned above except that the intracellular recording solution was always supplemented with 30 μM Alexa Fluor 594 (Molecular Probes, Eugene, OR) to visualize cell and spine morphology. Addition of Alexa Fluor 594 was necessary since we were incapable of acquiring bright enough images using the mCherry signal at the wavelengths required to image eGFP-FXR1P. External solution was composed of 2.5 mM MNI-Glutamate (Tocris, Ellisville, MO or Femtonics, Budapest, Hungary) dissolved in normal Ringer solution saturated with 95% O_2/5% CO_2. A 4 ml solution of MNI-Glutamate was recycled via a peristaltic pump for the duration of the experiment. Optimal imaging of Alexa 594 and eGFP-FXR1P was obtained at 900 nm and uncaging of MNI-glutamate was performed at 720 nm using a 60X, 1.0 numerical aperture water-objective, thereby minimizing the uncaging spot (Mai Tai mode-locked Ti-Sapphire lasers; Newport Spectra Physics). Clearly visible spines located on basal dendrites less than *ca.* 100 μm from the cell body and extending in parallel to the plane of imaging were chosen for uncaging. We chose sections of dendrites with at least one FXR1P-positive spine. The uncaging spots were placed at the tip of 2-4 spines at an angle perpendicular to the dendrite using Olympus Fluoview v10 software. Uncaging was performed by illuminating each spot with 720 nm light for 1.0 ms at an interval of 300 – 500 ms and monitoring the underlying excitatory postsynaptic currents (2P-EPSCs) in voltage-clamp mode. This was repeated 5-10 times at 0.1 Hz to obtain average amplitudes for AMPA receptor currents (-70 mV) and 12-15 times to obtain average amplitudes for NMDA receptor currents (+40 mV). The uncaging spot was sometimes

repositioned during the course of an experiment to compensate for drifting. Laser power was kept constant for spines on the same dendritic segment and generally was the same during a single imaging session. Since statistical comparisons were made on neighboring spines from the same dendrite, no effort was made to standardize laser power across different dendritic segments and experimental days.

Statistical Analysis. All statistical analyses were performed using R (http://www.R-project.org) [178] with the following packages installed: Reshape [205], Hmisc[179], gplots [206]and plotrix [207]. Unpaired analyses between two groups of data were performed using two-tailed Welch t-tests. Paired analyses between two groups of data were performed using two-tailed paired t-tests. A two-way mixed (1 between, 1 within factor) ANOVA was performed on overall spine shape data. Chi square tests were performed on proportion data for FXR1P spine shapes. When the chi square test was found to be significant, a post hoc test was performed according to [208]. Briefly, we identified the row with the largest contribution to the chi-square total, eliminated it from the contingency table and repeated the chi-square test on the reduced table. For all tests, $p<0.05$ was chosen for statistical significance. The specific test used for each experiment is noted in the figure legends. All graphs were created using base graphics implemented in R except for cumulative probability plots which were plotted using the Ecdf function from Hmisc.

4.5 Results

Overexpression of FXR1P does not change spine number, morphology or function

We previously showed that eGFP-FXR1P forms discrete clusters along the dendrite and at the base of a subset of spines, similar to endogenous FXR1P [23]. These clusters contain ribosomal subunits and mRNAs suggesting that FXR1P could control mRNA translation at spines [23]. Since local mRNA translation is thought to play an important role in long-lasting structural and functional changes

to dendritic spines, we wanted to determine if overexpression of FXR1P would change spine number, morphology or function.

To test whether FXR1P caused any structural changes to spines during early postnatal development, we biolistically transfected CA1 pyramidal cells in hippocampal slices cultured from P7 mice at 7 days *in vitro* with either a farnesylated red fluorescent protein (RFPf), used to delineate fine processes such as dendritic spines, or a combination of RFPf and eGFP-FXR1P. After 48 hours of transfection, slices were fixed, mounted and imaged using a confocal microscope. We found that overexpressed eGFP-FXR1P clustered along the dendrite and at spines, a pattern we previously reported [23]. A total of 26 control (RFPf only) dendritic segments and 17 FXR1P expressing (RFPf/eGFP-FXR1P) dendritic segments were imaged and analyzed using either Reconstruct or NeuronStudio (see methods). Using both of these methods we found that overexpression of FXR1P caused no overall changes in spine density, spine length or spine head diameter (Figures 1-2). In addition, overexpression of FXR1P did not alter spine shapes (Figure 2D). Therefore, overexpression of FXR1P for forty-eight hours did not have a significant influence on the structure of CA1 pyramidal spines.

Although spine size and spine function are generally correlated [49], the overexpression or loss of certain proteins can sometimes lead to a dissociation between these two features [209,210]. To determine whether FXR1P regulates synapse function independently of synaptic structure, we overexpressed FXR1P in CA1 pyramidal cells at 8 days *in vitro* in hippocampal slices cultured from P8 rats and obtained whole-cell electrophysiological recordings from FXR1P expressing (mCherry/eGFP-FXR1P) and untransfected control cells forty-eight hours post-transfection. We measured synaptic function by looking at spontaneous miniature excitatory postsynaptic potentials (mEPSCs) measured in the presence of tetrodotoxin (TTX) to block action potentials. The amplitude of the mEPSCs is indicative of the strength of individual synapses, whereas the frequency of the mEPSCs is a read-out of either the number of synapses or presynaptic release probability [43]. We found that overexpression of FXR1P did not cause a change in

mEPSC amplitude nor frequency at this developmental stage (Figure 3), supporting the structural results above and suggesting that FXR1P does not have an overall effect on synapse number, synapse strength or presynaptic release probability.

FXR1P associates with large, mushroom shaped spines with strong synapses

We previously showed that FXR1P clusters are found along the length of the dendrite but target only a small subset of dendritic spines, approximately 20% [23]. Since the large majority of these clusters are immobile over the time-course of minutes to hours, we asked if there might be differences in structure or function between the spines containing FXR1P clusters and non-containing spines. Using the same structural dataset used above, we scored each spine for the presence or absence of an FXR1P cluster. A spine was scored as FXR1P-positive if it contained an FXR1P cluster within its traced perimeter (Reconstruct) or if it visually contained an FXR1P cluster in 3D volume reconstructions (Imaris). A representative image of the localization of FXR1P clusters at spines is shown in Figure 4A. By comparing spines scored as FXR1P-positive to neighboring FXR1P-negative spines we found that FXR1P-positive spines were on average 16% longer ($p=0.00098$) and had 16% larger spine head diameters ($p=0.0073$) than FXR1P-negative spines (Figure 4C, D). Using the shape-analysis features of NeuronStudio, we found that FXR1P-positive spines were more likely to be mushroom-shaped than expected from the proportions of mushroom, stubby and thin spines across the dendrites analyzed (Figure 4B; χ^2 goodness-of-fit $p<0.00001$). We were also able to confirm the differences in spine length ($p=0.006$) and spine head diameter ($p=0.004$) between FXR1P-positive and FXR1P-negative spines when the data was re-analyzed in three dimensions using NeuronStudio (Figure 5). These results demonstrate a structural difference between FXR1P-containing and non-containing spines.

Since the structural and functional properties of dendritic spines do not always correlate, we wanted to determine whether the increase in spine size was concomitant with an increase in synaptic strength. In order to compare synaptic function at FXR1P-positive and FXR1P-negative spines, we turned to two-photon

glutamate uncaging, a method which allows researchers to probe synaptic function at the level of the individual synapse. For this experiment, rat hippocampal slices prepared at P8 were biolistically transfected at 8 days *in vitro* with mCherry and eGFP-FXR1P. Forty-eight hours post-transfection, transfected cells, bathed in 2.5 mM MNI-glutamate, were identified and targeted for whole-cell electrophysiological recordings. Cells were filled with Alexa 594 to delineate dendritic spines. An image of a patched, transfected CA1 pyramidal cell is shown in Figure 6A (left). We then identified a segment of basal dendrite containing at least one FXR1P-positive spine and zoomed in until individual FXR1P-positive and FXR1P-negative spines were clearly visible (Figure 6A, right). A spine was scored as FXR1P-positive if it contained an FXR1P cluster at the base, neck or head of the spine. Post-hoc analysis of eGFP-FXR1P fluorescence intensity confirmed that FXR1P-positive spines contained at least two-fold higher integrated signal intensity than FXR1P-negative spines. Glutamate was then uncaged in succession (300-500 ms delay) at selected spines (Figure 6B) at both -70 mV and +40 mV. FXR1P-positive spines were directly compared to their negative neighbors thus minimizing the influence of differences in local laser intensity on current amplitudes. We found that FXR1P-positive spines had 50% larger AMPAR-mediated two-photon uncaging-evoked EPSCs amplitudes (2P-EPSCs, -70 mV) than their negative neighbors ($p=0.011$; Figure 6B, C). Importantly, NMDA receptor-mediated responses were unchanged as the average 2P-EPSC amplitude measured at 100 ms after the peak amplitude at + 40 mV was similar between positive and negative spines ($p=0.71$; Figure 6D). Spines that were probed using two-photon glutamate uncaging were also visually categorized into mushroom, stubby and thin. This analysis confirmed that FXR1P-positive spines were more likely to be mushroom-shaped than their negative counterparts (Figure 7; Pearson's chi-square test $p=0.006$). These results demonstrate that FXR1P-positive spines have increased synaptic strength compared to their negative neighbors.

4.6 Discussion

We previously demonstrated that FXR1P clustered with ribosomes and mRNAs at ~20% of dendritic spines, pointing to a potential role for FXR1P in controlling mRNA translation at spines [23]. Here, we demonstrate that FXR1P clusters preferentially at a subset of large, mushroom-shaped spines with greater synaptic strength without changing overall spine density, spine size or spine shape.

Since FXR1P is present only at ~20% of spines, it is perhaps not surprising that we were unable to detect any differences in overall spine density, spine size or strength. One potential explanation for this lack of overall change is that FXR1P is only performing its function locally at a subset of spines, and since the changes at each spine are quite small, this change is diluted when we look at the properties of all the spines together. However, because the difference is only seen when we compare FXR1P(+) to FXR1P(-) spines, it is important to keep in mind that our results point simply to a correlation between the presence of an FXR1P cluster and the size and strength of the spine [23]. We are therefore unable to distinguish between the possibility that FXR1P is targeting large, strong spines or is directly causing them to get bigger and stronger in the first place. Regardless, preferential localization at large, strong spines, which represent the mature population of dendritic spines, suggests that FXR1P may play some local role in maintaining or creating mature spines.

Since dendritic spines grow and get stronger in response to certain patterns of synaptic activity, FXR1P clusters could be tagging recently activated spines. If this is the case, one would expect FXR1P clusters to be mobile and to move towards active spines. Although we previously found that the majority of FXR1P clusters in dissociated hippocampal cultures are immobile, certain small clusters are mobile even in these spontaneously active cultures [23]. This result predicts that certain patterns of synaptic activity may be able to stimulate the movement of FXR1P clusters towards spines. Indeed, researchers have found that RNA-binding proteins and mRNAs increase their motility when neurons are stimulated using bath application of BDNF or DHPG, pharmacological agents known to induce

protein synthesis and synaptic plasticity [13,108]. In addition, polyribosomes appear to redistribute from the dendritic shaft into a subset of large spines after L-LTP [190] leading to the idea that translational machinery moves towards active synapses to support spine growth or maintenance. In order to test whether this holds true for FXR1P, two-photon glutamate uncaging could be used to induce L-LTP at single FXR1P(-) synapses and movement in surrounding FXR1P clusters could be monitored using time-lapse imaging [47,48].

In addition to being associated with polyribosomes after L-LTP, large spines are also more likely to contain a spine apparatus, synaptopodin and the endoplasmic reticulum [211–214]. The spine apparatus is an extension of the smooth endoplasmic reticulum and is thought to be involved in activity-dependent spine growth or spine stabilization [214]. Synaptopodin, an actin-binding protein, is tightly associated with the spine apparatus [214,215]. Mice lacking synaptopodin also lack the spine apparatus and have impaired LTP and learning [216], suggestive of a role for synaptopodin in regulating spine plasticity. Indeed, Vlachos et al.[217] demonstrated that overexpressed synaptopodin is associated with spines that are 50% larger and stronger than synaptopodin negative spines. Additional evidence for specialized organelles, proteins and plasticity mechanisms at large spines comes from a study conducted by Holbro et al.[213]. They found that an eGFP-tagged marker of the ER was more prevalent at large, strong spines [213]. ER(+) but not ER(-) spines showed mGluR-dependent calcium-induced calcium release events and expressed mGluR-dependent long-term depression [213]. These results suggest that large spines have specialized organelles and proteins which may aid in their maturation, stabilization and ability to undergo synaptic plasticity. It would be interesting to determine whether FXR1P(+) spines are also associated with the ER and synaptopodin and/or whether FXR1P controls the local translation of mRNAs important for setting up these structures.

One important issue to raise is whether FXR1P clusters are found at large spines simply because of space issues. Is FXR1P randomly distributed in the dendrite and its association with large spines a coincidence due to hindrance? There are two reasons that make this unlikely. First, unlike the spine apparatus,

synaptopodin and the ER which are found invading the spine or associated with the spine head or neck, FXR1P clusters are more than twice as likely to be found at the base of the spine versus the spine head; the spine base, being a part of the dendrite, presumably offers no hindrance to FXR1P clusters [23]. Secondly, FXR1P clusters are associated with a population of spines that, on average, are larger and stronger than the surrounding spines. This does not necessarily mean that FXR1P clusters are always found at the base of the largest, strongest spines on the dendrite, but that on the whole, the population of FXR1P containing spines is larger and stronger than FXR1P negative spines. These results support the idea that the association between FXR1P and spines is not simply a coincidence due to hindrance or random localization, but instead that FXR1P associates with a subset of spines with distinct structural and functional properties.

One long-standing issue in the Fragile X field is whether the autosomal paralogs of FMRP, FXR1P and FXR2P, can compensate functionally for the loss of FMRP [31]. All three proteins associate with polyribosomes and mRNAs, are found at dendritic spines and are expressed in similar patterns in the mammalian central nervous system, begging the question of whether they perform redundant functions [21,22,24]. However, the fact that loss of FMRP leads to intellectual disability and altered spine density and spine morphology in humans means that the other two paralogs, which show normal expression patterns in human patients, cannot compensate for all FMRP functions [54]. In support of this, Coffee et al.[218] have found that human FMRP, but not human FXR1P nor FXR2P, is able to rescue neuronal deficits in the Drosophila *Fmr1* null. We have extended these findings by demonstrating that in mammalian hippocampal neurons, overexpression of FXR1P results in a different phenotype than overexpression of FMRP. Whereas postsynaptic expression of FMRP caused synapse elimination, we found that FXR1P overexpression caused no differences in spine density or mEPSC frequency [143]. This suggests that FXR1P is not involved in new spine growth or spine elimination. Instead, we found that FXR1P associated with a subset of large, strong dendrites spines, suggestive of a role for FXR1P in activity-dependent spine maturation or spine stabilization.

If FMRP and FXR1P are playing different roles at spines, the next question one can ask is whether FMRP and FXR1P share the same or different mRNA targets. FXR1P and FMRP share some functional redundancy in binding to kissing complex RNAs, at least *in vitro* [192]. FMRP binds to approximately 800 brain mRNAs *in vivo*, including PSD95, CaMKIIα, Arc and MAP1B, all proteins which are involved in modulating spine shape and function [20,98,145,164,219,220]. Similar studies have yet to be conducted to identify FXR1P target mRNAs in the brain. However, researchers have identified several FXR1P targets in non-neuronal tissues, including *TNFα*, *talin2* and *desmoplakin* mRNAs [32,33,156]. Interestingly, glial-derived TNFα increases AMPA receptor content at synapses when action potential firing is suppressed [221]. Whether FXR1P controls the local synthesis and release of TNFα from neurons to influence synaptic plasticity is unknown. Talin2 and Desmoplakin may also control spine plasticity through their roles as adhesion complex proteins linking transmembrane proteins such as integrins and cadherins to the actin cytoskeleton. Although a role for Talin2 and desmoplakin at spines has yet to be demonstrated, it is intriguing to note that integrins and cadherins both play important roles in controlling spine plasticity [222]. Whether *talin2* and *desmoplakin* are also FXR1P mRNA targets in neurons remains to be demonstrated. Therefore, at least in terms of these identified targets, it seems likely that FMRP and FXR1P may be controlling distinct, but perhaps overlapping, populations of mRNAs. These differences may help explain the differing roles for these two proteins at dendritic spines.

How is FXR1P controlling its target mRNAs? Results suggest that FXR1P plays a role at the level of mRNA translation and not mRNA stability, although this could be target-dependent [32,33,156]. In two separate studies, FXR1P was shown to both repress and enhance the translation of *TNFα* mRNA, raising the intriguing possibility that FXR1P could be having a context-dependent influence on mRNA translation [32,33]. Indeed, converging evidence suggests that both FXR1P and FMRP function with the microRNA-RNA-induced silencing complex (miRNA-RISC) to control mRNA translation in a context and activity-dependent manner [32,145]. In line with this, FXR1P, but not FXR2P nor FMRP, was found to regulate

the processing of the brain-specific pre-miR-9 and pre-miR-124, again demonstrating a unique role for FXR1P [223]. Based on these results we propose that FXR1P suppresses the translation of mRNAs as they are transported and stored in the dendrite. Upon synapse activation, FXR1P clusters mobilize to the spine and enhance the translation of mRNAs important for increasing or maintaining spine size and synaptic strength.

We have shown that FXR1P preferentially clusters at large, mature spines. Since spines mature in an activity-dependent manner, this result suggests that FXR1P controls the activity-dependent translation of mRNAs important for spine growth or spine maintenance. Since large spines are thought to represent long-lasting memories, FXR1P may also be important for learning and memory. In this regard, it is interesting to note that polymorphisms in the *Fxr1p* gene are associated with autism-spectrum disorders and schizophrenia [158,159], disorders that are linked to abnormal synapses or brain connectivity. Therefore, proper FXR1P function could be required for normal spine growth, neuronal connectivity and learning and memory.

4.7 Acknowledgements

This work was supported by the Canadian Institutes of Health Research, Canada Research Chairs Program, Canadian Foundation for Innovation and the National Institutes of Health grant 1R21DA026053-01 (U.S.A) (K.K.M.). D.C. was supported through a Frederick Banting and Charles Best CIHR Doctoral Research Award and an FRSQ Doctoral Award. The authors would like to thank Dr. Danuta Radzioch (McGill University) for the eGFP-FXR1P construct and Dr. Roger Tsien (Howard Hughes Medical Institute; UCSD) for the mRFP construct.

4.8 Figures

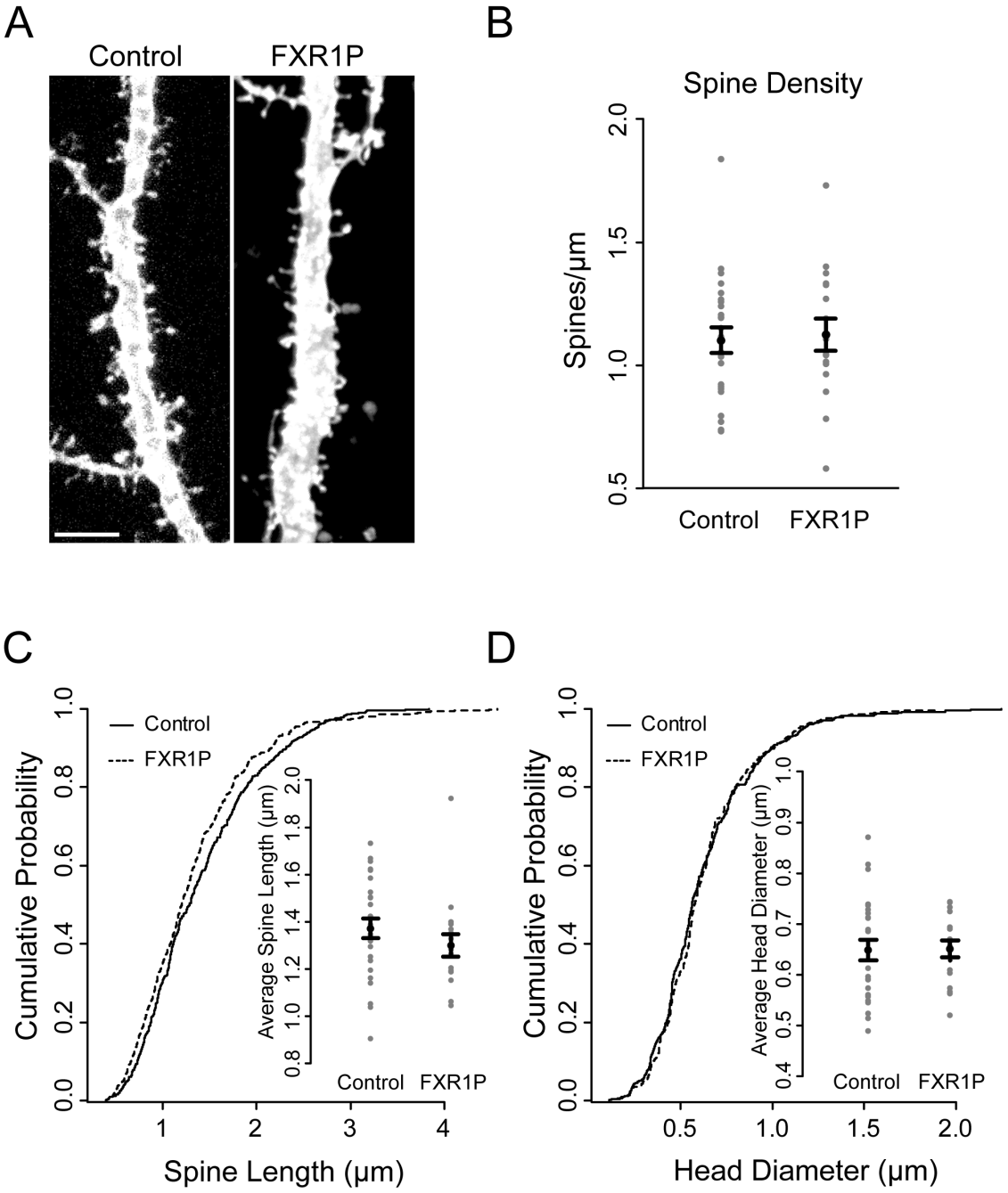
A
Control
FXR1P
B
Spine Density
Spines/µm
0.5
1.0
1.5
2.0
Control
FXR1P
C
Cumulative Probability
0.0
0.2
0.4
0.6
0.8
1.0
Control
FXR1P
Spine Length (µm)
1
2
3
4
Average Spine Length (µm)
0.8
1.0
1.2
1.4
1.6
1.8
2.0
Control
FXR1P
D
Cumulative Probability
Control
FXR1P
Head Diameter (µm)
0.5
1.0
1.5
2.0
Average Head Diameter (µm)
0.4
0.5
0.6
0.7
0.8
0.9
1.0
Control
FXR1P

Figure 1: Postsynaptic overexpression of FXR1P does not cause a significant change in spine density or spine morphology. This data was obtained by manually quantifying spines from 26 control and 17 FXR1P-expressing dendrites using Reconstruct (see methods). A total of 1138 and 895 spines from control and FXR1P expressing dendrites were quantified, respectively. **A.** Representative images of CA1 apical dendrites from control and FXR1P expressing cells transfected with farnesylated red fluorescent protein (RFPf) and RFPf/eGFP-FXR1P respectively. Scale bar = 10 μm. **B.** Quantification of spine density in control versus FXR1P expressing dendrites. Data is displayed as scattergrams with means +/- standard errors superimposed. Spine densities were not significantly different between the two conditions (Control: 1.10 +/- 0.05 spines/μm, FXR1P: 1.12 +/- 0.07 spines/μm, p=0.80) **C, D.** Cumulative probability plots for spine lengths (**C**) and spine head diameters (**D**). Note that the cumulative probability plots are based on random samples of 500 spines taken from both control and FXR1P expressing dendrites. *Insets.* Scattergrams displaying the average spine length (**C**) and average spine head diameter (**D**) for each dendritic segment. Average spine length and average spine head diameter are not significantly different between control and FXR1P dendrites (Average spine length: control: 1.37 +/- 0.04 μm FXR1P: 1.3 +/- 0.05 μm, p=0.27; average head diameter: control: 0.65 +/- 0.02 μm FXR1P: 0.65 +/- 0.02 μm, p=0.94). All values represent means +/- standard errors. Statistical analysis was performed using two-tailed, unpaired Welch two-sample t-tests.

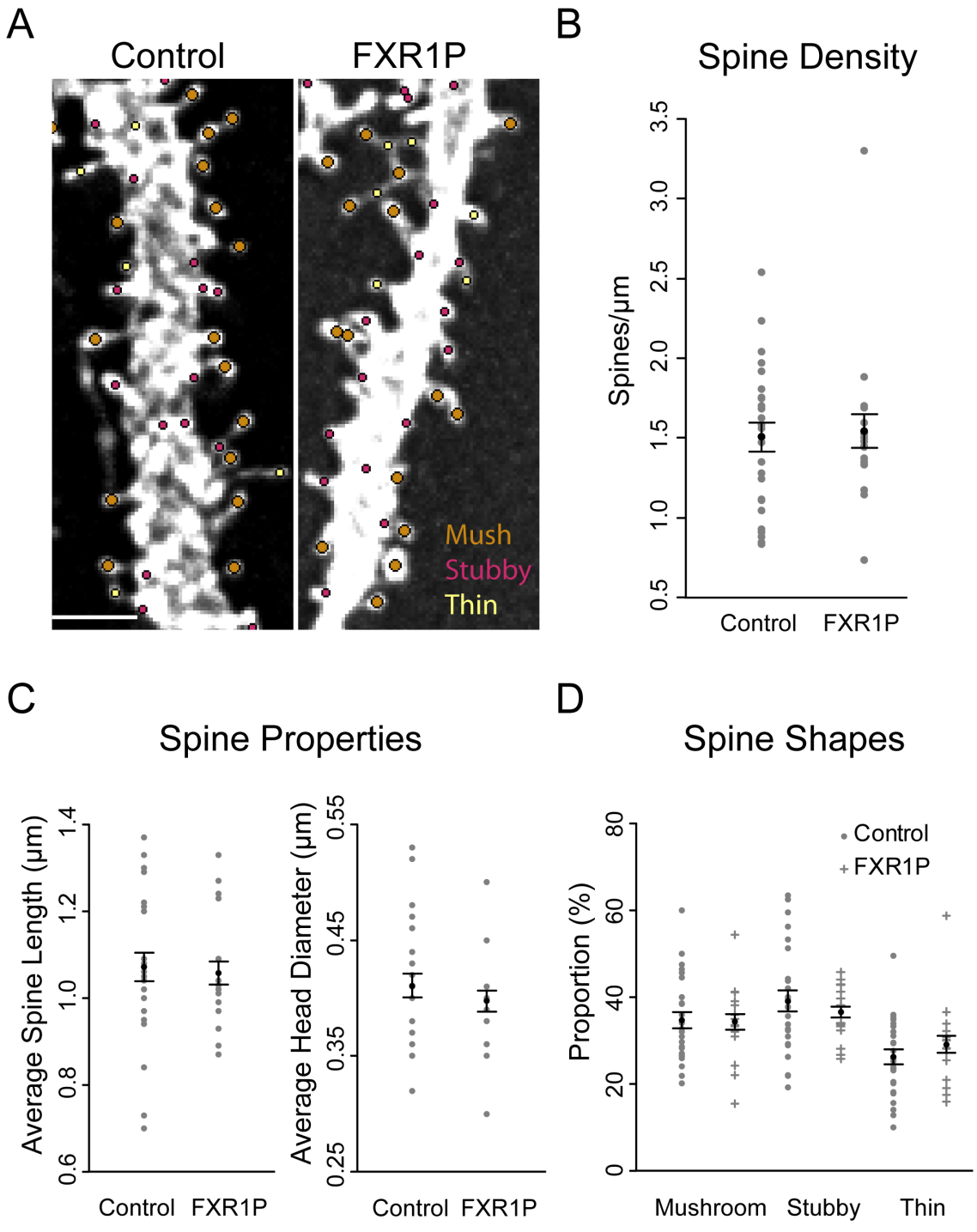
A
Control
FXR1P
Mush
Stubby
Thin
B
Spine Density
Spines/µm
0.5
1.0
1.5
2.0
2.5
3.0
3.5
Control
FXR1P
C
Spine Properties
Average Spine Length (µm)
0.6
0.8
1.0
1.2
1.4
Control
FXR1P
Average Head Diameter (µm)
0.25
0.35
0.45
0.55
Control
FXR1P
D
Spine Shapes
Proportion (%)
0
20
40
60
80
Control
FXR1P
Mushroom
Stubby
Thin

Figure 2: Spine analysis using automated three-dimensional detection and classification of spines (NeuronStudio) confirms similarity of spine density and spine morphology between control and FXR1P expressing dendrites. This data was obtained by quantifying spines from the same images, but not necessarily the same dendritic segments, of 26 control and 16 FXR1P-expressing dendrites (one dendrite could not be analyzed by NeuronStudio due to low fluorescent intensity). A total of 1929 and 1150 spines from control and FXR1P expressing dendrites were quantified, respectively. **A.** Representative images from control and FXR1P expressing cells demonstrating the classification of spines in NeuronStudio. Scale bar = 2.5 μm. **B.** Scattergrams of spine densities in control versus FXR1P expressing dendrites. Spine densities were not significantly different between the two conditions (Control: 1.63 +/- 0.13 spines/μm, FXR1P: 1.54 +/- 0.13 spines/μm, p=0.83) **C.** Scattergrams displaying the average spine length and average spine head diameter for each dendritic segment. Average spine length and average spine head diameter are not significantly different between control and FXR1P dendrites (Average spine length: control: 1.06 +/- 0.04 μm FXR1P: 1.06 +/- 0.03 μm, p=0.78; average head diameter: control: 0.41 +/- 0.01 μm FXR1P: 0.40 +/- 0.01 μm, p=0.40). **D.** Control and FXR1P expressing dendrites display similar proportions of mushroom, stubby and thin spines (Control: Mush: 35.32 +/- 1.96 % Stubby: 38.70 +/- 2.71 % Thin: 25.99 +/- 1.77%, FXR1P: Mush: 34.29 +/- 2.20 % Stubby: 36.60 +/- 1.62 % Thin: 29.11 +/- 2.48 %. Two-way mixed ANOVA, Genotype*Shape p=0.45). All values represent means +/- standard errors. Unless otherwise stated, statistical analysis was performed using two-tailed, unpaired Welch two-sample t-tests.

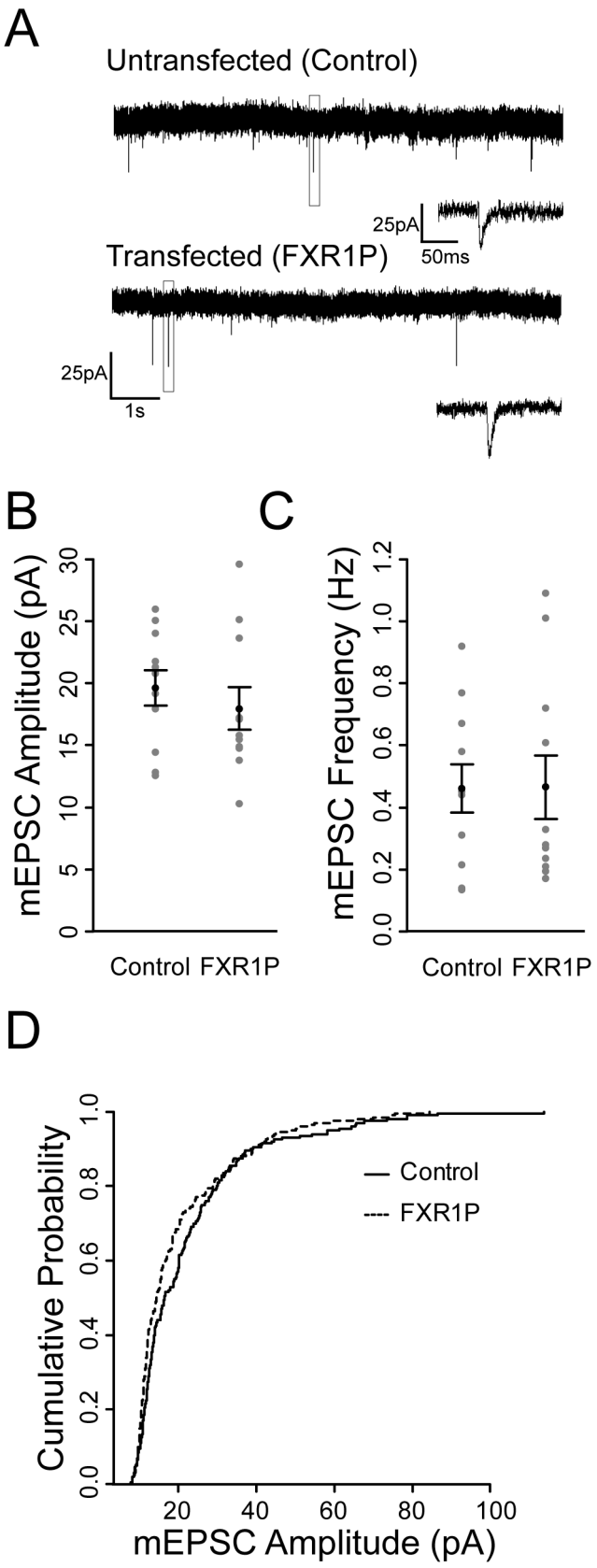
A
Untransfected (Control)
25pA
50ms
Transfected (FXR1P)
25pA
1s
B
mEPSC Amplitude (pA)
0
5
10
15
20
25
30
Control FXR1P
C
mEPSC Frequency (Hz)
0.0
0.2
0.4
0.6
0.8
1.0
1.2
Control FXR1P
D
Cumulative Probability
0.0
0.2
0.4
0.6
0.8
1.0
Control
FXR1P
20
40
60
80
100
mEPSC Amplitude (pA)

Figure 3: Similar mEPSC amplitudes and frequencies in control versus FXR1P-expressing cells. Whole-cell voltage clamp recordings from 11 control and 11 FXR1P expressing cells in hippocampal slices. A total of 1839 and 1659 events were analyzed from control and FXR1P expressing cells, respectively. **A.** Representative traces of mEPSCs recorded from untransfected control and transfected mCherry/eGFP-FXR1P expressing cells. **B, C.** Scattergrams of mEPSC amplitudes and frequencies with means and standard errors superimposed. mEPSC amplitude and frequency were similar between the two conditions (mEPSC amplitude: control: -19.62 +/- 1.43 pA FXR1P: -17.97 +/- 1.72 pA, p=0.47; mEPSC frequency: control: 0.46 +/- 0.08 Hz FXR1P: 0.47 +/- 0.10 Hz, p=0.98). **D.** Cumulative probability plot of mEPSC amplitudes taken from 200 random events from control and FXR1P expressing cells, showing a small but non- significant decrease in FXR1P expressing cells (K-S test $p>0.05$). All values represent means +/- standard errors. Unless otherwise stated, statistical analysis was performed using two-tailed, unpaired Welch two-sample t-tests.

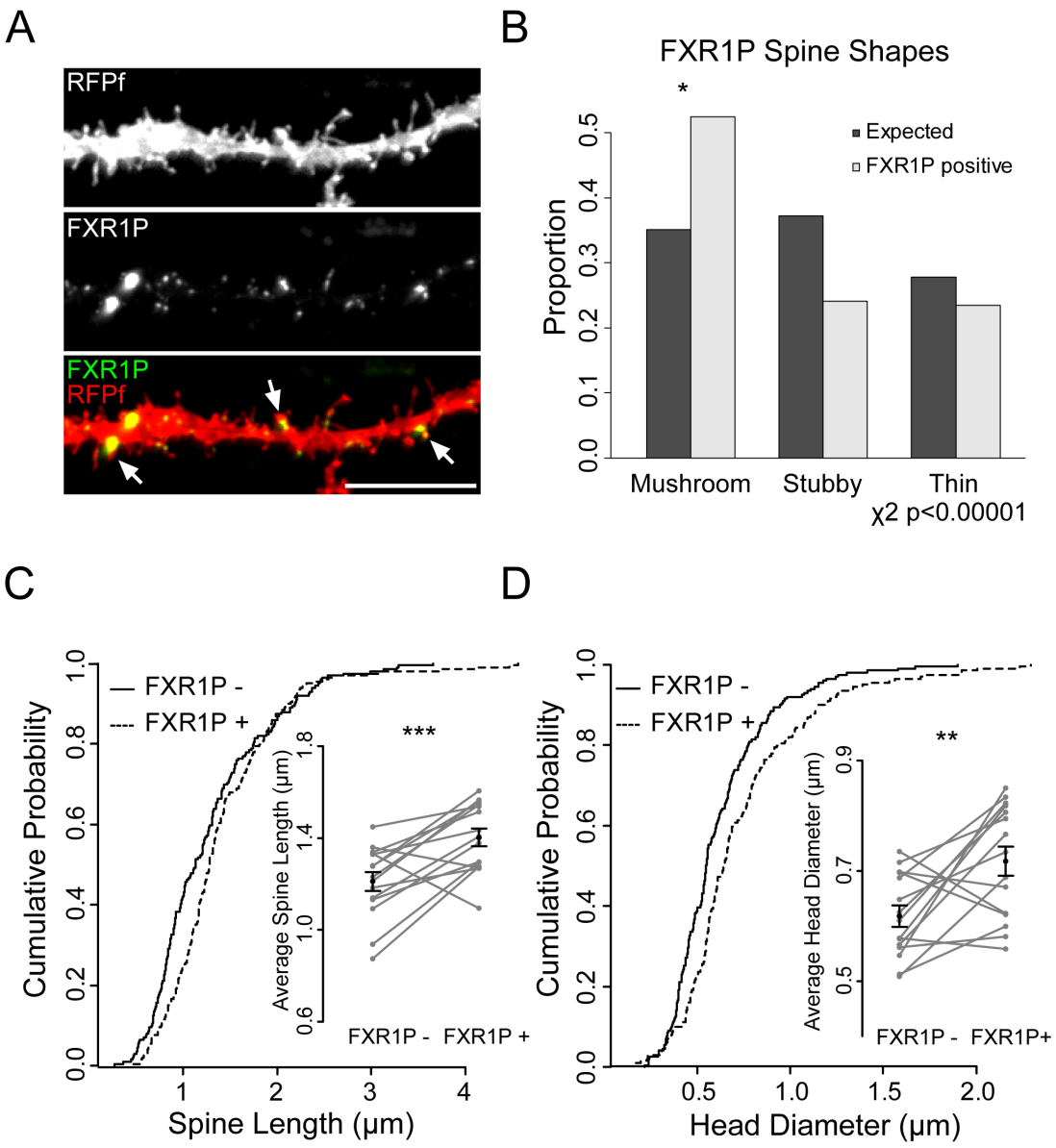
A
RFPf
FXR1P
FXR1P
RFPf
B
FXR1P Spine Shapes
*
Expected
FXR1P positive
Proportion
0.0
0.1
0.2
0.3
0.4
0.5
Mushroom
Stubby
Thin
χ2 p<0.00001
C
FXR1P -
FXR1P +
Cumulative Probability
0.0
0.2
0.4
0.6
0.8
1.0
1
2
3
4
Spine Length (μm)
***
Average Spine Length (μm)
0.6
1.0
1.4
1.8
FXR1P - FXR1P +
D
FXR1P -
FXR1P +
Cumulative Probability
0.0
0.2
0.4
0.6
0.8
1.0
0.5
1.0
1.5
2.0
Head Diameter (μm)
**
Average Head Diameter (μm)
0.5
0.7
0.9
FXR1P - FXR1P+

Figure 4: FXR1P clusters are preferentially located at a subset of large, mushroom-shaped spines. This data represents a comparison of spines containing FXR1P clusters with their negative neighbors. Dendrites with less than 4 FXR1P-positive spines were excluded from the analysis. A total of 15 dendritic segments and 199 FXR1P-positive and 696 FXR1P-negative spines were analyzed (Reconstruct). A. A representative image of a segment of CA1 apical dendrite from a cell expressing RFPf and eGFP-FXR1P showing the discrete localization of FXR1P in clusters along the dendrite and at a subset of spines. Arrows point to FXR1P-positive spines. Scale bar = 10 μm. B. FXR1P-positive spines were classified as mushroom, stubby or thin using NeuronStudio. 14 dendritic segments and 166 FXR1P-positive and 969 FXR1P-negative spines were analyzed. FXR1P was found at a higher proportion of mushroom-shaped spines than expected ($\chi 2$ goodness-of-fit $p<0.00001$; asterisk denotes significant difference). C, D. Cumulative probability plots for spine lengths (C) and spine head diameters (D). Note that the cumulative probability plots are based on the whole sample of 199 FXR1P-positive spines and a random sample of 199 FXR1P-negative spines. Insets. Scattergrams displaying the average spine length (C) and average spine head diameter (D) of FXR1P-positive and FXR1P-negative spines. Lines join averages from the same dendritic segment. Means and standard errors are superimposed. FXR1P-positive spines are on average longer and have larger spine head diameters than FXR1P-negative spines (Average spine length: FXR1P-negative: 1.21 +/- 0.04 μm FXR1P-positive: 1.40 +/- 0.04 μm, $p=0.00098$; average head diameter: FXR1P-negative: 0.62 +/- 0.02 μm FXR1P-positive: 0.72 +/- 0.03 μm, $p=0.0073$). All values represent means +/- standard errors. Statistical analysis was performed using two-tailed, paired t-tests. ** $p<0.01$, *** $p<0.001$.

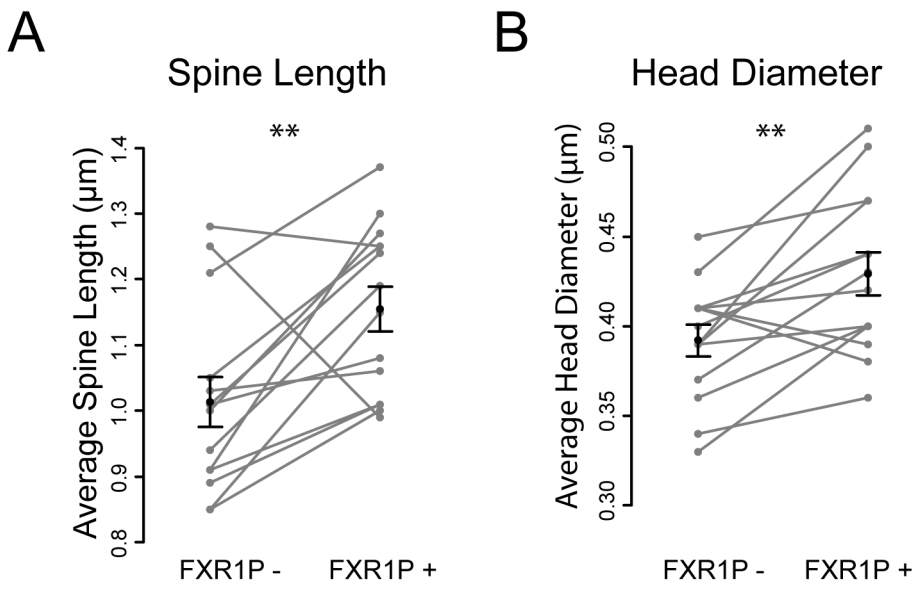

Figure 5: Independent analysis of spine size using NeuronStudio confirms preferential localization of FXR1P at large spines. Dendrites with less than 4 FXR1P-positive spines were excluded from the analysis. A total of 14 dendritic segments and 166 FXR1P-positive and 969 FXR1P-negative spines were analyzed. **A, B.** Scattergrams displaying the average spine length (**C**) and average spine head diameter (**D**) of FXR1P-positive and FXR1P-negative spines. Lines join averages from the same dendritic segment. Means and standard errors are superimposed. FXR1P-positive spines are on average longer and have larger spine head diameters than FXR1P-negative spines (Average spine length: FXR1P-negative: 1.10 +/- 0.04 µm FXR1P-positive: 1.16 +/- 0.03 µm, p=0.006; average head diameter: FXR1P-negative: 0.39 +/- 0.01 µm FXR1P-positive: 0.43 +/- 0.01 µm, p=0.004). All values represent means +/- standard errors. Statistical analysis was performed using two-tailed, paired t-tests. ** $p<0.01$.

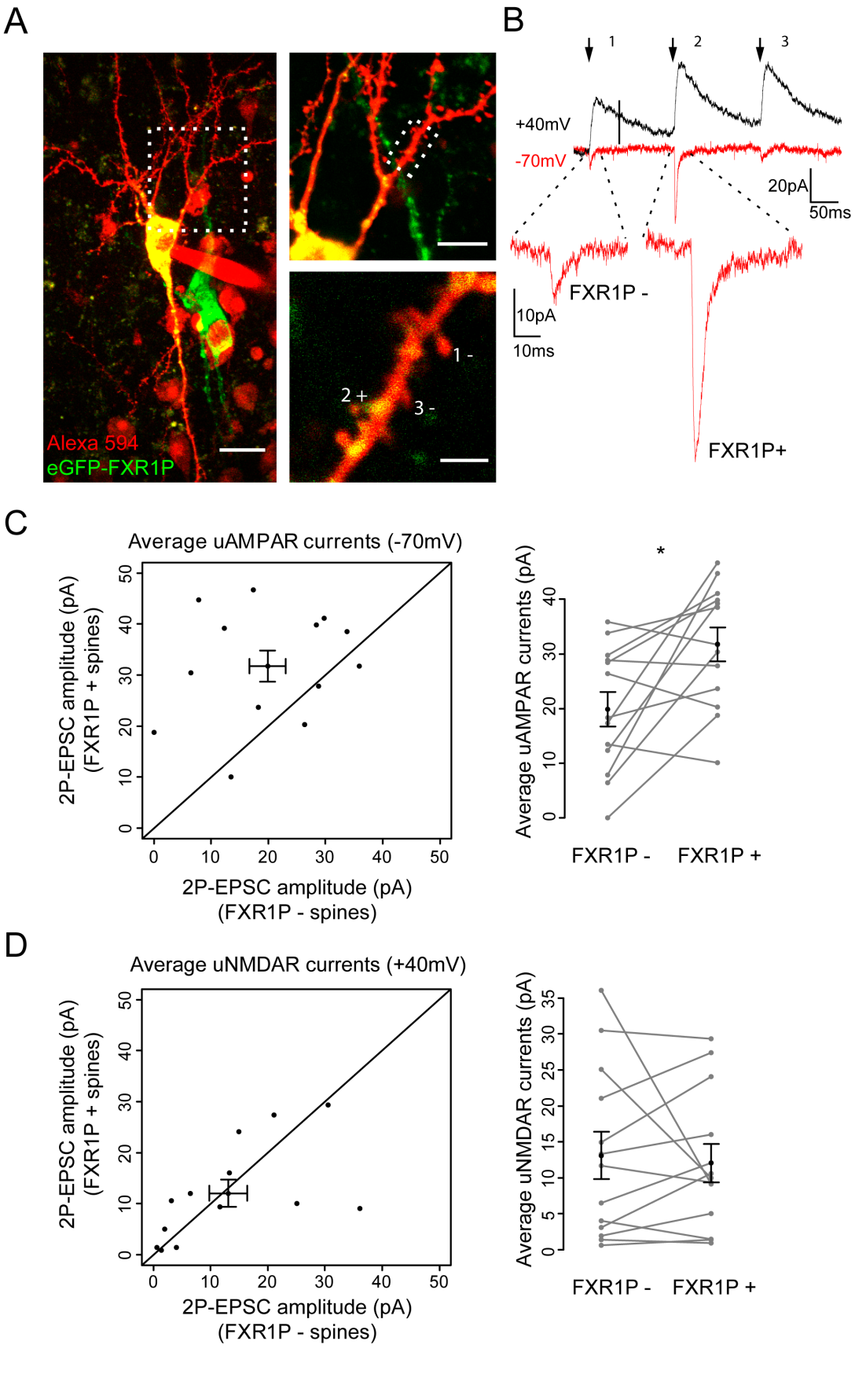
A
Alexa 594
eGFP-FXR1P
1 -
2 +
3 -
B
1
2
3
+40mV
-70mV
20pA
50ms
FXR1P -
10pA
10ms
FXR1P+
C
Average uAMPAR currents (-70mV)
2P-EPSC amplitude (pA)
(FXR1P + spines)
2P-EPSC amplitude (pA)
(FXR1P - spines)
*
Average uAMPAR currents (pA)
FXR1P -
FXR1P +
D
Average uNMDAR currents (+40mV)
2P-EPSC amplitude (pA)
(FXR1P + spines)
2P-EPSC amplitude (pA)
(FXR1P - spines)
Average uNMDAR currents (pA)
FXR1P -
FXR1P +

Figure 6: FXR1P clusters are preferentially located at spines with larger AMPA receptor currents. Two-photon glutamate uncaging was used to probe the AMPA and NMDA receptor content of neighboring FXR1P-positive and FXR1P-negative spines. A total of 20 FXR1P-positive and 27 FXR1P-negative spines from 13 dendritic segments were analyzed (5 mCherry/eGFP-FXR1P expressing cells). **A.** *Left* Representative image of an electrode patched onto a FXR1P expressing cell. For imaging purposes, cells were filled with 30 μm Alexa 594. Scale bar = 10 μm. White box indicates region used in higher magnification view. *Right* Higher magnification view of the basal dendrites (top) and a dendritic segment selected for glutamate uncaging (bottom). Scale bar = 10 μm and 2.5 μm respectively. Glutamate was uncaged onto 2 FXR1P-negative spines and 1 FXR1P-positive spine in the order shown. There was a 300 ms delay between each 1.0 ms laser pulse. **B.** Average traces of the currents obtained by uncaging glutamate on those 3 spines while voltage-clamped at -70 mV (red traces) and +40 mV (black traces). AMPA receptor currents were measured by taking the maximum amplitude of each peak at -70 mV and an estimate of the NMDA receptor current was taken 100 ms from the peak at +40 mV (black line). FXR1P-positive spines have significantly larger AMPA receptor current responses. Arrows denote uncaging pulse (720 nm, 1 ms). **C, D.** Dot plots and scattergrams displaying the average AMPA receptor (uAMPAR) currents (**C**) and average NMDA receptor (uNMDAR) currents (**D**) of FXR1P-positive (average of responses from 1-3 spines) and FXR1P-negative spines (average of responses from 1-3 spines) on the same dendritic segments. Lines join averages from the same dendritic segment. Means and standard errors are superimposed. FXR1P-positive spines have 50% larger AMPA receptor currents but similar NMDA receptor currents as FXR1P-negative spines (average uAMPA receptor current: FXR1P-negative: 19.91 +/- 3.17 pA FXR1P-positive: 31.75 +/- 3.10 pA, p=0.011; average uNMDA receptor current: FXR1P-negative: 13.09 +/- 3.29 pA FXR1P-positive: 12.05 +/- 2.67 pA, p=0.71). All values represent means +/- standard errors. Statistical analysis was performed using two-tailed, paired t-tests. * $p < 0.05$.

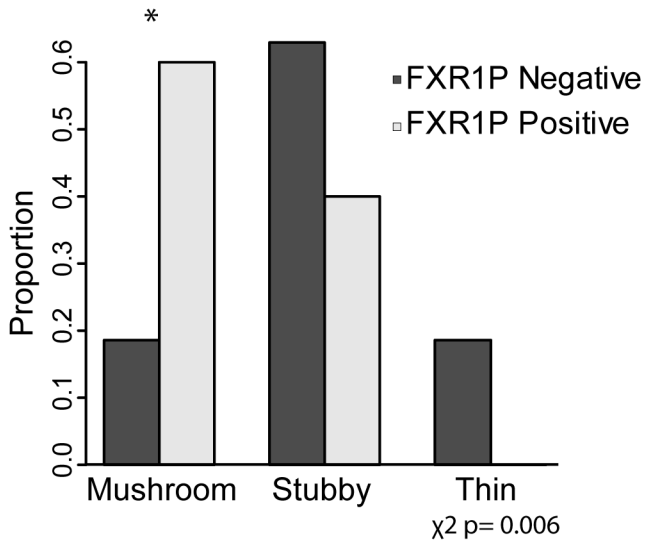

Figure 7: Independent confirmation that FXR1P preferentially clusters at mushroom-shaped spines. An estimate of spine shape was made by visual inspection of each spine. A spine was classified as mushroom if its head diameter was significantly greater than its neck width (large, bulbous head), thin if it was long with no separate head and stubby if it was short with no visible neck region. FXR1P clusters were more likely to be found at mushroom-shaped spines than stubby-shaped spines, whereas FXR1P-negative spines were more likely to be stubby in shape (Pearson's chi-square test p=0.006; asterisk denotes significant difference).

CHAPTER 5:

TARGETED DELETION OF THE FMRP PARALOG FXR1P ALTERS DENDRITIC SPINES AND ENHANCES LATE-PHASE LTP

Denise Cook, David Stellwagen, Keith K. Murai

5.1 Relationship to overall project

In the previous two chapters we presented evidence that FXR1P is highly colocalized with the translational machinery in the dendrite and at a subset of large, strong, mushroom-shaped spines, suggesting that it is involved in the local translational control of mRNAs important for spines. To further these studies and address the necessity of FXR1P for spine development and synaptic plasticity, we generated a conditional knockout of FXR1P where FXR1P is selectively deleted in the postnatal forebrain. The results of these studies are presented here.

5.2 Abstract

Long-lasting changes to the structure and function of excitatory synapses require new protein synthesis. This protein synthesis is triggered by synaptic activity and regulated by molecular mechanisms which act on mRNA transport, localization and translation, ensuring that the correct subsets of mRNAs are translated at the right time and place. The spatiotemporal control of protein synthesis is achieved in two ways: by signaling pathways which control the translation of all mRNAs and by RNA-binding proteins which act on specific subsets of mRNAs. Although the importance of general translational control mechanisms in synaptic plasticity is well-established, much less is known about the role of individual RNA-binding proteins in this process. Fragile X Related Protein 1 (FXR1P) is a member of the Fragile X family of RNA-binding proteins known to be involved in translational control and synaptic plasticity. We have previously shown that overexpressed FXR1P clusters with the translational machinery at a subset of large, mature dendritic spines, suggesting that FXR1P may be involved in activity-dependent spine maturation or spine maintenance.

However, it is unknown whether FXR1P is required for spine development and synaptic plasticity. We hypothesized that removal of FXR1P would reduce spine density and spine size, and lead to alterations in long-term synaptic plasticity. To test this, we generated a conditional knockout mouse where FXR1P was deleted from excitatory neurons in the postnatal mouse forebrain. Using diolistic labeling and 3D automated quantification methods, we compared spine density, size and shape between wild-type and FXR1P conditional knockout mice. We then used field recordings to determine whether loss of FXR1P led to a change in synaptic plasticity. We found that loss of FXR1P resulted in a reduction in the density and size of spines, whilst leading to an enhancement in late-phase long-term potentiation (L-LTP). These results indicate that FXR1P plays a critical role in the control of spine number, spine size and L-LTP.

5.3 Introduction

Controlling gene expression at the level of mRNA translation allows cells to rapidly synthesize new proteins in order to adapt to a changing external environment. In neurons, proper translational control is required for long-lasting synaptic plasticity and cognitive function [6,92,224,225]. Indeed, convergent evidence suggests that deficits in translational control, leading either to an increase or decrease in the normal levels of protein synthesis, may underlie certain forms of intellectual disability and autism-spectrum disorders [226,227]. Although many studies have characterized the importance of general translational control mechanisms in synaptic plasticity and cognition, much less is known about the role of gene-specific translational control mechanisms in these processes.

In mature neurons, activity-dependent mRNA translation is controlled at two main levels. The first level of control consists of signaling pathways which lead to global increases in mRNA translation in response to synaptic activity, such as the extracellular signal-regulated kinase (ERK) and mammalian target of rapamycin (mTOR) pathways (general translational control). By manipulating these pathways using genetic mouse models, researchers have shown that ERK and mTOR signaling play important roles in protein-synthesis dependent synaptic

plasticity and learning and memory [7,8,87]. The second level of control consists of cis-acting sequences in the 3' and 5' untranslated regions (UTRs) of each mRNA and the trans-acting RNA-binding proteins which bind to these sequences (gene-specific control). These RNA-binding proteins are involved in the transport, storage and translational control of their subsets of mRNAs [12]. The importance of this second level of translational control in synaptic plasticity and cognition comes from a large body of literature on one particular neuronal RNA-binding protein, Fragile X Mental Retardation Protein (FMRP). FMRP controls the translation of approximately 800 brain mRNAs [20]. Loss of FMRP leads to Fragile X Syndrome (FXS), a syndrome characterized by intellectual disability, autism and an overabundance of long, immature dendritic spines [16,18,54,228]. FMRP knockout mice recapitulate some of the human phenotypes, demonstrating subtle abnormalities in the structure and function of dendritic spines, enhanced protein-synthesis dependent metabotropic glutamate receptor-dependent long-term depression (mGluR-LTD) and deficits in learning and memory [136,228–233]. The role of FMRP in spine formation, synaptic plasticity and cognition supports the theory that translational control is an important switch for synaptic plasticity and memory storage and points to the need to study the neuronal function of other similar RNA-binding proteins.

FMRP is one of a family of three RNA-binding proteins with highly similar gene structures and RNA-binding domains [234]. Its two autosomal paralogs, Fragile X Related Protein 1 (FXR1P) and Fragile X Related Protein 2 (FXR2P), have received considerably less attention from researchers. The few studies on FXR2P knockout mice have revealed that FXR2P plays a similar, yet distinct, role to FMRP in synaptic plasticity and behaviour [28,31]. However, due to the lack of a viable full knockout mouse model for FXR1P [155], comparatively little is known about the function of FXR1P in the mammalian brain. Similar to FMRP and FXR2P, FXR1P is expressed in neurons in many brain regions, including the hippocampus, cortex and Purkinje cells in the cerebellum [21,22]. Like FMRP, FXR1P controls the translation of its target mRNAs in non-neuronal cells; however its mRNA targets in the brain have yet to be identified [32,33,156]. We have

previously shown that FXR1P associates with the translational machinery in clusters along the dendrite and at a subset of larger, functionally stronger dendritic spines, pointing to an important role for FXR1P at spines [23]. However, it is unknown whether loss of FXR1P would result in abnormalities to spines and long-lasting synaptic plasticity. By studying FXR1P we hope to improve our understanding of the important players in synapse strengthening and long-term memory formation. We hypothesized that FXR1P, like its paralog FMRP, may control spine density, spine size and protein-synthesis dependent synaptic plasticity. To test this, we developed a knockout mouse model where FXR1P is selectively deleted from excitatory neurons in the postnatal mouse forebrain. We then studied these conditional FXR1P knockout mice (FXR1P cKO) for differences in spines, basal synaptic transmission, protein-synthesis independent forms of short-term plasticity and protein-synthesis dependent forms of long-term plasticity. Loss of FXR1P decreased spine density and spine size, but surprisingly led to enhanced protein-synthesis dependent L-LTP, without affecting basal synaptic transmission and short-term plasticity. These results suggest that FXR1P controls the translation of a subset of mRNAs important for maintaining spines and long-lasting synaptic plasticity.

5.4 Materials and Methods

Ethics Statement with regards to animal use. All experiments involving mice were approved by the Montreal General Hospital Facility Animal Care Committee (Protocol ID#5758) and followed the guidelines of the Canadian Council on Animal Care. All animals used in experiments were housed in groups of three-five mice.

Generation of FXR1P conditional knockout mice Since the full FXR1P knockout dies at birth due to abnormalities in skeletal and heart muscle [155], we turned to a conditional knockout approach in order to study the effect of loss of FXR1P on the development of the postnatal mouse hippocampus. This strategy also allowed us to eliminate any influences of loss of FXR1P on earlier stages of neuronal development, such as neurogenesis. We obtained the floxed *Fxr1* line from Dr.

David Nelson through the Baylor College of Medicine Fragile X Mutant Mouse Facility. The generation of this line has been described previously [155]. The neomycin cassette has been excised to restore normal FXR1P levels and function [155], which we verified independently by western blotting. The mice are viable, fertile and have been backcrossed into a C57BL/6 background for at least 10 generations. The Cre recombinase-driver line chosen for this study was the αCaMKII-Cre T29-1 line (The Jackson Laboratory, Bar Harbor, Maine). This line has been characterized by several laboratories to show Cre-mediated recombination in excitatory neurons of the postnatal forebrain starting around the third postnatal week, with complete recombination in CA1 excitatory neurons by eight weeks [235–238]. This line has also been backcrossed for at least 10 generations.

To generate FXR1P conditional knockout mice, we first crossed the αCaMKII-Cre double transgenic (αCaMKII-Cre tg/tg) with the floxed *Fxr1* (*Fxr1* fl/fl*)* line to generate the double heterozygote mouse (αCaMKII-Cre tg/+; *Fxr1* fl/+). Genotypes were verified using standard polymerase chain reaction (PCR) using the following primers: Cre Forward: 5'- GCG GTC TGG CAG TAA AAA CTA TC-3', Cre Reverse: 5'-GTG AAA CAG CAT TGC TGT CAC TT-3' and Fxr1 Forward (LoxP site 1): 5'-GAT AGT GCT GTG TGT AGC TCC G-3', Fxr1 Reverse (LoxP site 1) 5'-GCT CCT GGC CCC TAG CAA C-3'. We then crossed αCaMKII-Cre tg/+; *Fxr1* fl/+ with αCaMKII-Cre tg/tg to establish the αCaMKII-Cre tg/tg; *Fxr1* fl/+ breeder line. Since the transgenic αCaMKII-Cre line was generated via random insertion and the site of insertion is unknown, SYBR green quantitative-PCR was performed to separate hemizygote from homozygote αCaMKII-Cre mice. Once the αCaMKII-Cre tg/tg; *Fxr1* fl/+ line was established, it was maintained by crossing with the αCaMKII-Cre tg/tg line. In order to avoid any potential influences of reduction of FXR1P levels on the parenting behaviour of female mice, experimental animals were generated, in most cases, by crossing male αCaMKII-Cre tg/tg; *Fxr1* fl/+ with female *Fxr1* fl/+ to generate αCaMKII-Cre tg/+; *Fxr1* fl/fl (FXR1P cKO), αCaMKII-Cre tg/+; *Fxr1* fl/+ (FXR1P cHET) and αCaMKII-Cre tg/+; *Fxr1* +/+ (WT).

In order to track cells which have undergone Cre-mediated recombination, we also crossed male αCaMKII-Cre tg/tg; *Fxr1* fl/+ with female Tomato tg/tg; *Fxr1* fl/+ to generate αCaMKII-Cre tg/+; Tomato tg/+ WT, FXR1P cHET and FXR1P cKO mice. Tomato is a reporter line which expresses a membrane-bound red fluorescent protein (tdTomato) in the absence of Cre expression and a membrane-bound green fluorescent protein (EGFP) after Cre-mediated recombination (B6.129(Cg)-Gt(ROSA)26Sor$^{tm4(ACTB-tdTomato,-EGFP)/Luo}$/J, The Jackson Laboratory, Bar Harbor, Maine). The Tomato line has been backcrossed into a C57BL/6 background for at least five generations. The presence of the tomato transgene was verified using standard PCR and the following primers: wild-type forward: 5'-CTC TGC TGC CTC CTG GCT TCT-3', wild-type reverse: 5'-CGA GGC GGA TCA CAA GCA ATA-3', mutant reverse: 5'- CTG CCA AGT AGG AAA GTC CC-3'.

Cryostat sections and immunohistochemistry. A qualitative study of Cre-mediated recombination across development was performed on one set of male and female αCaMKII-Cre tg/+; Tomato tg/+ mice at different ages (Figure 1). To validate the loss of FXR1P in adult mice, we examined male and female aged-matched WT, FXR1P cHET and FXR1P cKO mice between postnatal days 56-70 (4 males, 5 females). For both experiments, images shown are representative of the staining pattern obtained across multiple sections (Figure 1) and also multiple animals (Figure 2). Transcardial perfusion and cryostat sectioning was performed as previously described [23]. 30 μm sections were collected in Dulbecco's phosphate buffered saline (DPBS), permeabilized for 15 minutes using 1% Triton-X 100/DPBS, blocked for 1 hour using 10% normal goat serum/DPBS/0.1% Triton-X 100, and incubated overnight at 4 °C with primary antibody (various, see next section) diluted in 0.1% Triton-X 100/DPBS/1% normal goat serum. Sections were washed three times for 20 minutes using 0.1% Triton-X 100/DPBS/1% normal goat serum and incubated with Alexa Fluor secondary antibodies (see next section) for 1 hour. Sections were washed three times for 20 minutes and then mounted using SlowFade Gold antifade reagent (Invitrogen). Sections were imaged at 10X (0.4 numerical aperture) using an Ultraview spinning disk confocal

system (PerkinElmer, Wellesley, MA) connected to an Eclipse TE2000 (Nikon, Tokyo, Japan) and a cooled CCD 12-bit Hamamatsu ORCA-ER camera. Exposure time was 3000 milliseconds. Images of entire hippocampi were created by stitching together neighboring single plane images with at least 20% overlap using the Photomerge application of Photoshop CS3 Extended.

Antibodies used for immunofluorescence.. For detecting FXR1P in free-floating cryostat sections, we used a rabbit polyclonal antibody against FXR1P at 1:5000 (#ML13) which has been described previously [23,167]. Other antibodies used included rabbit anti-MAP2 (Millipore, 1:1000), mouse anti-GFAP (GFAP, 1:1000), human anti-ribosomal P antibodies (Immunovision, 1:5000), mouse anti-NeuN (Millipore, 1:5000) and rabbit anti-GFP (Invitrogen, 1:1000). Secondary antibodies used were Alexa 568-conjugated goat anti-mouse IgG, Alexa 488- and 647- goat anti-rabbit IgG and Alexa 647-conjugated goat anti-human IgG (all at 1:500; Molecular Probes).

CA1 Lysates and Western Blotting. To verify and quantify the loss of FXR1P from the CA1 region of the hippocampus, we prepared CA1 lysates from three sets of age-matched male and female WT, FXR1P cHET and FXR1P cKO mice between postnatal days 50-60 (8 females, 1 male). To isolate the CA1 region of the adult hippocampus, we first dissected out the hippocampi from a single mouse and placed them into ice-cold DPBS. The hippocampi were then cut into 300 μm transverse slices using a tissue chopper (McIllwain). Slices were transferred back to ice-cold PBS, separated using fine forceps and the CA1 region (both the cell bodies and stratum radiatum) from each intact slice was carefully dissected out using a scalpel blade. The CA1 pieces were then collected and quickly frozen on dry ice. Whole cell lysates were obtained by homogenizing the CA1 regions from each mouse in 100 μl of RIPA buffer (1% Triton X-100, 1% sodium deoxycholate, 0.1% SDS, 20 mM Tris pH 8.0, 150 mM NaCl and 1mM EDTA) using a gel-loading tip. Lysates were left on ice for 30 minutes, sonicated for 10 seconds and spun at 13,200 rpm for 10 minutes. Supernatants were collected and protein concentration was determined using a BCA assay (Pierce). 20 μg of total protein was run on a 10% SDS-PAGE gel and transferred to a PVDF membrane.

Membranes were cut at the appropriate molecular weight marker and incubated with either #ML13 (1:50,000-1:100,000) and anti-GAPDH (Abcam, 1:10,000) as a loading control. We quantified the expression profile of FXR1P relative to GAPDH using densitometry and the ImageJ Gel Analysis Plugin (http://rsb.info.nih.gov/ij/docs/menus/analyze.html#gels). We first normalized the intensity of FXR1P bands to GAPDH by dividing the area measurements returned by ImageJ and then expressed the level of FXR1P as a percentage of the level obtained in the corresponding wild-type sample. This was repeated and averaged across 2 blots. The averages and standard errors of the mean are shown in Figure 2 (n = 3 mice per genotype).

DiI labeling and imaging of CA1 dendrites and spines in hippocampal slices The spine analysis was performed on five sets of male-only WT and FXR1P cKO littermate pairs at postnatal day 60. Mice were rapidly transcardially perfused with ice-cold DPBS followed by 40 ml of fixative (4% paraformaldehyde/0.1 M phosphate buffer; pH 7.4) delivered at 20 ml/min using a syringe-pump (Harvard Apparatus). The brain was post-fixed for 10 minutes in 10 mL of fixative and then transferred to DPBS. For each animal, the hippocampi were removed and cut into 300 μm slices using a tissue chopper. We obtained approximately 15-20 slices per animal. Slices were then transferred to a 24-well plate containing DPBS.

CA1 dendrites and cells were labelled using the lipophilic fluorescent dye, DiI (Molecular Probes, Life Technologies, Burlington, ON). This dye incorporates itself into the cell membrane and diffuses through the membrane, filling dendrites and dendritic spines. DiI was introduced into fixed hippocampal slices using a method called Diolistics [239]. Briefly, we coated 100 mg of tungsten with 3 mg of DiI dissolved in 100 μl of methylene chloride. This was repeated so that 200 mg of DiI-coated tungsten was collected in a 15 ml conical tube, resuspended in 3 ml of ddH_2O and sonicated for 3 minutes. This suspension was then drawn into polyvinylpyrrolidone (PVP)-coated Tefzel tubing mounted on a Bio-Rad tubing preparation station. We allowed the tungsten particles to settle, removed the solution and dried the tubing for 5 minutes using nitrogen gas. The tubing was then cut into cartridges and loaded into a Bio-Rad Gene Gun. DiI-

coated tungsten bullets were introduced into hippocampal slices through a 3 μm Millipore Isopore filter with helium gas pressure set to 120 psi.

For imaging of CA1 dendrites and spines, we selected hippocampal slices with a low density of DiI labelling in order to get only a few dendrites per imaging field. We imaged 2-3 apical dendritic segments in stratum radiatum (approximately 100 μm from the cell body layer and close to the point of bifurcation of the apical dendrite) from 5-6 hippocampal slices per animal. Imaging was performed in the red (568nm) channel using a 60X oil immersion objective objective (60X Plan Fluor 1.25 numerical aperture) mounted on an Ultraview spinning disk confocal system (PerkinElmer, Wellesley, MA) connected to an Eclipse TE2000 (Nikon, Tokyo, Japan). Image acquisition was performed using Metamorph. Exposure time was 3000 ms. Z-stacks were formed using a z-step of 0.3 μm. A total of 66 wild-type and 69 FXR1P cKO apical dendritic segments from five mice per genotype were imaged and analyzed. All manipulations (perfusion, DiI labelling, imaging and analysis) were performed blind to the genotype of the animal.

Analysis of spine parameters and spine shapes using three-dimensional automated quantification in NeuronStudio. Spine density, spine size and spine shape were analyzed using NeuronStudio [204]. We first deconvolved each image using a 3D blind deconvolution algorithm from AutoDeblur with standard settings for confocal microscopy (Autoquant, Media Cybernetics, Maryland). 16-bit deconvolved image stacks were then loaded into ImageJ and images were enhanced for contrast by saturating 0.01% of the pixels in each image (Enhance Contrast plugin) in order to get the images in a dynamic range suitable for NeuronStudio. Voxel size was set to X: 0.109 μm Y: 0.109 μm, Z: 0.300 μm. Neurites were automatically traced by the software. Spines were detected and classified as mushroom, stubby or thin using default settings. Spine detection was verified using the 3D viewer and any erroneously defined spines were manually removed. Average spine densities, spine parameters and proportion of spine shapes were then calculated and compared between wild-type and FXR1P cKO mice.

Field recordings. Experiments were performed on acute hippocampal slices obtained from 5-9 months old age-matched male and female WT and FXR1P cKO mice. Animals were anesthetized using 5-10 drops of isofluorane and quickly decapitated. The whole brain was removed (usually within 75 seconds) and transferred to a beaker containing ice-cold regular artificial cerebrospinal fluid (ACSF) with the following composition (in mM): NaCl 124, KCl 3, NaH_2PO_4 1.25, $CaCl_2$ 2, $MgSO_4$ 1, $NaHCO_3$ 26, D-Glucose 10 and saturated with 95% O_2/5% CO_2. After 1 minute the brain was removed, trimmed and mounted on the stage of a Leica VT1200 S (Leica Microsystems Inc., Concord, ON). The stage was filled with ice-cold regular ACSF, constantly bubbled with a mixture of 95% O_2 and 5% CO_2. Coronal slices were cut with a thickness of 300-400 μm at a speed of 0.1 mm/sec and 2 mm amplitude and transferred to a home-made submersion chamber containing bubbled regular ACSF at a temperature of 31.5°C (5 month old animals) and 36.5°C (9 month old animals) for 25-30 minutes after which the chamber was placed on the bench at room temperature. Approximately eight to twelve slices were collected per animal. Slices were allowed to recover in the submersion chamber for at least four hours [240]. In general, one animal was sacrificed per day, except for certain early-LTP studies where two animals (one per genotype) were sacrificed and experiments performed back-to-back. Experiments were performed on 1-2 slices per animal. The entire experiment, from brain slicing to analysis, was performed blind to genotype.

After the recovery period, one slice was transferred to a submersion chamber mounted on an electrophysiology rig, perfused with bubbled, regular ACSF at a rate of approximately 3 ml/min and maintained at 28-31°C. Extracellular field excitatory postsynaptic potentials (fEPSPs) were evoked by stimulation of the Schaffer collateral/commissural fiber pathway using a monopolar glass electrode filled with regular ACSF (tip resistance= 0.5-1 MΩ) placed in the middle portion of the CA1 stratum radiatum 250-500 μm away from a glass recording electrode filled with regular ACSF (tip resistance= 0.4-1.3 MΩ) and also placed in the middle portion of the stratum radiatum. Recordings were filtered at 3 KHz, digitized at 20 KHz and acquired with Clampex (Axon

Instruments). fEPSPs were evoked by delivering a 0.1 ms, 30-50 μA biphasic pulse at 0.033-0.067 Hz. Slices were kept for further experimentation if the amplitude of the fiber volley was less than one-third the amplitude of the fEPSP and if the amplitude of the fEPSP increased with increasing stimulation intensity. Input-output curves were generated by stimulating with different intensities (30 μA, 50 μA, 70 μA, 100 μA, 150 μA, 200 μA) and comparing the amplitude of the fiber volley to the initial slope of the fEPSP. The initial slope of the fEPSP was measured as the maximum slope across a 1 ms time-window after the end of the fiber volley. For all subsequent experiments, stimulation intensity was set to elicit a fEPSP with a slope that was approximately 40% of maximum obtained slope.

Paired-pulse facilitation was determined by delivering pulses at an inter-pulse interval of 25 ms, 50 ms, 100 ms and 200 ms. 5-10 sweeps delivered at 0.067 Hz were then averaged and used to calculate the % facilitation (slope fEPSP2/slope fEPSP1*100). A two-way mixed ANOVA (Within-subject factor: interval, Between-subject factor: genotype) was used to determine differences between genotypes.

For early-LTP, baseline fEPSPs were elicited by delivering pulses at 0.033-0.067 Hz until a stable 10 minute baseline was achieved. Average baseline slopes were comparable between genotypes (WT: 0.19 +/- 0.01 mV/ms, FXR1P cKO: 0.17 +/- 0.01 mV/ms, t-test $p > 0.05$). E-LTP was then induced with a single train of high frequency stimulation (1 x 100 Hz) using baseline stimulation intensity. Potentiation was then measured for 60 minutes post-LTP using baseline stimulation frequencies. Data were collected and presented as the average slope of the fEPSP from five-ten individual traces (2.5 minute time-frame) and then normalized to the average baseline slope from the 10 minute period. An unpaired, two-tailed Welch's t-test was performed on the average of the last five points from each genotype (last 12.5 minutes).

For late-LTP, baseline fEPSPs were elicited by delivering pulses at 0.033-0.067 Hz until a stable 30 minute baseline was achieved. Average baseline slopes were comparable between genotypes (WT: 0.20 +/- 0.02 mV/ms, FXR1P cKO:

0.16 +/- 0.01 mV/ms, t-test $p > 0.05$). L-LTP was then induced using four trains of high frequency stimulation with a 20 second interval (4 x 100 Hz) using baseline stimulation intensity. Potentiation was then measured for 180 minutes post-LTP using baseline stimulation frequencies. Data were collected and presented as the average slope of the fEPSP from five-ten individual traces (2.5 minute time-frame) and then normalized to the average baseline slope for the 30 minute period. An unpaired, two-tailed Welch's t-test was performed on the average of the last five points from each genotype (last 12.5 minutes).

Statistical Analysis. All statistical analyses were performed using R (http://www.R-project.org) [178] with the following packages installed Reshape [205], Hmisc [179], gplots [206] and plotrix [207]. Unpaired analysis between two groups of data was performed using two-tailed Welch t-tests. A two-way mixed (1 between, 1 within factor) ANOVA was performed on the paired-pulse facilitation data. The specific test used for each experiment is noted in the figure legends. All graphs were created using Excel (Microsoft).

5.5 Results

Characterization of the αCaMKII-Cre driver line

The full knockout of FXR1P dies at birth due to abnormalities in skeletal and heart muscle development, precluding its use as a mouse model to study FXR1P function in the adult brain [155]. To circumvent this issue, we developed a conditional knockout strategy to delete FXR1P from excitatory neurons in the postnatal forebrain by using the αCaMKII-Cre T29-1 Cre-recombinase driver line. We chose this strategy since it allows us to study the function of FXR1P in synaptic plasticity without having to worry about potential roles for FXR1P in early neuronal development, such as neurogenesis, axon growth and guidance and dendrite development, roles that have been demonstrated for its paralog FMRP [241–243].

Although the αCaMKII-Cre T29-1 driver line has been extensively characterized and causes Cre expression in excitatory neurons in the postnatal mouse forebrain starting at approximately three weeks, we noted that there were

certain discrepancies in the literature depending on which reporter line had been used [235,236]. This occurs for various reasons, including the fact that certain reporter lines are inserted into loci that are not well-expressed or accessible to Cre-recombinase in certain cell-types or the sensitivity of the chosen reporter line is too low to reveal small populations of recombined cells. To address this issue and to determine the earliest time-point at which Cre/loxP recombination occurs, we crossed αCaMKII-Cre T29-1 to the mT/mG reporter line, a reporter line which drives high expression in the majority of cell types in the mouse, allowing us to be more confident about the pattern of recombination reported by this line [244]. We wanted an accurate picture of the spatial and temporal pattern of Cre-recombination in order to determine 1) whether we could use the reporter line to study the structure of CA1 dendrite spines in young FXR1P cKO mice and 2) the earliest time-point at which we could be confident that almost 100% of CA1 cells had recombined.

By imaging hippocampi from αCaMKII-Cre tg/+; Tomato tg/+ mice at different developmental stages we found that Cre-loxP recombination occurred in excitatory neurons of the CA1 region of the hippocampus starting around postnatal day 12 (Figure 1A). The number of recombined cells in the CA1 region increased gradually, with a peak of recombination occurring between postnatal days 22-30. At this stage, membrane-targeted EGFP (mEGFP) allowed sufficient resolution to image dendrites and dendritic spines when Cre-loxP recombination density was fairly low (Figure 1B). By postnatal day 60, the large majority of CA1 cells had undergone recombination. Interestingly, we also saw recombination in the dentate gyrus and CA3 regions starting at later developmental time-points (P16 +). Note that CA3 cells expressed lower levels of the EGFP-reporter, making them difficult to see at this magnification. In addition, we noted that perforant path axons contacting the outer molecular layer of the dentate gyrus recombined by postnatal day 10, which was the earliest time-point examined (data not shown). By making a montage of a sagittal section of the entire P30 mouse brain, we found that Cre-loxP recombination also occurred in other forebrain regions outside of the hippocampus, including the olfactory bulb

and cortex, as has been previously shown for this αCaMKII-Cre driver line [235] (data not shown). Recombination was not seen in the cerebellum and midbrain regions.

Characterization of the conditional FXR1P knockout

The reporter study described above gave us a better idea of the spatial and temporal pattern of Cre-loxP recombination in the mouse hippocampus. However, since the timing and pattern of recombination is not always the same between different genes and since the loss of FXR1P also depends on the rate of degradation of its mRNA and protein, we used a specific FXR1P antibody (#ML13) to verify the loss of FXR1P at different time-points. We started with postnatal day 60 since we were confident from our reporter study (Figure 1) that at this time-point the majority of excitatory neurons in the CA1 region should have lost FXR1P. We stained free-floating sections with anti-FXR1P and anti-NeuN antibodies and imaged the hippocampus from wild-type, FXR1P cHET and FXR1P cKO mice. NeuN was used as a control to delineate the neuronal cell layers of the hippocampus. Our staining showed that FXR1P levels were lost from the majority of pyramidal cells in the CA1 region of the hippocampus in FXR1P cKO versus wild-type mice (Figure 2A). The FXR1P cHET also showed a reduction in FXR1P levels. At this age, we also found that FXR1P was lost from a significant fraction of excitatory cells in the CA3 region and dentate gyrus. However, a region between CA3 and CA1, presumably CA2, continued to express FXR1P at high levels. This is consistent with previous reports using the αCaMKII-cre driver line [235].

To confirm the loss of FXR1P using an independent method and quantitatively assess the amount of FXR1P reduction in knockout mice, we prepared hippocampal lysates from the CA1 region of three sets of wild-type, FXR1P cHET and FXR1P cKO mice (Figure 2B). Using SDS-PAGE and Western blotting techniques, we found that FXR1P levels were reduced to 52% and 15% of wild-type levels in the FXR1P cHET and FXR1P cKO, respectively

(Figure 2C). Interneurons and glial cells may account for the residual expression seen in the FXR1P cKO mouse.

According to our results using the mT/mG reporter line, Cre-loxP recombination also occurred in the cortex, but not in the cerebellum. To confirm these results using FXR1P staining, we imaged the cortex and cerebellum from wild-type and FXR1P cKO mice. We found that many cells in the cortex had lost FXR1P expression (Figure 2D). However, as expected, FXR1P expression was maintained in the Purkinje cells of the cerebellum (Figure 2E). Note that Purkinje cells are negative for NeuN, as previously published [245].

We also tried to determine the earliest time-point at which loss of FXR1P could be detected. Sections from P18 wild-type and cKO mice were stained with the anti-FXR1P antibody. In order to track recombined cells, these mice also contained the mT/mG reporter line. We found incomplete and sporadic loss of FXR1P in mEGFP expressing cells, indicating that at this time-point, the FXR1P protein was still in the process of being degraded in certain cells (data not shown). We then stained sections from P28 wild-type and cKO mice and found that most mEGFP positive cells had lost FXR1P expression (data not shown). However, since there were still a large number of CA1 cells with mTomato and FXR1P expression at this time-point (~40%) we chose to perform the rest of the experiments in this study on adult (>P60) wild-type and FXR1P cKO mice.

We first looked at whether loss of FXR1P resulted in any changes to the gross morphology of the hippocampus by staining free-floating sections using antibodies against markers for mature neuronal cell bodies (NeuN), dendrites (MAP2), ribosomes (P0) and astrocytes (GFAP). We saw no qualitative changes in NeuN expression in the CA1 region between wild-type and FXR1P cKO (Figure 2A). Staining for MAP2 showed no overt differences in dendrites between the cKO and wild-type (Figure 3A). Since we previously showed that the majority of FXR1P is colocalized with ribosomes [23], we were also interested in determining whether loss of FXR1P led to any changes in the expression or localization of ribosomes. We found no qualitative differences in the level or

pattern of staining of the large ribosomal subunit (Figure 3B). We also saw that P0 staining extended into the proximal dendrites of both wild-type and cKO CA1 neurons (Figure 3B, inset). We then looked at whether loss of FXR1P affected astrocytes, by staining with anti-GFAP (Figure 3C). We found that the pattern of GFAP staining was similar between wild-type and FXR1P cKO hippocampi. These results demonstrate that the loss of FXR1P is not causing any changes to the gross morphology of the hippocampus.

Loss of FXR1P reduces spine density and spine size

We were next interested in determining whether loss of FXR1P leads to a difference in spine density, spine size or spine shape. We used diolistics to label CA1 dendrites and spines in perfusion-fixed hippocampal slices from five sets of adult male wild-type and FXR1P cKO mice. Spinning-disk confocal imaging was used to image apical dendrites in the stratum radiatum of CA1 (~100 μm from the pyramidal cell layer). We used the three-dimensional automated quantification software NeuronStudio to measure dendrite widths, spine sizes and to classify spines as mushroom, stubby or thin. On visual inspection dendrites and spines seemed largely normal in the FXR1P cKO mice (Figure 4A), however quantification revealed several notable differences. Firstly, we found that dendrite widths were 14% larger in FXR1P cKO mice ($p=0.063$; Figure 4B). Secondly, we found that loss of FXR1P led to a 15% decrease in spine density ($p=0.014$; Figure 4C) and resulted in an 8% decrease in spine length ($p=0.043$; Figure 4D, F). However, spine head diameters were similar between wild-type and FXR1P cKO mice ($p=0.75$; Figure 4E, G). In addition, we found no significant differences in the proportion of mushroom, stubby and thin spines in wild-type and FXR1P cKO mice (data not shown).

Loss of FXR1P does not change basal synaptic properties or paired-pulse facilitation

Having found that loss of FXR1P reduced spine density and spine size, we wondered whether these structural changes would be reflected in changes to basal synaptic properties. By stimulating the Schaffer collateral pathway and recording field potentials in the stratum radiatum, we found no significant differences in the

input-output relationship between wild-type and FXR1P cKO mice (Figure 5A-C). Representative traces from one wild-type and FXR1P cKO slice are shown in Figure 5A. Averaged data from 18 wild-type and 19 cKO mice are shown in Figure 5B. This data was then averaged and presented in Figure 5C. Next, we looked at whether FXR1P cKO mice had altered pre-synaptic plasticity, measured by determining the paired-pulse facilitation ratio in response to two temporally spaced stimuli. Representative traces from a wild-type and cKO slice with an interpulse duration of 50 ms are shown in Figure 6A. We found no significant differences between genotypes in average paired-pulse facilitation at any of the inter-pulse intervals examined (ANOVA genotype*interval, p=0.77; Figure 6B). These results demonstrate that loss of FXR1P does not influence basal synaptic function and short-term pre-synaptic plasticity.

Loss of FXR1P enhances L-LTP but not E-LTP

Early-phase long-term potentiation (E-LTP) refers to a short-lived increase in synaptic strength (1-2 hours) that is normally induced using a weak stimulation protocol. This form of short-term synaptic plasticity requires the modification of pre-existing proteins at the synapse but is independent of new protein synthesis [7]. In contrast, late-phase LTP (LTP) is a long-lasting increase in synaptic strength (> 3 hours) that is induced using a strong stimulation protocol and requires rapid new protein synthesis [7,51,246]. We were therefore interested in determining whether loss of FXR1P led to a differential effect on E-LTP versus L-LTP. We first examined whether loss of FXR1P led to any differences in E-LTP. E-LTP was induced using a single train of high frequency stimulation (HFS: 1 x 100 Hz). Representative traces from a wild-type and cKO slice are shown in Figure 7A. We found that E-LTP, measured as a change in the initial slope of the fEPSP at 60 minutes post-HFS, was similar between wild-type and FXR1P cKO mice (p=0.71; Figure 7B). We then induced L-LTP (L-LTP) using four massed trains of HFS separated by a 20 second interval (4 x 100 Hz). Representative traces are shown in Figure 8A. When data from several animals were combined and averaged, we found that L-LTP was significantly increased by 40% at three hours post-HFS in

the FXR1P cKO versus wild-type mice (p=0.05; Figure 8B, C). These results suggest that loss of FXR1P enhances protein-synthesis dependent forms of LTP.

5.6 Discussion

Translational control of gene expression plays an important role in long-lasting forms of synaptic plasticity and long-term memory formation and storage. Here, we demonstrate that conditional loss of the specific translational regulator FXR1P decreases spine density and spine size, but at the same time enhances L-LTP. This suggests that FXR1P controls the translation of a subset of mRNAs required for maintaining proper spine structure and long-lasting synaptic plasticity.

First, we found that the FXR1P cKO had significantly less spines and smaller spines than wild-type animals, demonstrating that FXR1P plays a role in maintaining spine density and spine morphology. While this is consistent with our previous results demonstrating localization of overexpressed FXR1P at large, strong dendritic spines (Chapter 4), it is difficult to reconcile this finding with the enhanced L-LTP we see using electrophysiological measures. Since synaptic strength and size are generally correlated, a propensity for enhanced L-LTP would point to an increase in the number of large spines, not small spines. This paradox may be explained in several ways. First, it is thought that small spines are "learning" spines and have the ability to increase in size and strength in response to synaptic activity, whereas large spines act as "memory" spines and are more resistant to change [197,199]. Therefore, the increase in small spines in the FXR1P cKO may allow for enhanced L-LTP through either an increase in the number of spines undergoing L-LTP or an increase in the amount of potentiation at each spine. Secondly, the number of spines actually participating in strong memories in the FXR1P cKO mice may only be a small fraction of the total spine population. Therefore, the effect could be diluted when considering all spines. Although technically challenging, spines in the FXR1P cKO could be directly targeted using two-photon glutamate uncaging to look at whether loss of FXR1P leads to enhanced structural and functional L-LTP at single spines [47,48].

Importantly, we found that loss of FXR1P led to a selective enhancement in L-LTP and not E-LTP. This may be expected since E-LTP does not depend on new protein synthesis, whereas L-LTP does. However, several knockout mouse models of general translational regulators, notably eIF2α kinases, actually show conversion of E-LTP into L-LTP and weak memories into strong ones [10,11,93]. eIF2α phosphorylation represses global mRNA translation and CREB-dependent gene transcription, two key components of long-lasting synaptic plasticity. It is hypothesized that in mouse models where eIF2α phosphorylation is reduced, basal mRNA translation and CREB-dependent gene expression is enhanced, leading to increased expression of plasticity-related proteins and a lower threshold for inducing L-LTP [10,11]. However, since FXR1P forms part of the second level of translational regulation, it is likely that the first levels of translation regulation, such as ERK and mTOR signaling pathways and eIF2α dephosphorylation, still require a strong stimulus in order to be activated. In this regard, the FXR1P knockout is more similar to the forebrain-specific knockout of FKBP12, which also demonstrates a selective enhancement of L-LTP, but not E-LTP [8]. Since FKBP12 is an inhibitor of the mTOR signaling pathway, it is likely that other breaks, similar to the ones in the FXR1P cKO, need to be alleviated by a strong stimulus in order to induce L-LTP.

Loss of FXR1P leads to an immediate enhancement in L-LTP (Figure 8). This is consistent with the idea that L-LTP is divided into two distinct phases: 1) an early, transcription-independent but translation-dependent phase and 2) a transcription and translation-dependent phase [7,247]. Indeed, protein-synthesis inhibitors applied during the induction of L-LTP lead to an immediate decrease in the level of LTP, whereas transcription-inhibitors lead to a deficit in L-LTP maintenance [7]. Converging evidence points to an important role for rapid local protein synthesis in this initial phase of L-LTP. For example, researchers have shown that polyribosomes, mRNAs, translation factors, components of the mTOR and ERK signaling pathways and RNA-binding proteins are all found in the dendrites and at synapses [86,248]. In addition, BDNF induced L-LTP occurs in dendrites severed from the cell body, demonstrating that proteins can be

synthesized locally in response to synaptic activity [249]. This allows for the rapid and precise insertion of plasticity-related proteins into activated synapses. Whether FXR1P controls the local synthesis of these plasticity-related proteins is currently unknown. However, we have recently demonstrated that FXR1P is properly positioned to be involved in local translational control. In particular, we found that FXR1P formed small clusters in the dendrite and at a subset of large, mature dendritic spines [23]. Importantly, these clusters colocalized with ribosomes and mRNAs. Together, these results strongly support a role for FXR1P in the local translation of proteins related to L-LTP.

One important question that is raised by this study is: How does FXR1P control mRNA translation? Several studies point to a role for FXR1P in translational repression of its target mRNAs [33,156], although one study suggests that FXR1P could also activate translation [32]. In addition, a more recent study suggests that FXR1P regulates the levels of micro-RNAs, small non-coding RNAs involved in translational repression and mRNA degradation [223,250]. Our results showing enhanced L-LTP suggest that FXR1P represses the translation of plasticity-related proteins. We therefore predict that in the absence of FXR1P the mRNAs for these plasticity-related proteins are easier to translate and this leads to increased synapse strengthening. What is the identity of these plasticity-related proteins? Researchers have identified αCaMKII, PKMζ, Arc/Arg3.1 and BDNF as proteins that are upregulated during L-LTP induction and that play important roles either in the expression or maintenance of L-LTP [6]. Whether the basal or activity-dependent expression of these proteins is altered in the FXR1P cKO is currently under investigation. In addition, it is interesting to note that FXR1P binds to and represses the translation of *talin2* and *desmoplakin* mRNAs in heart muscle [156]. Although a role for Talin2 and desmoplakin at the postsynaptic density has yet to be established, they are both adaptor proteins linking cell-surface receptors to the actin cytoskeleton at focal adhesions and desmosomes, respectively. Since actin-remodeling plays an important role in structural spine plasticity and LTP, it is intriguing to wonder whether Talin2 and desmoplakin form part of these

plasticity-related proteins. Studies will need to be conducted to look at whether these two mRNAs are targets of FXR1P in the brain.

Our results showing a decrease in spine density and spine length along apical dendrites in area CA1 of the hippocampus and enhanced L-LTP are a striking contrast to the results researchers have obtained in the FMRP knockout mice. Loss of FMRP in humans is characterized by an increase in spine density and spine length, with an overabundance of filopodial, immature-looking spines [54]. Although the phenotypes appear more subtle and are region and age-specific in the FMRP knockout mice, a consistent phenotype appears to be an increase in spine length [19], which is opposite to the phenotype described here in the FXR1P cKO. In addition, a consistent phenotype observed in area CA1 in the FMRP knockout is enhanced protein-synthesis dependent mGluR-LTD, with no difference in L-LTP, and inconsistent differences in E-LTP [28,136,251–253]. Whether there are differences in mGluR-LTD in the FXR1P cKO remains to be tested. These disparate results lead to two models for the potential functional roles of FXR1P and FMRP in neurons. The first is one where FXR1P and FMRP regulate distinct, but perhaps overlapping, subsets of mRNAs, with FXR1P regulating the synthesis of "LTP proteins" and FMRP regulating the synthesis of "LTD proteins". The second is one where FXR1P and FMRP regulate the same mRNAs, but in opposite ways, with one acting as an activator of mRNA translation and the other acting as a repressor. Evidence suggesting that both FXR1P and FMRP can act as translational activators depending on the specific transcript and context supports this second model [32,148]. However, a detailed comparison of the mRNA targets for FXR1P and FMRP in the mouse hippocampus will be needed to help address this model.

What might be the behavioural consequences of loss of FXR1P? Based on results obtained from other translational regulators, specifically models with lower levels of eIF2α phosphorylation and increased CREB-dependent gene expression, a decrease in the threshold for inducing L-LTP is correlated with memories being formed quicker and easier in response to weak training paradigms

[10,11]. In contrast, in the FKBP12 conditional knockout, which shows an L-LTP phenotype similar to the FXR1P cKO, there is enhanced contextual fear memory, normal spatial memory but enhanced perseveration, indicating that enhanced memory formation may come with unexpected side-effects, such as an inability to forget old information [8]. Whether this is the case in the FXR1P cKO remains to be tested.

Here we demonstrate that translational control via the RNA-binding protein FXR1P is required for proper spine development and synaptic plasticity. These results provide support for the importance of specific translational controllers in the long-lasting strengthening of synaptic connections. Recent results suggest that any deviation in the levels of synthesized proteins can lead to deficits or enhancements in synaptic plasticity and cognitive function and this may underlie certain neurodevelopmental disorders such as autism spectrum disorders and Fragile X Syndrome [226]. By having a complete understanding of translational control in neurons, we may one day be able to treat these disorders by manipulating the levels of translational control back to a normal range by targeting specific RNA-binding proteins such as FXR1P.

5.7 Acknowledgements

This work was supported by the Canadian Institutes of Health Research (K.K.M.), Canada Research Chairs Program (K.K.M), Canadian Foundation for Innovation (K.K.M) and the National Institutes of Health grant 1R21DA026053-01 (U.S.A) (K.K.M. and D.S.). D.C. was supported through a Frederick Banting and Charles Best CIHR Doctoral Research Award and an FRSQ Doctoral Award. The authors would like to thank Dr. David Nelson for the floxed *Fxr1* mice and Edith Hanna for excellent technical support.

5.8 Figures

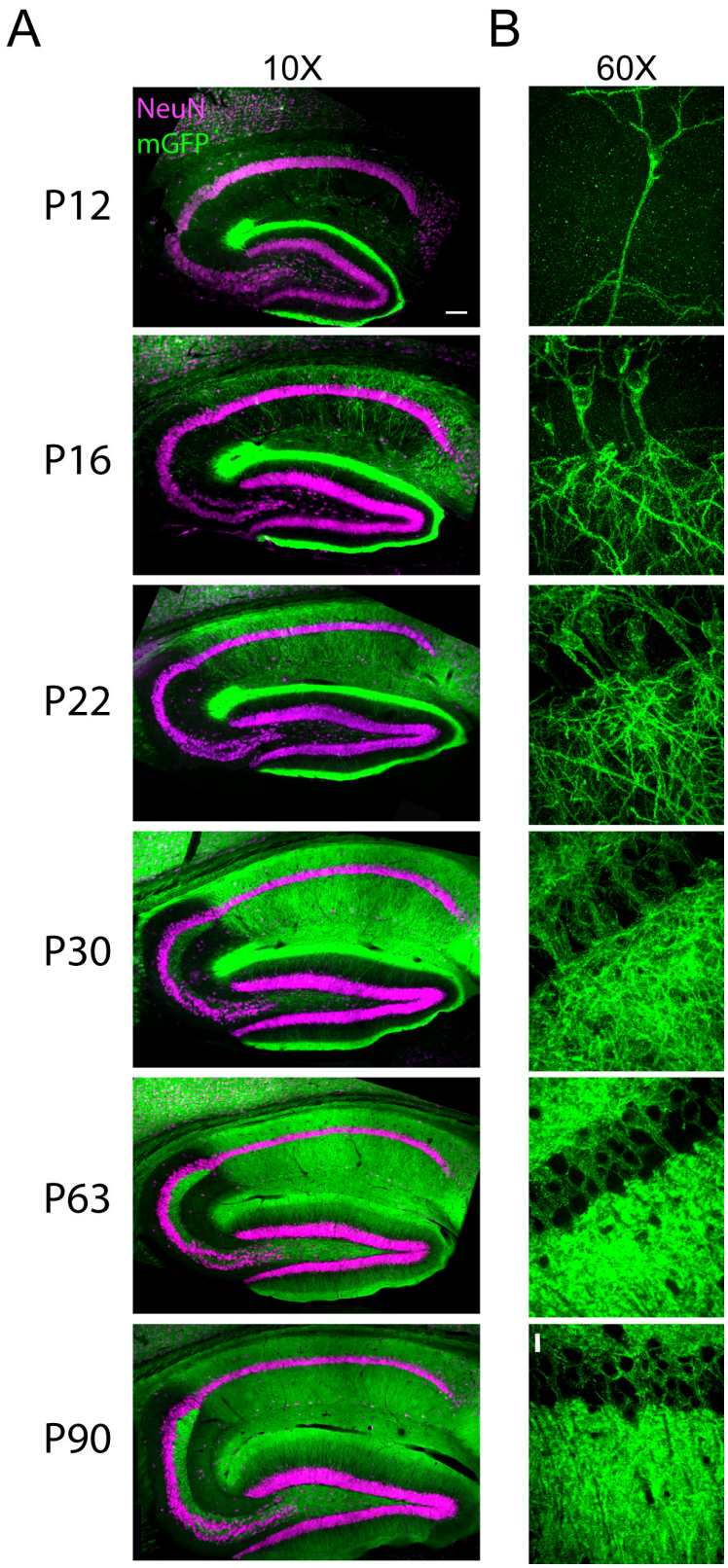

Figure 1: Cre expression using the αCaMKII-Cre (T29-1) driver line leads to a development-specific pattern of recombination in the postnatal mouse hippocampus. We crossed the αCaMKII-Cre (T29-1) driver line with a membrane-Tomato/membrane-GFP (mTomato/mGFP) reporter line in order to follow the pattern of Cre-recombination across postnatal development in the mouse hippocampus. **A.** 10X images of the hippocampus taken at different developmental time-points demonstrating the pattern of Cre-recombination. NeuN (magenta) staining delineates the cell body layers. Scale bar = 100 μm. B. High magnification view of the CA1 cell body layer showing the density of cells expressing mGFP. Scale bar = 10 μm.

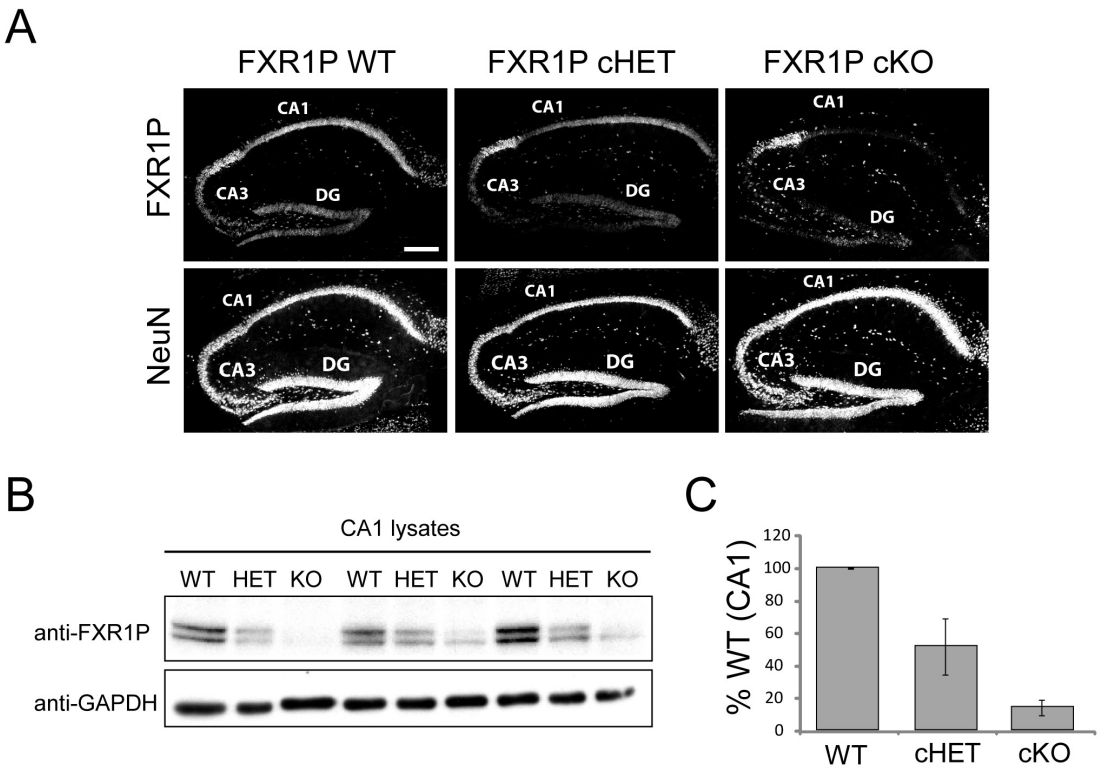
A
FXR1P WT
FXR1P cHET
FXR1P cKO
FXR1P
NeuN
CA1
CA3
DG
B
CA1 lysates
WT HET KO WT HET KO WT HET KO
anti-FXR1P
anti-GAPDH
C
% WT (CA1)
120
100
80
60
40
20
0
WT
cHET
cKO
D
Cortex
Layer VI
FXR1P
NeuN
FXR1P
NeuN
WT
cKO
E
Cerebellum
FXR1P
NeuN
FXR1P
NeuN

Figure 2: αCaMKII-Cre recombination results in loss of FXR1P in the CA1 region of the adult hippocampus. A. 10X images of hippocampal sections taken from P60 WT, FXR1P cHET and FXR1P cKO mice stained with an anti-FXR1P antibody (#ML13) and anti-NeuN antibody to delineate cell body layers. FXR1P is lost in a dose-dependent manner from the majority of CA1 excitatory pyramidal cells in the FXR1P HET and KO mice. Scale bar = 200 μm. **B.** Western blots from lysates prepared from the CA1 region of 3 sets of FXR1P WT, cHET and cKO mice. FXR1P was probed using an anti-FXR1P antibody (#ML13) which recognizes the medium isoforms (c and d) and anti-GAPDH was used as a loading control. FXR1P levels are reduced compared to wild-type levels in the FXR1P cHET and cKO mice. **C.** Quantification of the integrated intensity of the FXR1P signal, normalized for GAPDH and expressed as a percent of wild-type expression levels (n= 3 WT, 3 cHET, 3 cKO mice). **D, E.** Representative images (10X) taken from a region of the cortex (D) and cerebellum (E) stained with anti-FXR1P (#ML13) and anti-NeuN. FXR1P is lost from a large proportion of cells in the cortex, but is maintained in the Purkinje cells in the cerebellum. Scale bar = 100 μm.

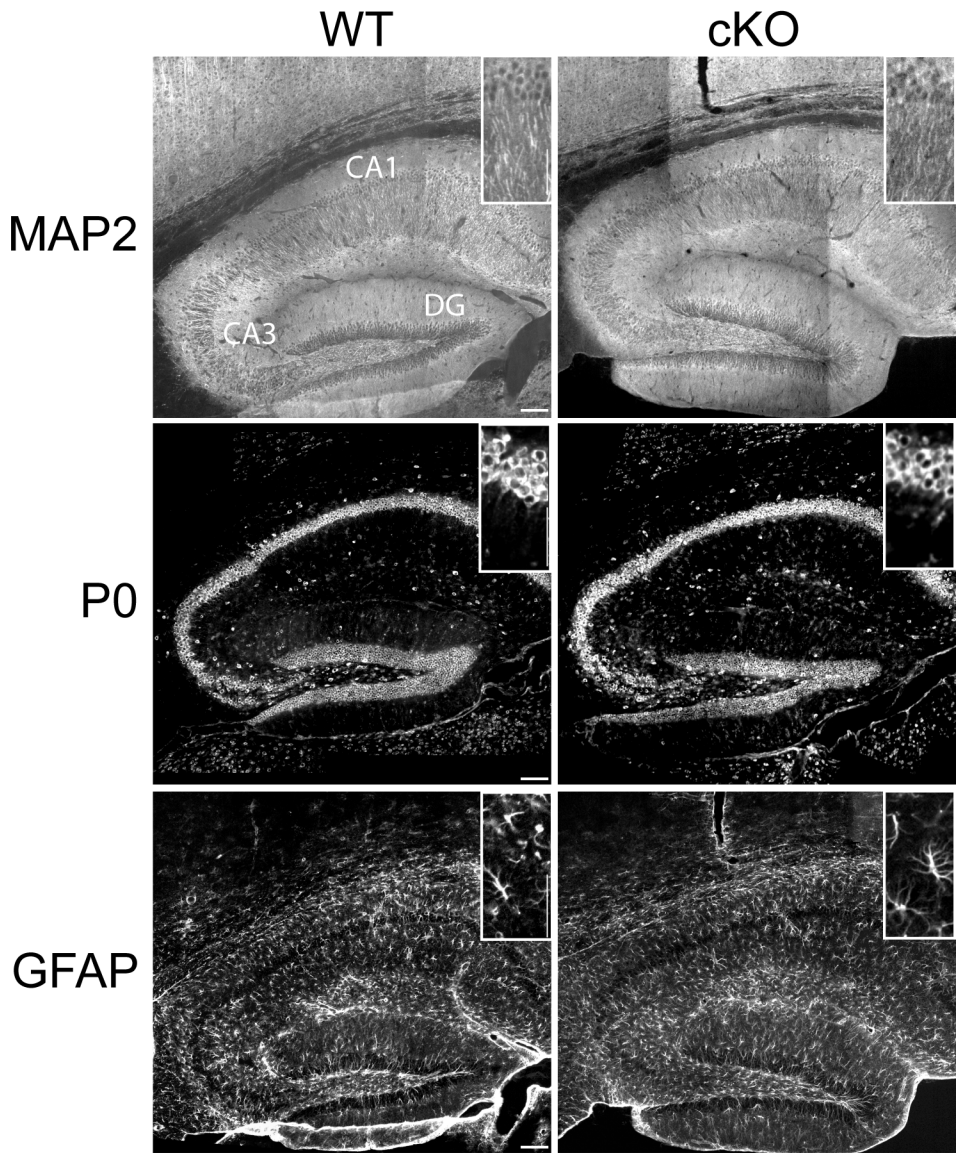

Figure 3: Loss of FXR1P does not disrupt the gross morphology of the hippocampus. Representative images (10X) of MAP2, P0 and GFAP staining taken from the hippocampus of an FXR1P WT and KO mouse. Loss of FXR1P caused no obvious differences in the levels or pattern of expression of MAP2, P0 and GFAP. Scale bar = 100 μm. *Insets* Higher magnification views of MAP2, P0 and GFAP staining. Scale bar = 50 μm.

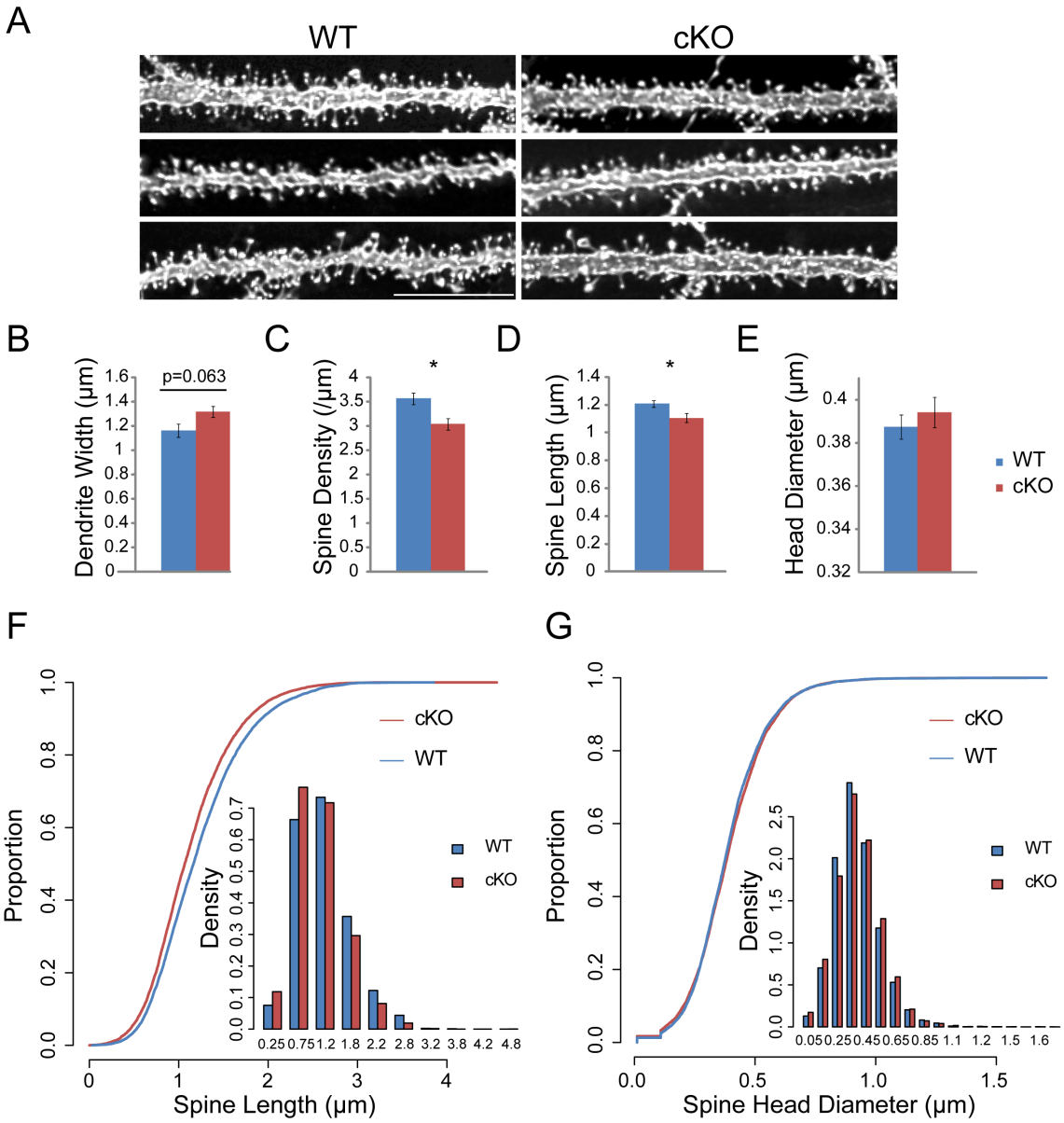
A
WT
cKO
B
Dendrite Width (µm)
p=0.063
C
Spine Density (/µm)
*
D
Spine Length (µm)
*
E
Head Diameter (µm)
WT
cKO
F
Proportion
cKO
WT
Density
WT
cKO
Spine Length (µm)
G
Proportion
cKO
WT
Density
WT
cKO
Spine Head Diameter (µm)

Figure 4: Loss of FXR1P reduces spine density and spine lengths. A total of five mice per genotype were used in this analysis. All quantifications were performed using NeuronStudio. **A.** Representative images of DiI-filled dendrites and dendritic spines taken from WT and FXR1P cKO mice. Scale bar = 10 μm. **B.** Loss of FXR1P leads to a trend towards wider apical dendrites (WT: 1.16 +/- 0.06 μm KO: 1.32 +/- 0.05 μm, p = 0.063). **C.** Loss of FXR1P leads to a significant 15% decrease in spine density on apical dendrites (WT: 3.56 +/- 0.12 μm^{-1}, KO: 3.04 +/- 0.12 μm^{-1}; p = 0.014). **D.** Spine lengths on apical dendrites are reduced by 8% in the FXR1P cKO (WT: 1.21 +/- 0.02 μm, KO: 1.11 +/- 0.03 μm, p = 0.043). **E.** No change in average spine head diameters (WT: 0.39 +/- 0.006 μm, KO: 0.39 +/- 0.007 μm, p = 0.48). **F, G.** Cumulative probability and histograms showing the distributions of spine lengths (F) and spine head diameters (G) from apical dendrites in WT and cKO mice (n= 8543 WT spines, n= 7635 KO spines). The distribution of spine lengths is shifted to the left in FXR1P KO mice (F), whereas only small differences exist in the distribution of spine head diameters (G). n = 5 WT and 5 cKO mice (all male). All values represent means +/- standard errors. Statistical analysis was performed using unpaired two-tailed t-tests.*$p<0.05$.

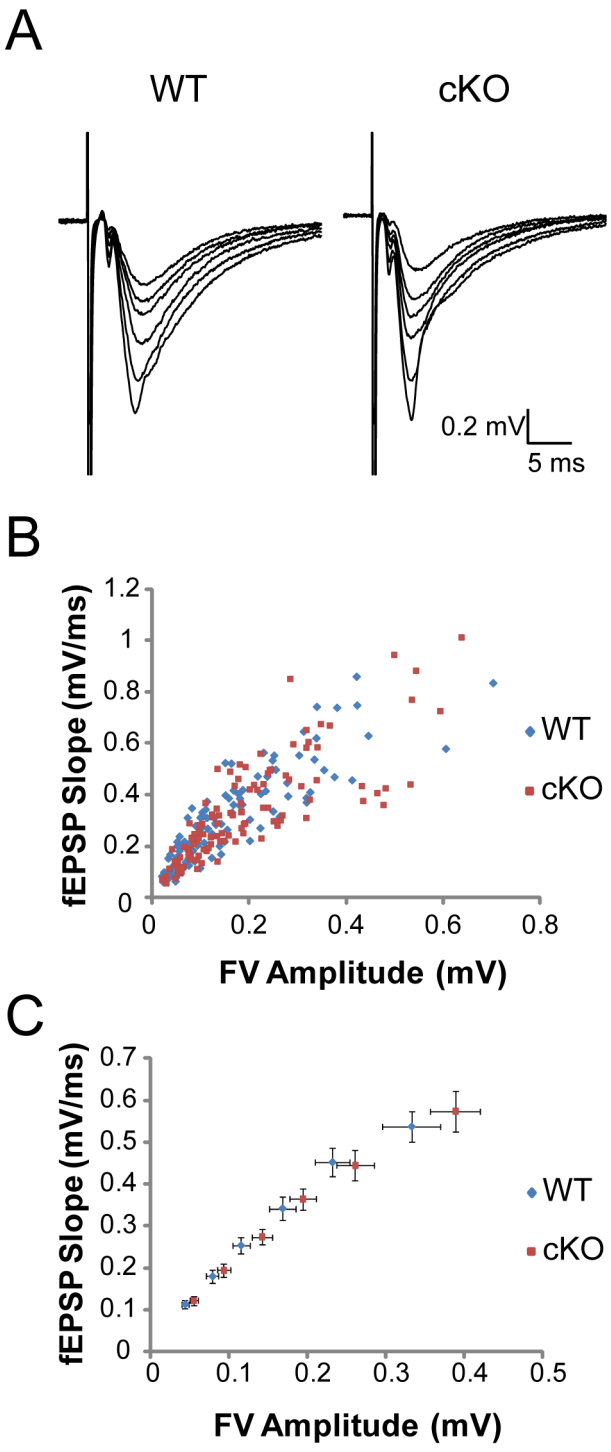
A
WT
cKO
0.2 mV
5 ms
B
fEPSP Slope (mV/ms)
FV Amplitude (mV)
WT
cKO
C
fEPSP Slope (mV/ms)
FV Amplitude (mV)
WT
cKO

Figure 5: Basal synaptic transmission is unaltered in FXR1P cKO mice. A. Representative traces of fEPSPs from a WT and FXR1P cKO acute hippocampal slice. Each trace is an average of approximately 5 sweeps. **B.** An input-output curve for each animal was constructed by plotting the initial slope of the fEPSP against the amplitude of the fiber volley at increasing stimulation intensities. Responses from 1-4 slices per animal were averaged (n = 18 WT (12 females, 6 males) mice, n = 19 cKO (12 females, 7 males) mice). Responses were comparable between WT and FXR1P cKO mice. **C.** Averaged input-output curve showing similar slopes between WT and FXR1P cKO mice.

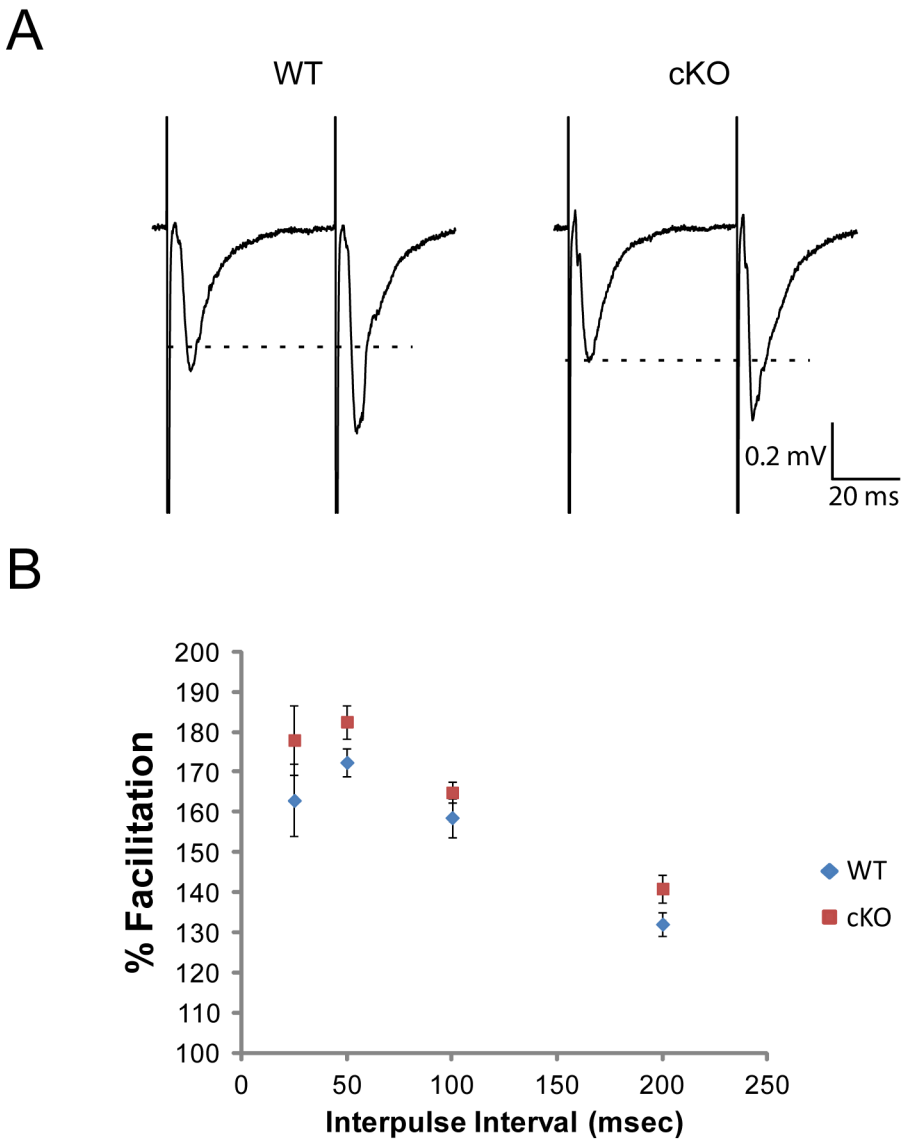

Figure 6: Short-term pre-synaptic plasticity is unaltered in FXR1P KO mice. Differences in short-term pre-synaptic plasticity were determined by measuring paired-pulse facilitation at different inter-stimulus intervals (25, 50, 100, 200 ms) in acute hippocampal slices. **A.** Representative traces of paired-pulse facilitation at a 50 ms interval from a WT and FXR1P cKO slice. Each trace is an average of 5 sweeps. **B.** Loss of FXR1P does not significantly alter paired-pulse facilitation (Two-way mixed ANOVA, genotype*inter-stimulus interval, p=0.77, main effect p=0.005 (Genotype); n = 7 WT mice (5 females, 2 males), n = 8 cKO (6 females, 2 males) mice). % Facilitation was calculated by dividing the initial slope of the second fEPSP by the initial slope of the first fEPSP.

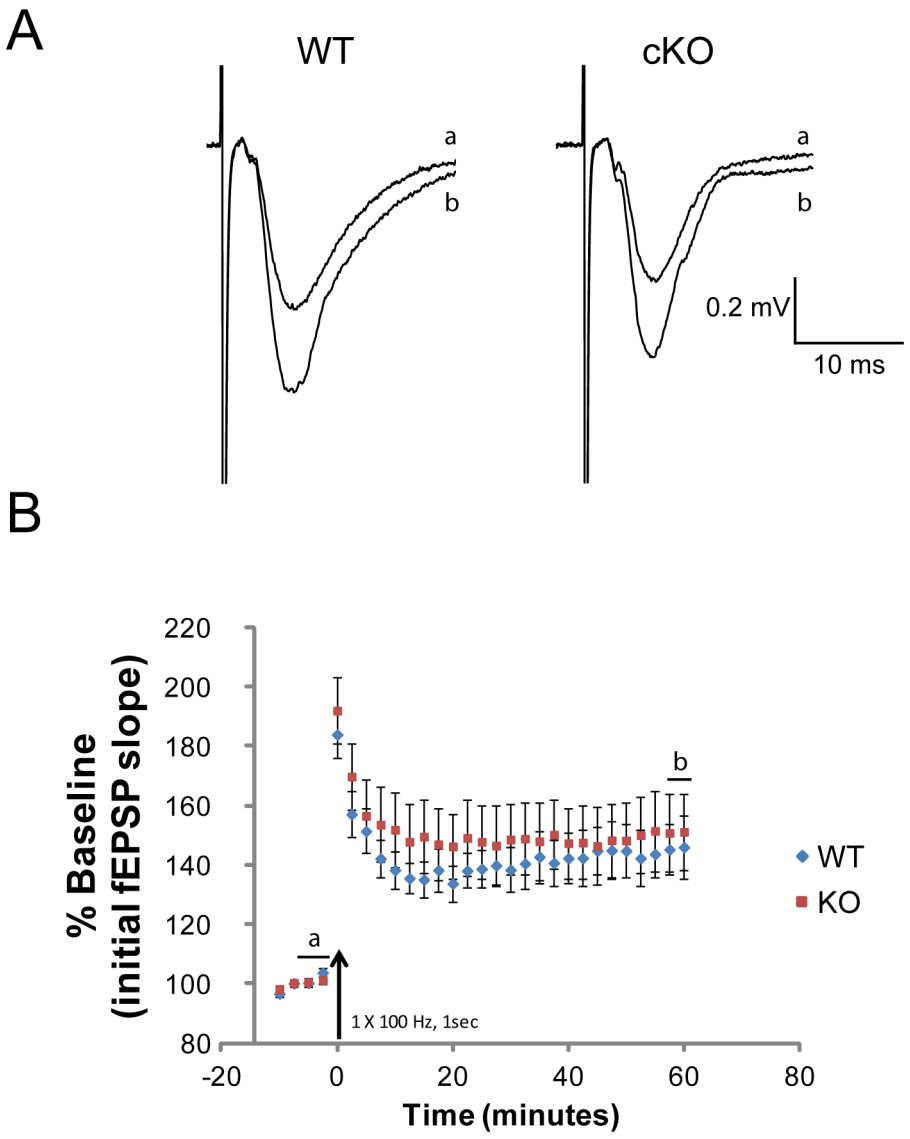

Figure 7: FXR1P cKO mice have normal E-LTP. A. Representative traces of E-LTP induced in a WT and FXR1P cKO hippocampal slice. Each trace is an average of 10 consecutive sweeps representing a) 5 minutes of baseline immediately preceding high frequency stimulation and b) the period from 55-60 minutes post-LTP. **B.** A single train of high frequency stimulation (HFS: 1x100 Hz) produced similar levels of E-LTP in WT (n = 8 mice (4 females, 4 males), 9 slices) and FXR1P KO animals (n = 10 mice (5 females, 5 males), 12 slices). E-LTP, measured between 50-60 minutes post-HFS, was unaltered by the loss of FXR1P measured using initial fEPSP slope (WT: 144.39 +/- 8.99%, KO: 150.34 +/- 12.89%, two-tailed, unpaired t-test p=0.71).

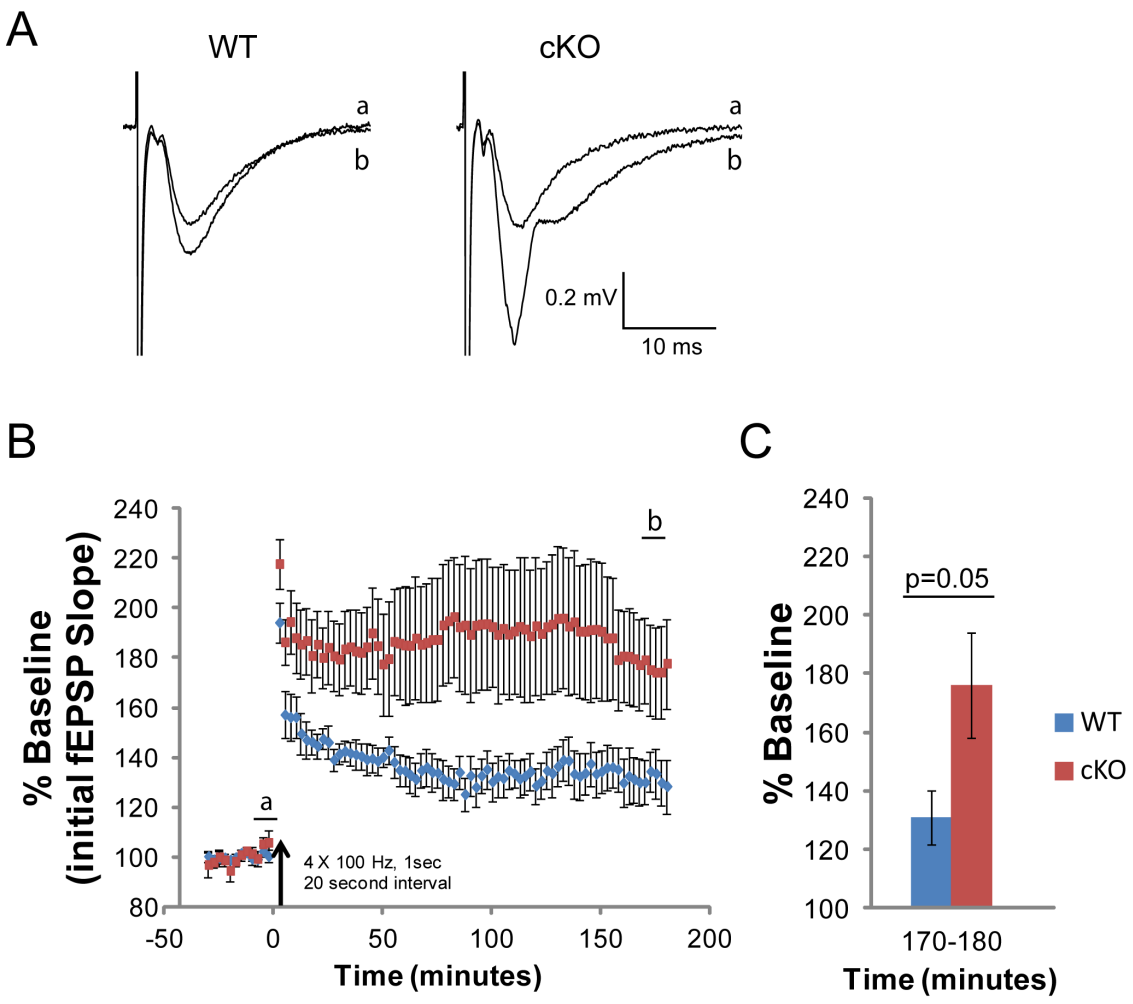

Figure 8: FXR1P cKO mice express enhanced L-LTP. A. Representative traces of L-LTP induced in a WT and FXR1P KO hippocampal slice. Each trace is an average of 10 consecutive sweeps representing a) 5 minutes of baseline immediately preceding high frequency stimulation and b) the period from 175-180 minutes post-LTP. **B.**Four trains of high frequency stimulation delivered at 20 second intervals (4xHFS) produced higher levels of potentiation in FXR1P cKO animals (n = 7 mice (4 female, 3 male), 7 slices) than WT animals (n = 7 mice (5 female, 2 males), 7 slices). **C.** L-LTP, measured between 170-180 minutes post-HFS, was 40% greater in FXR1P KO versus WT animals measured using initial fEPSP slope (WT: 131.14 +/- 9.25%, KO: 176.02 +/- 17.78%, two-tailed, unpaired t-test p=0.05).

CHAPTER 6:

FINAL CONCLUSIONS

6.1 Original contributions to knowledge

Our main goal in conducting the research presented in this doctoral thesis was to characterize the involvement of the RNA-binding protein FXR1P in local, gene-specific translational control of mRNAs important for spine development, synaptic plasticity and memory. We hypothesized that FXR1P controls the local translation of mRNAs required for proper spine development and long-lasting synaptic plasticity.

Prior to starting this research project, only a few studies had looked at the expression pattern of FXR1P in the mammalian brain and none had described a functional role for FXR1P. Research into the functional role of FXR1P in the brain was restricted by the fact that, unlike the full knockouts of both FMRP and FXR2P which are both viable, the knockout mouse of FXR1P dies shortly after birth [155]. We addressed this issue by creating a postnatal forebrain-specific knockout of FXR1P. This strategy allowed us to study how loss of FXR1P affected spine development, synaptic physiology and behaviour in adult mice.

However, before getting to these crucial final experiments, we first performed a full characterization of the expression pattern, subcellular localization and overexpression phenotype of FXR1P in hippocampal neurons. The aim of Chapter 3 was to address the first part of our hypothesis—that FXR1P controls the local translation of mRNAs in neurons. We chose to address this aim indirectly by looking at the expression and localization pattern of FXR1P in cultured hippocampal neurons. We predicted that if FXR1P is controlling local mRNA translation, then it should be found in dendrites colocalized with ribosomes and mRNAs. Our major original finding from these experiments was that FXR1P associated with the protein synthesis machinery in dendrites and at the base of a subset of dendritic spines. Although this result does not by itself demonstrate that FXR1P directly controls mRNA translation, the tight association of both

endogenous and exogenous FXR1P with the translational machinery is strong support for some role in mRNA metabolism, whether it is mRNA transport, anchoring, stability or translational control. We also made several smaller, but equally important, original findings. We found that the expression of FXR1P, FMRP and FXR2P, as well as the ribosomal subunit L7, were highest during the first two postnatal weeks and gradually decreased into adulthood. Since this correlates with a period of high synaptic plasticity, it suggests that FXR1P, like FMRP and FXR2P, could also play an important role in synapse formation, maintenance or plasticity. Additionally, we found that FXR1P colocalized with its paralogs FMRP and FXR2P in clusters along the dendrite. Although confocal imaging does not have sufficient resolution to allow us to determine whether FXR1P, FMRP and FXR2P are sharing the same mRNAs targets, this result does show that there is a close association of RNPs containing FXR1P, FMRP and FXR2P. Importantly, we were also able to demonstrate that overexpressed eGFP-FXR1P showed a similar expression pattern and colocalization with the protein synthesis machinery as endogenous FXR1P, allowing us to use this construct to study whether overexpression of FXR1P alters the structure and function of dendritic spines (Chapter 4). Overall, the results from Chapter 3 are a strong indication that FXR1P could be locally controlling mRNAs important for spine development and synaptic plasticity.

Our next goal was to determine whether FXR1P plays a role in spine development. As a first step to address this goal, we tested whether increasing the levels of FXR1P, by overexpressing eGFP-FXR1P in organotypic hippocampal slices, altered spine density, spine morphology or synaptic function (Chapter 4). We found that overexpressing FXR1P did not induce significant changes to overall spine density, spine morphology or synapse function. However, by comparing the small subset of FXR1P-positive dendritic spines (~20%) to FXR1P-negative spines we found that these spines were on average larger, more likely to be mushroom-shaped and contained more AMPA receptors than their negative counterparts. Although this result only shows a correlation between FXR1P clusters and large, mushroom-shaped, and functionally stronger spines, it

does suggest that FXR1P may be involved in creating or maintaining mature dendritic spines.

Our next aim was to directly test whether FXR1P is required for spine development and synaptic plasticity. To address this aim, we generated a postnatal forebrain-specific knockout of FXR1P. This approach allowed for the efficient deletion of FXR1P in the postnatal forebrain starting around postnatal day 12 (P12) and complete in the hippocampal CA1 area by P60. In support of a role for FXR1P in maintaining mature dendritic spines, we found that CA1 pyramidal cells from adult FXR1P cKO mice had less spines and smaller spines than wild-type mice (Chapter 5). Paradoxically, however, we found that loss of FXR1P actually led to enhanced L-LTP. Importantly, we also showed that loss of FXR1P did not alter basal synaptic transmission, paired-pulse facilitation and E-LTP, which unlike L-LTP, do not require rapid new protein synthesis. Altogether, these results suggest that FXR1P is essential for maintaining dendritic spine density and size and for regulating specific aspects of long-term synaptic plasticity.

6.2 Significance to behaviour

Our results are the first demonstration that like FMRP, FXR1P is also required for maintaining proper synaptic structure, function and plasticity. Complete absence of FMRP leads to moderate to severe behavioural consequences in humans, including intellectual disability and autism [16,18]. However, the behavioural consequences in mice are much more subtle and mixed, with several studies reporting conflicting results in learning/memory paradigms including the Morris water maze and fear conditioning tests. FMRP knockout mice display normal spatial learning and memory in the Morris water maze, but take significantly longer to re-learn the location of the platform if it is moved to the opposite quadrant (reversal learning) [229,231,254]. This may indicate a deficit in behavioural flexibility, increased perseveration or interference of the old memory [254]. However, other studies have reported no differences in the Morris water maze, an effect that has led some researchers to conclude that the subtle behavioural deficits are dependent on the background strain used in the study [230,252,255,256].

Similar results have been obtained using contextual fear conditioning, where either a subtle deficit or no deficit has been obtained [230]. These results indicate a subtle deficit in learning and memory in the FMRP knockout mice.

As mentioned in previous discussions, we have noted that results of gain-of-function and loss-of-function experiments with FXR1P show phenotypes opposite or different to those observed in studies on FMRP. For instance, whereas over-expressing FMRP caused synapse elimination [143], we have shown that overexpressed FXR1P localized to large, mature spines (Chapter 4). In addition, loss of FXR1P decreased spine density and spine length, whereas loss of FMRP is associated with increased spine density and spine length [19,54]. This argues that FXR1P is instead required for spine growth or maintenance. We have also shown a difference in synaptic plasticity between the two knockouts, with loss of FMRP leading to enhanced mGluR-LTD but no change in L-LTP, but loss of FXR1P leading to enhanced L-LTP [28,136]. Although it is difficult to compare results from these measures between the full FMRP knockout with our conditional FXR1P knockout, we nevertheless were interested in determining if these distinct phenotypes would be reflected in the behaviour of the FXR1P cKO mouse. We performed these experiments in cooperation with the Neurophenotyping Centre at the Douglas Hospital. The key results are summarized here. We found that FXR1P cKO mice performed similar to wild-type mice on both the regular version of the Morris water maze and contextual fear conditioning tests. However, FXR1P cKO mice were actually quicker at learning the new platform location when it was moved to the opposite quadrant. These results indicate that FXR1P cKO mice have normal learning and long-term memory, but display enhanced behavioural flexibility or executive function. Intriguingly, although the FXR1P cKO mice were better at learning the new platform location, they spent more time in the old quadrant location during the probe trial. Upon deconstructing the data further we realized that the mice were heading for the new location first, however once they realized that the platform was no longer there, decided to head back to the old location. Therefore, it appears that the FXR1P cKO mice are better at preserving and using both memories. This indicates that in addition to playing a

role in the hippocampus, FXR1P may also be important in the prefrontal cortex, a region that has been implicated in this type of executive function/behavioural flexibility. These results demonstrate that FXR1P cKO mice display an interesting behavioural phenotype that is different and potentially opposite to that seen in the FMRP knockout mouse.

6.3 Unanswered questions/future directions

These findings raise the intriguing possibility that FMRP and FXR1P may be functioning in similar, but opposing pathways, either because they bind to separate mRNA targets or because they bind to the same mRNA targets but function in opposite ways. Although it remains to be tested whether loss of FXR1P alters mGluR-LTD, our results are reminiscent of two papers that have demonstrated that Stau1 and Stau2 are required for L-LTP and mGluR-LTD, respectively [122,123]. Interestingly, Stau1 and Stau2 are present in distinct RNPs and associate with different mRNAs, which potentially explains their differential roles in synaptic plasticity [120]. We have found that FMRP, FXR1P and FXR2P show partial colocalization in RNPs along the dendrite [23]. However, due to the resolution limits of confocal microscopy it remains unclear if the proteins are present in the same RNPs or positioned in separate RNPs located close to each other. Also, since the nature of the mRNA composition of an RNP is currently unknown (whether it contains one type of mRNA or several) the fact that they may be present in the same RNPs does not necessarily mean that they are bound to the same mRNAs [12]. Whether FMRP and FXR1P bind to the same or different mRNA targets is currently being tested by one of our collaborators, Dr. Edouard Khandjian. In addition, we are currently using western blotting to screen for changes in the levels of synaptic proteins that may help explain the phenotypes seen in the FXR1P cKO mice. For instance, we are interested in probing for changes in proteins involved in increasing spine size or spine function such as PSD95, GluA1, Shank and Homer. However, since FXR1P may only have an influence on activity-dependent new protein synthesis, it may be necessary to employ more sophisticated techniques to isolate only this pool of newly synthesized proteins. This was previously performed using radioactive pulse-

chase labeling; however in recent years a new technique called bioorthogonal noncanonical amino acid tagging (BONCAT) has been developed to isolate the pool of newly synthesized proteins [257]. We plan to induce L-LTP in slices from wild-type and FXR1P cKO animals and use BONCAT to isolate the pool of newly synthesized proteins. We will then probe this subset of proteins for changes in the levels of our target synaptic proteins. Results from these types of experiments will provide more insight into the roles of FXR1P and may help elucidate the identity of proteins involved in L-LTP.

Since new proteins can be shared between two active synapses, the locus of new protein synthesis is likely the dendrite and not the individual synapse [47]. However, we and others have found that endogenous and exogenous RNA-binding proteins and mRNAs cluster in specific locations along the dendrite and at dendritic spines [12,23,108]. Therefore, if RNA-binding proteins and mRNAs are specifically localized and mostly immobile, how are proteins shared across the dendritic branch? First, it is likely that these RNPs represent storage sites of repressed mRNAs and not actively translating mRNAs. This is supported by several studies that indicate that RNPs or RNA granules dissolve and/or release their mRNAs in response to synaptic activity [106,107]. These mRNAs are no longer anchored by being part of the granule and are free to diffuse along the dendrite, allowing new proteins to be picked up by any active synapses. Second, bath application of BDNF and KCl increases the percentage of RNPs that are mobile, which may represent the redistribution of these particles to more active regions [13,108]. In support of this, our preliminary results using time-lapse imaging in dissociated hippocampal cultures suggest that some FXR1P clusters can travel from one spine to the next, as if they are sampling these spines for their metabolic demands. We predict that high levels of synaptic activity may lead to the anchoring of these mobile clusters at spines. In order to test for this, we could activate single spines using two-photon glutamate uncaging and look for directed movement and anchoring of FXR1P clusters at these spines. These clusters may then serve to exclusively provide these potentiated spines with mRNAs for spine growth and maintenance, leading to the correlation between FXR1P clusters and

large, strong spines that we noted in Chapter 4. Therefore, although RNPs are highly localized there are several possibilities to explain how mRNAs and proteins can be shared between activated spines.

In conclusion, this thesis provides the first description of the expression pattern, localization and function of the RNA-binding protein FXR1P in the hippocampus. Our results support the recent hypothesis put forth by Bear et al.[226] that loss of a translational regulator, potentially leading to subtle changes in the levels of plasticity-related proteins, can lead to unexpected consequences on synaptic plasticity and behaviour as presented here. Our results demonstrating enhanced L-LTP and improved behavioural flexibility in the FXR1P cKO support improved cognitive performance. However, it remains to be seen whether this improvement compromises other types of learning and behaviours. For instance, improved learning may make it more difficult to forget old or less useful information. Indeed, enhanced L-LTP has previously been associated with increased perseveration and autism-like behaviours [8]. More research is needed to determine whether these behavioural deficits are also seen in the FXR1P cKO mouse. Only with a complete functional and behavioural analysis of the FXR1P cKO mouse will we be able to determine whether FXR1P could be a potential drug target for treating cognitive impairments.

APPENDIX A:

A NEURON-ASTROCYTE CO-CULTURE SYSTEM TO INVESTIGATE ASTROCYTE SECRETED FACTORS IN MOUSE NEURONAL DEVELOPMENT

Emma V. Jones*, Denise Cook*, and Keith K. Murai
*These authors contributed equally to this work

Published in: Methods in molecular biology (Clifton, N.J.) 814: 341-52.

i. Abstract

Astrocytes secrete factors that promote neuron survival, synapse formation and plasticity. Understanding how these factors perform these roles requires a robust *in vitro* system that can effectively assess the impact of individual glial factors on neuronal properties. A classical approach to studying neuron-glial interactions *in vitro* uses a system where dissociated embryonic rat neurons are suspended over a feeder layer of rat astrocytes. Here, we describe a useful "sandwich" co-culture system where postnatal mouse hippocampal neurons are grown suspended above a feeder layer of mouse hippocampal astrocytes. We demonstrate that neurons in these cultures remain healthy beyond three weeks *in vitro* and develop more synapses compared to neurons grown without astrocytes. An advantage of this method is that astrocytes and neurons can be prepared separately from postnatal transgenic or knock-out mouse lines allowing one to study, for example, how wild-type neurons develop in the presence of astrocytes from a knock-out mouse line that lacks the expression of a specific astrocyte-secreted factor. We find this culture system to be a convenient and powerful approach to study the contribution of astrocyte-secreted molecules to neuron development.

1. Introduction

Astrocytes are the most abundant cells in the brain and were initially described as support cells that promote neuronal growth and survival [258]. More recent studies have revealed that astrocytes play an integral role in synaptic transmission and plasticity by regulating extracellular ion homeostasis, removing excess neurotransmitter from the synaptic cleft and releasing neuromodulatory factors [259,260]. In addition, astrocytes are important during synapse development. For example, neurons grown in the absence of astrocytes produce fewer functional synapses than neurons grown either with astrocytes or with astrocyte-conditioned media, suggesting that factors secreted by astrocytes are necessary for synaptic development [261]. To date, only a few of these factors have been identified (reviewed in [262,263]). Therefore, characterizing the full complement of these secreted factors remains an active area of neuroscience research.

To investigate the contribution of astrocyte-secreted factors in synapse development, we have developed a "sandwich" culture system using postnatal hippocampal neurons and astrocytes derived from mouse. This culture system is an adaptation of the method initially described by Gary Banker, where embryonic rat hippocampal neurons are grown at low-density above a feeder layer of astrocytes [264]. The original culture system was optimized for rat neurons, which are known to have better survival and growth than mouse neurons. The advantage of creating a mouse culture system is that it is compatible with transgenic or knock-out mouse models. This facilitates the production of "mix and match" cultures where wild-type or knock-out neurons can be cultured with wild-type or knock-out astrocytes. We find that our "sandwich" method of neuron-astrocyte co-culture produces postnatal mouse hippocampal neurons that survive beyond three weeks *in vitro* and elaborate complex dendritic arbors and produce dendritic spines (Figures 2 and 3). Since neurons are cultured in the absence of glial contact, this system is especially useful for investigating how astrocyte-secreted factors influence neuron survival and synapse development.

2. Materials

Common equipment, materials and solutions for dissections

1. Uncoated, sterile 10 cm dishes
2. Dissection microscope
3. Horizontal and vertical laminar flow hoods (*see* **Note 1**)
4. Autoclaved and fire-polished Pasteur pipettes (*see* **Note 2**)
5. 150 ml Sterile filter cups (Millipore, SCGVU01RE)
6. 10 ml and 60 ml syringes (BD-Falcon)
7. 0.22 μm filters (Fisher)
8. Haemocytometer
9. Fine-tipped dissection tools (i.e. Dumont no.5), microscissors and spatula (Fine Science Tools)
10. 12 well dishes (BD-Falcon)
11. Borate Buffer (0.1 M pH 8.5): Prepare separate solutions of 0.1 M boric acid, pH 5.6 (Sigma-Aldrich, B6768) and 0.1 M sodium tetraborate, pH 8.7 (Sigma-Aldrich, 221732). Combine in a 10:9 ratio (boric acid: sodium borate), filter-sterilize using sterile filter cups and store at 4ºC.

2.1 Material/solutions needed for the preparation of mouse hippocampal astrocytes

1. P0-P2 mouse pups (*see* **Note 3**)
2. 70 μm cell strainer (BD Biosciences, 352350)
3. 75 cm^2 tissue culture flasks (Sarstedt)
4. Sterile double distilled water (Invitrogen)
5. Poly-D-Lysine Hydrochloride (Sigma-Aldrich, P7886): Prepare stock solution by dissolving in borate buffer to 2 mg/ml. Filter-sterilize using syringe filter. Store at -20ºC. Dilute to 0.1 mg/ml in borate buffer at time of use (*see* **Note 4**).
6. Glial Growth Media: Minimum Essential Media containing Earle's salts and L-glutamine (Invitrogen, 11095080) supplemented with glucose 0.6% (v/v) (from 45% glucose solution, sterile, Sigma-Aldrich, G8769), 1%

penicillin-streptomycin (Invitrogen, 15140122) and 10% heat-inactivated horse serum (Invitrogen, 26050088). Store at 4ºC for up to one month.

7. Dissection Media: Hank's Buffered Salt Solution (Invitrogen, 141850052) supplemented with 10 mM HEPES (1 M stock, Invitrogen 15630080). Store at 4ºC.

2.2 Material/solutions needed for preparing the astrocyte feeder layer

1. Paraffin
2. Trypin-EDTA (0.025%, Invitrogen)
3. Fresh or frozen astrocytes

2.3 Material/solutions needed for freezing down astrocytes

1. Cryotubes (Nunc)
2. Sterile DMSO (Sigma-Aldrich)
3. Freezing Media: Glial Growth Media supplemented with 30% horse serum and 30% DMSO. Prepare fresh and leave on ice.

2.4 Material/solutions needed for preparing mouse hippocampal neurons

1. Litter of P0 mice (*see* **Note 3**)
2. 15 mm (circle) glass coverslips (Fisher, cat no. 12-545-83 'D'), acid-washed and sterilized (*see* **Note 5**).
3. Poly-L-Lysine Hydrobromide (Sigma-Aldrich, P2636): Prepare stock solution by dissolving in borate buffer to 2 mg/ml. Filter-sterilize using syringe filter. Store at -20ºC. Dilute to 0.1 mg/ml in borate buffer at time of use (*see* **Note 4**).
4. Neuronal Growth Media: Neurobasal-A (Invitrogen, 10888022) supplemented with 1% GlutaMAX-1 (Invitrogen, 35050061), 2% B-27 (Invitrogen, 17504044) and 1% penicillin/streptomycin (Invitrogen, 15140122). Store at 4°C for up to one month.
5. Papain (Sigma, P4762). Prepare a 1% solution in H_2O, filter-sterilize and store at -20ºC in 250 µl aliquots.
6. **Prepare fresh the day of dissection**: Solution A: 2.25 ml Neuronal Growth Media supplemented with 0.02% BSA, filter sterilized.

7. **Prepare fresh the day of dissection**: Solution B: 5 ml Neurobasal-A supplemented with 1% BSA and 1% trypsin inhibitor (Sigma, T4385), filter-sterilized. Divide into 2 tubes.
8. Cytosine β-D-arabinofuranoside (Ara-C) (Sigma, C1786). Prepare 3 mM aliquots in sterile ddH_2O, store at -20ºC.

3. Methods

The success of this method depends on careful planning, organization and attention to detail. As shown in Figure 1, it takes over one month to prepare neurons for experiments. Hippocampal astrocytes must be prepared at least 2 weeks before the planned neuron dissection (consider freezing down astrocytes to alleviate the process, see 3.3). Other smaller steps, including preparing paraffin dots, cleaning coverslips, coating and washing dishes must be carefully integrated into the schedule to ensure that the necessary materials are ready for each dissection. Although this method requires significantly more work than direct co-cultures of neurons and astrocytes, we found that our "sandwich" co-culture method produces reliable, healthy neuron cultures from postnatal (P0) mouse tissue (see Figures 2 and 3) that can be used to study the role of astrocytes in regulating neuronal development. For example, we can study how astrocyte-secreted factors control synapse formation by comparing synapses on wild-type neurons cultured with astrocytes prepared from either wild-type mice or knock-out mice. In addition, immunostaining, imaging and quantification of our cultures are aided by the fact that neurons can be plated at a low density with negligible glial contamination on the coverslips.

3.1. Preparation of mouse hippocampal astrocytes (approximately two weeks before neuron dissection)

1. One day before dissection, coat a 75 cm^2 flask with 5 ml of 0.1 mg/ml poly-D-lysine. Leave overnight in cell culture incubator (37ºC). The following day, wash flask twice with sterile water (*see* **Note 6**).

2. Prior to dissection, add 15-20 ml of Glial Growth Media to the flask and place in cell culture incubator to allow media to equilibrate to 37ºC, 5% CO_2.
3. Prior to dissection, pipette 3 mls of Glial Growth Media in a 50 ml tube and place in 37ºC water bath.
4. At the start of the dissection, remember to pre-warm the rest of the Glial Growth Media in a 37ºC water bath.
5. Turn on blower in horizontal flow hood containing dissection microscope. Wipe down all surfaces and dissection tools using 70% ethanol (*see* **Note 7**).
6. Prepare 3-4 10 cm dishes containing chilled Dissection Media (*see* **Note 8**).
7. Decapitate pups with sharp scissors (*see* **Note 9**). Place heads in a 10 cm dish containing Dissection Media.
8. Carefully pry away the skin and thin skull using either microscissors and/or no 5. forceps. Carefully remove brains with a small spatula and place in a fresh 10 cm dish containing Dissection Media (*see* **Note 10**).
9. To remove the hippocampi, split the brain in half between the cerebral hemispheres and separate the cortex from the diencephalon and brainstem. The hippocampus is found on the posterior half of the hemisphere. Remove the meninges and dissect out the hippocampus by cutting along the boundary between the hippocampus and the adjoining cortex.
10. Carefully transfer hippocampi to the 50 ml tube containing 3 ml pre-warmed Glial Growth Media.
11. Triturate the tissue twenty times using a fire-polished pipette with its aperture reduced to one-half of the original size until most of the clumps disappear (*see* **Note 11**).
12. Pass the cell suspension through a cell strainer to remove clumps and collect flow-through in a 50 ml tube containing ~7 ml of Glial Growth Media.

13. Centrifuge the cells at 1500 rpm for five minutes. At the end of the centrifugation, a small pellet of cells should be clearly visible.
14. Carefully aspirate, decant or pipette off the supernatant. Resuspend the cells in 5 ml Glial Growth Media and add to the flask that was placed in incubator at step 2. Carefully rock flask back and forth to evenly distribute cells and place in incubator (*see* **Note 12**).
15. Allow cells to attach for one day and replace media with fresh Glial Growth Media (*see* **Note 13**).
16. Change the media completely every three to four days until cells reach >70% confluency (*see* **Notes 13, 14**).
17. At this point, cells can be split to seed for the astrocyte feeder layer (proceed to 3.2) or frozen down for later use (proceed to 3.3).

3.2 Preparation of the astrocyte feeder layer (approximately five days before neuron dissection)

1. At least one day before seeding the astrocytes, prepare paraffin dots on two 12 well dishes (*see* **Note 15**). Sterilize under UV light for 2-3 hours.
2. Coat wells using 0.1 mg/ml poly-D-lysine (at least 500 µl per well). Leave overnight in incubator at 37ºC.
3. Wash 12 well dishes twice using sterile water (*see* **Note 6**).
4. At least twenty minutes before seeding astrocytes, add 1 ml of Glial Growth Media to each well and place dishes in incubator.
5. Add bottle of Glial Growth Media and 20 ml of plain MEM to 37ºC water bath.
6. If using fresh astrocytes for the feeder layer, rinse the flask with 20 ml warmed plain MEM, aspirate and then incubate with 5 ml trypsin-EDTA (0.025%) at 37°C until cells lift off (~3-5 minutes) (*see* **Note 16**). Add 5-10 ml Glial Growth Media and collect cells into a 50 ml tube.
7. Centrifuge at 1500 rpm for five minutes. Resuspend cells in 2 ml and count cell concentration using a haemocytometer (*see* **Note 17**).
8. Plate 80,000 cells/well (roughly 10^6 cells per dish) (*see* **Note 18**).

9. If using frozen astrocytes, retrieve appropriate number of vials (10^6 cells per 12 well dish) from the liquid nitrogen and quickly thaw in water bath at 37ºC. Add to 50 ml tube containing 10 ml Glial Growth Media, centrifuge at 1500 rpm for 5 minutes, and resuspend in 13 ml Glial Growth Media. Add 500 µl of astrocyte suspension to each well.
10. Change media one day after plating. Culture cells for 5-7 days prior to neuron dissection, with full media changes every 2-3 days.

3.3 Freezing down astrocytes

1. Dilute astrocyte suspension 1:1 in cold freezing media (final concentration: Glial Growth Media + 20% horse serum + 15% DMSO).
2. Add approximately 10^6 cells (1 ml) per cryotube (enough cells for one 12 well dish).
3. Place tubes in a stryofoam rack (or a suitable container for slow freezing of cells) and place in a -80ºC freezer overnight.
4. Transfer vials to liquid nitrogen after twenty-four hours. Astrocytes can be stored for up to six months in liquid nitrogen.

3.4 Preparation of mouse hippocampal neurons

1. Change media on astrocyte feeder cultures to Neuronal Growth Media 24-72 hours prior to dissection.
2. At least one day prior to dissection, coat coverslips (in 12-well dishes) with 0.1 mg/ml poly-L-lysine (at least 500 µl per well). Leave overnight in incubator at 37ºC.
3. Wash coverslips twice using sterile water (*see* **Note 6**).
4. During the preparation for dissection, add 1 ml of Neuronal Growth Media to each well and place dishes in the incubator to equilibrate to 37ºC, 5% CO_2. Pre-warm additional Neuronal Growth Media and Solution A in a 37ºC water bath.
5. To dissect out hippocampi of P0 mice, follow 3.1, steps 5-9.
6. Transfer hippocampi to Solution A. Add one aliquot of papain (250 µl) and incubate in water bath at 37ºC for 10-15 minutes (with swirling every 3-4 minutes to mix).

7. During this incubation, warm both tubes of Solution B in a 37ºC water bath.
8. Fire-polish a Pasteur pipette without changing its width. Transfer hippocampi (leaving behind as much of the solution as possible) to a 50 ml tube containing 2 ml Neuronal Growth Media. Triturate eight times to break up tissue (*see* **Note 11**).
9. Transfer supernatant to tube containing 2.5 ml Solution B. Triturate eight times using a fire-polished Pasteur pipette with its aperture reduced to one-half of the original size.
10. Allow any larger clumps to settle to the bottom of the tube, then transfer supernatant to a second tube containing 2.5 ml Solution B. Triturate four times using a fire-polished Pasteur pipette with its aperture reduced to one-third of the original size.
11. Centrifuge the cells at 1000 rpm for five minutes. Carefully discard the supernatant, resuspend cells in 3 ml Neuronal Growth Media and count cell concentration using a haemocytometer. Plate cells at a density of approximately 80,000 cells/well (approximately 10^6 cells per dish) onto coverslips (*see* **Note 19**).
12. After three hours of plating (*see* **Note 20**), remove coverslips and place on top of paraffin dots (suspended above glial feeder layer) with neurons facing up.
13. After three days add Ara-C to a final concentration of 3 μM to prevent glial overgrowth.
14. Change one-third of the media every 3-4 days with fresh, pre-warmed Neuronal Growth Media.

4. Notes

1. The dissection is carried out in a horizontal flow hood and all preparation steps, pipetting, etc, are carried out in a vertical flow hood. At all steps, follow proper sterile technique to avoid bacterial and fungal contamination.

2. Pasteur pipettes are fire-polished by carefully exposing their tip to a Bunsen-burner flame for a few seconds. This is repeated until the edges become smooth and the tip is of the desired size. We normally fire-polish our autoclaved pipettes as needed under the vertical flow hood. Alternatively, Pasteur pipettes can be fire-polished in bulk on a regular lab bench and then autoclaved.
3. Matings are set up for forty-eight hours using C57/BL6 mice three weeks prior to desired time of dissection of astrocytes or neurons. On average, 6-8 females will yield a minimum of 1-2 litters. During the week of dissection, cages are checked daily to ensure appropriate staging of pups. For astrocyte cultures, we find that P1-P2 pups yield a good quantity of astrocytes. For healthy neuronal cultures, it is essential that the mice are less than twenty-four hours old.
4. Diluted poly-D-lysine and poly-L-lysine can be stored at 4ºC for several weeks.
5. To prepare coverslips for coating with poly-L-lysine, wash overnight in concentrated nitric acid followed by five twenty minute washes in distilled water. Coverslips are sterilized under the hood with 70% ethanol, air-dried and placed into 12 well dishes.
6. Dishes with paraffin dots and sterilised coverslips can be prepared in advance and stored in plastic wrap for several months. Coated flasks, dishes and coverslips can be prepared in advance, wrapped in plastic wrap and stored at 4ºC for several weeks.
7. Alternatively, the dissection can be performed using careful sterile technique on a regular lab bench.
8. We normally pour the chilled dissection media (4ºC) into dishes at the beginning of the dissection and leave them at room temperature during the dissection (20-30 minutes). However, it may be necessary to keep the dishes on ice if the dissection takes more than forty-five minutes. This will prevent the brains from become soft and difficult to dissect.

9. We normally use an entire C57/BL6 litter (6-10 pups). We find that the astrocytes grow better if at least six pups are used.
10. The more intact the brains are when they are removed, the easier it will be to find and dissect out the hippocampus. Be very vigilant at this stage.
11. Trituration involves pipetting the hippocampi up and down several times through a fire-polished Pasteur pipette to break down the tissue to a suspension of single cells. This should be done quickly but gently to ensure that the tissue is successfully broken down. Avoid introducing too many bubbles into the media. The media should become cloudy if the trituration is successful.
12. It should take approximately 60-90 minutes to complete the dissection, trituration and plating of astrocyte and neuronal cells.
13. Before removing the medium, slap the flask 5-10 times against your hand to dislodge loosely attached cells (such as contaminating oligodendrocyte progenitors and microglia).
14. Depending on the amount of starting material, this normally takes 7-10 days**.**
15. Paraffin dots are prepared by melting paraffin wax in a 50 ml beaker using a hot plate. We normally do this under a vertical flow hood. The paraffin should be hot, but not boiling. We submerge the tip of a paperclip in the paraffin and carefully add the small bit of wax to the well. It should take 1-2 seconds for the paraffin to harden (if longer, reduce the temperature of the wax). This is repeated twice for each well to place three dots per well in a triangular pattern. Fresh paraffin should be substituted every two to three months.
16. Sometimes the astrocytes remain adherent even after five minutes. Be sure to check under the microscope to see if the astrocytes have dislodged. If not, slap the flask several times to release the cells. Pipetting up and down against the side of the dish once the Glial Growth Media is added can also help.
17. We usually get 4 million cells from a 70-90% confluent flask.

18. Alternatively, astrocytes can be frozen down at this point (see 3.3).
19. An average sized litter (6-9 pups) usually yields 4-6 million cells. The density of neurons seeded can be altered depending on the application. We find 80,000 cells per well produces cultures that are of sufficient low-density for imaging single neurons. Higher densities may be used for biochemistry studies. Please note that much lower densities may delay the maturation of the cultures and reduce neuronal survival.
20. We use a short plating step in Neuronal Growth Media, which is serum-free. This reduces the number of astrocytes that are able to attach to the coverslip.

Figures

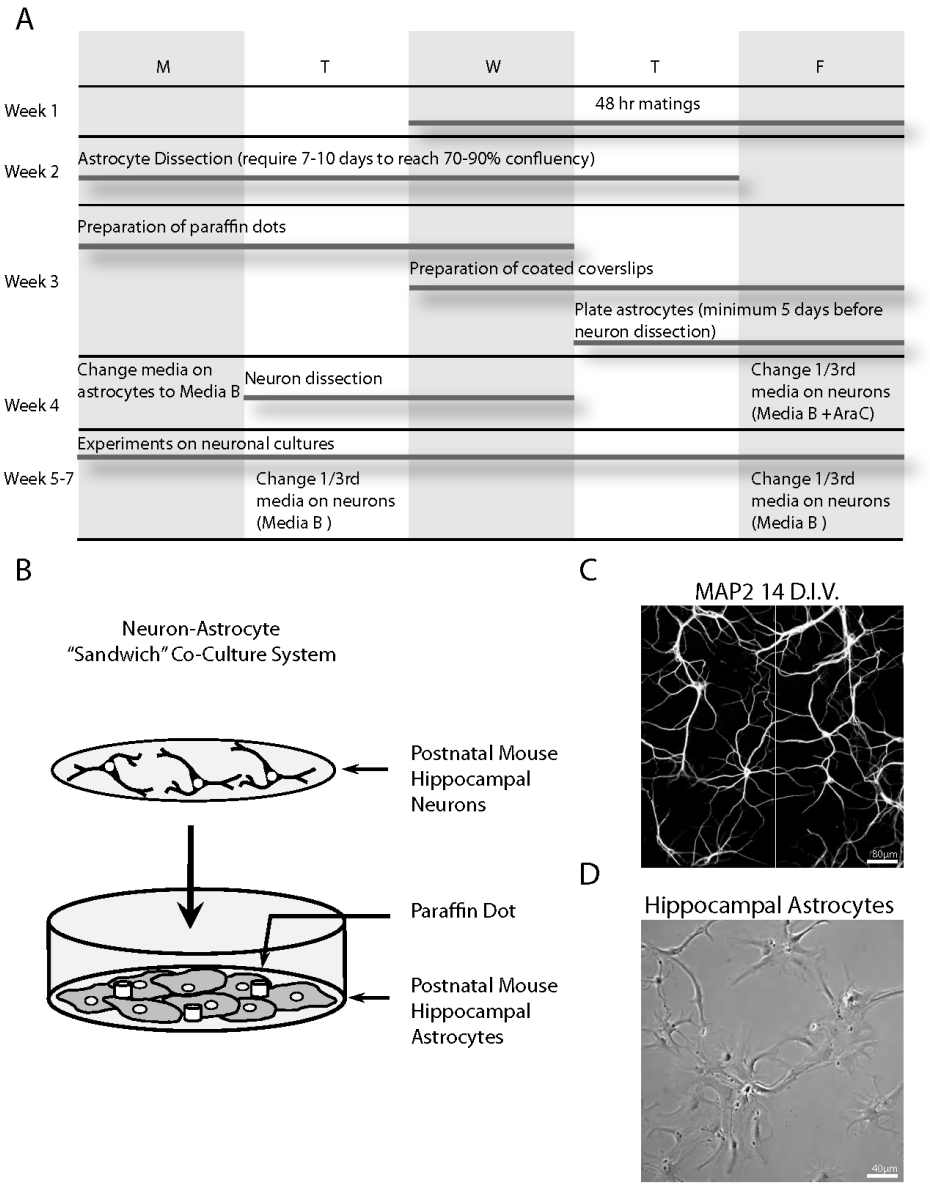

Figure 1: Timeline for dissections and diagram depicting the "sandwich" co-culture method. A. Calendar describing the major steps involved in preparing the "sandwich" hippocampal astrocyte-neuron co-culture system. These steps are explained in 3.1-3.4. **B.** Schematic showing the astrocyte feeder layer below the neurons which are plated onto a coverslip and placed face-up on top of paraffin dots in the well. **C.** MAP2 staining of a representative culture at 14 days *in vitro* (DIV) showing typical neuron density and mature dendritic arbors. **D.** Phase contrast image of the astrocyte feeder layer showing typical astrocyte density at neuron plating.

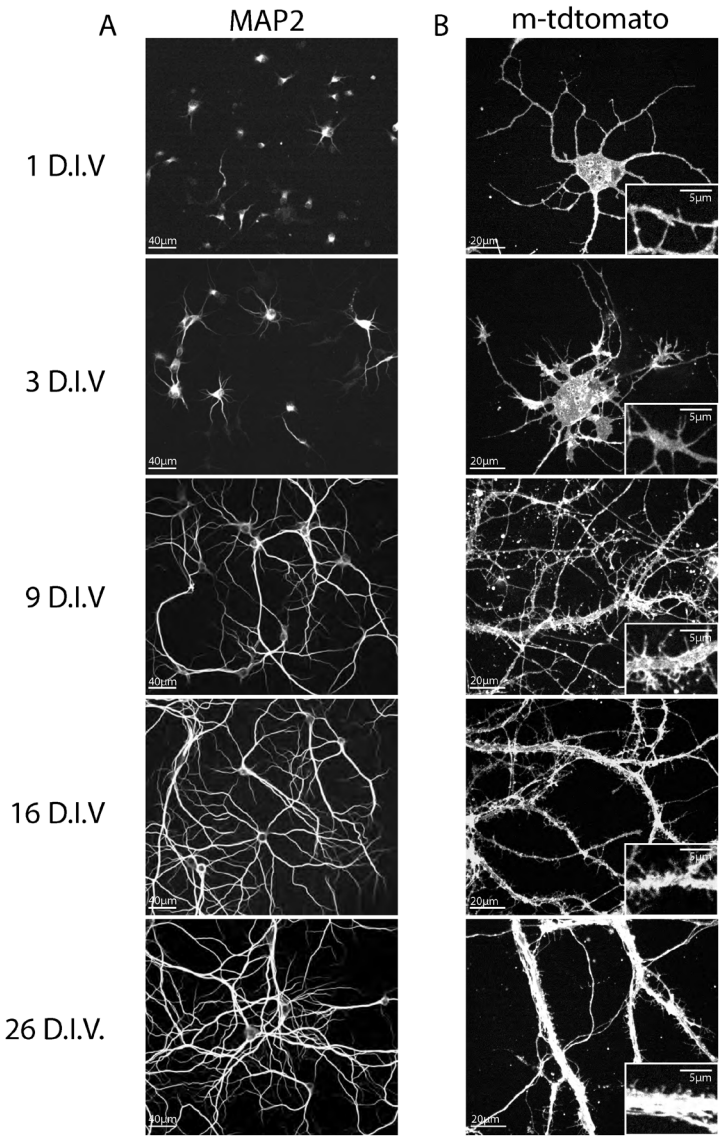

Figure 2: Development of dendrites and spines of postnatal hippocampal neurons grown using the co-culture "sandwich" method. A. MAP2 immunostaining of neurons at different DIV. MAP2 is a marker for proximal dendrites and is used here to show the typical morphology of neurons at different developmental time points. Between 1-3 DIV, MAP2-positive neurites are short and immature. By 9 DIV, dendrites are more elaborate. Dendrites continue to grow and thicken between 9 and 26 DIV. B. Neurons from wild-type mice and a transgenic mouse line expressing a membrane-targeted red fluorescent protein (m-tdtomato) were cultured together to allow the visualization of dendrites, axons and spines of a subset of neurons in culture. Here we follow the development of spines in the cultures. Between 1-3 DIV, processes start to form, sometimes with axonal and dendritic growth cones. By 9 DIV, small filopodial-like spines are visible. These spines continue to mature into more typical mushroom spines by 16-21 DIV.

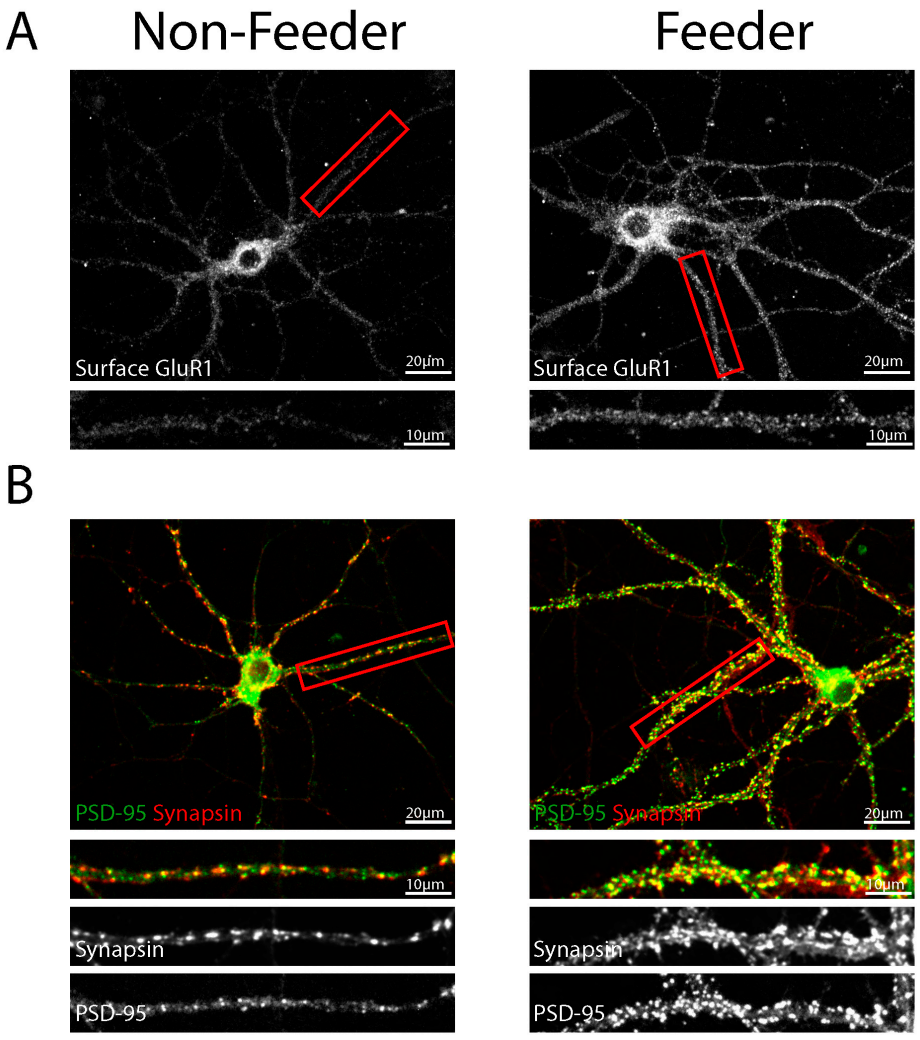

Figure 3: Comparison of synapses in mouse hippocampal neurons grown with or without an astrocyte feeder layer at 14 DIV. Neurons grown with an astrocyte feeder layer develop more synapses and have increased surface AMPA-type glutamate receptors. **A.** Immunostaining for surface GluR1, an AMPA receptor subunit, reveals an increase in the number and intensity of synaptic GluR1 punctae on dendrites of neurons cultured with an astrocyte feeder layer. **B.** Immunostaining showing co-localisation of presynaptic synapsin (red) and postsynaptic PSD-95 (green) to indicate synaptic punctae. Neurons grown with an astrocyte feeder layer have an increased number of synapses.

APPENDIX B:

CHARACTERIZATION OF THE METHOD USED TO OVEREXPRESS FXR1P IN HIPPOCAMPAL SLICES

We first decided to use a Semliki Forest virus to overexpress eGFP-FXR1P in CA1 neurons in mouse organotypic hippocampal slices. We chose this method because the modified PD strain of Semliki Forest virus drives high expression of exogenous proteins in the absence of visible toxic effects to neurons in hippocampal slices [265,266].

We engineered a viral vector to overexpress both eGFP-FXR1P and a membrane targeted version of mCherry (mCherryf) to visualize CA1 dendrites and spines. Using spinning disk confocal microscopy, we found eGFP-FXR1P clustered in the cell body and dendrites of CA1 neurons (Figure 1). eGFP-FXR1P clustered at a subset of spines, in contrast to RFP-actin, which clustered at all spines (Figure 1).

We soon recognized two important drawbacks to this approach. The first is that overexpressed FMRP, a related protein, creates FMRP and FXR1P containing stress granules in heterologous cells [185]. In addition, endogenous FMRP and FXR1P move into stress granules when neuron-like heterologous cells and hippocampal neurons are stressed with arsenite [267,268]. The second drawback is that Semliki Forest virus induces stress granules in heterologous cells [269]. No one has reported whether the modified version of Semliki Forest virus, which inhibits host protein synthesis to a lesser extent than the original version, induces stress granules in the hippocampal neurons it infects [265]. Nor has anyone ever reported whether overexpressed versions of FMRP or FXR1P induce stress granules in neurons. Since stress granules sequester and repress mRNAs when cells are stressed and could be detrimental to a study on mRNA translation, it was important to us to first determine whether our virus induces stress granules in neurons and whether eGFP-FXR1P localizes to stress granules in neurons.

To determine whether modified Semliki Forest virus induces stress granules in neurons, CA1 neurons were infected with a virus expressing membrane targeted eGFP (eGPFf) or membrane targeted mCherry (mCherryf). We then performed immunofluorescence using antibodies directed against two well-characterized markers of stress granules, TIA-1 and G3BP, to determine whether infected cells contain stress granules [102]. Using confocal imaging, we showed that TIA-1 and G3BP were unclustered in the cytoplasm of uninfected cells, but were clustered in the cytoplasm of infected cells (Figure 2). We also noted nuclear depletion of TIA-1 in infected cells. Thus, neurons infected with our modified Semliki Forest virus, even those expressing very low levels of fluorescent protein (Figure 2a, top right corner), contained stress granules.

To determine whether overexpressed eGFP-FXR1P clusters with stress granules, CA1 neurons were infected with a virus expressing eGFP-FXR1P and mCherryf and immunofluorescence was performed using antibodies against TIA-1 and G3BP. We showed that eGFP-FXR1P clusters in the cell body and proximal dendrites of CA1 neurons were TIA-1 and G3BP positive (Figure 3). In contrast, eGFP-FXR1P clusters in the distal dendrites were neither TIA-1 nor G3BP positive (Figure 4). It is unclear whether this is an antibody sensitivity issue or whether distal dendrites do not form TIA-1 and G3BP positive stress granules. It is therefore unclear whether eGFP-FXR1P clusters in distal dendrites are stress granules. Nevertheless, it is clear that eGFP-FXR1P clusters contained stress granule markers in infected neurons. These experiments convinced us to look for an alternative approach to overexpress eGFP-FXR1P in neurons.

An alternative approach to transfect neurons in slice culture is to use the Helios Gene Gun from BioRad [203]. This system uses high pressure to bombard slices with gold particles coated with a plasmid encoding a protein of interest. Transfection efficiencies tend to be low because the plasmid must enter the nucleus in order to express protein. In addition, no one has ever tested whether hippocampal neurons transfected with the gene gun form stress granules.

To test this, we coated gold particles with a plasmid encoding eGFPf and transfected hippocampal slices using the gene gun. We then performed

immunofluorescence using an antibody against TIA-1. We showed that TIA-1 did not cluster in neurons transfected with the gene gun (Figure 5). This suggests that stress granules do not form when the gene gun is used and that this method can be used as an alternative to overexpress eGFP-FXR1P.

Using the gene gun, we next determined whether eGFP-FXR1P clusters in CA1 dendrites in the absence of the added stress and whether these clusters are stress granules. We coated gold particles with plasmids encoding eGFP-FXR1P and membrane-targeted red fluorescent protein (RFPf) and transfected them into hippocampal slices using the gene gun. We used the antibody against TIA-1 to determine whether stress granules formed. We found that eGFP-FXR1P still clustered in CA1 dendrites and that these clusters were not TIA-1 positive (Figure 5). This suggests that in the absence of stress eGFP-FXR1P clusters are not stress granules. In addition, clusters of overexpressed mCherry-FMRP were not positive for TIA-1 either (Figure 5). To our knowledge, this is the first demonstration that constructs overexpressing FXR1P or FMRP do not form stress granules in neurons.

These results opened our eyes to the potential drawbacks and caveats of using viruses to study translational control. Viruses, because of their convenience and high infection rates of neurons, have been widely adopted by neuroscientists, even those studying local translation [77]. However, viruses are well-known to co-opt the cellular protein synthesis machinery, even when modified to be less toxic. Therefore, care must be taken to control for the potential artifacts induced using this approach. In our case, we determined that the influence of the virus on the properties of FXR1P was too high a risk to take for this PhD project, and decided to use biolistic transfection and not viral techniques for all experiments in organotypic slices.

Figures

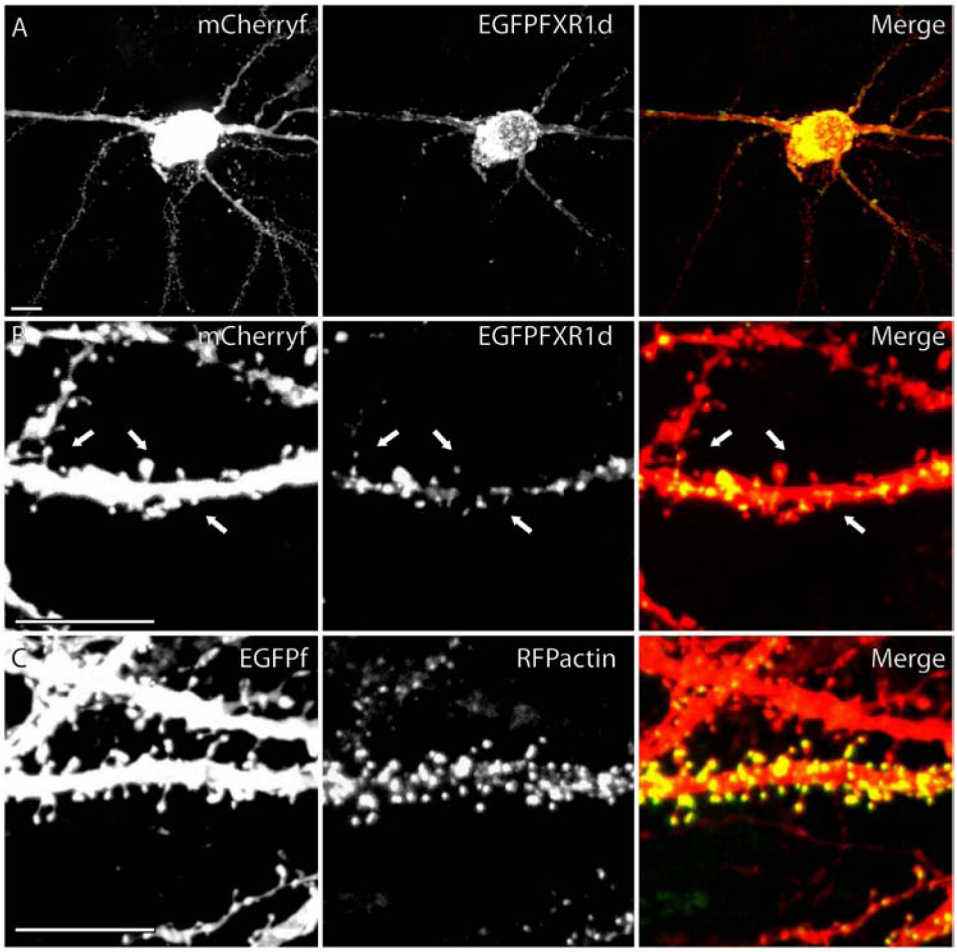

Figure 1: EGFP-FXR1P clusters in the dendrite shaft and at a subset of dendritic spines. A. We used Semliki Forest Virus to overexpress EGFP-FXR1P with farnesylated mCherry in CA1 pyramidal cells in the mouse hippocampus. We found that EGFP-FXR1P formed clusters in the cytoplasm and dendrite. **B.** A segment of dendrite showing clusters of EGFP-FXR1P in the dendrite and at a subset of spines (arrows). **C.** In contrast, RFPactin clusters at every spine. Scale bar= 10µm.

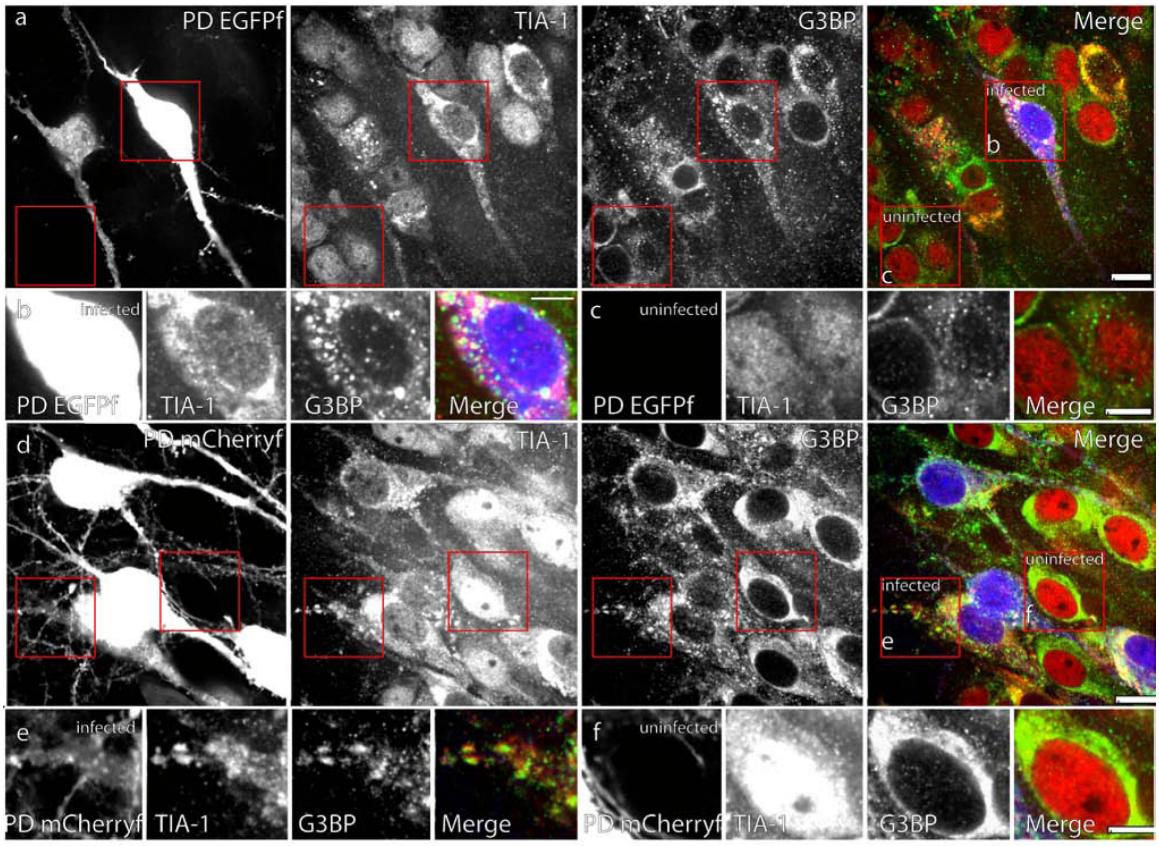

Figure 2: Stress granules form in cells infected with Semliki Forest Virus. a. We infected neurons with Semliki Forest Virus expressing farnesylated EGFP. Slices were stained using antibodies against TIA-1 and G3BP. TIA-1 and G3BP cluster in infected cells. **b.** Magnified image of an infected cell showing TIA-1 and G3BP clusters. **c.** Example of two uninfected cells showing diffuse expression of TIA-1 and G3BP. **d.** We infected neurons with Semliki Forest Virus expressing farnesylated mCherry. TIA-1 and G3BP cluster in infected cells. **e.** TIA-1 and G3BP cluster in the proximal dendrite of an infected cell. **f.** TIA-1 and G3BP are diffusely expressed in an uninfected cell. Scale bar= 10 µm (a, d); scale bar= 5 µm (b,c,e,f).

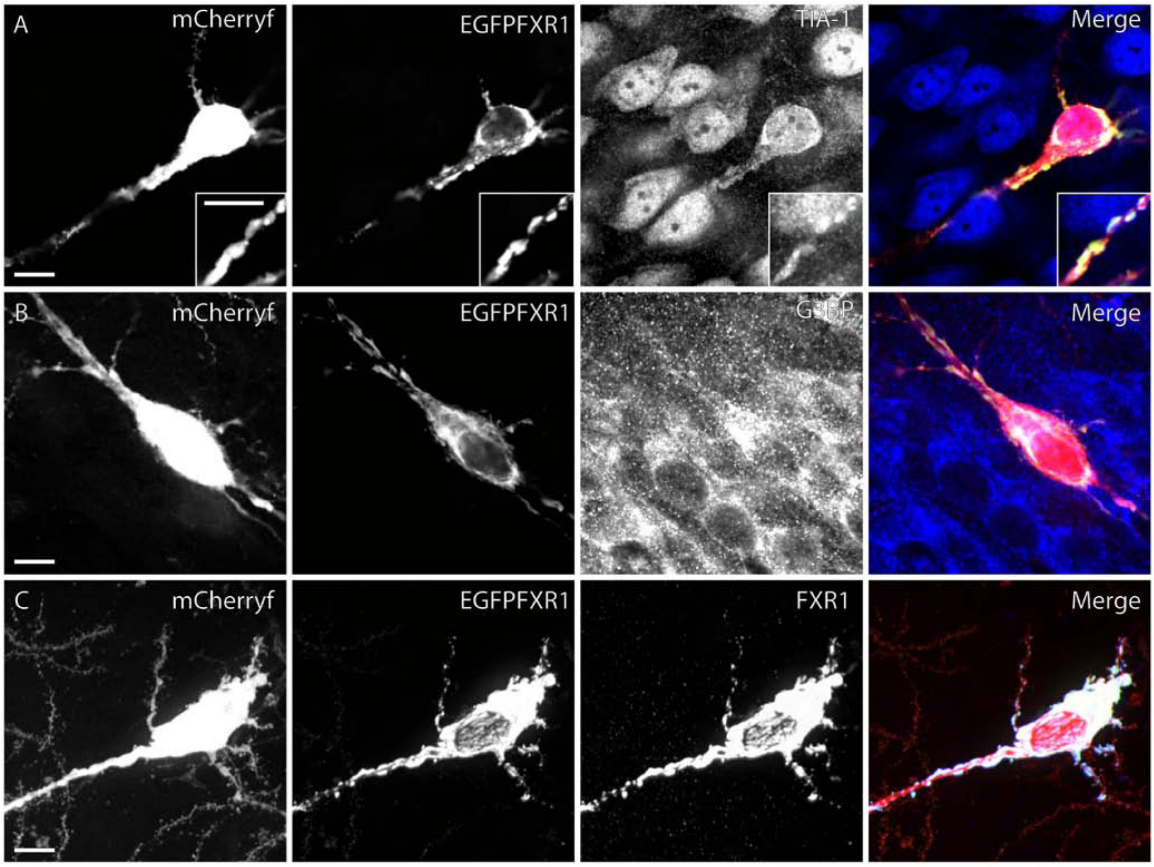

Figure 3: EGFP-FXR1P clusters in stress granules in the cytoplasm of infected cells. A. We infected slices with Semliki Forest Virus expressing EGFP-FXR1P and farnesylated mCherry. We show that EGFPFXR1clusters are TIA-1 positive. Clusters in the proximal dendrite are magnified in the inset. **B.** EGFP-FXR1P clusters are also G3BP positive. **C.** To confirm that EGFP-FXR1P is not degraded we show that EGFP-FXR1P clusters are positive for FXR1 using an antibody directed against the C-terminus of the proteins. Scale bar= 10 μm; inset scale bar= 5 μm.

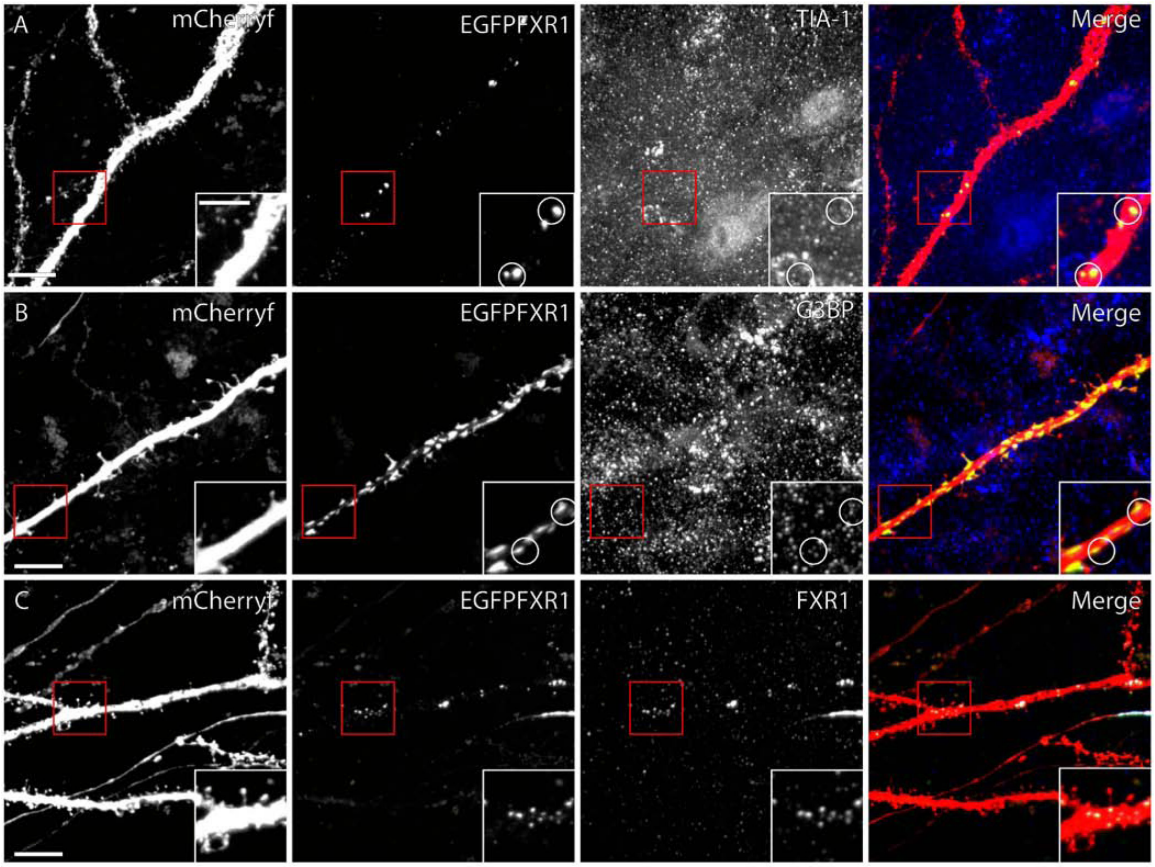

Figure 4: EGFP-FXR1P clusters are not positive for stress granule markers in the distal dendrites of infected cells. A. We infected slices with Semliki Forest Virus expressing EGFP-FXR1P and farnesylated mCherry. We show that EGFP-FXR1P clusters in distal dendrites are not TIA-1 positive. Clusters in the distal dendrite are magnified in the inset. B. EGFP-FXR1P clusters in distal dendrites are not G3BP positive. Clusters in the distal dendrite are magnified in the inset. C. As a control, we demonstrate that these clusters are FXR1P-positive using an anti-FXR1P antibody (Y19). Clusters in the distal dendrite are magnified in the inset. Scale bar= 10 µm; inset scale bar= 5 µm.

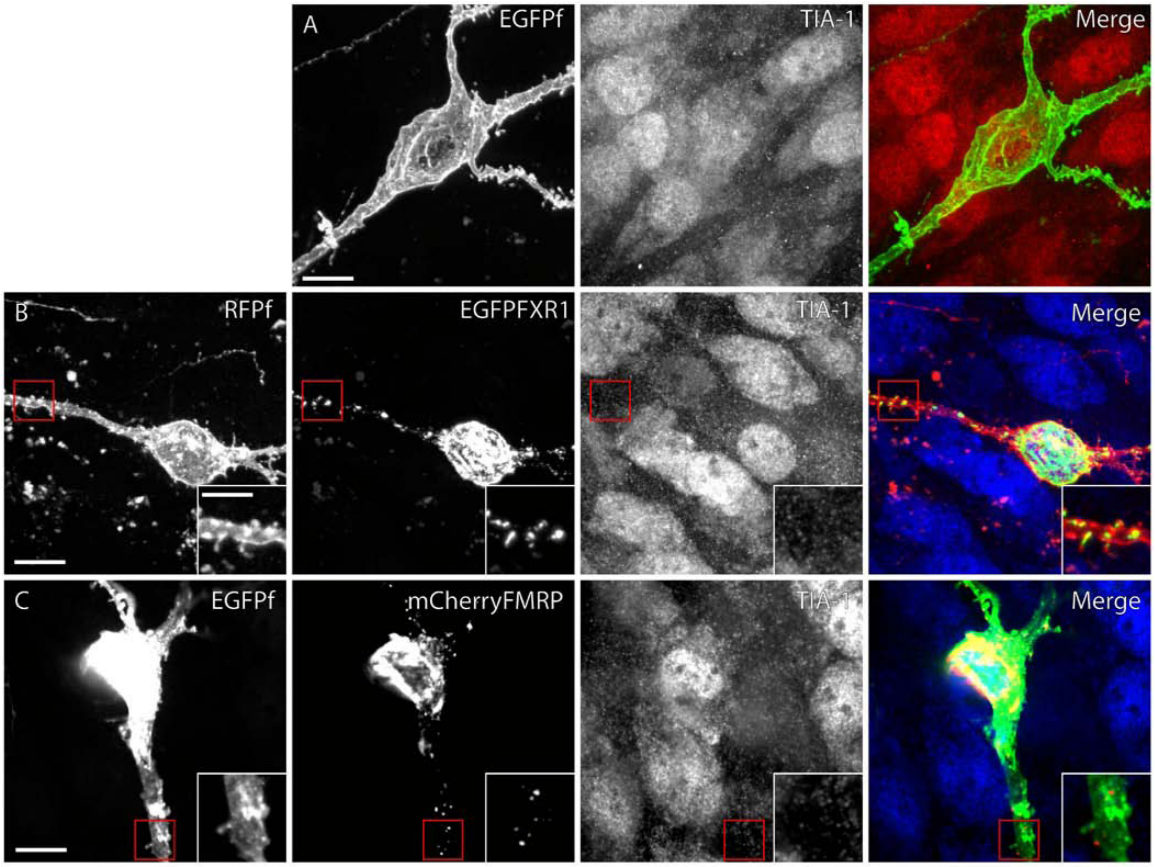

Figure 5: EGFP-FXR1P and mCherry-FMRP cluster in the absence of stress granule formation. A. We transfected hippocampal slices using the gene gun. TIA-1 did not cluster in cells transfected with farnesylated EGFP. **B.** EGFP-FXR1P clusters are not TIA-1 positive. **C.** In addition, mCherry-FMRP clusters are not TIA-1 positive. Scale bar= 10 µm; inset scale bar= 5 µm.

APPENDIX C:

CHARACTERIZATION OF THE METHOD USED TO KNOCKDOWN/KNOCKOUT FXR1P EXPRESSION IN HIPPOCAMPAL SLICES

After we found that eGFP-FXR1P overexpression led to clustering of the protein at the base of a subset of large, mature dendritic spines (presented in Chapter 2), we decided to look for an approach to knockdown/knock-out FXR1P in order to determine whether loss of FXR1P would lead to a change in spine shape or function. Since the gain-of-function study only allowed us to conclude that there was a correlation between FXR1P clusters and spine size, establishing a loss-of-function model would allow us to determine whether FXR1P expression was required for the proper development of spine density and spine morphology.

We settled on two different approaches to knockdown/knockout FXR1P expression: 1) small interfering RNAs (siRNAs) and 2) a conditional knockout in mice. Exogenous siRNAs are designed to target the mRNA of interest and are introduced into cells using one of a number of different transfection/infection methods. Once delivered into the cytoplasm of cells, siRNAs combine with the RNA-induced silencing complex (RISC) to target and degrade the mRNA of interest. A mouse genetic approach using a complete knockout of *Fxr1* would have been the most straight foward model system to use. However, the full knockout dies at birth, therefore we had to develop a conditional knock-out approach.

The goal was to develop these two methods in parallel since they both have their advantages and disadvantages. The advantages of starting with an siRNA approach is that 1) it is quicker to develop, 2) it is less costly and 3) you have better control of the timing of loss of the protein of interest. Since RNAi involves interfering with gene expression at the mRNA level the knockdown occurs faster than with a genetic deletion approach. The disadvantages, however, are that 1) siRNAs are prone to off-target effects and therefore a number of

controls, usually a rescue experiment, are necessary, 2) protein levels are reduced but often not fully eliminated and 3) they cannot be used as easily or effectively for acute electrophysiology experiments and behavioural studies (in-utero electroporation of plasmid containing the siRNA or viral infection to target a large number of cells *in vivo* is necessary). The advantages of the conditional knock-out approach are that 1) specific cell types can be targeted at specific times depending on the promoter used to drive Cre recombinase expression ,2) all *in vivo* studies are greatly simplified, including spine analysis, electrophysiology and behavioural experiments in adult animals and do not require any extra manipulations and 3) *in vitro* studies can also be performed, if necessary, by transfecting slices from the floxed *Fxr1* mice with a Cre-expressing vector. The disadvantages are 1) mouse lines are expensive and time-consuming to maintain, 2) it can take up to a year to get to the stage where you are generating animals for experiments, 3) compensatory mechanisms can sometimes come into play if the protein is lost during development/over a long period of time, 4) depending on mRNA/protein stability, it can take a long time between when the gene is excised and complete loss of the protein.

With these advantages/disadvantages in mind, we went ahead with screening siRNAs for FXR1P knock-down in parallel with setting up the mouse colonies required for the genetic approach. We settled on a strategy to test 4 siRNAs obtained from Qiagen (Figure 1). Two of these siRNAs were targeted against the 3' untranslated region (#6, #7) and the other two are targeted to the open reading frame (#5, #8). Since siRNAs often have off-target effects, one of the ways to control for this is to select two siRNAs targeted against different regions of the mRNA. The rationale is that since the sequences of the siRNAs are different, their off-target effects should also be different. Therefore, if both siRNAs show the same results this must be due to the knockdown of the protein of interest. However, if both siRNAs are used at levels which saturate the endogenous siRNA/microRNA system, then the same set of off-target effects may be seen. Therefore, a rescue control is always the best to confirm that the phenotype is actually due to knockdown of the protein of interest.

With these caveats in mind, we first went about looking for a mouse heterologous cell line which was suitable for testing our siRNAs. We found that NIH3T3 cells expressed FXR1P and its two other family members (Figure 2A, C). These cells were also easy to transfect with 10 nM of a control, fluorescent siRNA using HiPerfect transfection reagent with transfection efficiency around 80-90% (Figure 2B). We then tested for knockdown of FXR1P using western blotting techniques and found a ~50% loss of protein (Figure 3). We used the best two siRNAs against different regions of the mRNA (#5 and #6) to look at the time-course of FXR1P knockdown and found that by 72 hours post-transfection FXR1P levels were significantly reduced (Figure 4). This reduction was maintained up to 120 hours post-transfection, at which point, probably due to the fact that the cells are dividing and diluting out the siRNA, the levels of FXR1P started increasing again (data not shown). We were also able to show, using immunofluorescence, that FXR1P levels were significantly reduced in a large percentage of cells (Figure 5). This also served as a control for the FXR1P antibody.

With these excellent results we then went on to test these two siRNAs in neurons. Neurons are traditionally more difficult to transfect with plasmid DNA than heterologous cells; however, studies had shown high transfection efficiency with siRNAs [270]. However, we found that the HiPerfect transfection reagent that worked well in NIH3T3 cells was highly toxic for neurons (data not shown). We therefore had to switch to RNAiMax. We found that a large number of neurons incorporated a fluorescent siRNA (50 nM) both when transfected at 2 and 10 days *in vitro* (Figure 6). However, when we tested for FXR1P knockdown we unexpectedly discovered that our negative (scrambled siRNA) and positive (siRNA against ERK) control siRNA significantly increased the FXR1P levels (Figure 7). This was repeated several more times with the same result. Although there was a significant loss of FXR1P compared to the negative control siRNA, the difference between FXR1P levels in untransfected or mock transfected cells and FXR1P siRNA transfected cells was not very large. The increase in FXR1P levels that we noted was troubling because it meant that the exogenous siRNAs

were somehow blocking the normal pathways which control FXR1P expression. Indeed, a paper was subsequently published on microRNA control of FXR1P expression [271]. These results, in addition to the fact that FXR1P may actually function through the RISC pathway [32], convinced us to pursue a mouse genetic approach to study FXR1P function in neurons. The validation and work-up of that approach are presented in Chapter 3.

However, as noted previously, the siRNA approach does offer several advantages over a genetic approach and therefore these results may be put to good use in the future. For instance, despite our negative results in neurons, the FXR1P siRNAs were very successful in NIH3T3 cells. This approach could potentially be used to look for changes in the stability or translation of candidate mRNA targets of FXR1P or to study the influence of FXR1P knockdown on the translation of a reporter mRNA. In addition, further optimization using different concentrations of siRNAs or different transfection reagents could be used to try to improve the results obtained in neurons.

Figures

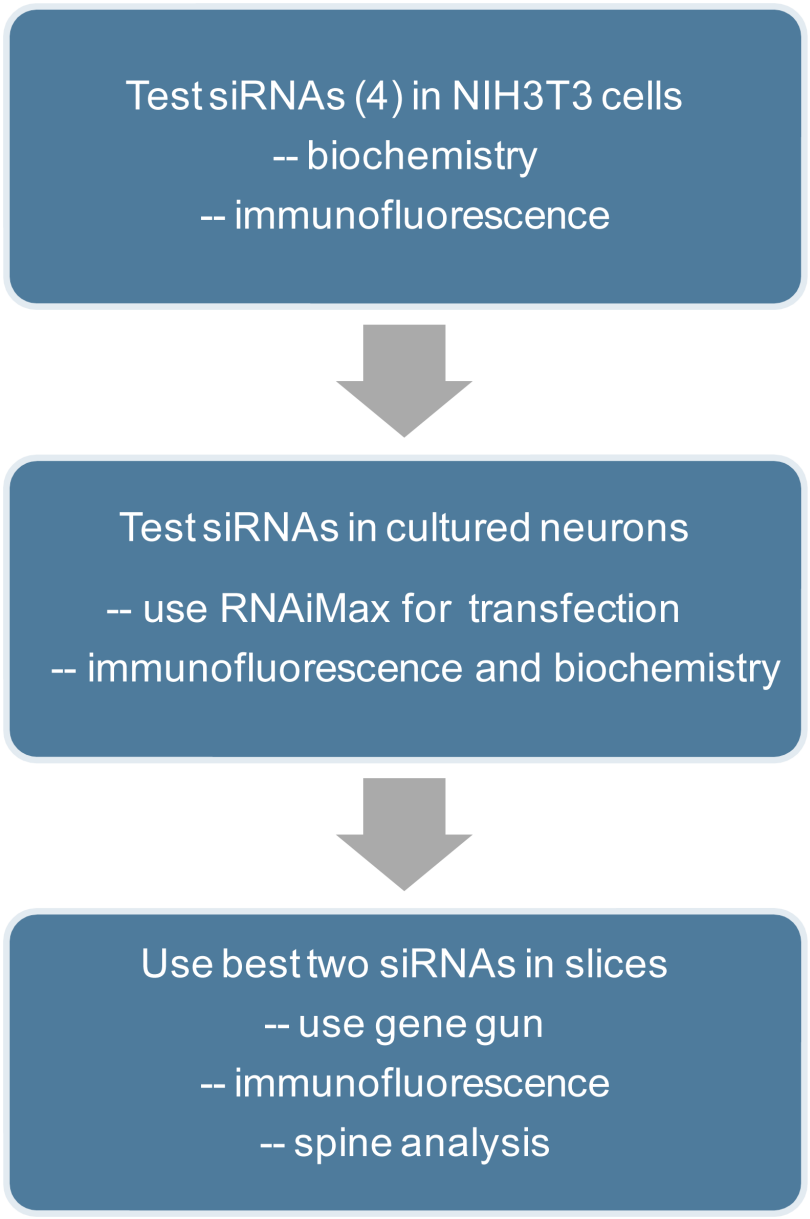

Figure 1: Strategy for testing and selecting siRNAs to knockdown FXR1P in organotypic slices.

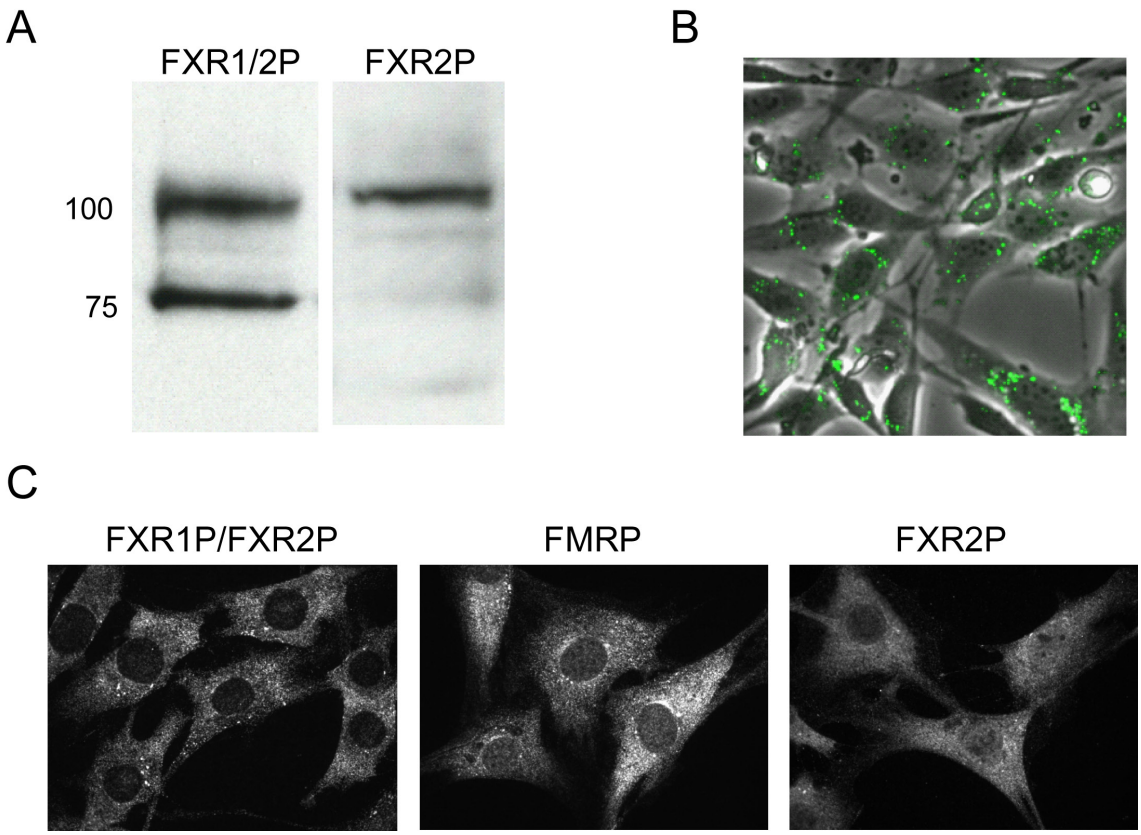

Figure 2: NIH3T3 cells are a good model system to test siRNAs for FXR1P knockdown. A. Western blots showing that Fragile X Proteins are expressed in NIH3T3 cells. **B.** Using a 488 Alexa Fluor-tagged control siRNA and HiPerfect transfection reagent we found that NIH3T3 displayed a high transfection efficiency. **C.** Confocal imaging was used to demonstrate expression of all three Fragile X proteins in NIH3T3 cells.

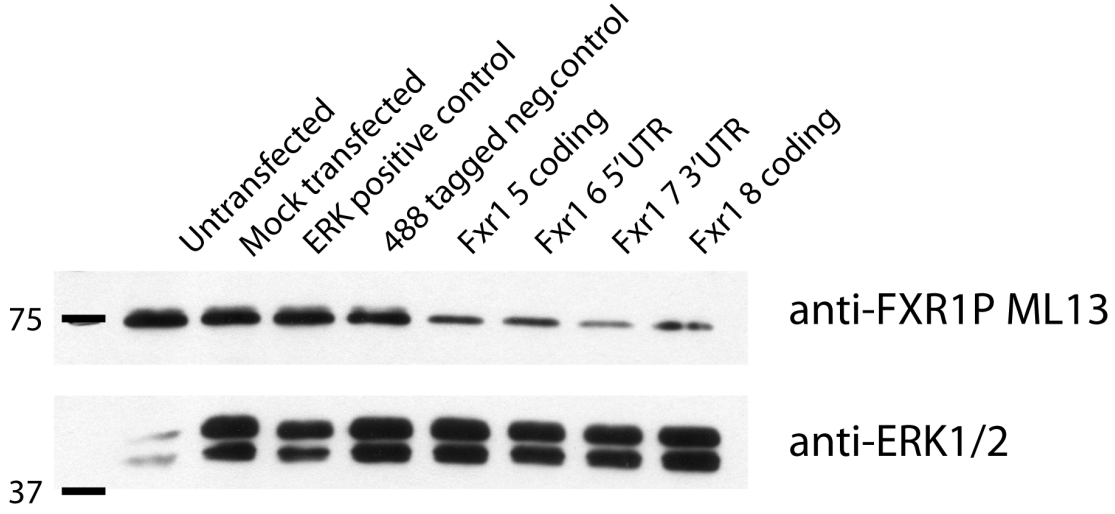

Figure 3: FXR1P knockdown in NIH3T3 cells using 4 Qiagen siRNAs.

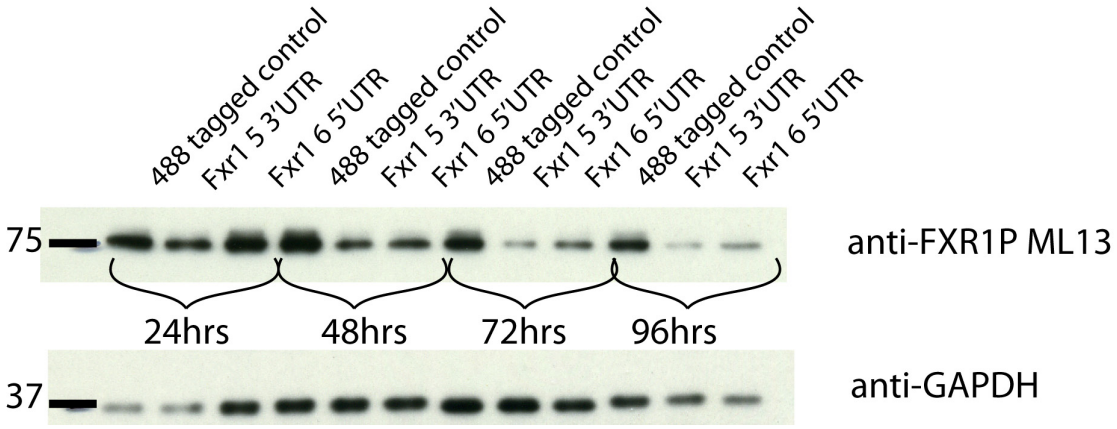

Figure 4: Time-course of FXR1P knockdown.

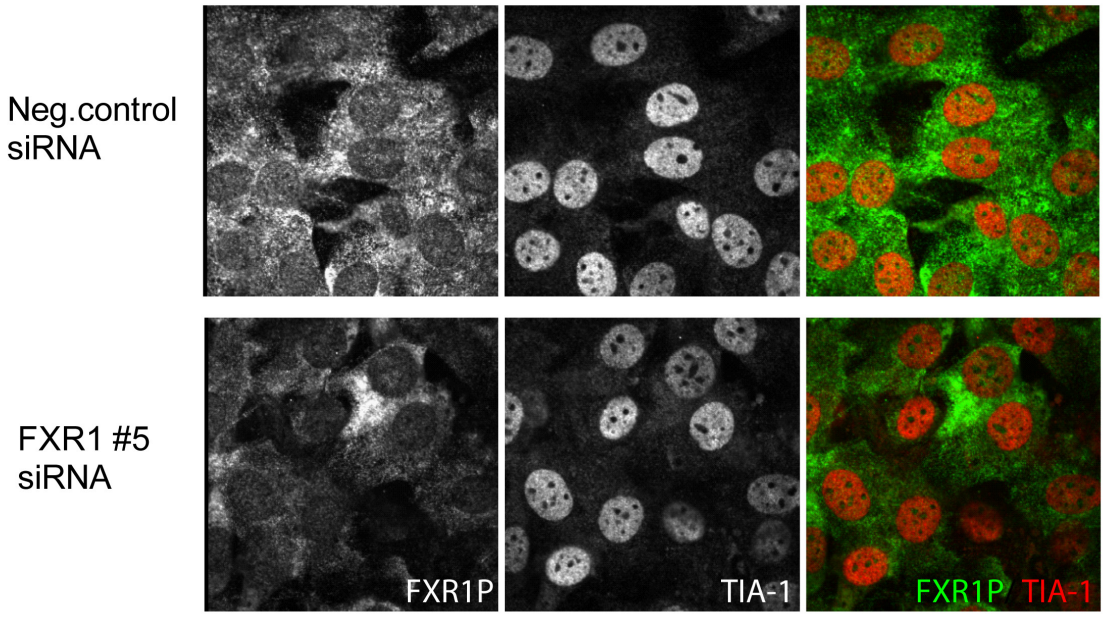

Figure 5: Immunofluorescence demonstrating FXR1P knockdown in the majority of NIH3T3 cells.

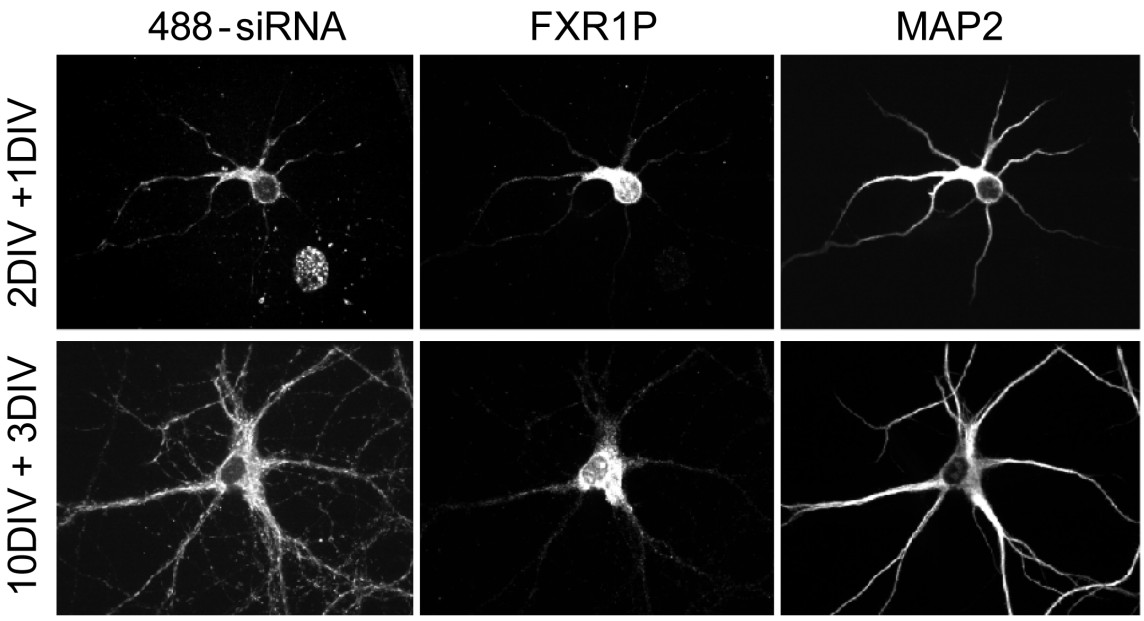

Figure 6: Hippocampal neurons can be transfected with siRNAs.

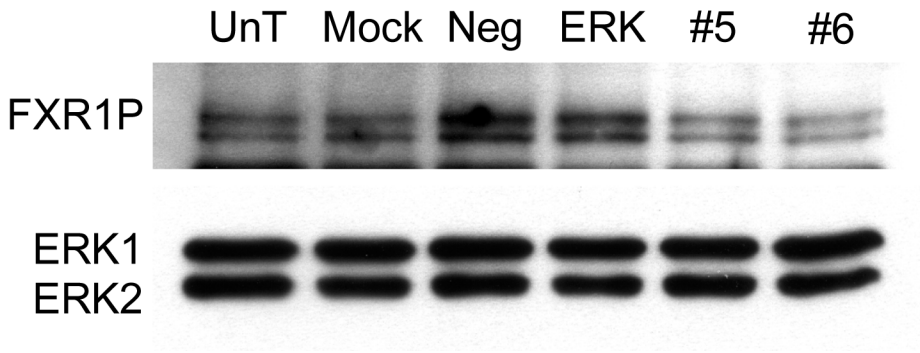

Figure 7: Control siRNAs increase FXR1P expression.

CHAPTER 10:

BIBLIOGRAPHY

1. Xu T, Yu X, Perlik AJ, et al. Rapid formation and selective stabilization of synapses for enduring motor memories. *Nature*. 2009;462(7275):915–9.

2. Govindarajan A, Kelleher RJ, Tonegawa S. A clustered plasticity model of long-term memory engrams. *Nature reviews neuroscience*. 2006;7(7):575–83.

3. Yang G, Pan F, Gan W-B. Stably maintained dendritic spines are associated with lifelong memories. *Nature*. 2009;462(7275):920–4.

4. Steward O, Schuman EMM. Protein synthesis at synaptic sites on dendrites. *Annual review of neuroscience*. 2001;24(1):299–325.

5. Schuman EM, Dynes JL, Steward O. Synaptic regulation of translation of dendritic mRNAs. *The Journal of neuroscience*. 2006;26(27):7143–6.

6. Costa-Mattioli M, Sossin WS, Klann E, Sonenberg N. Translational control of long-lasting synaptic plasticity and memory. *Neuron*. 2009;61(1):10–26.

7. Kelleher RJ, Govindarajan A, Jung H-Y, Kang H, Tonegawa S. Translational control by MAPK signaling in long-term synaptic plasticity and memory. *Cell*. 2004;116(3):467–79.

8. Hoeffer C a, Tang W, Wong H, et al. Removal of FKBP12 enhances mTOR-Raptor interactions, LTP, memory, and perseverative/repetitive behavior. *Neuron*. 2008;60(5):832–45.

9. Banko JL, Poulin F, Hou L, et al. The translation repressor 4E-BP2 is critical for eIF4F complex formation, synaptic plasticity, and memory in the hippocampus. *The Journal of neuroscience*. 2005;25(42):9581–90.

10. Costa-Mattioli M, Gobert D, Harding H, et al. Translational control of hippocampal synaptic plasticity and memory by the eIF2alpha kinase GCN2. *Nature*. 2005;436(7054):1166–73.

11. Costa-Mattioli M, Gobert D, Stern E, et al. eIF2alpha phosphorylation bidirectionally regulates the switch from short- to long-term synaptic plasticity and memory. *Cell*. 2007;129(1):195–206.

12. Doyle M, Kiebler M a. Mechanisms of dendritic mRNA transport and its role in synaptic tagging. *The EMBO journal*. 2011;30(17):3540–52.

13. Elvira G, Wasiak S, Blandford V, et al. Characterization of an RNA granule from developing brain. *Molecular & cellular proteomics*. 2006;5(4):635–51.

14. Kanai Y, Dohmae N, Hirokawa N. Kinesin transports RNA: isolation and characterization of an RNA-transporting granule. *Neuron*. 2004;43(4):513–25.

15. Fatemi SH, Folsom TD. The role of fragile X mental retardation protein in major mental disorders. *Neuropharmacology*. 2011;60(7-8):1221–6.

16. Hagerman R, Hoem G, Hagerman P. Fragile X and autism: Intertwined at the molecular level leading to targeted treatments. *Molecular autism*. 2010;1(1):12.

17. Boyle L, Kaufmann WE. The behavioral phenotype of FMR1 mutations. *American journal of medical genetics. Part C, Seminars in medical genetics*. 2010;154C(4):469–76.

18. Verkerk AJ, Pieretti M, Sutcliffe JS, et al. Identification of a gene (FMR-1) containing a CGG repeat coincident with a breakpoint cluster region exhibiting length variation in fragile X syndrome. *Cell*. 1991;65(5):905–914.

19. Buzzi A, Marino DD. *Molecular and Cellular Aspects of Mental Retardation in the Fragile X Syndrome: From Gene Mutations to Spine Dysmorphogenesis*. (Kreutz MR, Sala C, eds.). Vienna: Springer Vienna; 2012:517–551.

20. Darnell JCC, Van Driesche SJ, Zhang C, et al. FMRP Stalls Ribosomal Translocation on mRNAs Linked to Synaptic Function and Autism. *Cell*. 2011;146(2):247–261.

21. Tamanini F, Willemsen R, van Unen L, et al. Differential expression of FMR1, FXR1 and FXR2 proteins in human brain and testis. *Human molecular genetics*. 1997;6(8):1315–22.

22. Bakker CE, de Diego Otero Y, Bontekoe C, et al. Immunocytochemical and biochemical characterization of FMRP, FXR1P, and FXR2P in the mouse. *Experimental cell research*. 2000;258(1):162–70.

23. Cook D, del Rayo Sanchez-Carbente M, Lachance C, et al. Fragile X Related Protein 1 Clusters with Ribosomes and Messenger RNAs at a Subset of Dendritic Spines in the Mouse Hippocampus Chavis P, ed. *PLoS one*. 2011;6(10):e26120.

24. Siomi MC, Zhang YAN, Siomi H, Dreyfuss G. Specific sequences in the fragile X syndrome protein FMR1 and the FXR proteins mediate their binding to 60S ribosomal subunits and the interactions among them. *Molecular and cellular biology*. 1996;16(7):3825–3832.

25. Zhang Y, O'Connor JP, Siomi MC, et al. The fragile X mental retardation syndrome protein interacts with novel homologs FXR1 and FXR2. *The EMBO journal*. 1995;14(21):5358–66.

26. Levenga J, Buijsen RAM, Rife M, et al. Ultrastructural analysis of the functional domains in FMRP using primary hippocampal mouse neurons. *Neurobiology of disease*. 2009;35(2):241–50.

27. Tamanini F, Van Unen L, Bakker C, et al. Oligomerization properties of fragile-X mental-retardation protein (FMRP) and the fragile-X-related proteins FXR1P and FXR2P. *Biochem J*. 1999;523:517–523.

28. Zhang J, Hou L, Klann E, Nelson DL. Altered hippocampal synaptic plasticity in the FMR1 gene family knockout mouse models. *Journal of neurophysiology*. 2009;101(5):2572–80.

29. Zhang J, Fang Z, Jud C, et al. Fragile X-related proteins regulate mammalian circadian behavioral rhythms. *The American Journal of human genetics*. 2008;83(1):43–52.

30. Spencer CM, Serysheva E, Yuva-Paylor L a, et al. Exaggerated behavioral phenotypes in Fmr1/Fxr2 double knockout mice reveal a functional genetic interaction between Fragile X-related proteins. *Human molecular genetics*. 2006;15(12):1984–1994.

31. Bontekoe CJM, McIlwain KL, Nieuwenhuizen IM, et al. Knockout mouse model for Fxr2: a model for mental retardation. *Human molecular genetics*. 2002;11(5):487–98.

32. Vasudevan S, Steitz J a. AU-rich-element-mediated upregulation of translation by FXR1 and Argonaute 2. *Cell*. 2007;128(6):1105–18.

33. Garnon J, Lachance C, Di Marco S, et al. Fragile X-related protein FXR1P regulates proinflammatory cytokine tumor necrosis factor expression at the post-transcriptional level. *The Journal of biological chemistry*. 2005;280(7):5750–63.

34. Cajal S. The Croonian Lecture: La fine structure des centres nerveux. *Proceedings of the Royal Society of London*. 1894:444–468.

35. Neves G, Cooke SF, Bliss TVP. Synaptic plasticity, memory and the hippocampus: a neural network approach to causality. *Nature reviews neuroscience*. 2008;9(1):65–75.

36. Davis HP, Squire LR. Protein synthesis and memory: a review. *Psychological bulletin*. 1984;96(3):518–59.

37. Flexner JB, Flexner LB, Stellar E. Memory in Mice as Affected by Intracerebral Puromycin. *Science*. 1963;141(3575):57–59.

38. Penfield W, Milner B. Memory deficit produced by bilateral lesions in the hippocampal zone. *A.M.A. archives of neurology and psychiatry*. 1958;79(5):475–97.

39. Squire LR. The legacy of patient H.M. for neuroscience. *Neuron*. 2009;61(1):6–9.

40. Bliss T. Long-lasting potentiation of synaptic transmission in the dentate area of the anaesthetized rabbit following stimulation of the perforant path. *The Journal of physiology*. 1973:331–356.

41. Malenka RC. The long-term potential of LTP. *Nature reviews neuroscience*. 2003;4(11):923–6.

42. Yuste R, Bonhoeffer T, Yuste, Rafael, Tobias B. Morphological changes in dendritic spines associated with long-term synaptic plasticity. *Annual review of neuroscience*. 2001;24(1862):1071–89.

43. Lisman J, Raghavachari S. A unified model of the presynaptic and postsynaptic changes during LTP at CA1 synapses. *Science STKE*. 2006;2006(356):re11.

44. Lauri SE, Palmer M, Segerstrale M, et al. Presynaptic mechanisms involved in the expression of STP and LTP at CA1 synapses in the hippocampus. *Neuropharmacology*. 2007;52(1):1–11.

45. Fukazawa Y, Saitoh Y, Ozawa F, et al. Hippocampal LTP is accompanied by enhanced F-actin content within the dendritic spine that is essential for late LTP maintenance in vivo. *Neuron*. 2003;38(3):447–60.

46. Park M, Salgado JM, Ostroff L, et al. Plasticity-induced growth of dendritic spines by exocytic trafficking from recycling endosomes. *Neuron*. 2006;52(5):817–30.

47. Govindarajan A, Israely I, Huang S-YY, Tonegawa S. The dendritic branch is the preferred integrative unit for protein synthesis-dependent LTP. *Neuron*. 2011;69(1):132–46.

48. Tanaka J-I, Horiike Y, Matsuzaki M, et al. Protein synthesis and neurotrophin-dependent structural plasticity of single dendritic spines. *Science*. 2008;319(5870):1683–7.

49. Matsuzaki M, Ellis-Davies GC, Nemoto T, et al. Dendritic spine geometry is critical for AMPA receptor expression in hippocampal CA1 pyramidal neurons. *Nature neuroscience*. 2001;4(11):1086–92.

50. Nusser Z, Lujan R, Laube G, et al. Cell type and pathway dependence of synaptic AMPA receptor number and variability in the hippocampus. *Neuron*. 1998;21(3):545–59.

51. Frey U, Krug M, Reymann KG, Matthies H. Anisomycin, an inhibitor of protein synthesis, blocks late phases of LTP phenomena in the hippocampal CA1 region in vitro. *Brain research*. 1988;452(1-2):57–65.

52. Frey U, Morris RG. Synaptic tagging and long-term potentiation. *Nature*. 1997;385(6616):533–6.

53. Yu W, Lu B. Synapses and Dendritic Spines as Pathogenic Targets in Alzheimer's Disease. *Neural plasticity*. 2012;2012:1–8.

54. Irwin S a, Patel B, Idupulapati M, et al. Abnormal dendritic spine characteristics in the temporal and visual cortices of patients with fragile-X syndrome: a quantitative examination. *American journal of medical genetics*. 2001;98(2):161–7.

55. Takashima S, Becker L, Armstrong D. Abnormal neuronal development in the visual cortex of the human fetus and infant with Down's syndrome. A quantitative and qualitative Golgi study. *Brain research*. 1981;225:1–21.

56. Whitlock JR, Heynen AJ, Shuler MG, Bear MF. Learning induces long-term potentiation in the hippocampus. *Science*. 2006;313(5790):1093–7.

57. Kelleher RJ, Govindarajan A, Tonegawa S. Translational regulatory mechanisms in persistent forms of synaptic plasticity. *Neuron*. 2004;44(1):59–73.

58. Huber KM, Kayser MS, Bear MF. Role for Rapid Dendritic Protein Synthesis in Hippocampal mGluR-Dependent Long-Term Depression. *Science*. 2000;288(5469):1254–1256.

59. Autilio LA, Appel SH, Pettis P, Gambetti PL. Biochemical studies of synapses in vitro. I. Protein synthesis. *Biochemistry*. 1968;7(7):2615–22.

60. Morgan IG, Austin L. Synaptosomal protein synthesis in a cell-free system. *Journal of neurochemistry*. 1968;15(1):41–51.

61. Bodian D. A suggestive relationship of nerve cell RNA with specific synaptic sites. *Proceedings of the National Academy of Sciences of the USA*. 1965:418–425.

62. Kennedy M. Organelles and trafficking machinery for postsynaptic plasticity. *Annual review of neuroscience*. 2006:325–362.

63. Steward O, Ribak CE. Polyribosomes associated with synaptic specializations on axon initial segments: localization of protein-synthetic machinery at inhibitory synapses. *The Journal of neuroscience*. 1986;6(10):3079–85.

64. Steward O, Reeves TM. Protein-synthetic machinery beneath postsynaptic sites on CNS neurons: association between polyribosomes and other organelles at the synaptic site. *The Journal of neuroscience*. 1988;8(1):176–84.

65. Steward O. Alterations in polyribosomes associated with dendritic spines during the reinnervation of the dentate gyrus of the adult rat. *The Journal of neuroscience*. 1983;3(1):177.

66. Steward O, Falk PM. Polyribosomes under developing spine synapses: growth specializations of dendrites at sites of synaptogenesis. *Journal of neuroscience research*. 1985;13(1-2):75–88.

67. Levy B, Steward O, Levy WB. Preferential localization of polyribosomes under the base of dendritic spines in granule cells of the dentate gyrus. *The Journal of Neuroscience*. 1982;2(3):284–291.

68. Davis L, Banker GA, Steward O. Selective dendritic transport of RNA in hippocampal neurons in culture. *Nature*. 1987;330(6147):477–479.

69. Torre ER, Steward O. Demonstration of local protein synthesis within dendrites using a new cell culture system that permits the isolation of living axons and dendrites from their cell bodies. *The Journal of neuroscience*. 1992;12(3):762–72.

70. Torre ER, Steward O. Protein synthesis within dendrites: glycosylation of newly synthesized proteins in dendrites of hippocampal neurons in culture. *The Journal of neuroscience*. 1996;16(19):5967–78.

71. Eberwine J, Belt B, Kacharmina JE, Miyashiro K. Analysis of subcellularly localized mRNAs using in situ hybridization, mRNA amplification, and expression profiling. *Neurochemical research*. 2002;27(10):1065–77.

72. Miyashiro K, Dichter M, Eberwine J. On the nature and differential distribution of mRNAs in hippocampal neurites: implications for neuronal functioning. *Proceedings of the National Academy of Sciences of the USA*. 1994;91(23):10800–4.

73. Zhong J, Zhang T, Bloch LM. Dendritic mRNAs encode diversified functionalities in hippocampal pyramidal neurons. *BMC neuroscience*. 2006;7:17.

74. Muslimov IA, Nimmrich V, Hernandez AI, et al. Dendritic transport and localization of protein kinase Mzeta mRNA: implications for molecular memory consolidation. *The Journal of biological chemistry*. 2004;279(50):52613–22.

75. Steward O, Wallace CS, Lyford GL, Worley PF. Synaptic activation causes the mRNA for the IEG Arc to localize selectively near activated postsynaptic sites on dendrites. *Neuron*. 1998;21(4):741–51.

76. Weiler IJ, Greenough WT. Potassium ion stimulation triggers protein translation in synaptoneurosomal polyribosomes. *Molecular and cellular neuroscience*. 1991;2(4):305–14.

77. Aakalu G, Smith WB, Nguyen N, Jiang C, Schuman EM. Dynamic visualization of local protein synthesis in hippocampal neurons. *Neuron*. 2001;30(2):489–502.

78. Job C, Eberwine J. Identification of sites for exponential translation in living dendrites. *Proceedings of the National Academy of Sciences of the USA*. 2001;98(23):13037–42.

79. Sajikumar S, Frey JU. Late-associativity, synaptic tagging, and the role of dopamine during LTP and LTD. *Neurobiology of learning and memory*. 2004;82(1):12–25.

80. Sacktor TC. How does PKMζ maintain long-term memory? *Nature reviews neuroscience*. 2011;12(1):9–15.

81. Shema R, Sacktor T. Rapid erasure of long-term memory associations in the cortex by an inhibitor of PKM {zeta}. *Science*. 2007;317(August):951–953.

82. Si K, Choi Y-B, White-Grindley E, Majumdar A, Kandel ER. Aplysia CPEB can form prion-like multimers in sensory neurons that contribute to long-term facilitation. *Cell*. 2010;140(3):421–35.

83. Kang H, Schuman EM. Long-lasting neurotrophin-induced enhancement of synaptic transmission in the adult hippocampus. *Science*. 1995;267(5204):1658–62.

84. Frey U, Krug M, Brödemann R, Reymann K, Matthies H. Long-term potentiation induced in dendrites separated from rat's CA1 pyramidal somata does not establish a late phase. *Neuroscience letters*. 1989;97(1-2):135–9.

85. Miller S, Yasuda M, Coats JK, et al. Disruption of dendritic translation of CaMKIIalpha impairs stabilization of synaptic plasticity and memory consolidation. *Neuron*. 2002;36(3):507–19.

86. Tang SJ, Reis G, Kang H, et al. A rapamycin-sensitive signaling pathway contributes to long-term synaptic plasticity in the hippocampus. *Proceedings of the National Academy of Sciences of the USA*. 2002;99(1):467–72.

87. Hou L, Klann E. Activation of the phosphoinositide 3-kinase-Akt-mammalian target of rapamycin signaling pathway is required for metabotropic glutamate receptor-dependent long-term depression. *The Journal of neuroscience*. 2004;24(28):6352–61.

88. Gallagher SM, Daly C a, Bear MF, Huber KM. Extracellular signal-regulated protein kinase activation is required for metabotropic glutamate receptor-

dependent long-term depression in hippocampal area CA1. *The Journal of neuroscience*. 2004;24(20):4859–64.

89. Harding H, Novoa I, Zhang Y, Zeng H. Regulated translation initiation controls stress-induced gene expression in mammalian cells. *Molecular cell*. 2000;6:1099–1108.

90. Abel T. Memory Suppressor Genes: Inhibitory Constraints on the Storage of Long-Term Memory. *Science*. 1998;279(5349):338–341.

91. Chen A, Muzzio I a, Malleret G, et al. Inducible enhancement of memory storage and synaptic plasticity in transgenic mice expressing an inhibitor of ATF4 (CREB-2) and C/EBP proteins. *Neuron*. 2003;39(4):655–69.

92. Costa-Mattioli M, Sonenberg N, Richter JD. *Translational regulatory mechanisms in synaptic plasticity and memory storage.* 1st ed. Elsevier Inc. 2009:293–311.

93. Zhu PJ, Huang W, Kalikulov D, et al. Suppression of PKR promotes network excitability and enhanced cognition by interferon-γ-mediated disinhibition. *Cell*. 2011;147(6):1384–96.

94. Hussey GS, Chaudhury A, Dawson AE, et al. Identification of an mRNP complex regulating tumorigenesis at the translational elongation step. *Molecular cell*. 2011;41(4):419–31.

95. Olsen PH, Ambros V. The lin-4 regulatory RNA controls developmental timing in Caenorhabditis elegans by blocking LIN-14 protein synthesis after the initiation of translation. *Developmental biology*. 1999;216(2):671–80.

96. Clark IE, Wyckoff D, Gavis ER. Synthesis of the posterior determinant Nanos is spatially restricted by a novel cotranslational regulatory mechanism. *Current biology*. 2000;10(20):1311–4.

97. Scheetz A, Nairn A. NMDA receptor-mediated control of protein synthesis at developing synapses. *Nature neuroscience*. 2000:211–216.

98. Park S, Park JM, Kim S, et al. Elongation factor 2 and fragile X mental retardation protein control the dynamic translation of Arc/Arg3.1 essential for mGluR-LTD. *Neuron*. 2008;59(1):70–83.

99. Walden WE, Thach RE. Translational control of gene expression in a normal fibroblast. Characterization of a subclass of mRNAs with unusual kinetic properties. *Biochemistry*. 1986;25(8):2033–41.

100. Sutton M a, Taylor AM, Ito HT, Pham A, Schuman EM. Postsynaptic decoding of neural activity: eEF2 as a biochemical sensor coupling miniature synaptic transmission to local protein synthesis. *Neuron*. 2007;55(4):648–61.

101. Sossin WS, DesGroseillers L. Intracellular trafficking of RNA in neurons. *Traffic*. 2006;7(12):1581–9.

102. Kedersha N, Anderson P. Mammalian stress granules and processing bodies. *Methods in enzymology*. 2007;431(07):61–81.

103. Barbee S a, Estes PS, Cziko A-M, et al. Staufen- and FMRP-containing neuronal RNPs are structurally and functionally related to somatic P bodies. *Neuron*. 2006;52(6):997–1009.

104. Zeitelhofer M, Karra D, Macchi P, et al. Dynamic interaction between P-bodies and transport ribonucleoprotein particles in dendrites of mature hippocampal neurons. *The Journal of neuroscience*. 2008;28(30):7555–7562.

105. Vessey JP, Vaccani A, Xie Y, et al. Dendritic localization of the translational repressor Pumilio 2 and its contribution to dendritic stress granules. *The Journal of neuroscience*. 2006;26(24):6496–508.

106. Krichevsky AM, Kosik KS. Neuronal RNA granules: a link between RNA localization and stimulation-dependent translation. *Neuron*. 2001;32(4):683–696.

107. Shiina N, Shinkura K, Tokunaga M. A novel RNA-binding protein in neuronal RNA granules: regulatory machinery for local translation. *The Journal of neuroscience*. 2005;25(17):4420–34.

108. Antar LN, Afroz R, Dictenberg JB, Carroll RC, Bassell GJ. Metabotropic glutamate receptor activation regulates fragile x mental retardation protein and FMR1 mRNA localization differentially in dendrites and at synapses. *The Journal of neuroscience*. 2004;24(11):2648–55.

109. Ainger K, Avossa D, Morgan F, et al. Transport and localization of exogenous myelin basic protein mRNA microinjected into oligodendrocytes. *The Journal of cell biology*. 1993;123(2):431–41.

110. Knowles RB, Sabry JH, Martone ME, et al. Translocation of RNA granules in living neurons. *The Journal of neuroscience*. 1996;16(24):7812–20.

111. Miller LC, Blandford V, McAdam R, et al. Combinations of DEAD box proteins distinguish distinct types of RNA: Protein complexes in neurons. *Molecular and cellular neuroscience*. 2009;40(4):485–495.

112. Köhrmann M, Luo M, Kaether C, et al. Microtubule-dependent recruitment of Staufen-green fluorescent protein into large RNA-containing granules and subsequent dendritic transport in living hippocampal neurons. *Molecular biology of the cell*. 1999;10(9):2945–53.

113. Zhang HL, Eom T, Oleynikov Y, et al. Neurotrophin-induced transport of a beta-actin mRNP complex increases beta-actin levels and stimulates growth cone motility. *Neuron*. 2001;31(2):261–75.

114. Hüttelmaier S, Zenklusen D, Lederer M, et al. Spatial regulation of beta-actin translation by Src-dependent phosphorylation of ZBP1. *Nature*. 2005;438(7067):512–5.

115. Sasaki Y, Welshhans K, Wen Z, et al. Phosphorylation of zipcode binding protein 1 is required for brain-derived neurotrophic factor signaling of local beta-actin synthesis and growth cone turning. *The Journal of neuroscience*. 2010;30(28):9349–58.

116. Tiruchinapalli DM, Oleynikov Y, Kelic S, et al. Activity-dependent trafficking and dynamic localization of zipcode binding protein 1 and beta-actin mRNA in dendrites and spines of hippocampal neurons. *The Journal of neuroscience*. 2003;23(8):3251–61.

117. Eom T, Antar LN, Singer RH, Bassell GJ. Localization of a beta-actin messenger ribonucleoprotein complex with zipcode-binding protein modulates the density of dendritic filopodia and filopodial synapses. *The Journal of neuroscience*. 2003;23(32):10433–44.

118. St Johnston D, Beuchle D, Nüsslein-Volhard C. Staufen, a gene required to localize maternal RNAs in the Drosophila egg. *Cell*. 1991;66(1):51–63.

119. Mallardo M, Deitinghoff A, Müller J, et al. Isolation and characterization of Staufen-containing ribonucleoprotein particles from rat brain. *Proceedings of the National Academy of Sciences of the USA*. 2003;100(4):2100–5.

120. Furic L, Maher-Laporte M, DesGroseillers L. A genome-wide approach identifies distinct but overlapping subsets of cellular mRNAs associated with Staufen1- and Staufen2-containing ribonucleoprotein complexes. *RNA*. 2008;14(2):324–35.

121. Duchaîne TF, Hemraj I, Furic L, et al. Staufen2 isoforms localize to the somatodendritic domain of neurons and interact with different organelles. *Journal of cell science*. 2002;115(Pt 16):3285–95.

122. Lebeau G, Maher-Laporte M, Topolnik L, et al. Staufen1 regulation of protein synthesis-dependent long-term potentiation and synaptic function in hippocampal pyramidal cells. *Molecular and cellular biology*. 2008;28(9):2896–907.

123. Lebeau G, Miller LC, Tartas M, et al. Staufen 2 regulates mGluR long-term depression and Map1b mRNA distribution in hippocampal neurons. *Learning & memory*. 2011;18(5):314–26.

124. Goetze B, Tuebing F, Xie Y, et al. The brain-specific double-stranded RNA-binding protein Staufen2 is required for dendritic spine morphogenesis. *The Journal of cell biology*. 2006;172(2):221–31.

125. Richter JD. CPEB: a life in translation. *Trends in biochemical sciences*. 2007;32(6):279–85.

126. Wu L, Wells D, Tay J, et al. CPEB-mediated cytoplasmic polyadenylation and the regulation of experience-dependent translation of alpha-CaMKII mRNA at synapses. *Neuron*. 1998;21(5):1129–39.

127. Huang Y-S, Jung M-Y, Sarkissian M, Richter JD. N-methyl-D-aspartate receptor signaling results in Aurora kinase-catalyzed CPEB phosphorylation and alpha CaMKII mRNA polyadenylation at synapses. *The EMBO journal*. 2002;21(9):2139–48.

128. Alarcon J, Hodgman R. Selective modulation of some forms of schaffer collateral-CA1 synaptic plasticity in mice with a disruption of the CPEB-1 gene. *Learning & memory*. 2004:318–327.

129. Berger-Sweeney J, Zearfoss NR, Richter JD. Reduced extinction of hippocampal-dependent memories in CPEB knockout mice. *Learning & memory*. 2006;13(1):4–7.

130. Nilsen TW. Mechanisms of microRNA-mediated gene regulation in animal cells. *Trends in genetics*. 2007;23(5):243–9.

131. Fabian MR, Cieplak MK, Frank F, et al. miRNA-mediated deadenylation is orchestrated by GW182 through two conserved motifs that interact with CCR4-NOT. *Nature structural & molecular biology*. 2011;18(11):1211–1217.

132. Lugli G, Larson J, Martone ME, Jones Y, Smalheiser NR. Dicer and eIF2c are enriched at postsynaptic densities in adult mouse brain and are modified by neuronal activity in a calpain-dependent manner. *Journal of neurochemistry*. 2005;94(4):896–905.

133. Schratt GM, Tuebing F, Nigh EA, et al. A brain-specific microRNA regulates dendritic spine development. *Nature*. 2006;439(7074):283–9.

134. Siegel G, Obernosterer G, Fiore R, et al. A functional screen implicates microRNA-138-dependent regulation of the depalmitoylation enzyme APT1 in dendritic spine morphogenesis. *Nature cell biology*. 2009;11(6):705–16.

135. Edbauer D, Neilson JR, Foster K a, et al. Regulation of synaptic structure and function by FMRP-associated microRNAs miR-125b and miR-132. *Neuron*. 2010;65(3):373–84.

136. Huber KM, Gallagher SM, Warren ST, Bear MF. Altered synaptic plasticity in a mouse model of fragile X mental retardation. *Proceedings of the National Academy of Sciences of the USA*. 2002;99(11):7746–50.

137. Nosyreva ED, Huber KM. Metabotropic receptor-dependent long-term depression persists in the absence of protein synthesis in the mouse model of fragile X syndrome. *Journal of neurophysiology*. 2006;95(5):3291–5.

138. Laggerbauer B, Ostareck D, Keidel EM, Ostareck-Lederer a, Fischer U. Evidence that fragile X mental retardation protein is a negative regulator of translation. *Human molecular genetics*. 2001;10(4):329–38.

139. Zalfa F, Giorgi M, Primerano B, et al. The fragile X syndrome protein FMRP associates with BC1 RNA and regulates the translation of specific mRNAs at synapses. *Cell*. 2003;112(3):317–27.

140. Muddashetty RS, Kelić S, Gross C, Xu M, Bassell GJ. Dysregulated metabotropic glutamate receptor-dependent translation of AMPA receptor and

postsynaptic density-95 mRNAs at synapses in a mouse model of fragile X syndrome. *The Journal of neuroscience*. 2007;27(20):5338–48.

141. Bassell GJ, Warren ST. Fragile X syndrome: loss of local mRNA regulation alters synaptic development and function. *Neuron*. 2008;60(2):201–14.

142. Napoli I, Mercaldo V, Boyl PP, et al. The fragile X syndrome protein represses activity-dependent translation through CYFIP1, a new 4E-BP. *Cell*. 2008;134(6):1042–54.

143. Pfeiffer BE, Huber KM. Fragile X mental retardation protein induces synapse loss through acute postsynaptic translational regulation. *The Journal of neuroscience*. 2007;27(12):3120–30.

144. Ceman S, O'Donnell WT, Reed M, et al. Phosphorylation influences the translation state of FMRP-associated polyribosomes. *Human molecular genetics*. 2003;12(24):3295–305.

145. Muddashetty RS, Nalavadi VC, Gross C, et al. Reversible Inhibition of PSD-95 mRNA Translation by miR-125a, FMRP Phosphorylation, and mGluR Signaling. *Molecular cell*. 2011;42(5):673–88.

146. Todd PK, Mack KJ, Malter JS. The fragile X mental retardation protein is required for type-I metabotropic glutamate receptor-dependent translation of PSD-95. *Proceedings of the National Academy of Sciences of the USA*. 2003;100(24):14374–8.

147. Weiler IJ, Spangler CC, Klintsova AY, et al. Fragile X mental retardation protein is necessary for neurotransmitter-activated protein translation at synapses. *Proceedings of the National Academy of Sciences of the USA*. 2004;101(50):17504–9.

148. Bechara EG, Didiot MC, Melko M, et al. A novel function for fragile X mental retardation protein in translational activation. *PLoS biology*. 2009;7(1):e16.

149. Fähling M, Mrowka R, Steege A, et al. Translational regulation of the human achaete-scute homologue-1 by fragile X mental retardation protein. *The Journal of biological chemistry*. 2009;284(7):4255–66.

150. Cheever A, Ceman S. Translation regulation of mRNAs by the fragile X family of proteins through the microRNA pathway. *RNA biology*. 2009;6(2):175–8.

151. Siomi MC, Siomi H, Sauer WH, et al. FXR1, an autosomal homolog of the fragile X mental retardation gene. *The EMBO journal*. 1995;14(11):2401–8.

152. Sittler a, Devys D, Weber C, Mandel JL. Alternative splicing of exon 14 determines nuclear or cytoplasmic localisation of fmr1 protein isoforms. *Human molecular genetics*. 1996;5(1):95–102.

153. Kirkpatrick LL, McIlwain K a, Nelson DL. Alternative splicing in the murine and human FXR1 genes. *Genomics*. 1999;59(2):193–202.

154. Khandjian EW, Corbin F, Woerly S, Rousseau F. The fragile X mental retardation protein is associated with ribosomes. *Nature genetics*. 1996;12(1):91–3.

155. Mientjes EJ, Willemsen R, Kirkpatrick LL, et al. Fxr1 knockout mice show a striated muscle phenotype: implications for Fxr1p function in vivo. *Human molecular genetics*. 2004;13(13):1291–302.

156. Whitman S a, Cover C, Yu L, et al. Desmoplakin and Talin2 Are Novel mRNA Targets of Fragile X-Related Protein-1 in Cardiac Muscle Whitman; Dsp and Tln2 Are mRNA Targets of FXR1 in the Heart. *Circulation research*. 2011;85724:1–10.

157. Lachance C, Thuraisingam T, Garnon J, Roter E, Radzioch D. Posttranscriptional gene expression regulation in CpG-activated macrophages depends on FXR1P RNA-binding protein. *FEMS immunology and medical microbiology*. 2007;51(2):422–30.

158. Stefansson H, Ophoff R a, Steinberg S, et al. Common variants conferring risk of schizophrenia. *Nature*. 2009;460(7256):744–7.

159. Rehnström K, Ylisaukko-oja T, Nummela I, et al. Allelic variants in HTR3C show association with autism. *American journal of medical genetics. Part B, Neuropsychiatric genetics*. 2009;150B(5):741–6.

160. Frey U, Huang YY, Kandel ER. Effects of cAMP simulate a late stage of LTP in hippocampal CA1 neurons. *Science*. 1993;260(5114):1661–1664.

161. Wells DG. RNA-binding proteins: a lesson in repression. *The Journal of neuroscience*. 2006;26(27):7135–8.

162. O'Donnell WT, Warren ST. A decade of molecular studies of fragile X syndrome. *Annual review of neuroscience*. 2002;25:315–338.

163. Bardoni B, Davidovic L, Bensaid M, Khandjian EW. The fragile X syndrome: exploring its molecular basis and seeking a treatment. *Expert reviews in molecular medicine*. 2006;8(8):1–16.

164. Brown V, Jin P, Ceman S, et al. Microarray Identification of FMRP-Associated Brain mRNAs and Altered mRNA Translational Profiles in Fragile X Syndrome. *Cell*. 2001;107(4):477–487.

165. Kao D-II, Aldridge GM, Weiler IJ, Greenough WT. Altered mRNA transport, docking, and protein translation in neurons lacking fragile X mental retardation protein. *Proceedings of the National Academy of Sciences of the USA*. 2010;107(35):15601–6.

166. Khandjian EW, Bardoni B, Corbin F, et al. Novel isoforms of the fragile X related protein FXR1P are expressed during myogenesis. *Human molecular genetics*. 1998;7(13):2121–8.

167. Mazroui R, Huot ME, Tremblay S, et al. Fragile X Mental Retardation protein determinants required for its association with polyribosomal mRNPs. *Human molecular genetics*. 2003;12(23):3087–3096.

168. Devys D, Lutz Y, Rouyer N, Bellocq JP, Mandel JL. The FMR-1 protein is cytoplasmic, most abundant in neurons and appears normal in carriers of a fragile X premutation. *Nature genetics*. 1993;4(4):335–340.

169. Khandjian EW, Huot M-EE, Tremblay S, et al. Biochemical evidence for the association of fragile X mental retardation protein with brain polyribosomal ribonucleoparticles. *Proceedings of the National Academy of Sciences of the USA*. 2004;101(36):13357–62.

170. Kaech S, Banker G. Culturing hippocampal neurons. *Nature protocols*. 2006;1(5):2406–2415.

171. Matesic DF, Lin RC. Microtubule-associated protein 2 as an early indicator of ischemia-induced neurodegeneration in the gerbil forebrain. *Journal of neurochemistry*. 1994;63(3):1012–20.

172. Bassell GJ, Zhang H, Byrd AL, et al. Sorting of beta-actin mRNA and protein to neurites and growth cones in culture. *The Journal of neuroscience*. 1998;18(1):251–265.

173. Li Q, Lau A, Morris TJ, et al. A syntaxin 1, Galpha(o), and N-type calcium channel complex at a presynaptic nerve terminal: analysis by quantitative immunocolocalization. *The Journal of neuroscience*. 2004;24(16):4070–81.

174. Zinchuk V, Zinchuk O. Quantitative colocalization analysis of confocal fluorescence microscopy images. *Current protocols in cell biology*. 2008;Chapter 4(June):Unit 4.19.

175. Stoppini L, Buchs P a, Muller D. A simple method for organotypic cultures of nervous tissue. *Journal of neuroscience methods*. 1991;37(2):173–182.

176. Haber M, Zhou L, Murai KK. Cooperative astrocyte and dendritic spine dynamics at hippocampal excitatory synapses. *The Journal of neuroscience*. 2006;26(35):8881–8891.

177. Lo DC. Neuronal transfection using particle-mediated gene transfer. *Current protocols in neuroscience*. 1998;Chapter 3:Unit 3 15.

178. Team RDC. R: A Language and Environment for Statistical Computing. 2011.

179. Anon. Hmisc S function library. http://biostat.mc.vanderbilt.edu/twiki/bin/view/Main/Hmisc. 2003.

180. Wickham H. *Ggplot2 : elegant graphics for data analysis*. New York: Springer; 2009:viii, 212 p.

181. Huot ME, Mazroui R, Leclerc P, Khandjian EW. Developmental expression of the fragile X-related 1 proteins in mouse testis: association with microtubule elements. *Human molecular genetics*. 2001;10(24):2803–11.

182. Sorra KE, Harris KM. Overview on the structure, composition, function, development, and plasticity of hippocampal dendritic spines. *Hippocampus*. 2000;10(5):501–511.

183. Say E, Tay H-GG, Zhao ZS, et al. A functional requirement for PAK1 binding to the KH(2) domain of the fragile X protein-related FXR1. *Molecular cell*. 2010;38(2):236–49.

184. Jacobs T, Causeret F, Nishimura YV, et al. Localized activation of p21-activated kinase controls neuronal polarity and morphology. *The Journal of neuroscience*. 2007;27(32):8604–8615.

185. Mazroui R, Huot M-EE, Tremblay S, et al. Trapping of messenger RNA by Fragile X Mental Retardation protein into cytoplasmic granules induces translation repression. *Human molecular genetics*. 2002;11(24):3007–17.

186. Kedersha NL, Gupta M, Li W, Miller I, Anderson P. RNA-binding proteins TIA-1 and TIAR link the phosphorylation of eIF-2 alpha to the assembly of mammalian stress granules. *Journal of cell biology*. 1999;147(7):1431–1442.

187. Zito K, Scheuss V, Knott G, Hill T, Svoboda K. Rapid functional maturation of nascent dendritic spines. *Neuron*. 2009;61(2):247–58.

188. Wang DO, Martin KC, Zukin RS. Spatially restricting gene expression by local translation at synapses. *Trends in neurosciences*. 2010;33(4):173–82.

189. Kosik KS, Krichevsky AM. The message and the messenger: delivering RNA in neurons. *Science STKE*. 2002;2002(126):pe16.

190. Ostroff LE, Fiala JC, Allwardt B, Harris KM. Polyribosomes redistribute from dendritic shafts into spines with enlarged synapses during LTP in developing rat hippocampal slices. *Neuron*. 2002;35(3):535–45.

191. Antar LN, Dictenberg JB, Plociniak M, Afroz R, Bassell GJ. Localization of FMRP-associated mRNA granules and requirement of microtubules for activity-dependent trafficking in hippocampal neurons. *Genes, brain, and behavior*. 2005;4(6):350–359.

192. Darnell JC, Fraser CE, Mostovetsky O, Darnell RB. Discrimination of common and unique RNA-binding activities among Fragile X mental retardation protein paralogs. *Human molecular genetics*. 2009;18(17):3164–77.

193. Gessert S, Bugner V, Tecza A, et al. FMR1/FXR1 and the miRNA pathway are required for eye and neural crest development. *Developmental biology*. 2010;341(1):222–235.

194. Ethell IM, Pasquale EB. Molecular mechanisms of dendritic spine development and remodeling. *Progress in neurobiology*. 2005;75(3):161–205.

195. Zuo Y, Lin A, Chang P, Gan W-B. Development of long-term dendritic spine stability in diverse regions of cerebral cortex. *Neuron*. 2005;46(2):181–9.

196. Holtmaat AJGD, Trachtenberg JT, Wilbrecht L, et al. Transient and persistent dendritic spines in the neocortex in vivo. *Neuron*. 2005;45(2):279–91.

197. Yasumatsu N, Matsuzaki M, Miyazaki T, Noguchi J, Kasai H. Principles of long-term dynamics of dendritic spines. *The Journal of neuroscience*. 2008;28(50):13592–608.

198. Kasai H, Fukuda M, Watanabe S, Hayashi-Takagi A, Noguchi J. Structural dynamics of dendritic spines in memory and cognition. *Trends in neurosciences*. 2010;33(3):121–9.

199. Kasai H, Matsuzaki M, Noguchi J, Yasumatsu N, Nakahara H. Structure–stability–function relationships of dendritic spines. *Trends in neurosciences*. 2003;26(7):360–368.

200. Berning S, Willig KI, Steffens H, Dibaj P, Hell SW. Nanoscopy in a living mouse brain. *Science*. 2012;335(6068):551.

201. Tada T, Sheng M. Molecular mechanisms of dendritic spine morphogenesis. *Current opinion in neurobiology*. 2006;16(1):95–101.

202. Pfeiffer BE, Zang T, Wilkerson JR, et al. Fragile X mental retardation protein is required for synapse elimination by the activity-dependent transcription factor MEF2. *Neuron*. 2010;66(2):191–7.

203. Lo D. Neuronal Transfection Using Particle-Mediated Gene Transfer. *Current protocols in neuroscience*. 2001:1–12.

204. Rodriguez A, Ehlenberger DB, Dickstein DL, Hof PR, Wearne SL. Automated three-dimensional detection and shape classification of dendritic spines from fluorescence microscopy images. *PloS one*. 2008;3(4):e1997.

205. Wickham H. Reshaping Data with the reshape Package. *Journal Of Statistical Software*. 2007;21(12):1–20.

206. Lumley T, Warnes MGR. The gplots Package. *Text*. 2009.

207. Lemon J. Plotrix: a package in the red light district of R. *RNews*. 2006;6(4):8–12.

208. Markowski E. A Systematic Method for Teaching Post Hoc Analysis of Chi-Square Tests. *Decision sciences journal of innovative education*. 2009;7(1):59–65.

209. Béïque J-C, Lin D-T, Kang M-G, et al. Synapse-specific regulation of AMPA receptor function by PSD-95. *Proceedings of the National Academy of Sciences of the USA*. 2006;103(51):19535–40.

210. Wang X, Yang Y, Zhou Q. Independent expression of synaptic and morphological plasticity associated with long-term depression. *The Journal of neuroscience*. 2007;27(45):12419–29.

211. Ostroff LE, Cain CK, Bedont J, Monfils MH, Ledoux JE. Fear and safety learning differentially affect synapse size and dendritic translation in the lateral amygdala. *Proceedings of the National Academy of Sciences of the USA*. 2010;107(20):9418–23.

212. Spacek J, Harris KM. Three-dimensional organization of smooth endoplasmic reticulum in hippocampal CA1 dendrites and dendritic spines of the immature and mature rat. *The Journal of neuroscience*. 1997;17(1):190–203.

213. Holbro N, Grunditz A, Oertner TG. Differential distribution of endoplasmic reticulum controls metabotropic signaling and plasticity at hippocampal synapses. *Proceedings of the National Academy of Sciences of the USA*. 2009;106(35):15055–60.

214. Segal M, Vlachos A, Korkotian E. The spine apparatus, synaptopodin, and dendritic spine plasticity. *The neuroscientist*. 2010;16(2):125–31.

215. Deller T, Merten T, Roth SU, Mundel P, Frotscher M. Actin-associated protein synaptopodin in the rat hippocampal formation: localization in the spine neck and close association with the spine apparatus of principal neurons. *The Journal of comparative neurology*. 2000;418(2):164–81.

216. Jedlicka P, Vlachos A, Schwarzacher SW, Deller T. A role for the spine apparatus in LTP and spatial learning. *Behavioural brain research*. 2008;192(1):12–9.

217. Vlachos A, Korkotian E, Schonfeld E, et al. Synaptopodin regulates plasticity of dendritic spines in hippocampal neurons. *The Journal of neuroscience*. 2009;29(4):1017–33.

218. Coffee RL, Tessier CR, Woodruff E a, Broadie K. Fragile X mental retardation protein has a unique, evolutionarily conserved neuronal function not shared with FXR1P or FXR2P. *Disease models & mechanisms*. 2010;3(7-8):471–85.

219. Darnell JC, Jensen KB, Jin P, et al. Fragile X mental retardation protein targets G quartet mRNAs important for neuronal function. *Cell*. 2001;107(4):489–99.

220. Zhang YQ, Bailey a M, Matthies HJ, et al. Drosophila fragile X-related gene regulates the MAP1B homolog Futsch to control synaptic structure and function. *Cell*. 2001;107(5):591–603.

221. Stellwagen D, Malenka RC. Synaptic scaling mediated by glial TNF-alpha. *Nature*. 2006;440(7087):1054–9.

222. McGeachie AB, Cingolani L a, Goda Y. A stabilising influence: Integrins in regulation of synaptic plasticity. *Neuroscience research*. 2011;70(1):24–9.

223. Xu X-L, Zong R, Li Z, et al. FXR1P But Not FMRP Regulates the Levels of Mammalian Brain-Specific microRNA-9 and microRNA-124. *The Journal of neuroscience*. 2011;31(39):13705–13709.

224. Costa-Mattioli M, Sonenberg N. *Translational control of gene expression: a molecular switch for memory storage.* Elsevier; 2008:81–95.

225. Gkogkas C, Sonenberg N, Costa-Mattioli M. Translational control mechanisms in long-lasting synaptic plasticity and memory. *The Journal of biological chemistry*. 2010;285(42):31913–7.

226. Auerbach BD, Osterweil EK, Bear MF. Mutations causing syndromic autism define an axis of synaptic pathophysiology. *Nature*. 2011;480(7375):63–8.

227. Kelleher RJ, Bear MF. The autistic neuron: troubled translation? *Cell*. 2008;135(3):401–6.

228. Bhakar AL, Dölen G, Bear MF. The Pathophysiology of Fragile X (and What It Teaches Us about Synapses). *Annual review of neuroscience*. 2012;(March):417–443.

229. Kooy RF, D'Hooge R, Reyniers E, et al. Transgenic mouse model for the fragile X syndrome. *American journal of medical genetics*. 1996;64(2):241–5.

230. Baker KB, Wray SP, Ritter R, et al. Male and female Fmr1 knockout mice on C57 albino background exhibit spatial learning and memory impairments. *Genes, brain, and behavior*. 2010;9(6):562–74.

231. Dutch-belgian T, Helm RVD, Oerlemans F, Hoogeveen T, Oostra BA. Fmrl Knockout M ice : A Model to Study Fragile X Mental Retardation. *Cell*. 1994;78:23–33.

232. Bakker CE, Oostra BA. Understanding fragile X syndrome: insights from animal models. *Cytogenetic and genome research*. 2003;100(1-4):111–23.

233. Cruz-Martín A, Crespo M, Portera-Cailliau C. Delayed stabilization of dendritic spines in fragile X mice. *The Journal of neuroscience*. 2010;30(23):7793–803.

234. Kirkpatrick LL, McIlwain K a, Nelson DL. Comparative genomic sequence analysis of the FXR gene family: FMR1, FXR1, and FXR2. *Genomics*. 2001;78(3):169–77.

235. Sonner JM, Cascio M, Xing Y, et al. Alpha 1 subunit-containing GABA type A receptors in forebrain contribute to the effect of inhaled anesthetics on conditioned fear. *Molecular pharmacology*. 2005;68(1):61–8.

236. Tsien JZ, Chen DF, Gerber D, et al. Subregion- and cell type-restricted gene knockout in mouse brain. *Cell*. 1996;87(7):1317–26.

237. Fukaya M, Kato A, Lovett C, Tonegawa S, Watanabe M. Retention of NMDA receptor NR2 subunits in the lumen of endoplasmic reticulum in targeted NR1 knockout mice. *Proceedings of the National Academy of Sciences of the USA*. 2003;100(8):4855–60.

238. Gould TD, O'Donnell KC, Picchini AM, et al. Generation and behavioral characterization of beta-catenin forebrain-specific conditional knock-out mice. *Behavioural brain research*. 2008;189(1):117–25.

239. Gan WB, Grutzendler J, Wong WT, Wong ROL, Lichtman JW. Multicolor "DiOlistic" labeling of the nervous system using lipophilic dye combinations. *Neuron*. 2000;27(2):219–25.

240. Sajikumar S, Navakkode S, Frey JU. Protein synthesis-dependent long-term functional plasticity: methods and techniques. *Current opinion in neurobiology*. 2005;15(5):607–13.

241. Saffary R, Xie Z. FMRP regulates the transition from radial glial cells to intermediate progenitor cells during neocortical development. *The Journal of neuroscience*. 2011;31(4):1427–39.

242. Antar LN, Li C, Zhang H, Carroll RC, Bassell GJ. Local functions for FMRP in axon growth cone motility and activity-dependent regulation of filopodia and spine synapses. *Molecular and cellular neuroscience*. 2006;32(1-2):37–48.

243. Lee A, Li W, Xu K, et al. Control of dendritic development by the Drosophila fragile X-related gene involves the small GTPase Rac1. *Development*. 2003;130(22):5543–52.

244. Muzumdar MD, Tasic B, Miyamichi K, Li L, Luo L. A global double-fluorescent Cre reporter mouse. *Genesis*. 2007;45(9):593–605.

245. Mullen RJ, Buck CR, Smith a M. NeuN, a neuronal specific nuclear protein in vertebrates. *Development*. 1992;116(1):201–11.

246. Scharf MT, Woo NH, Lattal KM, et al. Protein Synthesis Is Required for the Enhancement of Long-Term Potentiation and Long-Term Memory by Spaced Training. *Journal of neurophysiology*. 2002;87(6):2770–2777.

247. Bramham CR. Local protein synthesis, actin dynamics, and LTP consolidation. *Current opinion in neurobiology*. 2008;18(5):524–31.

248. Schuman EM. mRNA trafficking and local protein synthesis at the synapse. *Neuron*. 1999;23(4):645–8.

249. Kang H, Schuman EM. A requirement for local protein synthesis in neurotrophin-induced hippocampal synaptic plasticity. *Science*. 1996;273(5280):1402–6.

250. Fabian MR, Sonenberg N, Filipowicz W. Regulation of mRNA translation and stability by microRNAs. *Annual review of biochemistry*. 2010;79:351–79.

251. Lee HYY, Ge W-P, Huang W, et al. Bidirectional Regulation of Dendritic Voltage-Gated Potassium Channels by the Fragile X Mental Retardation Protein. *Neuron*. 2011;72(4):630–642.

252. Paradee W, Melikian HE, Rasmussen DL, et al. Fragile X mouse: strain effects of knockout phenotype and evidence suggesting deficient amygdala function. *Neuroscience*. 1999;94(1):185–92.

253. Godfraind JM, Reyniers E, De Boulle K, et al. Long-term potentiation in the hippocampus of fragile X knockout mice. *American journal of medical genetics*. 1996;64(2):246–51.

254. D'Hooge R, Nagels G, Franck F, et al. Mildly impaired water maze performance in male Fmr1 knockout mice. *Neuroscience*. 1997;76(2):367–76.

255. Dobkin C, Rabe a, Dumas R, et al. Fmr1 knockout mouse has a distinctive strain-specific learning impairment. *Neuroscience*. 2000;100(2):423–9.

256. Peier a M, McIlwain KL, Kenneson a, et al. (Over)correction of FMR1 deficiency with YAC transgenics: behavioral and physical features. *Human molecular genetics*. 2000;9(8):1145–59.

257. Dieterich DC, Link a J, Graumann J, Tirrell D a, Schuman EM. Selective identification of newly synthesized proteins in mammalian cells using bioorthogonal noncanonical amino acid tagging (BONCAT). *Proceedings of the National Academy of Sciences of the USA*. 2006;103(25):9482–7.

258. Le Roux P, Reh T. Regional differences in glial-derived factors that promote dendritic outgrowth from mouse cortical neurons in vitro. *The Journal of neuroscience*. 1994;14(8):4639–4655.

259. Araque A, Parpura V, Sanzgiri RP, Haydon PG. Tripartite synapses: glia, the unacknowledged partner. *Trends in neurosciences*. 1999;22(5):208–215.

260. Murai KK, Van Meyel DJ. Neuron glial communication at synapses: insights from vertebrates and invertebrates. *The neuroscientist*. 2007;13(6):657–66.

261. Ullian EM, Sapperstein SK, Christopherson KS, Barres BA. Control of synapse number by glia. *Science*. 2001;291(5504):657–61.

262. Barres BA. The mystery and magic of glia: a perspective on their roles in health and disease. *Neuron*. 2008;60(3):430–40.

263. Pfrieger FW. Role of glial cells in the formation and maintenance of synapses. *Brain research reviews*. 2010;63(1-2):39–46.

264. Banker GGK. *Culturing Nerve Cells*. MIT Press; 1998:666.

265. Lundstrom K, Abenavoli A, Malgaroli A, Ehrengruber MU. Novel Semliki Forest virus vectors with reduced cytotoxicity and temperature sensitivity for

long-term enhancement of transgene expression. *Molecular therapy*. 2003;7(2):202–9.

266. Ehrengruber MU, Schlesinger S, Lundstrom K. Alphaviruses: Semliki forest virus and Sindbis virus vectors for gene transfer into neurons. *Current protocols in neuroscience*. 2011;Chapter 4:Unit 4.22.

267. Kim SH, Dong WK, Weiler IJ, Greenough WT. Fragile X mental retardation protein shifts between polyribosomes and stress granules after neuronal injury by arsenite stress or in vivo hippocampal electrode insertion. *The Journal of neuroscience*. 2006;26(9):2413–8.

268. Dolzhanskaya N, Merz G, Aletta JM, Denman RB. Methylation regulates the intracellular protein-protein and protein-RNA interactions of FMRP. *Journal of cell science*. 2006;119(Pt 9):1933–46.

269. McInerney GM, Kedersha NL, Kaufman RJ, et al. Importance of eIF2alpha phosphorylation and stress granule assembly in alphavirus translation regulation. *Molecular biology of the cell*. 2005;16(8):3753–63.

270. Krichevsky AM, Kosik KS. RNAi functions in cultured mammalian neurons. *Proceedings of the National Academy of Sciences of the USA*. 2002;99(18):11926–9.

271. Cheever A, Blackwell E, Ceman S. Fragile X protein family member FXR1P is regulated by microRNAs. *RNA*. 2010;16(8):1530–9.